Moscow Institute of Physics and Technology
Department of Aerophysics and Space Research
Physics of Nonequilibrium Systems Laboratory

SUPERFAST HOMOGENEOUS PLASMA IGNITION OF HYDROGEN-OXYGEN AND AIR-FUEL SUPERSONIC FLOWS BY HIGH-VOLTAGE IONIZATION WAVE

First Stage Report, 01.01.1999-15.12.1999

Date Submitted: December 15, 1999

Edited by Dr. Andrei Yu. Starikovskii,
Moscow Institute of Physics and Technology
Physics of Nonequilibrium Systems Laboratory
Institutskii lane, 9, 141700,
Dolgoprudny, 141700, RUSSIA
Phone (+7-095)-408-6347
Fax (+7-095)-576-6528
E-mail astar@neq.mipt.ru
URL http://neq.mipt.ru

REPORT DOCUMENTATION PAGE

Form Approved OMB No. 0704-0188

1. AGENCY USE ONLY (Leave blank)	2. REPORT DATE	3. REPORT TYPE AND DATES COVERED
	15 December 1999	Final Report

4. TITLE AND SUBTITLE

Superfast Homogeneous Plasma Ignition of Hydrogen-Oxygen and Air-Fuel Supersonic Flows by High-Voltage Ionization Wave

5. FUNDING NUMBERS

F61775-99-

6. AUTHOR(S)

Dr. Andrei Starikovskii

7. PERFORMING ORGANIZATION NAME(S) AND ADDRESS(ES)

Moscow Inst. of Physics and Technology
Institutskii Lane, 9
Dolgoprudny 141700
Russia

8. PERFORMING ORGANIZATION REPORT NUMBER

N/A

9. SPONSORING/MONITORING AGENCY NAME(S) AND ADDRESS(ES)

EOARD
PSC 802 BOX 14
FPO 09499-0200

10. SPONSORING/MONITORING AGENCY REPORT NUMBER

SPC 99-4007

11. SUPPLEMENTARY NOTES

12a. DISTRIBUTION/AVAILABILITY STATEMENT

Approved for public release; distribution is unlimited.

12b. DISTRIBUTION CODE

A

13. ABSTRACT (Maximum 200 words)

This report results from a contract tasking Moscow Inst. of Physics and Technology as follows: 1) The contractor will perform experiments on ignition initiation by ionization wave in the H2-O2 mixture. Determine the ignition threshold shift. Study the combustion uniformity and synchronization in the system. 2) He will determine the active particle formation rate in ionization wave with the nanosecond time resolution. Measure electric field of ionization wave in hydrogen. Develop a numerical model determining the active particles generation in the fast ionization wave. Verify the numerical model with the use of experimental data.

14. SUBJECT TERMS

EOARD, Plasma Physics, Supersonic and Hypersonic Flows, Kinetic Theory, Deflagration and Detonation

15. NUMBER OF PAGES

205

16. PRICE CODE

N/A

17. SECURITY CLASSIFICATION OF REPORT	18. SECURITY CLASSIFICATION OF THIS PAGE	19. SECURITY CLASSIFICATION OF ABSTRACT	20. LIMITATION OF ABSTRACT
UNCLASSIFIED	UNCLASSIFIED	UNCLASSIFIED	UL

Contents

Chapter 1

Abstract

1.1 Main phases and results expected

1. Conduct experiments on ignition initiation by ionization wave in the H_2-O_2-N_2 mixture. Determine experimentally the ignition threshold shift. Study the combustion uniformity and synchronization in the system

2. Determine the active particle formation rate in ionization wave with the nanosecond time resolution. Measure electric field of ionization wave in hydrogen. Develop a numerical model determining the active particles generation in the fast ionization wave. Verify the numerical model with the use of experimental data.

1.2 Main results obtained

In the framework of the project the following work has been performed and results have been obtained:

- Experimental investigation of the structure of the ionization wave front:

    1. Measurements of the temporal and spatial behavior of electric field in the nanosecond discharge in the form of the fast ionization wave (FIW);
    2. Investigations of active particles formation rate in the fast ionization wave with the nanosecond time resolution;
    3. Measurements of electron density behind the FIW front and determination of the average energy of electrons. Analysis of different types of electron energy distribution functions (EEDF) usability for modelling of active particles formation in plasma.

- Experimental and numerical investigation of the oxidation of molecular hydrogen in H_2-O_2-N_2 stoichiometric mixture in nanosecond pulsed discharge:

    1. Measurements of an absolute concentration of electronically excited molecules H_2 in $a^3\Sigma_g^+$ - state;
    2. Measurements of the rate of hydrogen oxidation at different pressures;

3. Development of numerical code of gas excitation behind the FIW front in the high-current stage; development of the numerical code of chemical kinetics in the discharge afterglow. Verification of the numerical codes on the basis of comparison with the experiment;
4. Determination of main phases of kinetic processes and of the most important processes for each stage. Analysis of the role of reactions with participation of charged, electronically and vibrationally excited particles.

- Numerical modelling of the process of ignition for H_2-air, H_2-O_2 and CH_4-air mixtures at high temperatures under the action of FIW:

1. Calculations of ignition threshold shift for different concentrations of mixture components and gas pressures;
2. Analysis of ignition efficiency, which enable to plan experimental measurements of the initiation of ignition by FIW at high temperatures;
3. High-temperature boundary of transition to pure thermal mechanism of ignition initiation.

- Experimental system for the investigation of the ignition kinetics and determination of the ignition threshold shift in various mixtures in a wide range of the initial conditions (temperature, pressure, high-voltage impulse parameters) is adjusted. The systems for diagnostic of electrical parameters of the discharge, gas dynamic parameters of the shock wave and optical time-resolved emission spectroscopy system are prepared for the experiments.

- Experimental investigation of the decomposition of N_2O nitrogen oxide in nanosecond pulsed discharge:

1. Relative concentration profiles of electronically excited molecules N_2, NO and N_2^+ during N_2O decomposition in the discharge have been measured;
2. Experimental data of the rate of N_2O decomposition at different pressures have been obtained.

- Theoretical analysis of the elementary exchange reaction AB+C→A+BC with the random distribution of AB reagents over vibration energy.

1. The analytical expressions for microconstants of processes that correspond to certain vibration states of reagents AB(v) and products BC(w) with the use of vibronic terms model have been derived;
2. It has been proved that the values of microconstants are completely determined by the value and temperature dependence of the experimentally measurable rate constant of reaction AB+C→A+BC in thermally equilibrium conditions and value of energy release in reaction ΔH.

3. Comparison of calculations using the proposed model with calculations using other models and experimental data has been performed; the possibility to use the model for a qualitative analysis of vibration excitation effect on kinetics at various conditions of excitation – from strong shock waves at $T_{tr} \gg T_{vib}$ to highly non-equilibrium gas discharge at $T_{tr} \ll T_{vib}$ – has been proved.

- Numerical investigation of the role of vibrationally-excited molecules during the oxidation of molecular hydrogen in H_2-O_2-N_2 stoichiometric mixture in nanosecond pulsed discharge:

  1. The numerical model of gas excitation behind the FIW front in the high-current stage taking into account vibrational levels excitation has been developed;
  2. The numerical model of chemical kinetics in the complex system taking into account master equations for vibrational levels excitation/relaxation in the discharge afterglow and chemical reactions between excited reagents has been developed;
  3. The analysis of the role of reactions with participation of vibrationally excited particles has been performed.

- Numerical simulations of the properties of a positive streamer in CH_4-air mixtures in a nonuniform electric field in 1.5D-formulation.

  1. The production of active particles including atoms, radicals and electronically excited molecules by a long positive streamer versus gas composition, pressure, and temperature have been calculated. The results have been used to estimate the efficiency of the streamer-corona ignition of the combustion in the considered gaseous mixtures;
  2. The possibility of the ignition at high pressures of CH_4 : Air mixtures by a streamer discharge has been demonstrated. The ignition threshold versus the main parameters of the system has been determined.

- Numerical code for the modelling of discharge development in the form of the fast ionization wave was developed. The code is based on the solution of a non-stationary Boltzmann equation by Monte-Carlo Particle-In-Cell method.

  1. The governing role of the non-local effects in the propagation of pulsed discharges at high overvoltage and applicability of numerical results together with experimental data on population rates for high-energy emitting electron states for calculation of the energy branching in such a discharges have been demonstrated;
  2. It has been proved that the electron energy distribution function is governed by high-energy electrons in the vicinity of the nanosecond breakdown front.
  3. It has been obtained that the low-energy part of the EEDF in relatively low fields is close to the solution of stationary two-term approximation of Boltzmann equation at the appropriate electric field.

4. The rates of electron-impact processes near the fast ionization wave front, where the relaxation of the high-energy part of the EEDF leads to the significant differences in constant rate values in comparison with an equilibrium case have been calculated.

Part I

Experimental investigations of the fast ionization wave

Chapter 2

Experimental investigations of the fast ionization wave structure; time-resolved measurements of the electric field and rate of active particles production.

2.1 Fast ionization wave

The pulsed electric discharge in gases at essentially high overvoltage develops in the form of so called "fast ionization wave" (FIW) propagating at a velocity of $10^9 - 10^{10}$ cm/s. High electric fields in the FIW front and behind it result in the effective gas ionization, dissociation and excitation, at the same time the gas translation temperature does not essentially change. The non-equilibrium energy distribution makes it possible to provide the high efficiency of FIW, as an ignition initiator, at relatively low power consumption.

Important advantages of application of FIW, as an ignition source, are the spatial uniformity and short time of active particle generation (difference between the characteristic time of particle formation in FIW and the combustion and gas dynamic processes times is about three orders of magnitude).

To understand the basic features of the development and propagation of nanosecond discharge we performed a series of experiments to study the behavior of an electric field and an excitation of electronic degrees of freedom in the molecular nitrogen under the action of pulsed periodic discharge.

The kinetic scheme has been developed for the numerical modelling of the destruction of molecular hydrogen in the discharge. To check this scheme we investigated a hydrogen destruction experimentally.

Values of the electric field in the FIW front is still being researched. Estimations based on experimental investigations reviewed in [1] give two sets of reduced electric field values that are concerned with the type of generator used to initiate the FIW. For voltage pulse amplitudes of 15–25 kV, values of the reduced electric field are within the range of 50–2000 V cm^{-1} $Torr^{-1}$ for the pressures 10–30 Torr. For voltage pulse amplitudes from 250 to 300 kV, the reduced electric field was found to be in the range $\sim 400 - 6000$

V cm^{-1} $Torr^{-1}$ for the pressures 10–100 Torr. Theoretical investigations are few and give values from 520 V cm^{-1} $Torr^{-1}$, for the pressure of 10 Torr and voltage of 100 kV [2], to 1500 V cm^{-1} $Torr^{-1}$ for the same pressure and voltage of 250 kV [3]. As there is significant uncertainty between the different data, it seems to be reasonable to obtain the electric field in the FIW front by experimental methods.

Electric field measurements in such a system are complicated by the fact that a wide dynamic range (from tens -hundreds of V/cm behind the FIW front up to some kV/cm in the front) and good temporal resolution (electric field rises within, in any case, nanoseconds) are required.

In recent years, various non-perturbation methods of electric field measurements have been developed. They are based on the optical detection of the Stark effect. They may use either the laser-induced fluorescence probing of the Stark mixing in the gas containing molecules of special kind (NaK) [4] or 2+1 photon laser Stark spectroscopy of atomic hydrogen [5], or the registration and analysis of Stark splitting of the plasma - induced H Balmer delta emission in hydrogen [6]. The careful investigation of an electric field with temporal resolution of a few nanoseconds using methods mentioned above is made difficult by the fact that the mediocre dissociation degree in the fast ionization wave (no more than $\sim 10^{-4}$ [7]) leads to the poor signal-to-noise ratio.

Some efforts have been made to measure electric fields for the streamer - leader transition [8, 9] using the Pockels effect (double refraction modification under the electric field). The temporal resolution of this method is limited by optical - electrical conversion and may be diminished to picoseconds. There is another complication with Pockels device measurements: polarization of the dielectric in the strong electric field may be a reason for the local electric field gain near the probe. In such a case, ionization growth in the region will leads to charge-distribution distortion [10]. Calibration of the Pockels device in the known electric field excludes such errors and so will be accurate only below breakdown. So, the best measurements by Pockels devices are made at relatively low fields [11].

We deal with a combined approach which yields both the mean longitudinal electric field value in the FIW front and the electron density behind it. The basic idea of the method is a reconstruction of the charge q per unit length from the experimental measurements that takes into account the space sensitivity function of the detector which is determined from the special experiments. The electric field E and the electron concentration n_e were found on the basis of the deduced q value. The results are then compared with electronic levels excitation dynamics, obtained from the time-resolved emission spectroscopy measurements.

2.2 Experimental setup

The experimental apparatus is shown schematically in Fig. 2.1. Negative voltage pulses with a U=15.5 kV peak-pulse amplitude, 40 Hz repetitive frequency, and a 25 ns duration on half-height with a 3 ns rise time were used to initiate the FIW. The pulses were transmitted from the generator (1) through the coaxial electric cable to the high voltage electrode of the discharge tube. The length of the coaxial cable was chosen long enough to separate the first pulse created by the generator and the reflection of this pulse from the end of the discharge tube. The following reflected pulses could have appeared because of

the different impedances of the generator, the cable and the discharge tube. These were consequently prevented from influencing the results. Pulse amplitude was controlled by the low-inductive broad-band calibrated current shunt (2) that was included into cable shield break.

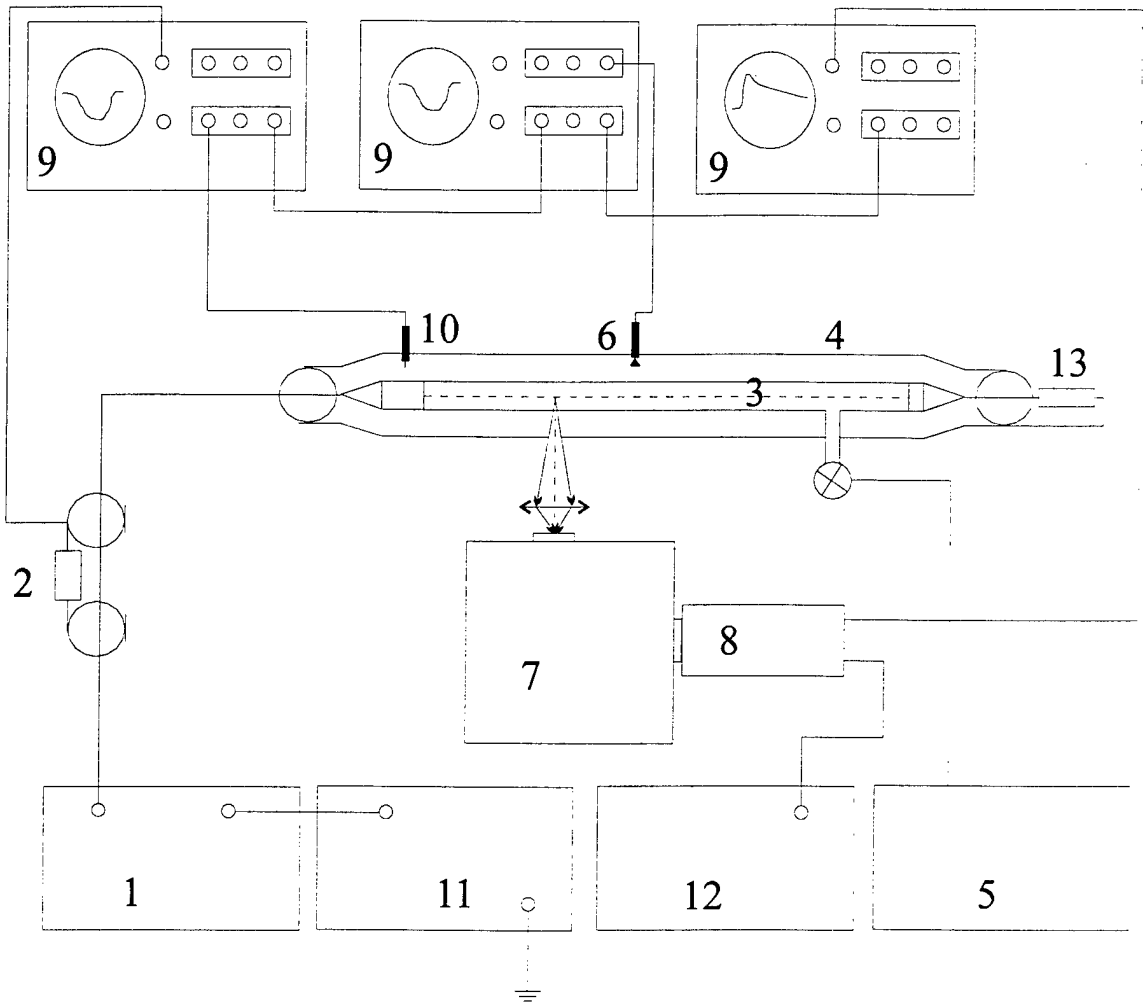

Figure 2.1: Schematic diagram of the apparatus. 1 – nanosecond pulsed generator; 2 – coaxial current shunt; 3 – discharge tube; 4 – metallic screen; 5 – vacuum system; 6 – capacitive detector; 7 – monochromator; 8 – photomultiplier; 9 – oscillographes; 10 – synchrogauge; 11,12 – power sources; 13 – 50 Ohm resistor.

As a rule, in the region corresponding to the optimal fast ionization wave propagation only two pairs of pulses are usually registered by the current shunt. Approximately 60% of the energy stored in the first pulse from the generator is lost to the plasma; 20% is added in the second pair of pulses, and $\sim$ 20% is disappeared in the generator [12]. It should be emphasized that all of the results presented here, unless explicitly stated otherwise, refer to the ionization wave initiated by the first pulse.

The glass discharge tube (3) of 60 cm length and 1.75 cm inner diameter with the plate electrodes at the ends was surrounded by a coaxial metallic screen of diameter 6 cm. The low voltage electrode was connected to the metallic screen by a coaxial electric cable with a matching resistance (13). The tube was pumped and filled with air by means of the

vacuum system (5). The pressure was controlled by three types of gauges: thermocouple gauge PMT-2 for the pressure range $10^{-3} - 10^{-1}$ Torr, pressure gauge 6MD×4S for the $10^{-1} - 10$ Torr and U-tube oil manometer for the $10 - 20$ Torr range. The space between the discharge tube and the metallic screen (4) was filled with air at atmospheric pressure.

A modification of the electrical signal along the tube was registered with the aid of a calibrated broad-band capacitive detector (6). The detector consists of a duct capacitor connected with a copper contact pad and the signal from the duct capacitor was registered by the oscillograph. As a result, the capacitive probe yields a voltage signal related to the presence of a charge density in the discharge cell where integration takes place over the whole charge distribution. The probe was moved in the narrow slit of the tube screen along the tube axis at intervals of 3 mm. The signal from the capacitive detector may be thought of in the following way. If the detector is placed at a point $\vec{r_d}$ of the configuration space, then assuming that directionality diagram of the probe is isotropic, the electric signal from the detector may be represented as

$$V(\vec{r_d}) = \int_{\Omega} \rho(\vec{r}) f_d(\vec{r_d} - \vec{r}) d^3r \tag{2.1}$$

Here, the region Ω is bounded by metallic screen, f_d is a space sensitivity function of the detector and $\rho(\vec{r})$ is a charge distribution.

It is known from the experimental observations that the fast ionization wave is an axially symmetric structure [12]. In such a situation, electric potential and the signal from the capacitive detector at the point $\vec{r_d}$ will be defined only by the charge q per unit length, ignoring any real charge distribution in the cross-section. Then

$$V(x_d) = \int_{-\infty}^{+\infty} q(x) f_d(x - x_d)\, \underset{\sim}{\mathrm{x}}, \tag{2.2}$$

where the actual integration limits are restricted by the width of the space sensitivity function.

The space sensitivity function of the capacitive probe was determined from the special experiments. In these experiments a signal from the detector was registered at the known charge distribution. The high voltage electrode described above was replaced by an electrode of 223 mm in length. The end plate of the electrode was then covered with a thin dielectric layer to prevent corona development and experiments were performed at atmospheric pressure. The probe was moved along the discharge tube at intervals of 1 mm and signal amplitude was registered. Simultaneously charge distribution in the region Ω was defined from the Laplacian solution assuming that the electrode is an equipotential surface. The space sensitivity function was then obtained on the basis of equation (2.2). It was found that the detector sensitivity function is a symmetric curve $\sim$ 4 cm in halfwidth.

Time delay Δt of the radiation front in the measurement cross section in comparison with the electric field front was measured by a narrow-band capacitive sensor and coaxial photocell FEK-22 (spectral range of sensitivity - 250 - 550 nm).

In experiments on determination of the absolute radiation intensity the radiation produced by separate transitions was recorded by an optical system that consists of a set of diaphragms, monochromator MDR-12 (7) and photomultiplier (8) 14ELY-FT (the spectral sensitivity range of the photocathode was 250–600 nm). The radiation was selected

in the direction perpendicular to the discharge device axis at a distance of 20 cm from the high-voltage electrode.

Measurements were performed in air and spectrally pure nitrogen at pressures from 1 Torr to 20 Torr for 0–0 transition of the second positive system (λ=337.1 nm) and 0–0 transition of the first negative system (λ=391.4 nm).

The width of each electron-vibration transition was experimentally determined with a spectral step of 0.25 Å. To eliminate the contribution of the adjacent bands into the signal and provide the constant sensitivity of the recording system in the whole transmission band the independent adjustment of input and output monochromator slots was used.

To obtain absolute characteristics the optical system was calibrated with the use of light sources with known absolute radiation densities: deuterium calibrated DDS-30 (spectral range 200-500 nm) and tungsten TRY-1100 (spectral range 350-700 nm).

The temporal resolution of the optical system was 1 ns at low pressures and 2 ns at high pressures and was determined by the time that was required in order that the breakdown front pass through the discharge tube section which radiation was gathered from. During synchronized recording of the electric field and radiation the temporal resolution was 1 ns.

All signals were registered on the oscillograph Tektronix TDS-380 and S9-4A (9) with synchro-signal taken from the gauge (10) positioned over the high-voltage electrode. Oscillographs were positioned in a shielded room and all cables were additionally screened to prevent high - frequency electrical noise. The oscillograms of the signals from the capacitive detector were processed using the specially elaborated software package.

Temporary resolution of both the electric and spectroscopic measurements was less than 2 ns. Experiments were performed in air for the pressure range 0.1–16 Torr. The pressure range was taken in order to optimize the FIW propagation for the high voltage pulse parameters previously mentioned.

2.3 FIW front velocity and attenuation

The FIW front velocity was taken as a velocity of the point on the front half-way up the signal amplitude by assuming that ionization wave front acceleration is constant. FIW front velocity V_{fr} dependence *versus* pressure is represented in Fig. 2.3 together with the attenuation coefficient G. This attenuation coefficient was determined according to the expression $G = (U_{50} - U_{450})/U_{50}$, where U_{50} and U_{450} – are the signal amplitudes at the points respectively situated at 50 and 450 mm from the high voltage electrode. Inasmuch as the ionization wave amplitude drops linearly along the length of the discharge tube, the attenuation coefficient allows an estimate of the wave amplitude at the arbitrary distance from the high voltage electrode. At the pressures which are typical for the region of increase of the $V_{fr}(P)$ dependence, FIW propagates along the tube with a near constant velocity. With the growth of pressure, the back of the ionization wave slows down first and eventually so does the front of the wave.

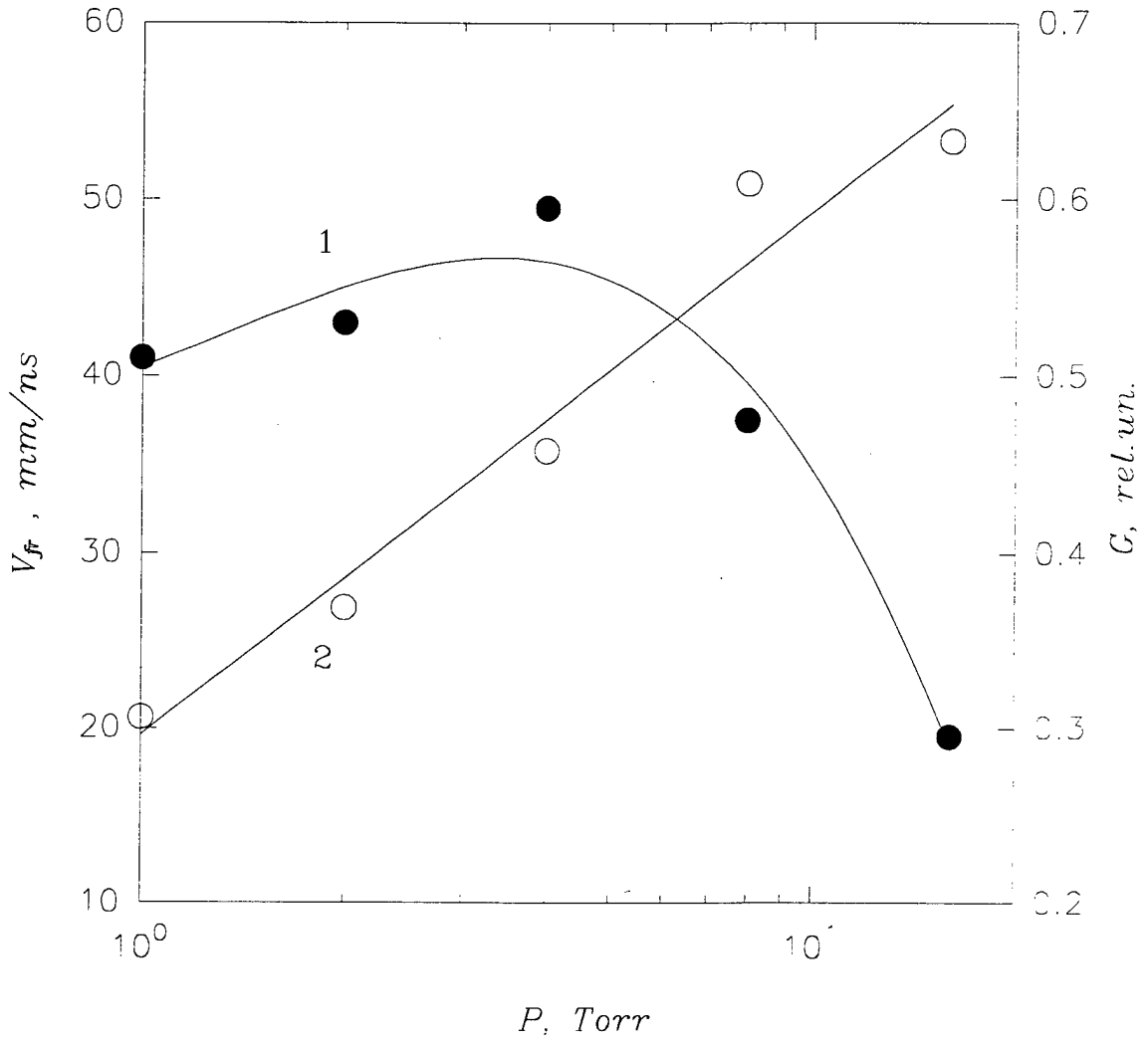

Figure 2.2: Dependence of the FIW front velocity V_{fr} (curve (1)) and the amplitude attenuation coefficient G (curve (2)) *versus* pressure.

2.4 Electric field in the FIW front and electron density behind the front

For all investigated pressures it was found that the electric field profiles are asymmetric in time. They rise to a peak value during 3-4 ns and then drop during ~2 ns, after that, a smooth decrease down to zero is observed.

Peak electric field values increase slightly with pressure: from 4.5 kV/cm when $P =$ 1 Torr to 8 kV/cm at 16 Torr in the cross section at distance 20 cm from the high voltage electrode. At the same time, peak values of the reduced electric field, represented in Fig. 2.3, curve (1), change by an order of magnitude within the investigated pressure range. It should be mentioned that data processing with an assumption of zero width for the detector sensitivity function $f_d = \delta(x - x_d)/C$ (where C is a constant) gives the same tendency for the E/P maximum value to diminish with pressure (compare curves (1) and (2) in Fig. 2.3). But as the absolute E/P values are $1.5 - 2$ times lower than the ones calculated with the real f_d; they can hence be used as an experimental estimation.

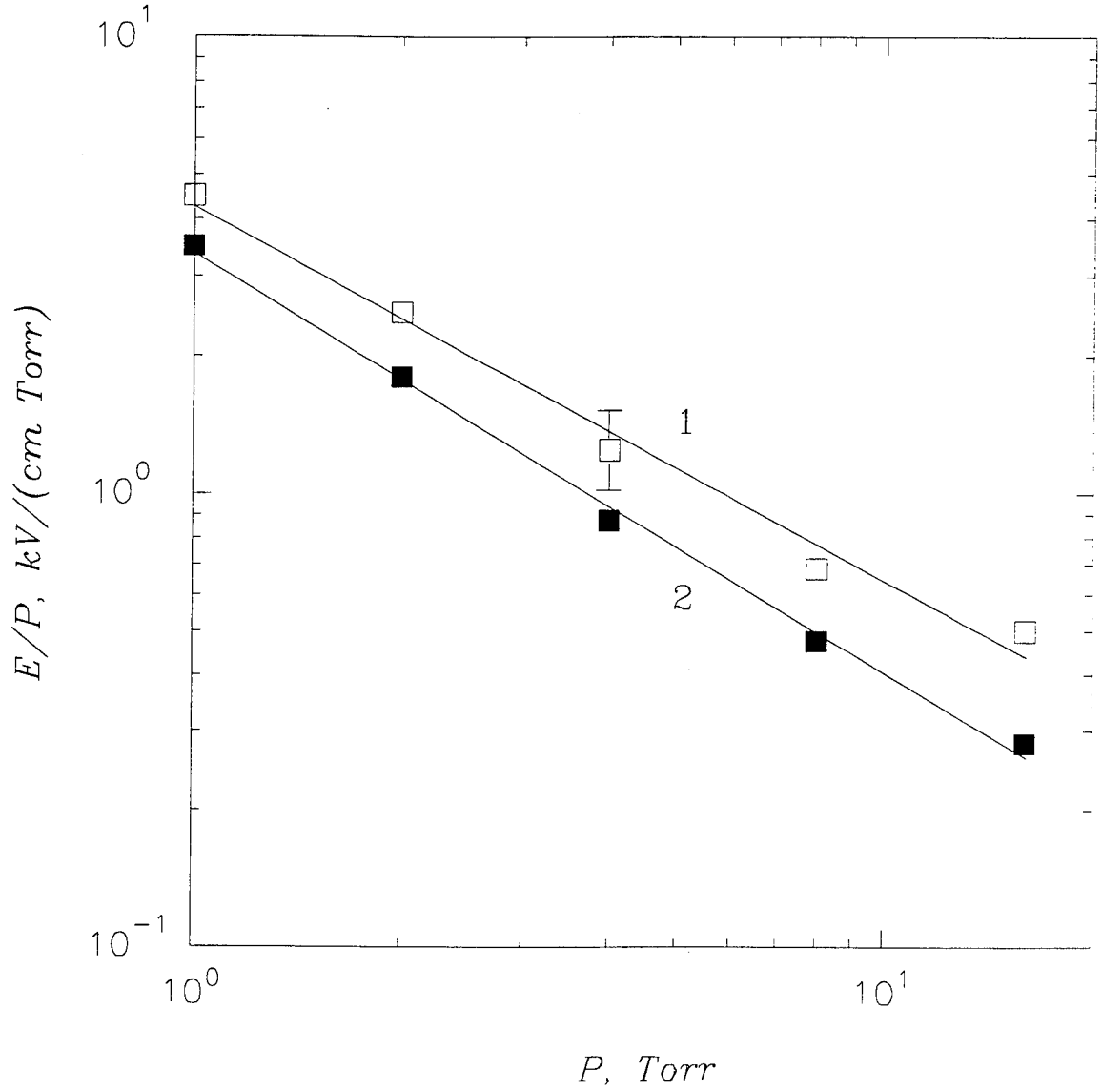

Figure 2.3: Peak values of the longitudinal reduced electric field *vs* pressure in the orthogonal section situated at position 20 cm, relative to the high voltage electrode. Curve (1) represents data recovered with real detector sensitivity function, curve (2) – with $f_d = \delta(x - x_d)/C)$.

The significant decrease of E/P values with pressure must sharply influence the energy distribution in the discharge. For example, at the pressure P=1 Torr the maximum reduced field reaches 4.5 kV/(cm · Torr) and so significantly exceeds the threshold for the electron runaway [13]. Alternatively, at the P=16 Torr, the peak E/P value reduces to 0.5 kV/(cm · Torr) so that the mean reduced electric fields correspond to effective ionization and electronic levels excitation.

It was found that the degree of ionization diminishes with pressure, whereas electron density dependence $n_e(P)$ has the form of a smooth curve with maximum value $n_e = 5{\cdot}10^{12}$ cm^{-3} at the pressure $P = 4$ Torr. It should be noticed that the maximum of the ionization wave front velocity is attained at the same pressure (see Fig. 2.3).

2.5 The rate of electron excited states population

The excited states population is determined by processes of excitation, radiative depopulation and quenching during collisions with heavy particles. The electron-excited particle concentration in FIW is small in comparison with the concentration of nitrogen molecules in the ground state. Therefore, under conditions of this study the upper electron level population is formed predominantly from the ground state by the direct electron impact. An equation that describes change in the excited state particle [N*] concentration shows up as follows:

$$\frac{d[N^*]}{dt} = Q - \frac{1}{\tau_0}[N^*] - k_{q(i)}^{N_2}[N_2][N^*] - k_{q(i)}^{O_2}[O_2][N^*], \tag{2.3}$$

Herein τ_0 – radiative lifetime of the associated level, $k_{q(i)}^{N_2}$ – constant of the rate of excited molecule (ions) quenching by N_2 molecules, $k_{q(i)}^{O_2}$ – constant of the rate of quenching by O_2 molecules, Q – the rate of nitrogen electron state excitation from the ground state by electron impact. The $Q(t)$ rate of excitation may be reconstructed for any time moment t from $[N^*]$ and $d[N^*]/dt$ values measured in the experiment.

On the other hand the population rate is determined by concentrations of electrons n_e and nitrogen molecules in the ground state $[N_2]$, excitation process section σ and electron energy distribution function $f(\varepsilon)$:

$$Q = n_e[\mathrm{N_2}] \int_{\varepsilon_k}^{+\infty} \sigma(\varepsilon)\sqrt{\frac{2\varepsilon}{m_e}}\sqrt{\varepsilon} f(\varepsilon) d\varepsilon = n_e[\mathrm{N_2}]\langle\sigma v\rangle, \tag{2.4}$$

where ε_k –energy threshold of the state excitation. For the electron energy distribution function the unit normalization with $\sqrt{\varepsilon}$ weight coefficient was adopted:

$$\int_0^{+\infty} \sqrt{\varepsilon} f(\varepsilon) d\varepsilon = 1 \tag{2.5}$$

To analyze the EEDF in the nanosecond discharge the numerical solution of Boltzmann stationary equation in two-term approximation and three different analytical dependencies were used.

In a number of paper [14, 15] the accuracy of two-term approximation was analyzed for molecular nitrogen by estimation of residual terms of expansion into Legandre series and comparison of the obtained results with modeling by Monte-Carlo method. It was shown that integral characteristics of the plasma, i.e. average and characteristic energies, diffusion and mobility coefficients determined by a low-energy part of EEDF, can be found with 25% error up to 1500 Td fields (1 Td=10^{-17} V·cm^2).

To solve numerically Boltzmann equation processes of elastic collisions [16], rotational excitation [17], population of the first ten vibrational levels of the main nitrogen molecule state [18, 19], excitation of the first 11 lower electron levels of N_2 molecule [20] and of Rydberg states, energy losses through dissociation [21, 22] and ionization [23, 24] processes were taken into account. It was assumed that: 1. electron-electron and electron-ion collisions do not essentially contribute into the process, which fits well for relatively low degree of gas ionization $\sim 10^{-4}$ and the total electron concentration of $\sim 10^{12}$ cm^{-3} at conditions of this study; 2. there is a spatially uniform version of EEDF which is in

equilibrium with the local electric field; the latter condition is obviously violated in strong fields in the vicinity of the ionization wave front, but in a few nanoseconds the following E/N decrease up to 100 - 400 Td makes it possible to use the two-term approximation.

A flow of fast electrons of energy about tens keV which is formed within the first several nanoseconds at the breakdown front where the reduced electric field is over the runaway threshold causes the generation of the secondary electrons which degrading spectrum is a power series and rather slowly decreases, as the energy increases [25].

When solving Boltzmann non-stationary equation in [26] it was shown that in molecular nitrogen at pressure of several Torrs the time of "cooling down" of the secondary electron spectrum in 10-100 eV energy range after the beam action is ceased makes up tens of nanoseconds, which can result in the considerable overenrichment of EEDF in this energy range for a short period of time in comparison with the results of analysis in two-term approximation.

For this reason a number of analytical dependencies for EEDF which are characterized by different behavior in the high energy range were additionally treated:

Maxwell distribution with ε_e average electron energy:

$$f_m(\varepsilon) = \frac{3\sqrt{3}}{\sqrt{2\pi}}\varepsilon_e^{-3/2}\exp\left(-\frac{3}{2}\frac{\varepsilon}{\varepsilon_e}\right) \tag{2.6}$$

Druyvesteyn distribution:

$$f_d(\varepsilon) = \frac{3\sqrt{3}}{4\Gamma[3/4]}\varepsilon_e^{-3/2}\exp\left(-\frac{9}{16}\left(\frac{\varepsilon}{\varepsilon_e}\right)^2\right), \tag{2.7}$$

Maxwell distribution is derived with the assumption that the transport scattering frequency is constant: $\nu_{tr}(\varepsilon) = const$. The more rapid fall at high energies is typical for Druyvesteyn distribution. The following is valid for it: $\nu_{tr}(\varepsilon) \sim \varepsilon^{1/2}$.

Additionally we examined EEDF associated with the condition of $\nu_{tr}(\varepsilon) \sim \varepsilon^{-1/4}$ and characterized by the slower than (2.6) and (2.7) decrease of the number of electrons in the distribution "tail":

$$f_{1/2}(\varepsilon) = 6\sqrt{3}\varepsilon_e^{-3/2}\exp\left(-2\sqrt{3}\left(\frac{\varepsilon}{\varepsilon_e}\right)^{1/2}\right) \tag{2.8}$$

The distribution $f_{1/2}$ (2.8) represents an intermediate version between the spectrum of the relaxing impulsed beam and stationary distribution in the external electric field. It appears to be the most adequate description of the process of high electron states population in the ionization wave that forms the beam-type electron distribution at the front. At the same time behind the FIW front the distribution close to the solution of Boltzmann equation in two-term approximation is formed in the low energy part of the spectrum.

2.6 Average energy and density of electrons in discharge

Independent measurements of FIW electron concentration and electric fields under the similar conditions [27] make it possible to analyze usability of EEDFs of various types at

conditions of discharge under high overvoltage at earlier stages.

Ratio W of $N_2(C^3\Pi_u, v'=0)$ and $N_2^+(B^2\Sigma_u^+, v'=0)$ level population rates at specified EEDF parametrically depends (2.4) on the average energy of electrons ε_e:

$$W(\varepsilon_e) = \frac{Q_{N_2(C^3\Pi_u)}}{Q_{N_2^+(B^2\Sigma_u^+)}} = \frac{\int_{\varepsilon_2}^{+\infty} \sigma_{2+}\varepsilon f(\varepsilon)d\varepsilon}{\int_{\varepsilon_1}^{+\infty} \sigma_{1-}\varepsilon f(\varepsilon)d\varepsilon} \tag{2.9}$$

The average energy ε_e can be determined for every EEDF by comparison of $W(\varepsilon_e)$ value calculated on the basis of (2.9) with population rate ratio experimentally determined from (2.3).

Cross-sections σ_{2+} and σ_{1-} were reconstructed from excitation function of nitrogen spectral bands with the use of Frank-Cordon known coefficients for the second positive [28] and the first negative [29] systems of nitrogen.

The electron density $n_e(t)$ can be calculated on the basis of (2.4) with the use of known average energy of electrons $\varepsilon_e(t)$ for every EEDF and experimental measured electron state population rates $Q(t)$:

$$n_e(t) = \frac{Q(t)}{[N_2]\int_{\varepsilon_k}^{+\infty} \sigma(\varepsilon)\sqrt{\frac{2\varepsilon}{m_e}}\sqrt{\varepsilon}f(\varepsilon)d\varepsilon} \tag{2.10}$$

Typical results for nitrogen at pressure of 4 Torr are presented in Fig. 2.4a-d. Plausible time interval of measurements is limited by $\tau \simeq 22$ ns period of time when the excitation rate becomes less than the quenching rate of the $N_2^+(B^2\Sigma_u^+, v'=0)$ level.

Electron recombination processes for such a period of time can be disregarded, and the decrease of the level excitation rate is caused by decrease of the electron energy. Hence, electron concentration is to be monotonically built up during the impulse and become stationary. We adopted this behavior of electron concentration as one of criteria of the actual EEDF approximation accuracy.

Conformity of the absolute value of maximum electron concentration to the n_e values experimentally obtained serves as the second criterion.

In paper [27] at identical conditions the dynamics of the electric field in discharge and electron concentration behind the FIW front were reconstructed on the basis of charge density measurements. Results of comparison of n_e calculated for various EEDF with experimental data are shown in Fig. 2.5.

It follows from Figs. 2.4, 2.5 that EEDF (2.8) which at $t \simeq 16$ ns makes it possible to reach stationary value of $n_e(t)$ adequately coinciding with the experimental electron concentration at various pressures meets the both criteria best of all.

2.7 Verification of self-consistency for various EEDF. Reduced electric field value.

To verify self-consistency of the solution obtained with the use of known dependencies $\varepsilon_e(t)$, $n_e(t)$ and integral ionization section [23] the k^i nitrogen ionization rate constant was calculated for the modeling EEDF (2.8):

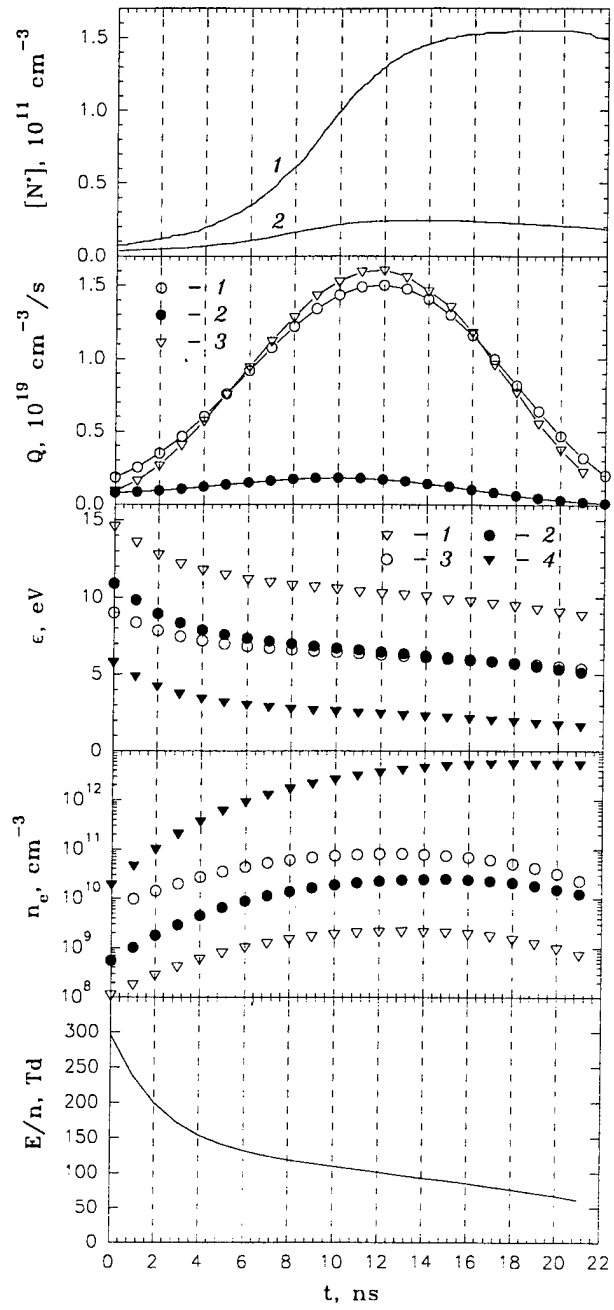

Figure 2.4: Typical results. Nitrogen, pressure $P = 4$ Torr. **a)** Experimental measured concentration of excited particles. 1 – in $N_2(C^3\Pi_u, v'=0)$ state, 2 – in $N_2^+(B^2\Sigma_u^+, v'=0)$ state. **b)** Excited particle concentration growth rate. 1 – in $N_2(C^3\Pi_u, v'=0)$ state, 2 – in $N_2^+(B^2\Sigma_u^+, v'=0)$ state, 3 – in $N_2(C^3\Pi_u, v'=0)$ state, calculation using $n_e(t)$ dependence obtained and excitation rate constant from the stationary two-term approximation. **c)** Dynamics of average electron energy change, calculation for different EEDFs. 1 – f_d, 2 – f_m, 3 – f_B, 4 – $f_{1/2}$. **d)** Dynamics of electron concentration change. Designations are the same. **e)** Dynamics of electric field change reconstructed by ε_e for $f_{1/2}$.

$$k^i(t) = \int_{\varepsilon_i}^{+\infty} \sigma_i(\varepsilon)\sqrt{\frac{2\varepsilon}{m_e}}\sqrt{\varepsilon} f_{1/2}(\varepsilon)d\varepsilon \tag{2.11}$$

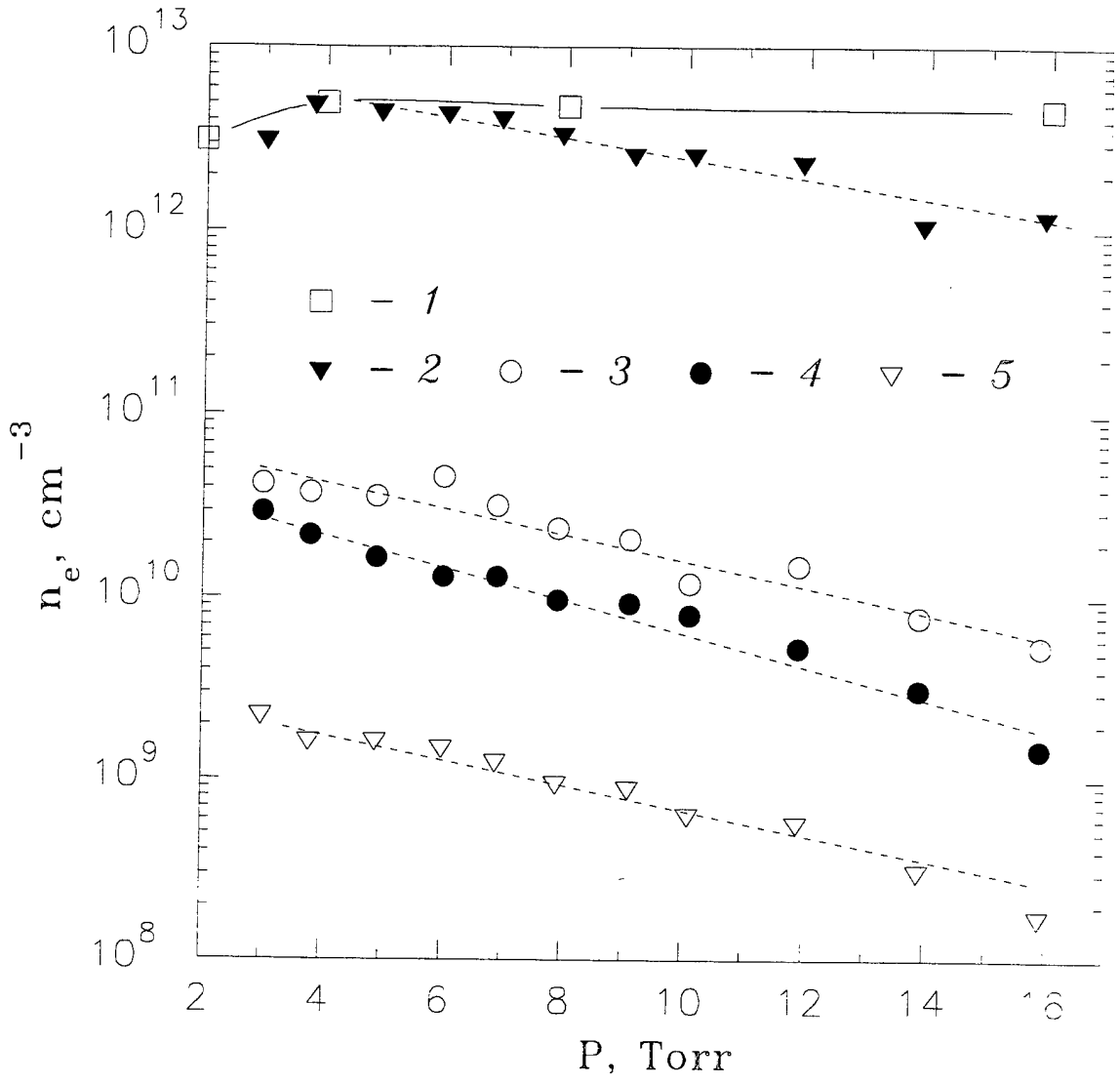

Figure 2.5: Pressure dependence of maximum electron concentration. 1 – measurement results, 2 – calculation for $f_{1/2}$, 3 – f_B, 4 – f_m, 5 – f_d.

On the other hand, it follows from the electron balance equation:

$$k^i(t) = \frac{1}{n_e n_0} \frac{dn_e}{dt} \tag{2.12}$$

Absolute ionization rate constants obtained from (2.11) and (2.12) coincide with each other within two times during the whole impulse. The ionization rate calculated in two-term approximation is approximately by the order of magnitude less and results in the essential discrepancy with the experimental observed values.

Thereby, considerable overpopulation of the EEDF high-energy part due to the degrading spectrum is to be taken into account in description of ionization and high level population rate.

The function of average electron energy dependence on reduced electric fields in nitrogen is known with the high accuracy [15] which makes it possible to determine E/N at any moment of time with the use of ε_e average electron energy obtained. In [15] the

good agreement between $\varepsilon_e(E/N)$ calculation in the frame of two-term approximation of Boltzmann equation and experimental data up to 500 Td is shown.

Since in low-energy part the $f_{1/2}$ and f_B functions virtually coincide at the same ε_e the further mathematical treatment is conducted for numerical solution of Boltzmann equation f_B at ε_e, average energy determined by $f_{1/2}$ modeling function. The electric field change calculated in such a manner during the radiation impulse is presented in Fig. 2.4e.

The section of $N_2(C^3\Pi_u)$ level excitation by electron impact is known with the good accuracy. The approximation of E/N dependence of this state excitation rate constant k_C calculated in the two-term approximation is given in [14]:

$$\lg k_C = -8.1 - \frac{218}{E/N} \tag{2.13}$$

where E/N is expressed in Td and k - in cm^3/s. The $N_2(C^3\Pi_u, v = 0)$ population rate was calculated taking into consideration the $(E/N)(t)$ and $n_e(t)$ dependencies obtained. The results are given in Fig. 2.4b. It is clear that the population rate of this relatively low level is adequately described by the calculation in the two-term approximation. The similar comparison for the $N_2(B^2\Sigma_u^+)$ high level results in the discrepancy between results of calculation in the two-term approximation and experiments by more than the order of magnitude.

2.8 Structure of the ionization wave front

As noted above, the reduced electric fields in the FIW front for the first several nanoseconds prior to the radiation impulse start are very high. If we base on the data of Fig. 2.4 c,d and adopt $\varepsilon_e = 6$ eV and $n_e = 2 \cdot 10^{10}$ cm^{-3} for electron energy and concentration directly behind the wave front we obtain a paradoxical result: the calculated current density $j = 0.1$ A/cm^2 is by more than the two orders of magnitude less than the current density $j_c \simeq 25$ A/cm^2 required to charge the discharge device capacitance per unit length. Since behind the FIW front the current density is to be constant with the accuracy up to the relatively slow change of the plasma potential as the discharge develops it is possible to make a conclusion that in the vicinity of the high field front the local approximation becomes improper and the current calculation based on the calculated electron concentration and energy becomes invalid.

We start from the fact that directly at the ionization wave front the fast electrons of n_e^f concentration predominantly contribute into the charge transfer and estimate their energy on the basis of spectral data obtained. The average energy of such electrons is to be over the velocity of the FIW front propagation which results in $\varepsilon_e \geq 5$ keV estimate at 4 Torr pressure and $v_{fr} \simeq 4 \cdot 10^9$ cm/s [27] associated velocity. The $N_2(C^3\Pi_u, v'=0)$ excitation section at these energies is a negligible small. Assuming that the electron distribution in FIW front is virtually monoenergetic we write for the $N_2^+(B^2\Sigma_u^+, v'=0)$ state:

$$\frac{[N_2^+(B^2\Sigma_u^+, v = 0)]_{min}}{\tau} = n_e^f [N_2] \sigma_{1-} \langle v \rangle \tag{2.14}$$

Herein, $\langle v \rangle$ – average electron energy. The $\Theta \sim 1$ cm radius is adopted as a characteristic length of electron path prior to their drift to the side wall of the discharge tube. Then,

the concentration corresponding to $[N_2^+(B^2\Sigma_u^+, v=0)]_{min}$ threshold of particle detection is generated for $\tau \simeq \Theta/v_{fr}$.

We estimate n_e^f characteristic electron concentration in the wave front on the basis of the fact that $en_e^f\langle v_x\rangle$ fast electron current density is to correspond to $q_C v_{fr}/S$ density of the current to charge the discharge device capacitance per unit length, where q_C - the charge per unit length:

$$n_e^f = q_C v_{fr}/eS\langle v_x\rangle. \tag{2.15}$$

Assuming that the main component of the electron velocity in the FIW front is directed along the discharge device axis, i.e. $\langle v\rangle \simeq \langle v_x\rangle$, at $[N_2] \simeq 10^{17}$ cm^{-3} from (2.14, 2.15) we obtain an estimate of the excitation section:

$$\sigma_{1^-} = \frac{eS}{\Theta q_c}\frac{[N_2^+(B^2\Sigma_u^+, v=0)]_{min}}{[N_2]}\frac{\langle v_x\rangle}{\langle v\rangle} \simeq 5\cdot 10^{-19}\ \text{cm}^2 \tag{2.16}$$

On the basis of the fact that the $\langle v_x\rangle$ projection can not be less than v_{fr} wave front velocity the accuracy of the assumption made is $1/2 < \langle v_x\rangle/\langle v\rangle < 1$ and, hence, at $n_e \simeq (2-4)\cdot 10^{10}$ cm^{-3} electron concentration the average energy in the wave front is $\varepsilon_e \simeq 20 \pm 5$ eV.

With a knowledge of the $\sigma_i \simeq 7\cdot 10^{-18}$ cm^2 total nitrogen ionization section for those energies it is possible to estimate the n_e concentration of the secondary electrons generated by n_e^f fast electrons prior to their drift to the wall: $n_e \simeq n_e^f[N_2]\sigma_i\Theta \simeq 2\cdot 10^{10}$ cm^{-3}, which is in good agreement with the electron concentration directly behind the high field front (Fig. 2.4) which was obtained in this study.

Fig.2.6 shows the temporal evolution of electric field impulse and the $N_2(C^3\Pi_u, v'=0)$ and $N_2^+(B^2\Sigma_u^+, v'=0)$ levels population at 4 Torr pressure in nitrogen. The time reference point of $Q(t)$ and the maximum electric field was chosen by matching of absolute values of $(E/N)(t)$ dependencies measured in [27] and calculated (Fig. 2.4e). The time shift obtained correlates well with Δt measured time delay between the electric signal and radiation.

As is seen from Fig.2.6 the radiation impulse starts behind the FIW front in $E/N \simeq$ 300 Td reduced fields. The maximum population rate determined by not only the electron state excitation rate constant but also the electron concentration is attained at $E/N \simeq$ 120 Td fields in the whole range of pressures contemplated.

Thereby, it is possible to argue that intensive generation of electrons as well as the electron state population take place behind the ionization wave front in residual fields and the moments of time when "electrical" and "luminous" FIW fronts come to the measurement cross section are essentially separated.

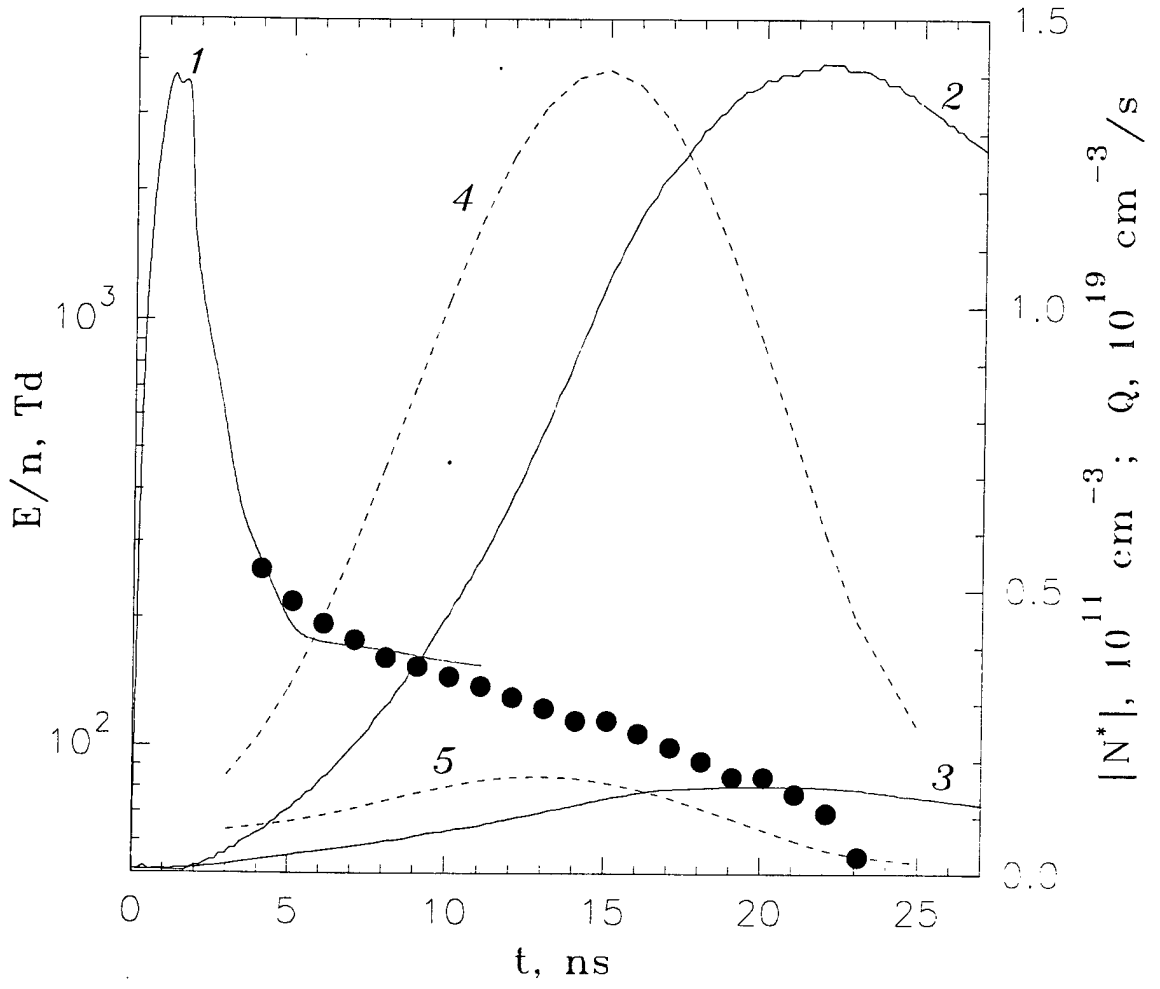

Figure 2.6: Temporal evolution of electric field, $N_2(C^3\Pi_u, v'=0)$ and $N_2^+(B^2\Sigma_u^+, v'=0)$ level population rate and value in nitrogen. 1 – electric field dynamics, measurements by capacitive divider, 2 – $N_2(C^3\Pi_u, v'=0)$ state particle concentration, 3 – $N_2^+(B^2\Sigma_u^+, v'=0)$ state particle concentration, 4 – $N_2(C^3\Pi_u, v'=0)$ state population rate, 5 – $N_2^+(B^2\Sigma_u^+, v'=0)$ state population rate, • – electric field values obtained in this study.

Part II

Numerical modelling of the fast ionization wave

Chapter 3

A Monte Carlo simulation of the Fast Ionization Wave development and propagation

Well-known approaches developed for the glow discharge modelling are unsuitable in the case of self-consistent modelling of pulsed nanosecond discharges, which are characterized by high values of electric field strength in the breakdown front – up to a several kTd.

In particular two-term approximation of Boltzmann equation failed to describe electrons behavior at high E/N; qualitatively new effects appear due to non-local nature of the task; high-energy so called "run-away" electrons carry noncompensated charge and provide an effective pre-ionization [114, 115].

In the other hand it is existence of the region with very strong electric fields allow to describe fast ionization waves as a separate class of discharges.

Modelling of such discharges requires the most general models, which imposes quite strict demands both on the input information (in particular, on the presence of differential cross-sections data for a wide range of electron energies) and on the numerical methods used.

In the present work a numerical code has been developed for the modelling of discharge development in the form of the fast ionization wave.

3.1 Boltzmann kinetic equation for electrons

To analyze a development and propagation of the fast ionization wave at high reduced electric field values let us consider a gas of electrons in the electric field $\vec{E}$ with a velocity distribution function $f(x, v, t)$. In such a case $f(x, v, t)dx^3dv^3$ represents a number of electrons which are situated at the time moment t in 6-dimensional volume element dx^3dv^3, and $(\vec{x}, \vec{v})$are their coordinates.

Electron acceleration under the electric field $\vec{E}$ is equal $-(e\vec{E})/m_e$. Assuming that electron does not change its velocity during a short time interval and does not change electric field strength in the same time interval δt, we shall obtain that electron with initial coordinates $(\vec{x}, \vec{v})$at $t = t_0$ will change coordinates for $(\vec{x'}, \vec{v'})$, which may be derived from the following relationship:

$$\vec{x'} = \vec{x} + \vec{v}\delta t \tag{3.1}$$

$$\vec{v'} = \vec{v} - \frac{e\vec{E}}{m}\delta t \tag{3.2}$$

Let us consider two small elements of the phase volume placed at the points $(\vec{x}, \vec{v})$and $(\vec{x'}, \vec{v'})$(Fig.3.1) of the 6-dimensional space of velocities and coordinates.

It is follows from equations (3.1) and (3.2), that part of electrons from volume element (d^3xd^3v) at point $(\vec{x}, \vec{v})$will move to volume element $(d^3x'd^3v')$ at point $(\vec{x'}, \vec{v'})$during a time interval δt.

At first order of a δt value we have $d^3xd^3v = d^3x'd^3v'$ and, consequently, number of molecules dN in the volume element with coordinates $(\vec{x}, \vec{v})$may be written as [117]:

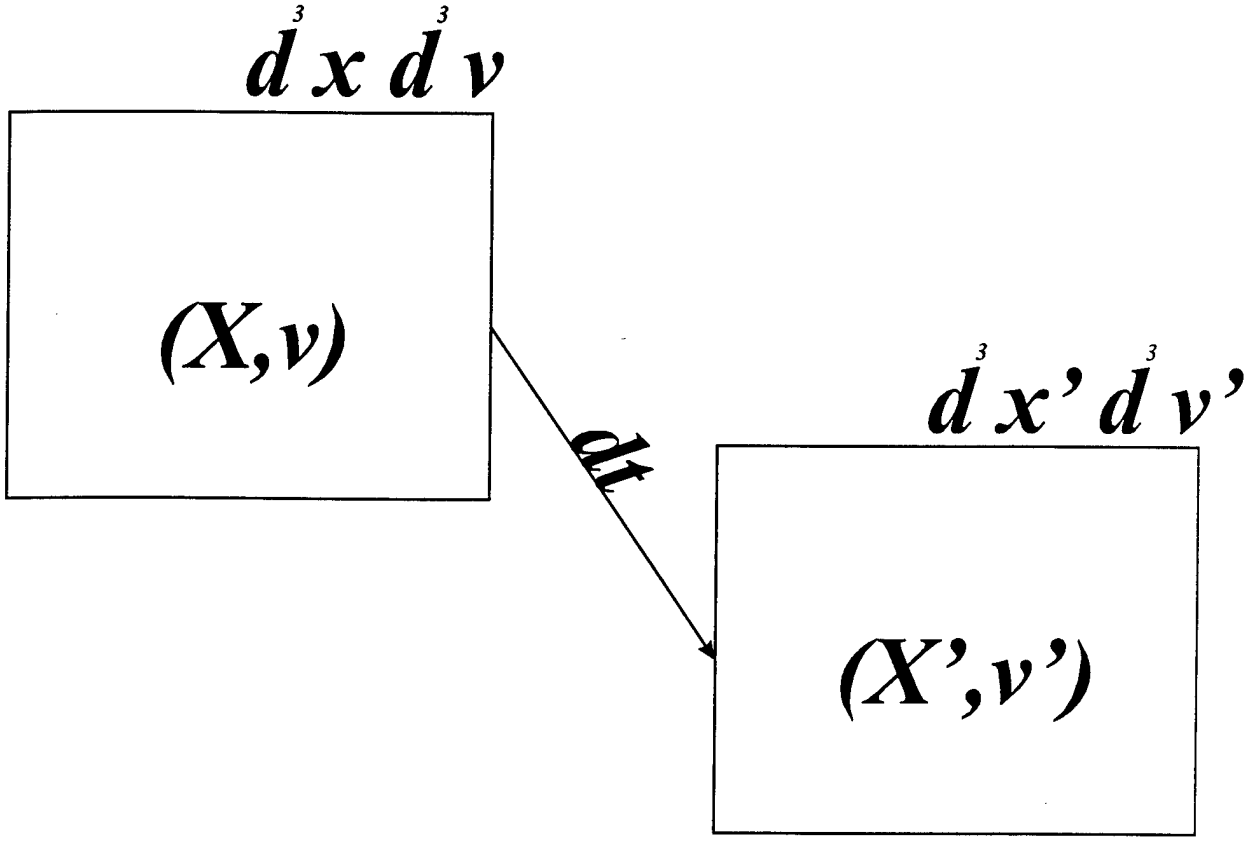

Figure 3.1: Volume element in the 6-dimensional phase space of velocities and coordinates of the system

$$dN = f(\vec{x}, \vec{v}, t)d^3xd^3v \tag{3.3}$$

at the same time number of electrons dN' in the volume element with $(\vec{x'}, \vec{v'})$coordinates will be

$$dN' = f(\vec{x}', \vec{v}', t + \delta t) d^3x d^3v \tag{3.4}$$

A total electron flow from $(\vec{x}, \vec{v})$– state to $(\vec{x'}, \vec{v'})$– state taking into account (3.1,3.2,3.3,3.4) may be written as

$$\begin{aligned} dN' - dN &= \left[f(\vec{x}', \vec{v}', t + \delta t) - f(\vec{x}, \vec{v}, t)\right] d^3x d^3v = \\ &= \left[f(\vec{x} + \vec{v}\delta t, \vec{v} - \frac{e\vec{E}}{m_e}\delta t, t + \delta t) - f(\vec{x}, \vec{v}, t)\right] d^3x d^3v = \\ &= \left[\frac{\delta f}{\delta t} + \vec{v} \cdot \nabla f - \frac{e\vec{E}}{m_e} \cdot \nabla_v f\right] \delta t d^3x d^3v \end{aligned} \tag{3.5}$$

where ∇_v — gradient operator in the space of velocities:

$$\nabla_v = \hat{i}(\partial/\partial v_x) + \hat{j}(\partial/\partial v_y) + \hat{k}(\partial/\partial v_z) \tag{3.6}$$

and $\hat{i}$, $\hat{j}$, $\hat{k}$ — unit vectors along v_x, v_y, v_z axis of the Cartesian coordinates in the velocity space.

But part of electrons placed in the volume element with coordinates $(\vec{x}, \vec{v})$at a time moment t will not reach volume element with coordinates $(\vec{x'}, \vec{v'})$at a time moment $t + \delta t$. These electrons will change their energy and/or direction of motion (that is a scattering will take place) due to collisions with molecules. Such a scattering will change a velocity distribution function $f(\vec{x}, \vec{v}, t)$.

Let us denote a variation of electron number in a volume $d^3x d^3v$ due to collisions as $(\delta f/\delta t)_c \delta t d^3x d^3v$. In such a case $(\delta f/\delta t)_c$ value is a velocity of f function changing in time due to electron - molecular collisions of all the types (elastic, non-elastic, superelastic, ionizing). Correction factor for a total electron flow from the $(\vec{x}, \vec{v})$- state to the $(\vec{x'}, \vec{v'})$- state due to the scattering will be written as

$$dN' - dN = \left(\frac{\delta f}{\delta t}\right)_c \delta t d^3x d^3v \tag{3.7}$$

and from (3.5), (3.7) follows that

$$\frac{\partial f}{\partial t} + \vec{v} \cdot \nabla f - \frac{e\vec{E}}{m} \cdot \nabla_v f = \left(\frac{\delta f}{\delta t}\right)_c \tag{3.8}$$

3.1.1 Boltzmann equation for an electron energy distribution function in the nearly isotropic case

In the case of an elastic electron-molecule collisions energy exchange between colliding particle is too small in comparison with a typical primary electron energy because of the great difference in the masses of the electron and molecule. At the same time deviation of velocity vector from its initial direction may be significant. If electron path between elastic collisions small in comparison with the path between the nonelastic ones, then due to large electron deviations their velocity distribution $f(\vec{v})$ practically does not depend upon velocity direction $\vec{v}$. Therefore we may use a following expansion for $f(\vec{v})$ [116]:

$$f(\vec{v}) \simeq f_0(v) + \frac{\vec{v}}{v} \cdot \vec{f}_1(v) \tag{3.9}$$

where f_0 and $\vec{f}_1$ — depend upon v only (more precisely, from the absolute value of $\vec{v}$) and $|\vec{f}_1| \ll f_0$.

Using such an expansion and taking into account elastic, inelastic and superelastic collisions one may derive from (3.8) in spatially isotropic case [118]:

$$\begin{aligned}\left(\frac{mu}{2e}\right)^{1/2}\frac{\partial f_0}{\partial t} &= \frac{E^2}{3}\frac{\partial}{\partial u}\left(\frac{u}{NQ_m}\frac{\partial f_0}{\partial u}\right) + \frac{2m}{M}\frac{\partial}{\partial u}\left(u^2 NQ_m f_0\right) + \\ &+ \frac{2mkT}{Me}\frac{\partial}{\partial u}\left(u^2 NQ_m \frac{\partial f_0}{\partial u}\right) + \\ &+ \sum_j \left[(u+u_j)f_0(u+u_j)N_0 Q_j(u+u_j) - u f_0(u) N_0 Q_j(u)\right] + \\ &+ \sum_j \left[(u-u_j)f_0(u-u_j)N_0 Q_{-j}(u-u_j) - u f_0(u) N_0 Q_{-j}(u)\right]\end{aligned} \tag{3.10}$$

where $Q_j(u)$ is a cross-section of molecule excitation from a ground state to jth excited one in nonelastic collisions with an electron, which had an energy u before a collision; $Q_m(u)$ is a cross-section of elastic electron- molecular collisions with an impulse transfer:

$$Q_m(u) = 2\Pi \int_0^{\Pi} (1 - \cos(\Theta)) I(\Theta, u) \sin(\Theta) d\Theta \tag{3.11}$$

N_0 is a molecule density in a ground state, N_j is a molecule density in a jth excited state, M is a molecule mass, m is a electron mass, e is a electron charge, E is a electric field strength, T is a gas temperature, u is a electron energy.

It is very easy to extend equation (3.10) for a gas mixture:

$$\begin{aligned}\left(\frac{mu}{2e}\right)^{1/2}\frac{\partial f_0}{\partial t} &= \frac{E^2}{3}\frac{\partial}{\partial u}\left(u\left[\sum_k N_k Q_m^k\right]^{-1}\frac{\partial f_0}{\partial u}\right) + 2m\frac{\partial}{\partial u}\left(u^2\left[\sum_k \frac{N_k Q_m^k}{M_k}\right] f_0\right) + \\ &+ \frac{2mkT}{Me}\frac{\partial}{\partial u}\left(u^2\left[\sum_k \frac{N_k Q_m^k}{M_k}\right]\frac{\partial f_0}{\partial u}\right) + \\ &+ \sum_j\sum_k \left[(u+u_{jk})f_0(u+u_{jk})N_{0k}Q_j^k(u+u_{jk}) - u f_0(u) N_{0k} Q_j^k(u)\right] + \\ &+ \sum_j\sum_k \left[(u-u_{jk})f_0(u-u_{jk})N_{jk}Q_{-j}^k(u-u_{jk}) - u f_0(u) N_{jk} Q_{-j}^k(u)\right]\end{aligned} \tag{3.12}$$

where N_k is a density of particles of k sort, M_k is a mass of every particle, Q_m^k, Q_j^k, Q_{-j}^k is a cross section of elastic, nonelastic and superelastic collisions of particles of k sort correspondingly; N_{jk} is a number of molecules of kind k, which are in the excited state j, and u_{jk} is an energy of this state.

In such a case $\vec{f_1}$ value may be expressed through a f_0:

$$\vec{f_1} = e\vec{E}(\partial f_0/\partial v)/mNvQ_m \tag{3.13}$$

3.1.2 Boltzmann equation for an electron energy distribution function in strong electric fields

In strong nonuniform in space electric fields expression (3.12) is not correct. There are two reasons for this fact: first, the change of electron energy distribution function (EEDF) in the given point of space because of electron transfer (term $\vec{v}\cdot\nabla f$ in equation (3.8)) becomes significant. Then, the condition for the expansion $f(\vec{x},\vec{v},t)$ (equation (3.9)), $f_1 \ll f_0$ is failed with an increase of electron average energy; nonelastic collision frequency becomes comparable or even higher than transport collision frequency.

Thus, for the description of pulsed discharges at high overvoltage a two-term approximation of the Boltzmann equation (3.9), (3.12), (3.13) which is suitable for different types of gas discharge may be used with a number of qualifications only.

In the most general case to model a development of the fast ionization wave it is necessary to solve nonuniform in space Boltzmann equation (3.8). This leads to the significant expenses in processor time due to increasing task dimension. Furthermore, in contrast to system of equations (3.9), (3.12), (3.13), the solution of equation (3.8) requires differential, and not integral cross-sections of all the processes with electrons. It should be noted that such a cross-sections are available for very restricted number of gases, which leads to some limitations on the direct modelling of the discharge using equation (3.8).

Data on differential scattering cross-section for nitrogen and algorithm of the solution of Boltzmann equation in the non-stationary space-nonequilibrium case of discharge development at high overvoltage will be given below.

Analytical approximations to differential scattering cross sections for electrons

We use a modified Coulomb scattering formula to approximate the angular distributions of scattered electrons as proposed in [119]. The reason for the modification is to allow for the fitting to data that is predominantly backward scattering, e.g., O_2 at low energies, and yet go over to the conventional form in the limit of predominantly forward scattering at high energies.

The modified differential scattering cross section $I(\Theta,\beta,u)$ is assumed to be

$$I = A * (1 - (1 - 2 * \beta(u) * [\cos(\Theta)]^{-2} \tag{3.14}$$

where Θ is the scattering angle, β is the "modified screening parameter" and is a function of the electron energy, and u is the electron energy. Here A is the conventional magnitude factor for Coulomb scattering and is a function of electron energy only. In the limits of small Θ and of large electron energies this has the same form as for conventional screened Coulomb scattering with β as the screening parameter.

Integration yields the total cross section Q_t:

$$Q_t = -((A * \Pi)/((-1 + \beta) * \beta)); \tag{3.15}$$

and the momentum transfer cross section Q_m

$$\begin{aligned} Q_m &= (2*\Pi*(A-2*A*\beta-A*\ln(2-2*\beta)+ \\ &+ A*\beta*\ln(2-2*\beta)+A*\ln(2*\beta)- \\ &- A*\beta*\ln(2*\beta))/((-1+\beta)*(-1+2*\beta)^2) \end{aligned} \tag{3.16}$$

so that the ratio of cross sections is

$$\begin{aligned} Q_m/Q_t &= (2*\beta*(-1+2*\beta+ \\ &+ \ln(2-2*\beta)-\beta*\ln(2-2*\beta)- \\ &- \ln(2*beta)+\beta*\ln(2*\beta)))/ \\ &(-1+2*\beta)^2; \end{aligned} \tag{3.17}$$

The differential scattering cross sections normalized to the total cross section is

$$I_{norm} = I(\Theta,\beta)/Q_t(\beta) \tag{3.18}$$

so that probability of scattering through an angle less than Θ_0 is

$$Q_{t_{prob}} = (A*\Pi - A*\Pi*\cos(\Theta_0))/(\beta*(1-\cos(\Theta_0)+2*\beta*\cos(\Theta_0))); \tag{3.19}$$

For $Theta_0 = \Pi$ this is Q_t as expected. For the given $Q_{t_{prob}}$ value $0 < Q_{t_{prob}} < Q_t$ one can find the scattering angle Θ_0:

$$\Theta_0 = \arccos((1-\beta-Q_{t_{prob}})/(1-\beta-Q_{t_{prob}}+2*\beta*Q_{t_{prob}})] \tag{3.20}$$

As in [119] this approach only attempt to fit the experimental angular distributions at energies for which the particular scattering cross section is important to the solution of the electron Boltzmann equation.

The empirical expressions used for the lowest two spherical harmonic components of the angular scattering are taken from Table I of [119]. The magnitudes of cross-sections for elastic scattering and for the various inelastic scattering processes will be discussed later.

- Elastic scattering of electrons by N_2 ($Q_0 = Q_t$ everywhere):

$$Q_1/Q_0 = -0.2*u^{1/2}/(0.025+u^{1/2})+1.2*(16*u^{1/2}+u)/(100+16*u^{1/2}+u); \tag{3.21}$$

$$Q_m/Q_0 = 1 - Q_1/Q_0; \tag{3.22}$$

$$\beta = 0.6/(1+(u/500)^{1/2}+(u/200)^{1.01})^{0.99}; \tag{3.23}$$

- Resonant vibrational excitation:

  Since the scattering is roughly isotropic:

$$\beta = 0.5 \tag{3.24}$$

- Lower triplet states — $A^3\Sigma_u^+$, $B^3\Pi_g$, and $W^3\Delta_u$:

$$Q_1/Q_0 = -u^2/(1500 + u^2); \tag{3.25}$$

$$Q_m/Q_0 = 1 - Q_1/Q_0; \tag{3.26}$$

$$\beta = 0.5 * (1 + (u/200)^2)/(1 + (u/282)^2); \tag{3.27}$$

- Upper triplet state — $C^3\Pi_u$:

$$Q_1/Q_0 = -0.2; \tag{3.28}$$

$$Q_m/Q_0 = 1 - Q_1/Q_0; \tag{3.29}$$

$$\beta = 0.647; \tag{3.30}$$

- Lower singlet state — $a^1\Pi_g$:

$$Q_1/Q_0 = (200000 + 160 * u^2 + u^4)/(200000 + 2600 * u^2 + u^4); \tag{3.31}$$

$$Q_m/Q_0 = 1 - Q_1/Q_0; \tag{3.32}$$

$$\beta = 0.4 * (u/150)^2/(1 + (u/300)^2 + (u/220)^4); \tag{3.33}$$

- Sum of singlets:

$$Q_1/Q_0 = u^2/(2500 + u^2); \tag{3.34}$$

$$Q_m/Q_0 = 1 - Q_1/Q_0; \tag{3.35}$$

$$\beta = 0.5/(1 + (u/370)^{2.5}); \tag{3.36}$$

The differential cross sections with the more detailed angular distributions [120, 121] can be used in such a calculations as well. A similar approximation was made for N_2 in [122].

Cross sections. N_2 - electron collisions

Cross sections used in this work are based on those used in [119, 123].

It has been pointed out by several authors that the vibrational excitation cross sections tabulated in [119, 123] (based on Schulz) should be updated on the basis of later beam experIments. However, authors of [119] find good agreement with six different experimental transport and rate coefficients using these cross sections. These coefficients are drift velocity, characteristic energy, ionization, metastable ($A^3\Sigma_u^+$) excitation, $C^3\Pi_u$ excitation, and N_2 heating at $E/n < 40$ Td via rotational excitation and anharmonic relaxation of vibrational excitation. They therefore believe one would have to have a very strong reason before making any significant change in these cross sections. For example, a preliminary investigation (Haddad and Phelps, unpublished) suggests that the changes in cross sections accompanying the use of a multiterm spherical harmonic code are small. As a second example, Hadded and Phelps found that the resonance in the rotational excitation cross section found theoretically by Onda and included in the cross sections recommended in [124] is inconsistent with swarm data and should be ignored.

In the present work we used a set of cross-section which describes following processes:

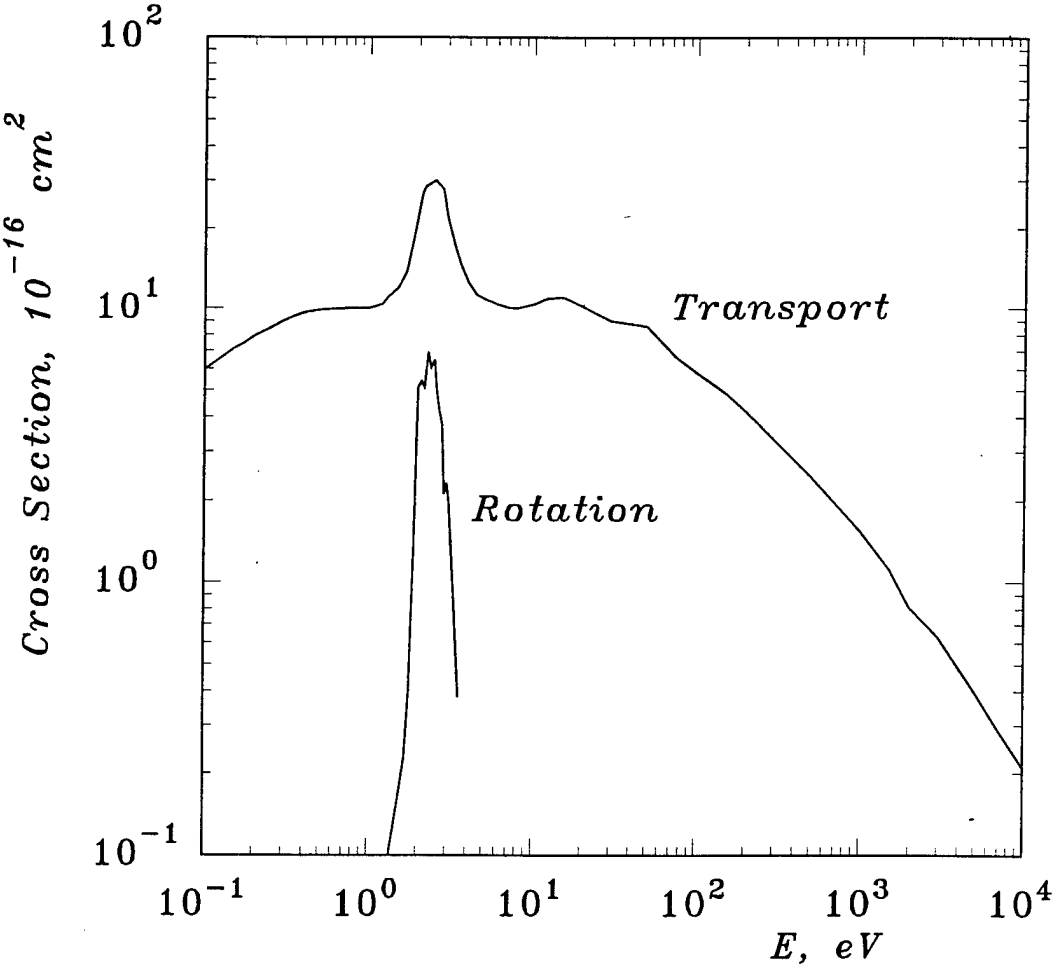

Figure 3.2: Transport cross-sections and excitation of rotational levels

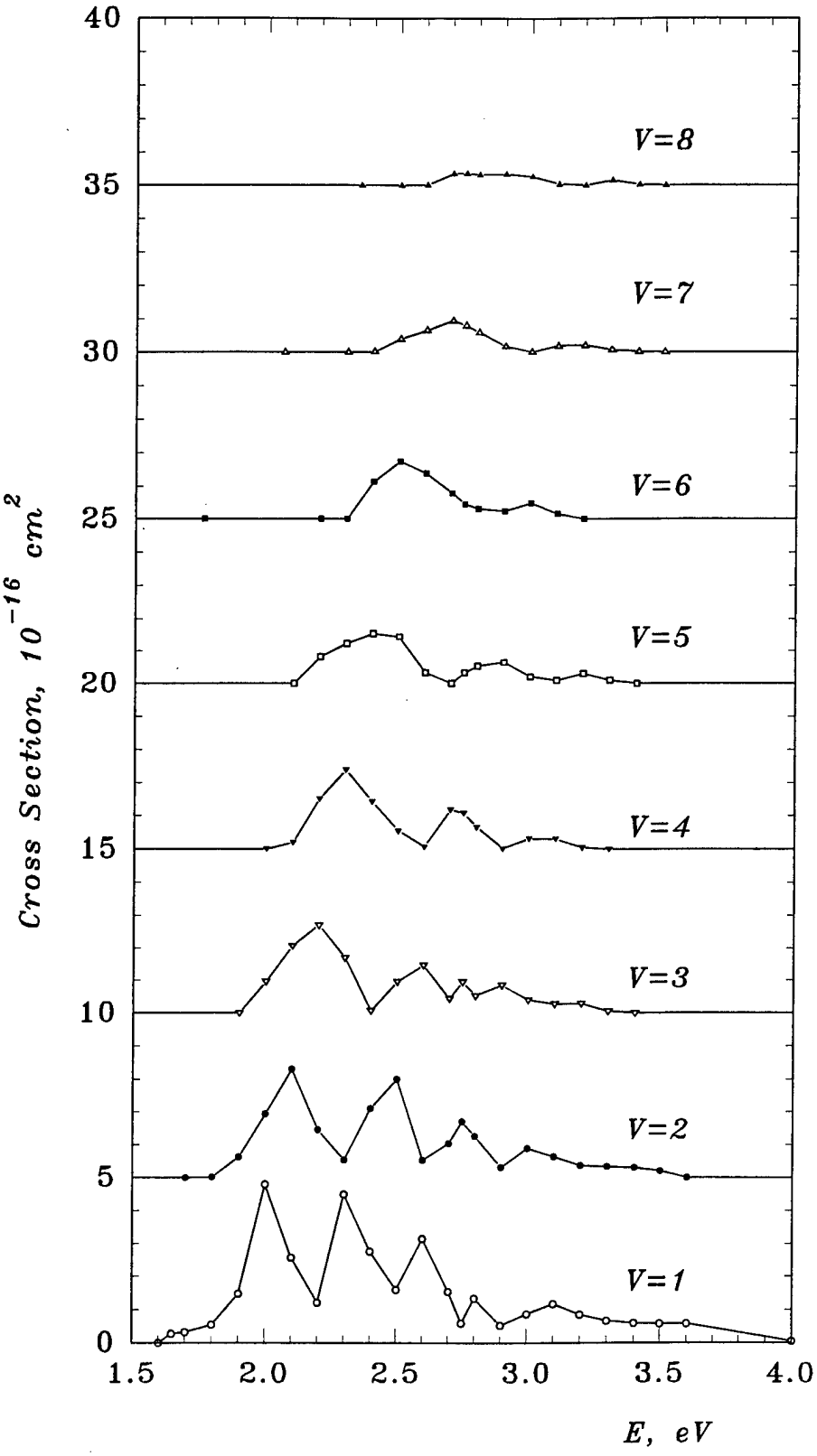

Figure 3.3: Cross-sections for the excitation of vibrational levels of N_2 molecule ground state

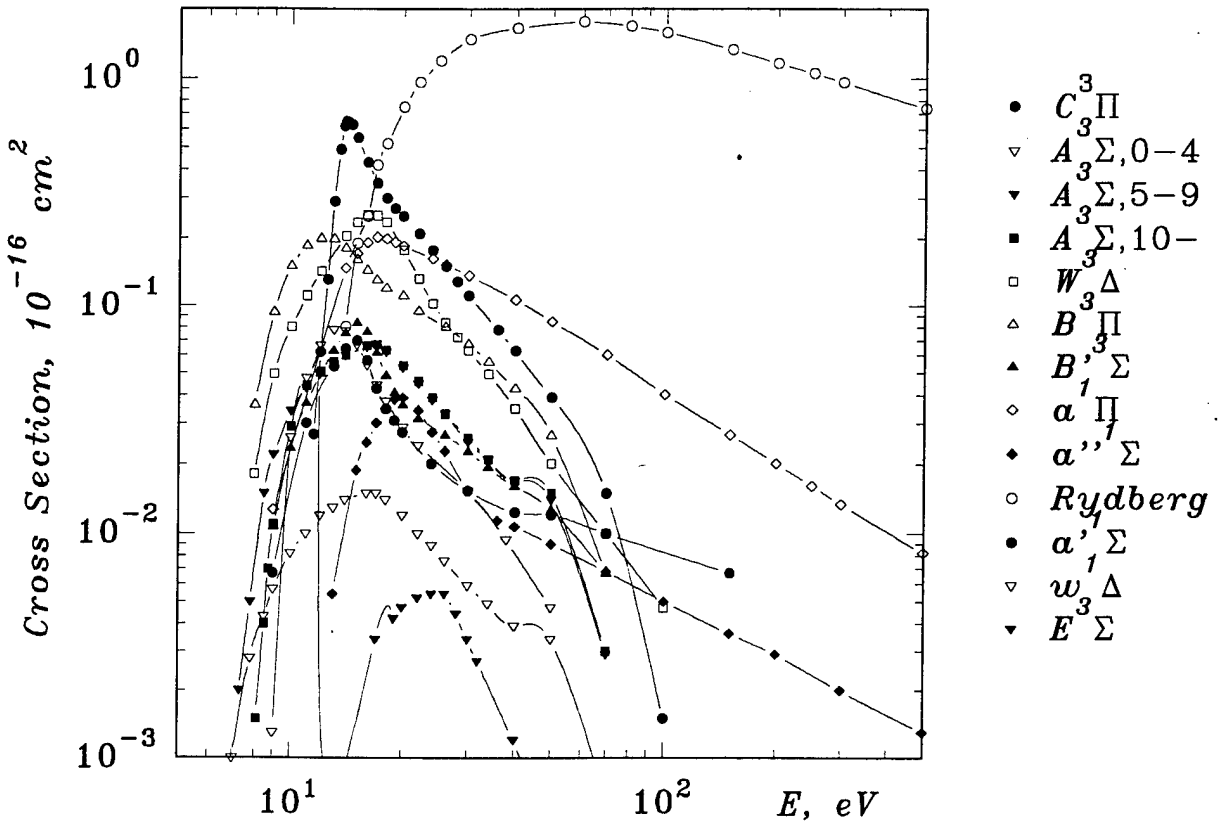

Figure 3.4: Cross-sections for N_2 electron levels excitation

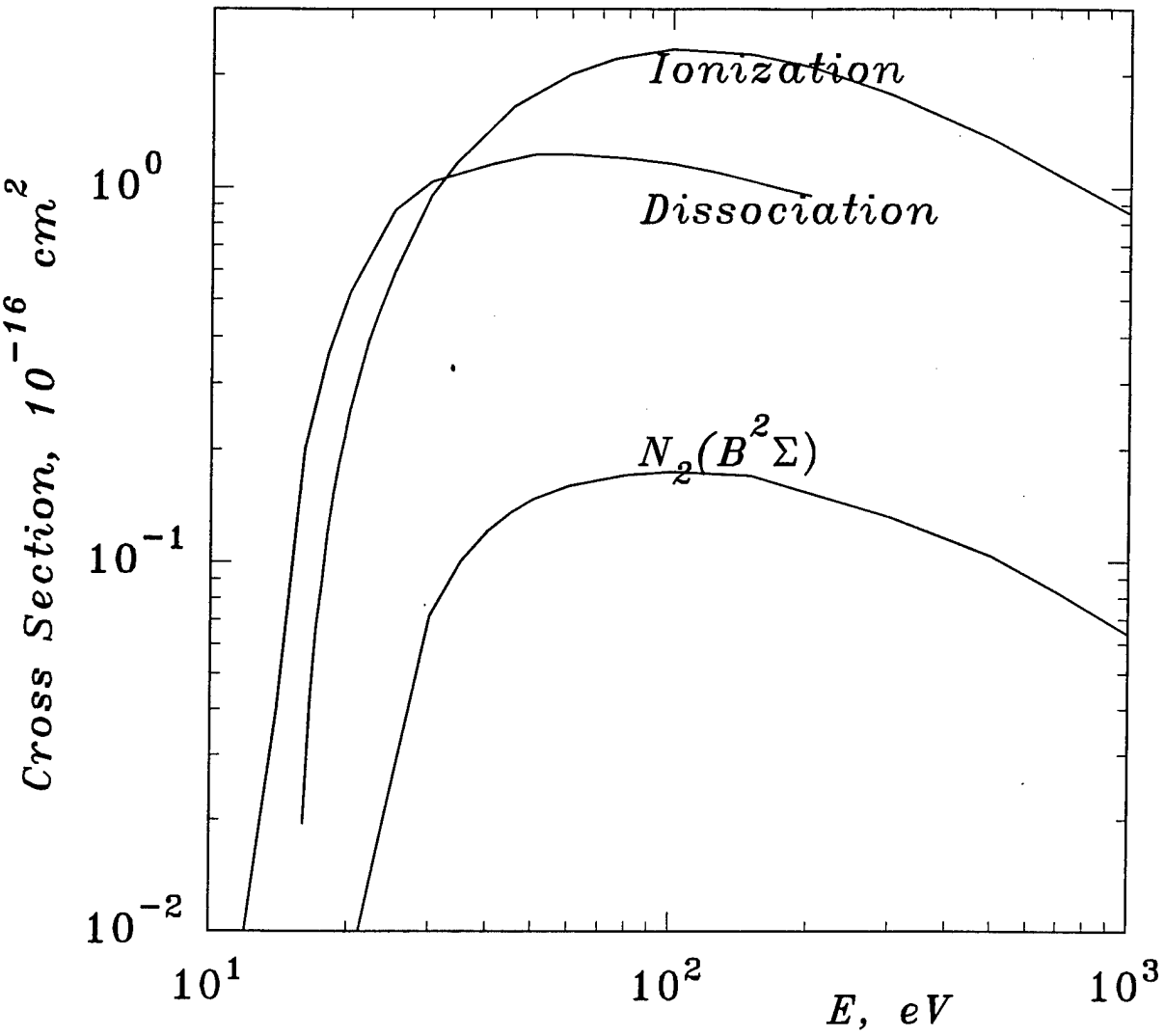

Figure 3.5: Cross-sections for ionization and dissociation of N_2 molecule by an electron impact

1. Elastic scattering (Fig.3.2)
2. Rotational levels excitation (Fig.3.2) (the energy loss is $\Delta E = 0.02$ eV)
3. An excitation of vibrational levels (Fig.3.3)
   - $v' = 1$, $\Delta E = 0.29$ eV
   - $v' = 2$, $\Delta E = 0.59$ eV
   - $v' = 3$, $\Delta E = 0.88$ eV
   - $v' = 4$, $\Delta E = 1.17$ eV
   - $v' = 5$, $\Delta E = 1.47$ eV
   - $v' = 6$, $\Delta E = 1.76$ eV
   - $v' = 7$, $\Delta E = 2.06$ eV
   - $v' = 8$, $\Delta E = 2.35$ eV
4. An excitation of electronic states (Fig.3.4)
   - $A^3\Sigma_u^+, v = 0, 4$, $\Delta E = 6.17$ eV
   - $A^3\Sigma_u^+, v = 5 - 9$, $\Delta E = 7.00$ eV
   - $A^3\Sigma_u^+, v > 10$, $\Delta E = 7.80$ eV
   - $B^3\Pi_g$ $\Delta E = 7.35$ eV
   - $W^3\Delta_u$ $\Delta E = 7.36$ eV
   - $B'^3\Sigma_u^-$ $\Delta E = 8.16$ eV
   - $a'^1\Sigma_u^-$, $\Delta E = 8.40$ eV
   - $a^1\Pi_g$, $\Delta E = 8.55$ eV
   - $w^1\Delta_u$, $\Delta E = 8.89$ eV
   - $C^3\Pi_u$, $\Delta E = 11.03$ eV
   - $E^3\Sigma_g^+$, $\Delta E = 11.88$ eV
   - $a''^1\Sigma$, $\Delta E = 12.25$ eV
   - *Rydberg*, $\Delta E = 12.487$ eV
5. Dissociation and ionization by an electron impact (fig.3.5)
   - $N(^4S^0) + N(^4S^0)$, $\Delta E = 9.76$ eV
   - N_2^+, $\Delta E = 15.60$ eV
   - $N_2^+(B^2\Sigma_u^+)$, $\Delta E = 18.80$ eV

To calculate a fraction of electron kinetic energy ΔE which is lost in elastic electron-molecular scattering let us consider a kinetics of the collision [117]. Energy and impulse conservation laws for a molecule of mass M and an electron of initial velocities $\vec{v}$ and $\vec{V}$ and final velocities $\vec{v}'$ and $\vec{V}'$ correspondingly may be written in a form:

$$\frac{1}{2}mv^2 + \frac{1}{2}MV^2 = \frac{1}{2}mv'^2 + \frac{1}{2}MV'^2 \tag{3.37}$$

$$m\vec{v} + M\vec{V} = m\vec{v'} + M\vec{V'} \tag{3.38}$$

A vector $\vec{V}$ may be resolved into two components: one of them is directed along the vector v, and another one is in perpendicular direction, that is

$$\vec{V} = a\vec{v} + \vec{b} \tag{3.39}$$

here $\vec{b}$ is a vector perpendicular to the v and located in the plane which contains both v and V (Fig.3.6).

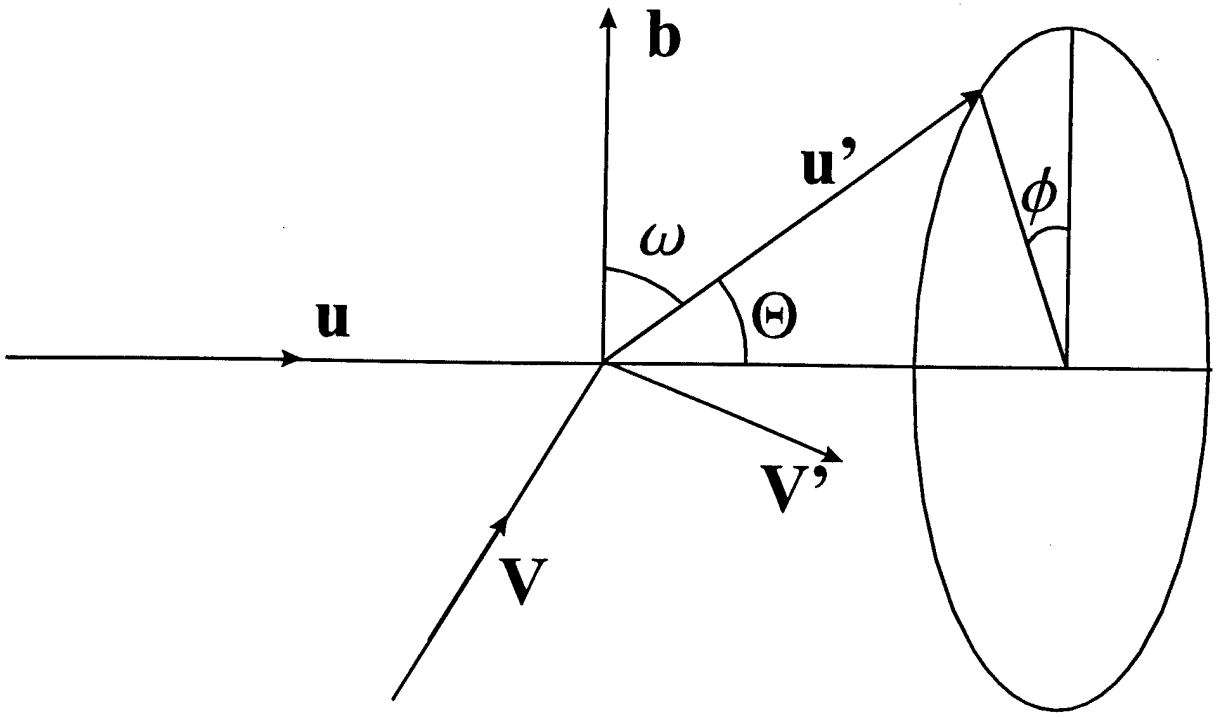

Figure 3.6: Velocity diagram for the electron-molecular collision

Then for the value of energy loss during a collisions it may be derived that:

$$\begin{aligned}
\Delta E &= \frac{1}{2}mv^2 - \frac{1}{2}mv'^2 = \\
&= \frac{1}{2}MV'^2 - \frac{1}{2}M(a^2v^2 + b^2) = \\
&= \frac{1}{2}M\left[\frac{m}{M}\vec{v}\left(1 + \frac{M}{m}a\right) + \vec{b} - \frac{m}{M}\vec{v'}\right]^2 - -\frac{1}{2}M(a^2v^2 + b^2) = \\
&= \frac{1}{2}M\left[\frac{m^2}{M^2}v^2\left(1 + \frac{M}{m}a\right)^2 + b^2 + \frac{m^2}{M^2}v'^2 - \frac{2m^2}{M^2}\vec{v}\cdot\vec{v'}\left(1 + \frac{M}{m}a\right) -\right.
\end{aligned}$$

$$-\frac{2m}{M}\vec{b}\cdot\vec{v'}\Big] - \frac{1}{2}M(a^2v^2+b^2) =$$

$$= \frac{1}{2}\frac{m^2}{M}(v^2+v'^2-2\vec{v}\cdot v') + ma(v^2-\vec{v}\cdot v') - m\vec{b}\cdot\vec{v'} \tag{3.40}$$

Because of dramatic difference in the masses of electron and molecule $v' \simeq v$ is correct and (3.40) may be transformed as

$$\Delta E = \left(\frac{m^2}{M}v^2 + m\vec{v}\cdot\vec{V}\right)(1-\cos(\Theta)) - mbv\cos(\omega) \tag{3.41}$$

where Θ is an angle of the electron scattering and ω is an angle between the vectors $\vec{b}$ and v'.

In a case when molecule motion is negligible (that is there is no energy transfer from molecules to electrons) an expression (3.41) takes especially simple form:

$$\Delta E = \frac{m^2}{M}v^2(1-\cos(\Theta)) \tag{3.42}$$

3.2 Numerical model

In the present work a new numerical code is developed for a modelling of the discharge in the form of the fast ionization wave. The code is based on the solution of non-stationary Boltzmann equation.

The equation which gives the EEDF dynamics in the fixed point of the phase space was described above (3.8). The method of separation on physical processes is used in the present work to solve this equation.

To obtain the solution $f(\vec{x},\vec{v},t)$ at the next time step $t' = t+\delta t$ following equations were solved sequentially:

$$\frac{\partial f}{\partial t} = \frac{e\vec{E}}{m}\cdot\nabla_v f \tag{3.43}$$

$$\frac{\partial f}{\partial t} = -\vec{v}\cdot\nabla f \tag{3.44}$$

and

$$\frac{\partial f}{\partial t} = \left(\frac{\delta f}{\delta t}\right)_c \tag{3.45}$$

Then the solution at every time moment $t' = t+\delta t$ may be then represented as a following sequence:

$$f(t+\delta t) = L_3L_2L_1f(t) \tag{3.46}$$

where L_1 is an operator which describes an energy exchange between an electric field and electrons, L_2 is an operator which describes electron motion in the physical space; and L_3 is an operator which describes an appearance and motion of electrons in a velocity space during their collisions with molecules.

The equations (3.43, 3.44) were solved numerically using implicit final difference schemes which approximate initial equations to order Δt and $(\Delta x)^2$. On every step an energy conservation (taking into account a heating on a step L_1) and a conservation of a total number of electrons was controlled. Transport equations were solved separately for every point of electron impulse phase space. At this case the non-local effects connected with a fast transfer of high-energy electrons in the physical space are taken properly into account.

On the step L_3 a variation of the electron energy distribution function in the collisions is calculated using the Monte-Carlo technique. At that on the current time step the probability of this collision is defined as a result of a comparison of random generator number and "segment of events" of the type of "elastic collision"... "nonelastic collision of type 1"... "nonelastic collision of type 2"... "ionization"... "NO COLLISIONS".

The probability of an electron scattering during time interval δt in a process of j – type at in collision with a molecule of k –type is calculated from the equation:

$$P_j^k = v_e \sigma_j^k(v_e) N_k \delta t \tag{3.47}$$

Every step the criterion $\sum\limits_{k,j} P_j^k = P_{coll} < 1$ is controlled. Therefore the probability for electron to move without collisions during a time interval δt is equal $P_{free} = 1 - P_{coll}$.

Different probabilities of electron scattering on different angles with respect to initial velocity vector depending upon impacting electron energy were taken into account for all processes except a direct ionization by an electron impact (see discussion above).

Let the scattering took place in the event of i – type. Angle distribution of the scattered electron in the scattering plane Θ is defined by a probability density $I(\Theta)/Q$. Another angle distribution (ϕ) was assumed to be uniform in all the cases.

To calculate final velocities let go over into coordinate system, in which a vector of initial electron velocity has the only component along an X – axis direction:

$$\begin{pmatrix} v_1 \\ v_2 \\ v_3 \end{pmatrix} = \begin{pmatrix} T_{11} & T_{31} & T_{21} \\ T_{21} & T_{11} & T_{31} \\ T_{31} & T_{21} & T_{11} \end{pmatrix} \cdot \begin{pmatrix} 1 \\ 0 \\ 0 \end{pmatrix} \cdot v_0 \tag{3.48}$$

In this coordinate system the rotation of vector coordinates $(1, 0, 0)$ on angles Θ and ϕ leeds to the following rearrangement of equations:

$$\begin{pmatrix} u_1 \\ u_2 \\ u_3 \end{pmatrix} = \begin{pmatrix} \cos(\Theta) \\ \sin(\Theta)\cos(\phi) \\ \sin(\Theta)\sin(\phi) \end{pmatrix} \cdot v_0 \tag{3.49}$$

and finally in initial coordinate system we have:

$$\begin{pmatrix} v_1' \\ v_2' \\ v_3' \end{pmatrix} = \begin{pmatrix} v_1 & v_3 & v_2 \\ v_2 & v_1 & v_3 \\ v_3 & v_2 & v_1 \end{pmatrix} \cdot \begin{pmatrix} \cos(\Theta) \\ \sin(\Theta)\cos(\phi) \\ \sin(\Theta)\sin(\phi) \end{pmatrix} \tag{3.50}$$

Taking into account energy losses in collisions ΔE we shall obtain for the components of the velocity of a scattered electron:

$$\begin{pmatrix} v_1'' \\ v_2'' \\ v_3'' \end{pmatrix} = \begin{pmatrix} v_1' \\ v_2' \\ v_3' \end{pmatrix} \cdot \sqrt{1.0 - \Delta E/E} \tag{3.51}$$

This defines new position of the velocity vector in a phase space and a certain part of electrons $0 < \alpha < 1$ moves from the initial phase-space cell to the appropriate one. Simultaneously a collision probability increases in $1/\alpha$ times. Such an organization of calculations provides a tolerance, a positivity and a monotony of a solution at time intervals of the order of $\tau \geq 10\tau_0$ where τ_0 is a free path time. From the other hand it gives a considerable gain in calculation time in comparison with a precise solution of the Boltzmann equation.

For a direct ionization a dependence of differential ionization cross-section *vs* energy of the secondary electron has been taken into account; secondary electron velocity distribution has been assumed isotropic in space. Probability of appearance of secondary electron of energy u_2 in the process of ionizing collision with primary electron of energy u_1 is defined as [125]:

$$P_{u_1,u_2} = \left((1.0 + (u_2)^2/169.0) \cdot (13.0\text{atan}((u_1 - \Delta u)/26.0))\right)^{-1} \tag{3.52}$$

where $\Delta u = u_2 + 15.6$ is an energetic threshold of an ionization process with an appearance of electron of energy u_2.

3.3 Results

3.3.1 0D calculations

As a first step 0D-calculations have been performed. They do not allow to reveal the role of space non-uniformity effects and the influence of these effects on the EEDF and on the rates of molecule excitation by an electron impact. From the other hand such an approach gives a scale of both non-stationary effects connected with a final time of the EEDF relaxation and deviation of rates of electron - molecular processes from equilibrium.

Calculations have been performed for the conditions of experiments described in this Report. In Figure 3.7 typical data on the electric field dynamics, population rates of $N_2^+(B^2\Sigma_u^+, v = 0)$ and $N_2(C^3\Pi_u, v = 0)$ states and appropriate densities in the front of a fast ionization wave are represented.

Electric field strength in a volume at 0D - calculations was specified from the experimental data; an initial electron density was taken to be $n_{e_0} = 10^8$ cm$^-3$. Nonuniform mesh in velocity space was used; moreover, a position of the cell center in velocity space depends quadratically in its number.

Such a distribution of mesh nodes allowed to compensate low density of energetic states (which increases as v^3 in a velocity space) at low energies and to provide a good energy resolution in a region of nonelastic processes threshold. Total amount of mesh nodes was $N = 80 \times 80 \times 80$, minimal velocity step was taken to be $\Delta v = 1.0 \times 10^4$ m/s (this value corresponds to an energetic resolution $\Delta e = 1.4 \times 10^{-4}$ eV).

Results obtained are represented in Figures 3.8, 3.9, 3.11, 3.10.

In Figure 3.8 the dynamics of reduced electric field, electron density, average velocity of electrons and their energy in nitrogen at a pressure 4 Torr are shown. The reduced electric

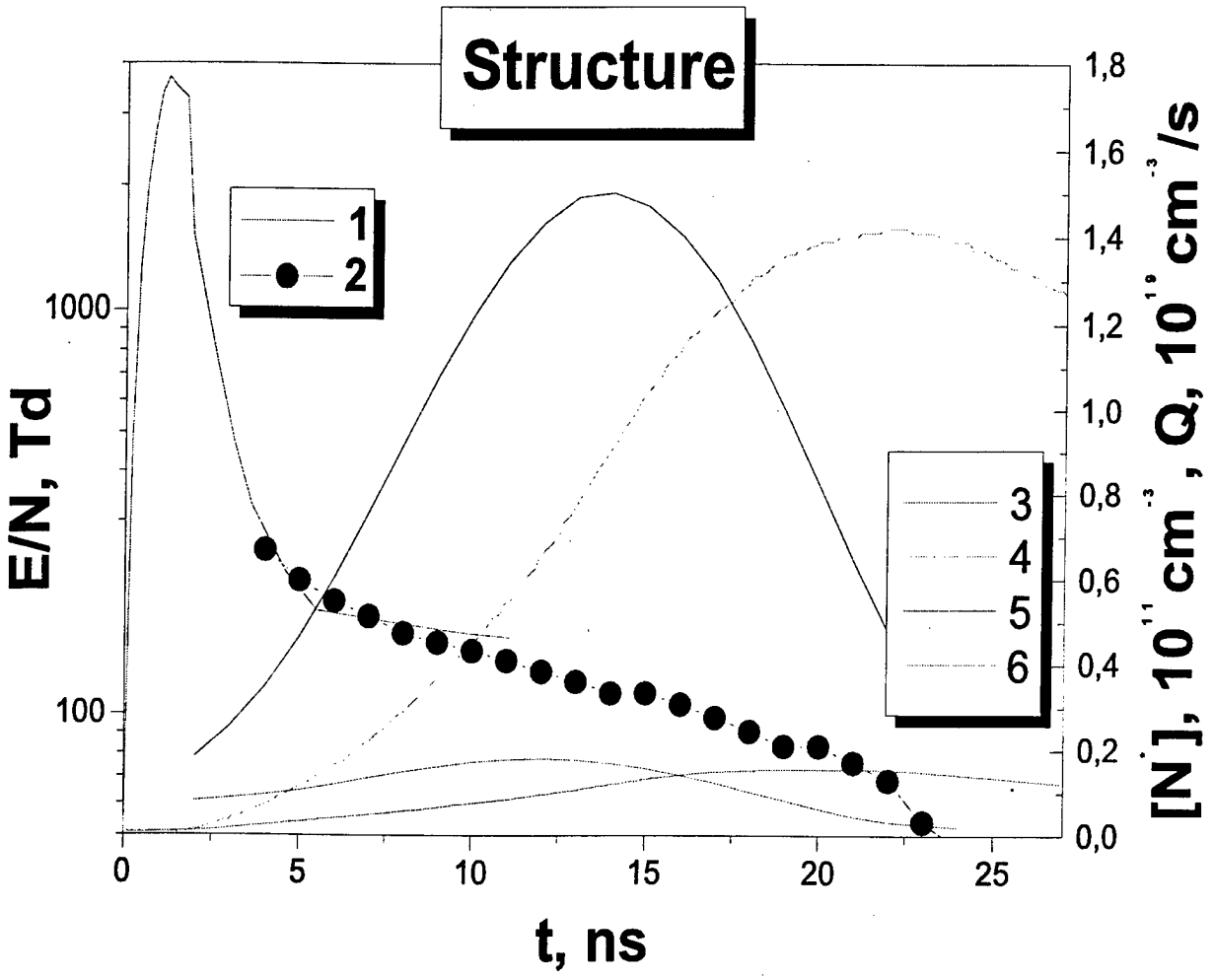

Figure 3.7: Breakdown structure: 1,2 — electric field; 3 — $[N_2^+(B^2\Sigma_u^+, v = 0)]$, 4 — $[N_2(C^3\Pi_u, v = 0)]$; 5 — population rate of the electronic state $N_2(C^3\Pi_u, v = 0)$; 6 — population rate of the electronic state $N_2^+(B^2\Sigma_u^+, v = 0)$. Experimental data.

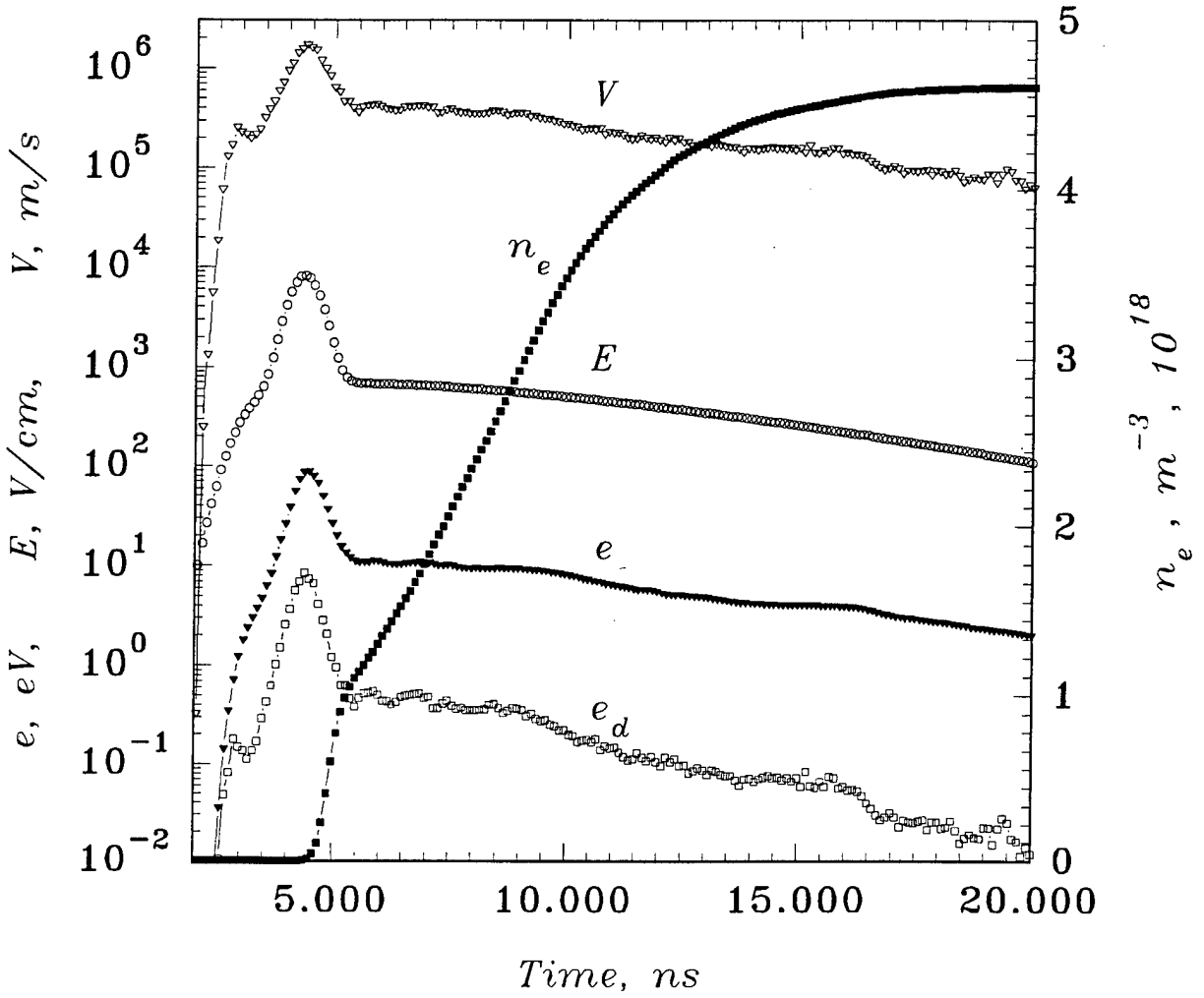

Figure 3.8: Electric field E, electron density n_e, velocity of directed motion v, mean electron energy ε and energy ε_d corresponding to velocity v, calculated in 0D model.

field dependence *vs* time is taken from experiments (Fig.3.7). In a whole experimental dependencies are well represented by the calculated dynamics of electron density: the required electron concentration as well as electron level population take place behind the FIW front in residual fields.

Slow change of the reduced electric field behind the wave front lead to the fact that average energy and average velocity of electrons in this region practically coincide with those calculated using two-term approximation of the Boltzmann equation (Fig.3.8). This may be explained by relatively fast relaxation of the swarm parameters of electrons; the rate of the relaxation exceeds significantly the rate of change in the reduced electric field.

On the contrary, in the region of electric field peak, which corresponds to the FIW front, the average electric energy changes with a characteristic time delay $\delta t \sim 0.5$ ns with respect to the electric field.

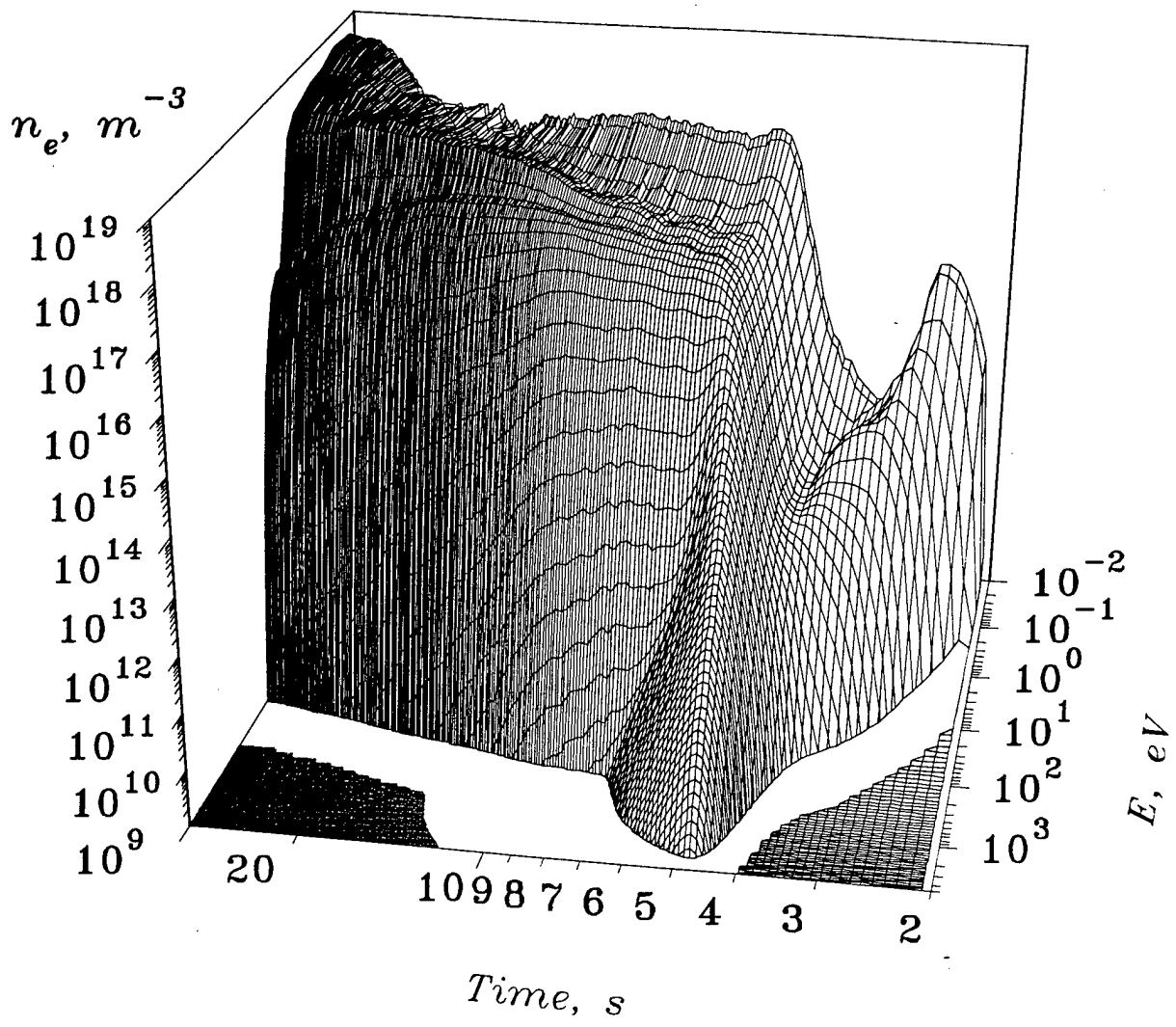

Figure 3.9: Typical behavior of an electron energy distribution function. 0D model. $P = 4$ Torr. Nitrogen.

Typical electron energy distribution function is represented in Fig.3.9. All the stages

of the EEDF formation are clearly seen. First of all the heating of an electron ensemble and population wave propagation take place at the time interval $\tau < 3$ ns. Then energy of electrons reaches value enough for the gas ionization. High reduced electric fields in the wave front cause strong electron heating up to the time $\tau \simeq 5$ ns. EEDF relaxation with E/n decrease is accompanied by continued gas ionization; and degradation spectrum of the secondary electrons governs the EEDF shape practically all the time of the high-voltage pulse.

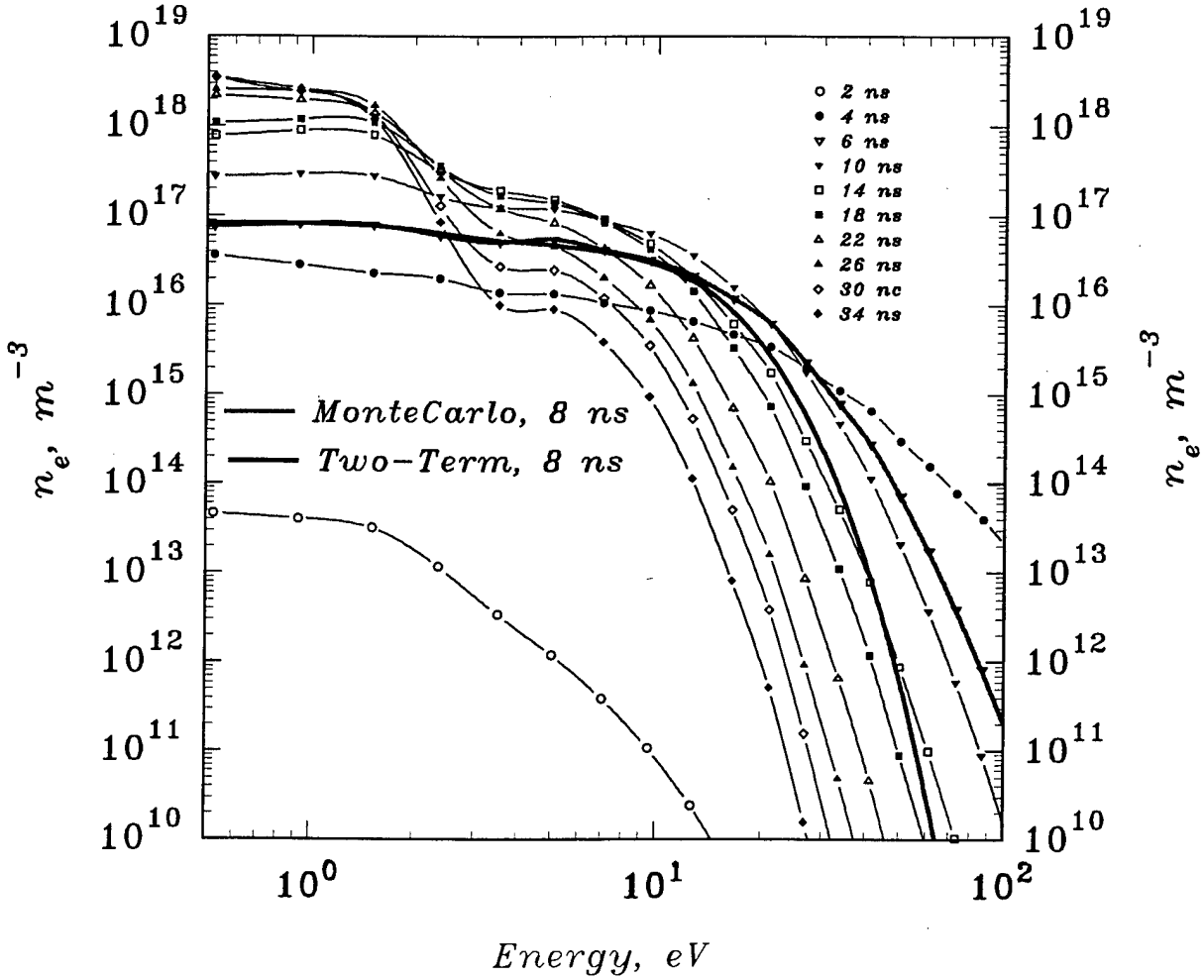

Figure 3.10: EEDF calculated in 0D model for different time moments (marked with numbers, ns, near the curves). Curves fB and fMC give a comparison of the stationary solution of Boltzmann equation in two-term approximation and Monte-Carlo solution.

The influence of the finite EEDF relaxation rate in the high-energy region on the shape of electron energy distribution function is demonstrated in Fig.3.10. Two electron distributions are represented in this Figure at the same time moment: the first one is calculated using the Monte-Carlo technique, and another one is calculated in frames of the two-term approximation of the Boltzmann equation.

It is clearly seen that functions coincide with each other at energies less than 10 eV and differ significantly at higher energies. Such a difference and an enrichment of high-energy

"tail" of the electron energy distribution function connected with a relatively slow EEDF relaxation. At fast decrease of the electric field value behind the FIW front a high-energy part of the distribution function loss an equilibrium with the electric field (Fig.3.10).

From the point of view of the elementary processes in the breakdown front and in its close vicinity nonstationary effects lead to the significant deviation of excitation, dissociation and ionization rates from the equilibrium. So, Fig.3.11 represents a comparison of rates of excitation of $C^3\Pi_u$ state of nitrogen and $B^2\Sigma_g$ state of N_2^+ ion calculated with Monte-Carlo technique and in the two-term approximation of the Boltzmann equation. In the breakdown front the excitation rates less than the rates obtained in the two-term approximation because of finite EEDF relaxation time. From the other hand, in a region of a field decrease these rates exceed "two-terms" values during all the time of discharge development.

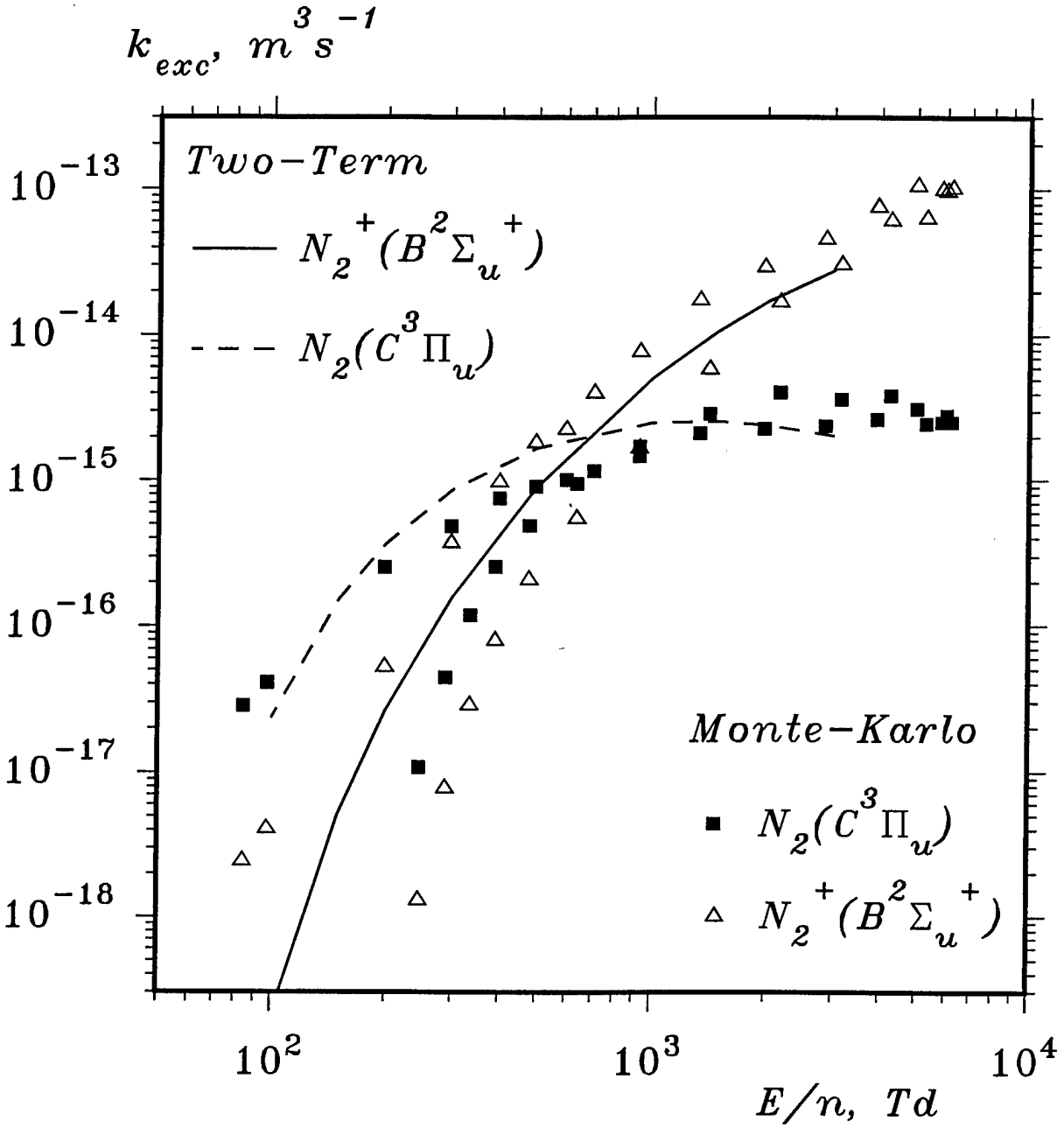

Figure 3.11: Comparison of total ionization and excitation rates. Points — calculations according to 0D Monte-Carlo model, solid lines — stationary solution of two-term approximation of Boltzmann equation. At starting point $E/n = 250$ Td.

3.3.2 1D calculations

A possibility to analyze the development of the fast ionization wave structure and the role of non-local effects, connected with "run-away" electrons arising in the breakdown front appears in the case of 1D - calculations. Conditions in the velocity space were the same as in 0D model. Distribution of the parameters in a physical space was calculated on a mesh, which contained 20 cell of size $\Delta x = 2$ cm.

The results of calculations of the initial stage of the FIW development – from the moment when the electric field becomes increase (see Fig.3.12) up to the moment of the FIW start – are represented in the Figures 3.13, 3.14, 3.15, 3.16. At this moment the motion of the point which characterizes a maximum of average electron energy along a discharge gap begins.

The dynamics of the EEDF at a distance 4 cm from the high-voltage electrode is represented in Fig.3.13. First of all relatively low-energy electrons come to this point. This causes by a low reduced electric fields on an initial stage of the discharge development and, consequently, by low values of average electron energy and weak EEDF anisothropy.

An increase in electric field strength heats an electron ensemble and provide a transition of part of electrons to the "run-away" regime. These fast electrons cause an active preionization before the wave front. Secondary electrons have relatively low energies and zero average velocity. This leads to a some decrease of average energy and velocity of electrons before the front in comparison with maximal possible values ($\varepsilon_{max} \simeq 2U_0$). At the same time electron energy and velocity of directed motion before the front exceed the same parameters in the front significantly.

Figures 3.14, 3.15 and 3.16 demonstrate clearly nonequilibrium and nonlocal character of the EEDF. They represent the average velocity of electrons, their average energy and electron energy distribution function *vs* distance from the high-voltage electrode at a time moment $\tau = 6$ ns.

The heating of a EEDF leads to an appearance of high-energy electrons flow before the wave front (Fig.3.14). Their average energy reach value of 1 keV. Electron energy in a wave front comprises 110-150 eV and slow decreases with a distance from the high-voltage electrode.

The electron energy distribution function at a large distances before the wave front becomes enriched significantly in the region of high energies. It looks like a so called "degradation spectrum", which is typical for the relaxation of an electron beam in the atmosphere (Fig.3.16).

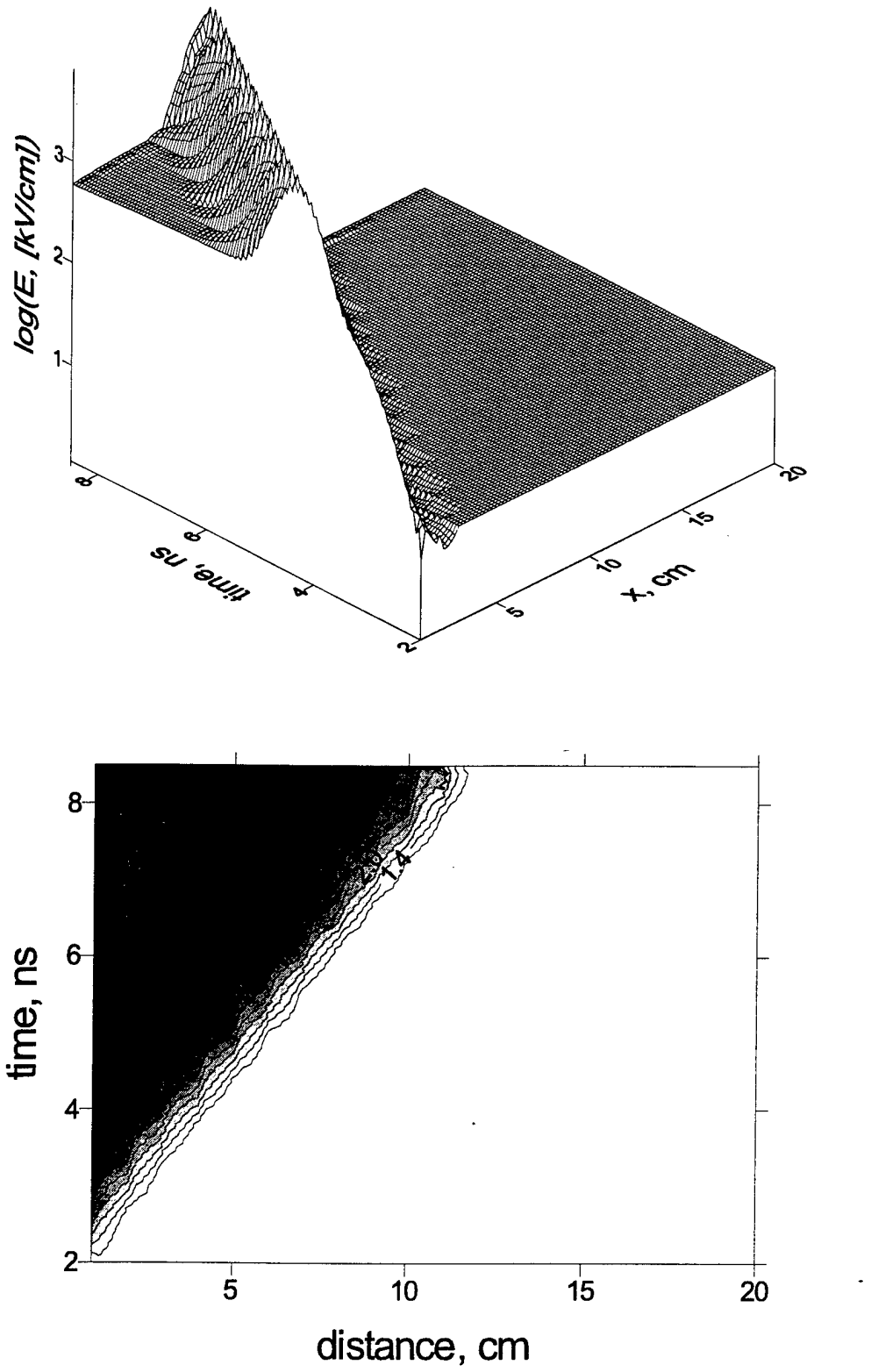

Figure 3.12: Reduced electric field dynamics in the discharge gap based on the experimental data. N_2, $p = 4$ Torr.

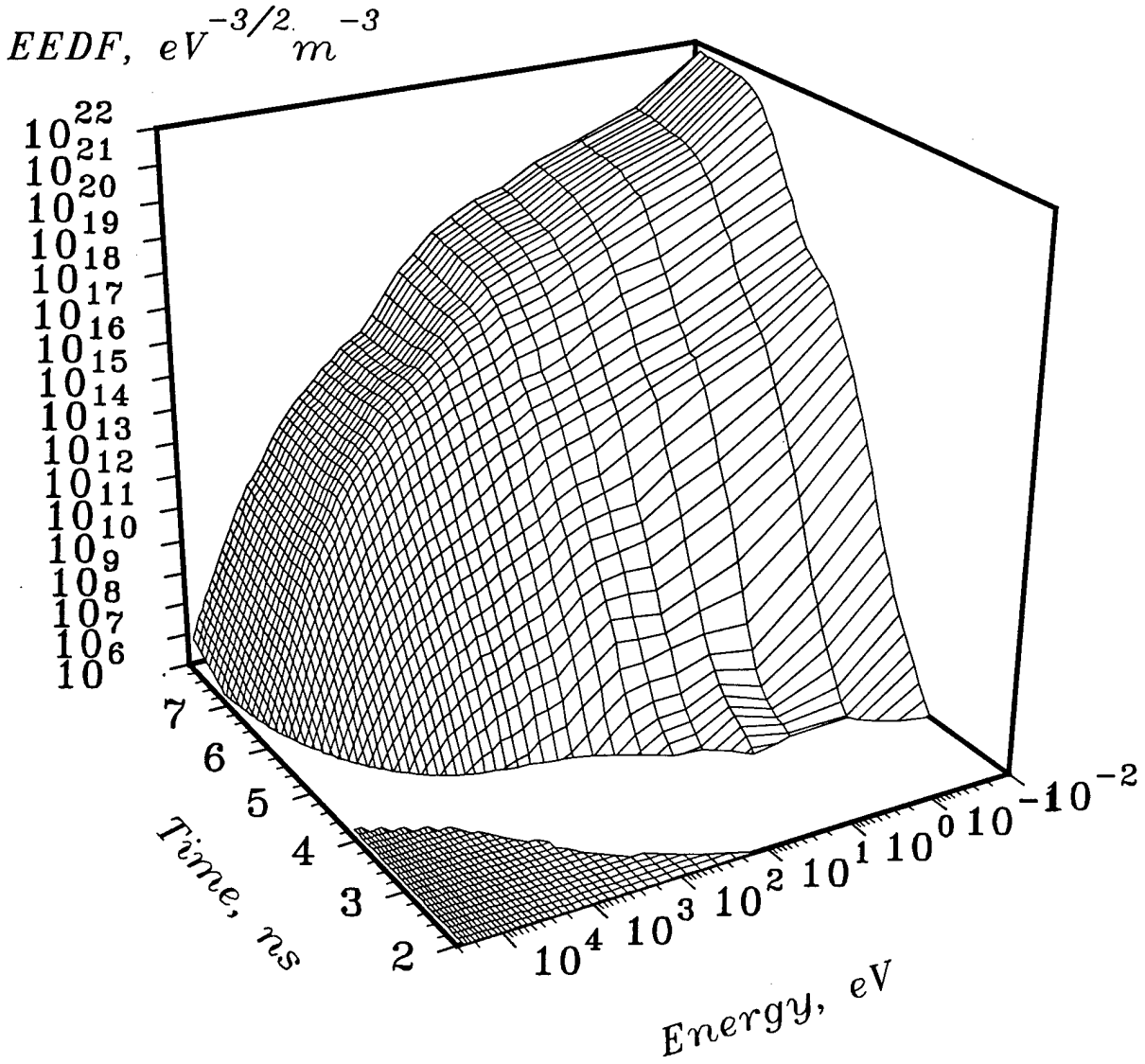

Figure 3.13: Electron energy distribution function n_e, calculated at the point $x = 4$ cm from high-voltage electrode with 1D 3V Monte-Carlo model. N_2, $p = 4$ Torr.

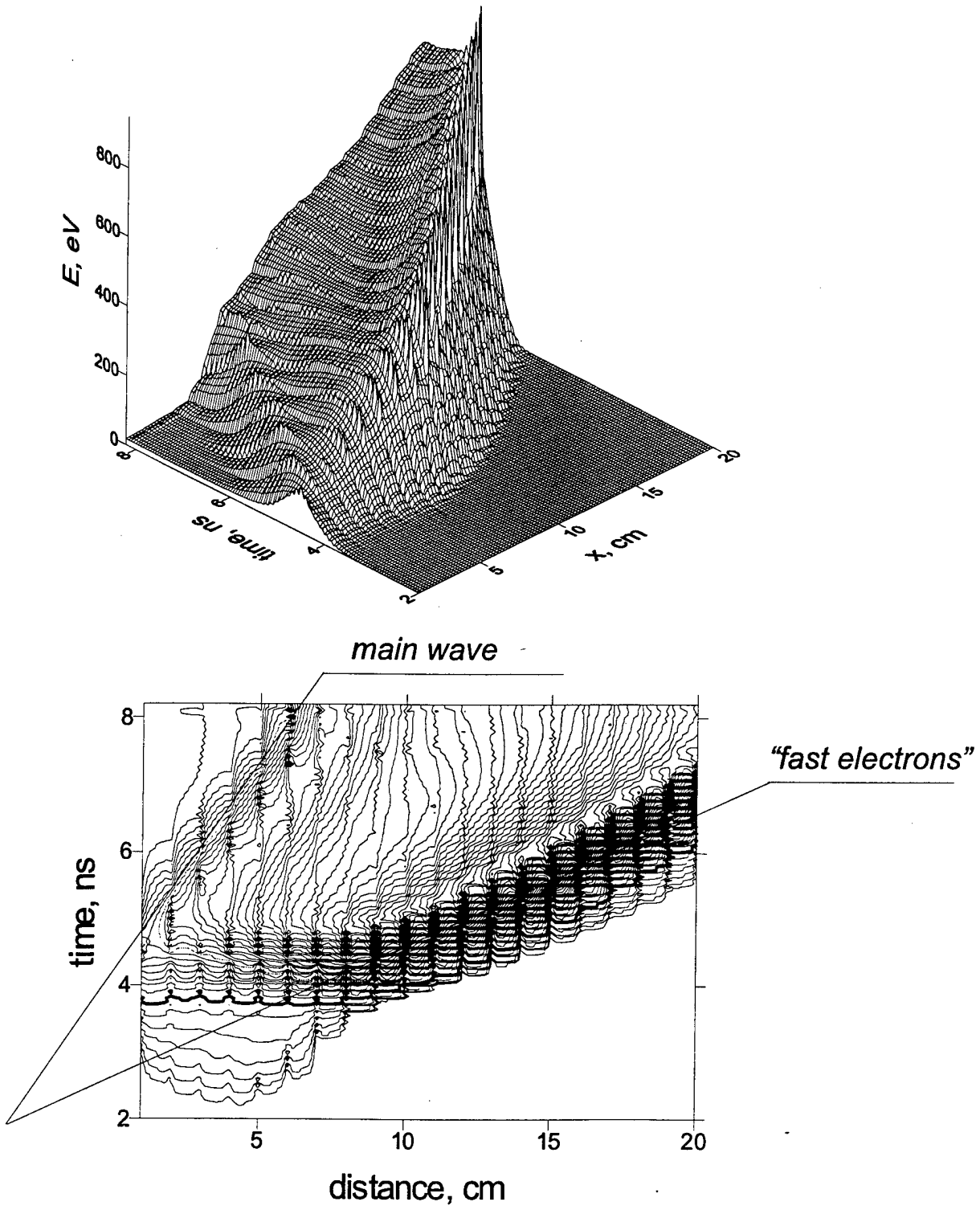

Figure 3.14: Mean electron energy *vs* time and coordinate. N_2, $p = 4$ Torr.

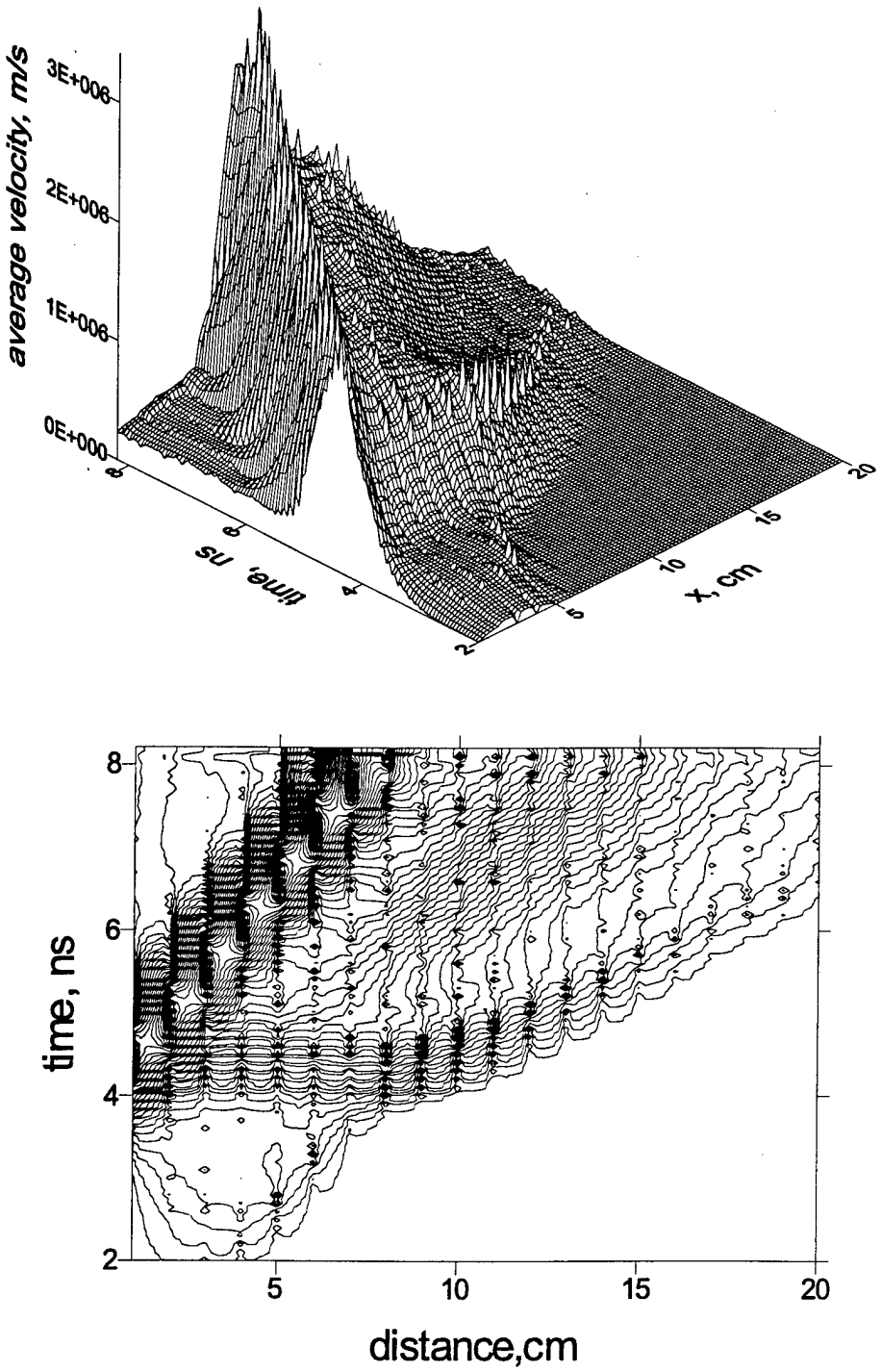

Figure 3.15: Average electron velocity V upon the time and coordinate. 1D Monte-Carlo model. $V_{wave} = 4 \times 10^7$ m/s. N_2, $p = 4$ Torr.

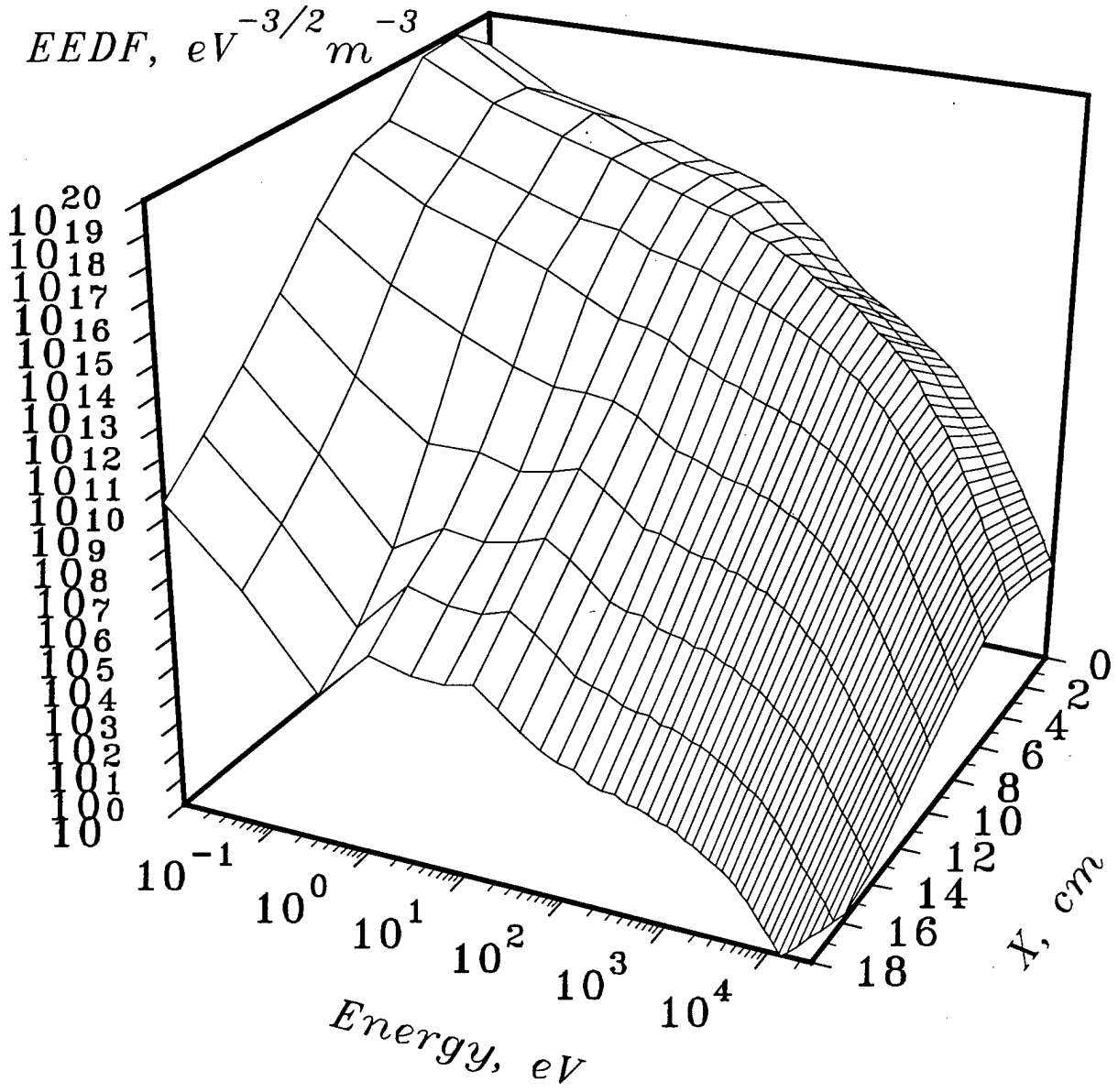

Figure 3.16: Electron energy distribution function *vs* coordinate at the time moment $t = 6$ ns; 1D Monte-Carlo model.

Results of calculation for the fast ionization propagation in nitrogen in a real experimental geometry (internal screen radius is 3.0 cm, internal radius of a discharge tube is 0.87 cm, external one is 1.07 cm, dielectric constant value for a glass is 4.9, high voltage pulse amplitude in a transmittance cable is -13.5 kV, wave resistance of a transmission line is 50 Ohm) have proved that near the ionization wave front electron energy distribution is characterized by a significant enrichment with high-energy electrons. These electrons propagation along a discharge gap, which is restricted mainly by their leaving from a discharge volume on the walls, provide the carry-over of the non-compensated charge and lead to an intensive gas pre-ionization behind the wave front. At the high field region front the electron energy distribution is close to the beam-type one with a predominance of high energy runaway electrons.

Further electron production takes place under strong electric fields in the breakdown front and the electron energy distribution function slowly comes to Maxwellian one. Sharp decrease of the electric field behind a breakdown front causes a slow decrease both in an electron energy and directed velocity of electrons; at the same time, the electron density increases.

The energy distribution in a region of relatively low electric fields far from the breakdown front acquires a typical non-Maxwellian form with a sharp decrease in the energy range which corresponds to the thresholds of non-elastic processes.

Thus, the results of the calculations 1) show a governing role of the non-local effects in the propagation of pulsed discharges at high overvoltage; 2) together with the experimental data on population rates for high-energy emitting electron states may be useful to develop a model of the energy branching in such a discharges.

-The electron energy distribution function is governed by high-energy electrons in the vicinity of the nanosecond breakdown front.

-The low-energy part of the EEDF in relatively low fields is close to the solution of stationary two-term approximation of Boltzmann equation at the appropriate electric field.

-Relaxation of the high-energy part of the EEDF leads to the significant differences in the rates of electron-impact processes near the fast ionization wave front.

Part III

Experimental investigations of plasma-chemical processes in the fast ionization wave

Chapter 4

Oxidation of molecular hydrogen by pulsed electric discharge in H_2-air mixture.

The key question for the investigation of ignition in the nonequilibrium conditions is the correlation between different processes on the stage of initiation. The relative importance of electronic (vibrational) levels excitation, dissociation and ionization of molecules is under consideration [30, 31].

To understand the main processes on the stage of ignition initiation in the pressure range $1 - 8$ Torr at a room temperature the process of oxidation of molecular hydrogen in the mixture H_2-O_2-N_2= 0.296 : 0.148 : 0.556 under the action of pulsed nanosecond discharge is investigated. On a base of a comparison of experimental data and results of calculations the analysis of plasmachemical kinetics processes in the system is performed.

4.1 Experimental setup

Discharge section is made of quartz tube 20 cm in length and 47 mm in diameter with flat high-voltage and ring low-voltage electrodes. In the low-voltage electrode there is an optical window from CaF_2 (0,16-1,1 μm). A nanosecond discharge is initiated by negative polarity pulses with $|U_{gen}| = 13$ kV amplitude, 25 ns duration on a half-height and 2 ns rise time.

The discharge tube was pumped through the hole in the low-voltage electrode to the pressure 2×10^{-3} Torr, controlled by a thermocouple gauge PMT-2, and filled by an investigated mixture. The pressure was controlled by a pressure gauge 6MD×4S and a U-tube oil manometer.

The pulse shape and amplitude control was realized by the low-inductive broad-band calibrated back current shunt included into the cable shield break. The length of coaxial cable was chosen long enough to separate first pulse created by the generator and the same pulse reflected from the discharge tube due to the different impedances of the cable and the discharge chamber. The current shunt was previously calibrated with the signal from the I1-7 pulsed generator (100 V amplitude, 30 ns duration, 2 ns rise time).

The radiation from plasma was recorded on the accumulation mode from the end plate of the discharge tube (MDR-23, 1.2 nm/mm, 1.2 m, 1200 unit/mm) with resolution

up to 0.6 Å. The registration scheme included monochromator MDR-23, photomultiplier FEY-100, RC-integration circuit and digital oscilloscope S9-8 coupled with a computer. The time constant of the integrating circuit made up 0.25s and provided operations with the high spectral resolution at a low noise level.

To obtain absolute spectral characteristics the optical system was calibrated with the use of light sources with known absolute radiation densities (DDS-30 and TPY-1100 calibrated).

4.2 Measured parameters

4.2.1 Absolute $H_2(a^3\Sigma_g^+ \rightarrow b^3\Sigma_u^+)$ emission

Under conditions of our experiments in low ultraviolet and visible bands the continuous spectrum is predominant in the discharge radiation ($H_2(a^3\Sigma_g^+ \rightarrow b^3\Sigma_u^+)$ transition).

A temporary behavior of concentration of H_2 in the ground state has been recalculated from the registration of absolute intensity of this transition on the wavelength $\lambda = 239$ nm with a spectral resolution $\Delta\lambda = 0.24$ nm.

Total intensity of the transition and, consequently, the concentration of molecular hydrogen in $a^3\Sigma_g^+$ - state were determined on the basis of registered in [32] distribution of the absolute intensity on the wavelengths knowing lifetime of the molecule and quenching rate constants.

Time of half-relaxation of concentration of H_2 molecules in the $a^3\Sigma_g^+$ - state to the quasistationary state is plotted in Fig. 4.1. When ionization wave crosses a discharge gap, at time moment $\tau_1 \simeq 5 - 7$ ns a phase of quasistationary high-current discharge reaches. The duration of this stage, where a general excitation of internal degrees of freedom takes place is $\tau_2 \simeq 15 - 17$ ns.

Characteristic times of hydrogen conversion oh this stage are $\tau = 15 - 30$ s, that is – $600 - 1200$ discharge pulses. It should be noted that in spite of the long summary time of process, plasmachemical reactions after each pulse last $10 - 20$ ms. This fact allow to exclude diffusion processes from the consideration.

The population of the $(H_2(a^3\Sigma_g^+))$ level takes place by an electron impact form the ground state of molecular hydrogen:

$$H_2 + e \rightarrow H_2(a^3\Sigma_g^+) + e \tag{4.1}$$

due both to a mediocre excitation of the gas during a current pulse and to a relaxation of electronic states between the pulses. Then the radiation intensity of $H_2(a^3\Sigma_g^+ \rightarrow b^3\Sigma_u^+)$ transition is proportional to molecular hydrogen concentration, constant rate of (4.1) process and electron density.

The absolute initial concentration of excited hydrogen molecules in $H_2(a^3\Sigma_g^+)$ - state *vs* gas pressure is represented in Fig. 4.2. The concentration of excited particles lies in the range $3 - 7 \times 10^{11}$ cm^{-3}, in a good agreement with [27, 32].

4.2.2 Electric pulse current and voltage measurements

The electron density and reduced electric field value were determined from the current and voltage measurements with nanosecond temporal resolution.

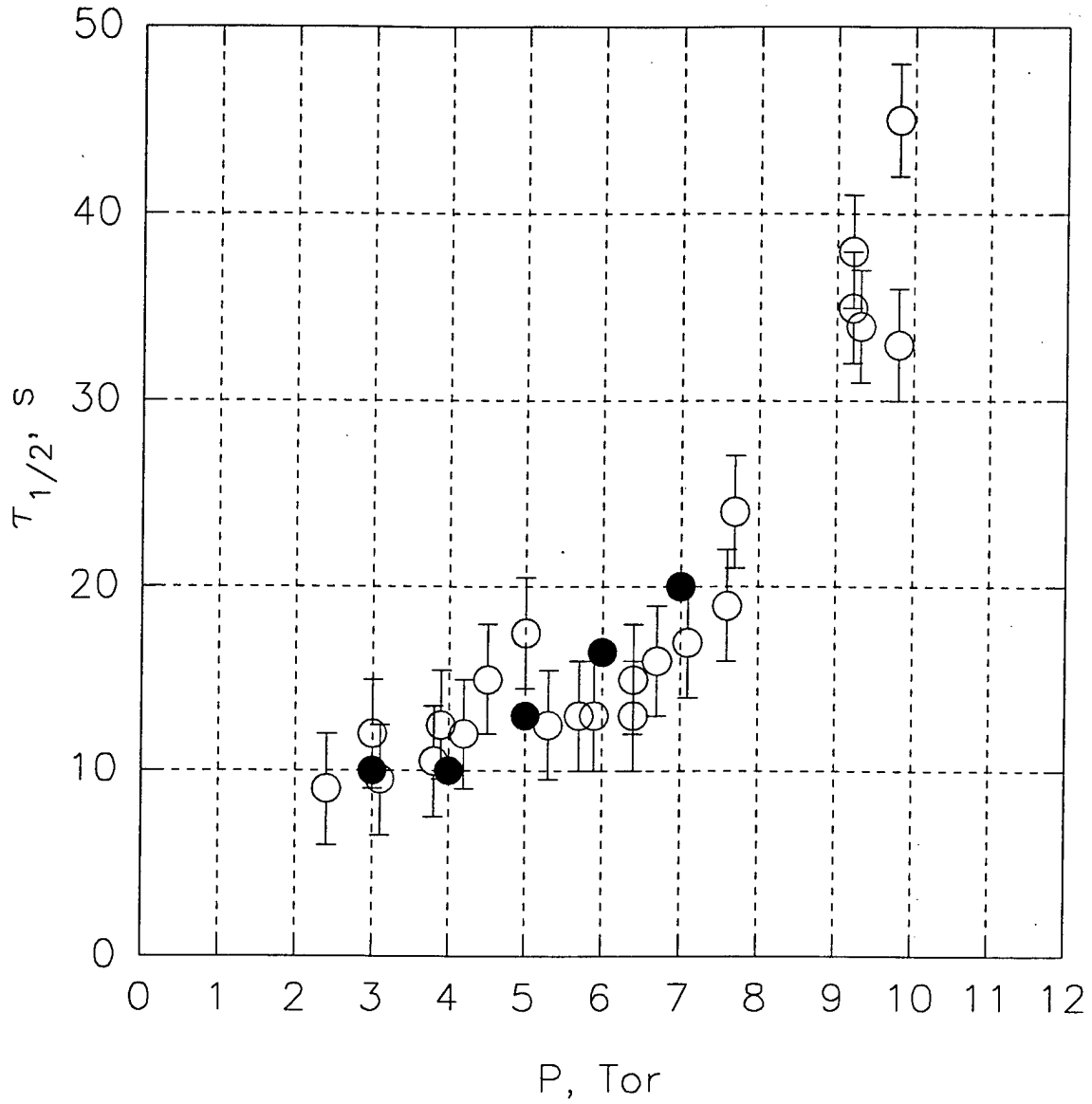

Figure 4.1: The half - time of relaxation of the $a^3\Sigma_g^+$ - stage to a quasistationary state in discharge *vs* pressure. Hollow symbols – experiments, filled ones – calculations.

Electric current in the discharge gap may be obtained as a sum of coming and reflected pulses $I = I_{gen} + I^{ref}$. The reflected from the discharge section pulse consists of two different in sign parts: reflected from the ionization wave front I_{fr}^{ref} and propagated with the velocity $V_{fr} = 3\ 10^9$ cm/s [7], and reflected from the low-voltage electrode when the breakdown is close the discharge gap I_{sc}^{ref}. Because of the high velocity of the wave front the Doppler effect should be taken into account:

$$I_{fr}^{ref}(t) = \frac{1+\beta}{1-\beta}\, I_{fr}^{ref,(measur)}\left(t\,\frac{1-\beta}{1+\beta}\right),$$

where $\beta = V_{fr}/c = 0.1$, c – light velocity in vacuum.

Coming I_{gen} *(1)*, reflected I^{ref} *(2)* and transmitted I *(3)* current pulses are represented in Fig. 4.3. Reflected pulse *(2)* is multiplied by (-1) and different parts of this pulse are

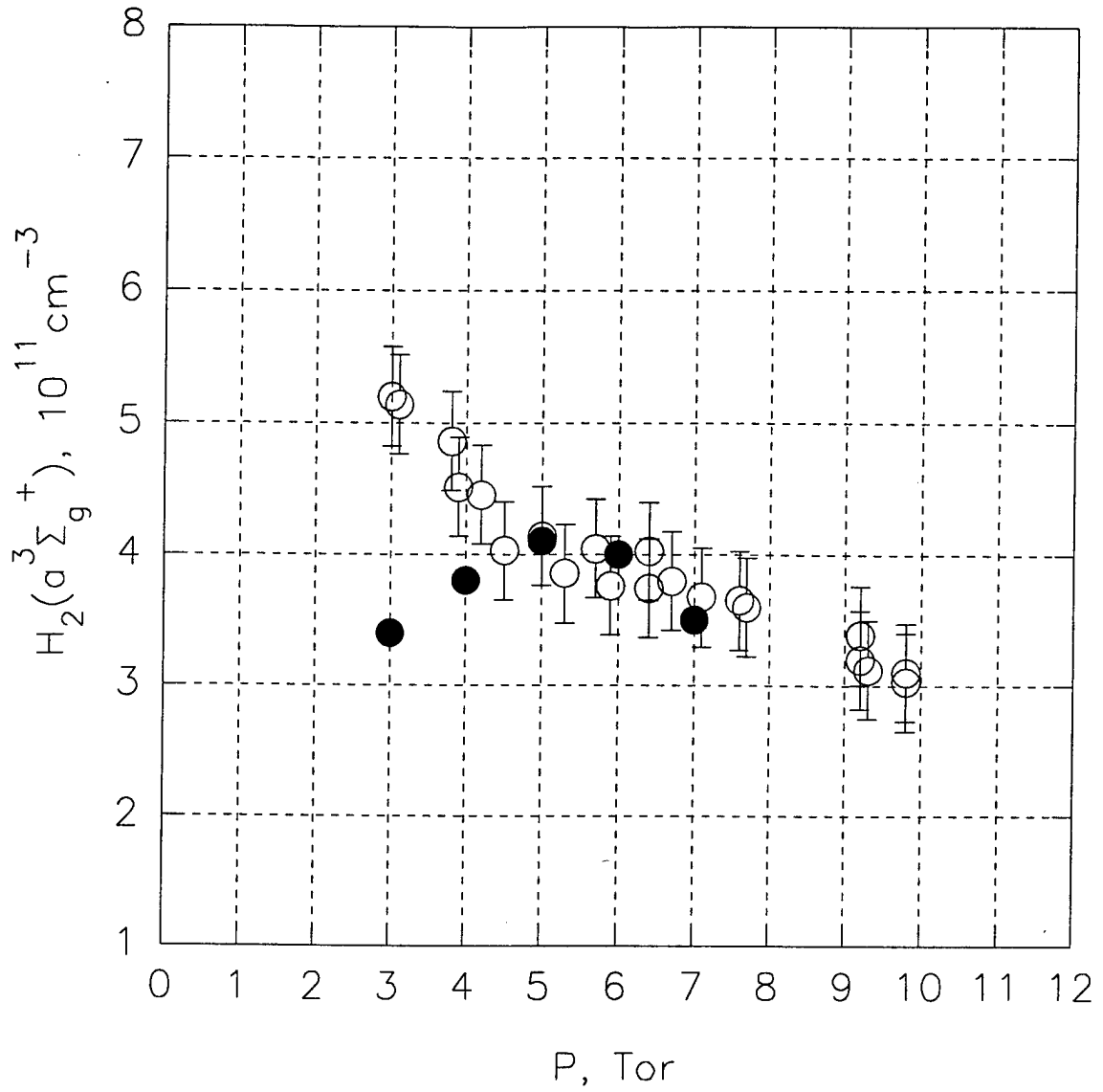

Figure 4.2: The peak concentration of molecular hydrogen in $H_2(a^3\Sigma_g^+)$ - stage *vs* pressure. Hollow symbols – experiments, filled ones – calculations.

marked with a thick solid (I_{fr}^{ref})and dashed (I_{sc}^{ref}) lines. In the same figure peak current *vs* pressure is represented. It is obviously seen that in the pressure range $3-7$ Torr peak current changes from $I = 300$ A at $P = 3$ Torr to $I = 155$ A at $P = 7$ Torr. The duration of current pulse remains equal $\tau_{pul} \simeq 16$ ns in this range of parameters.

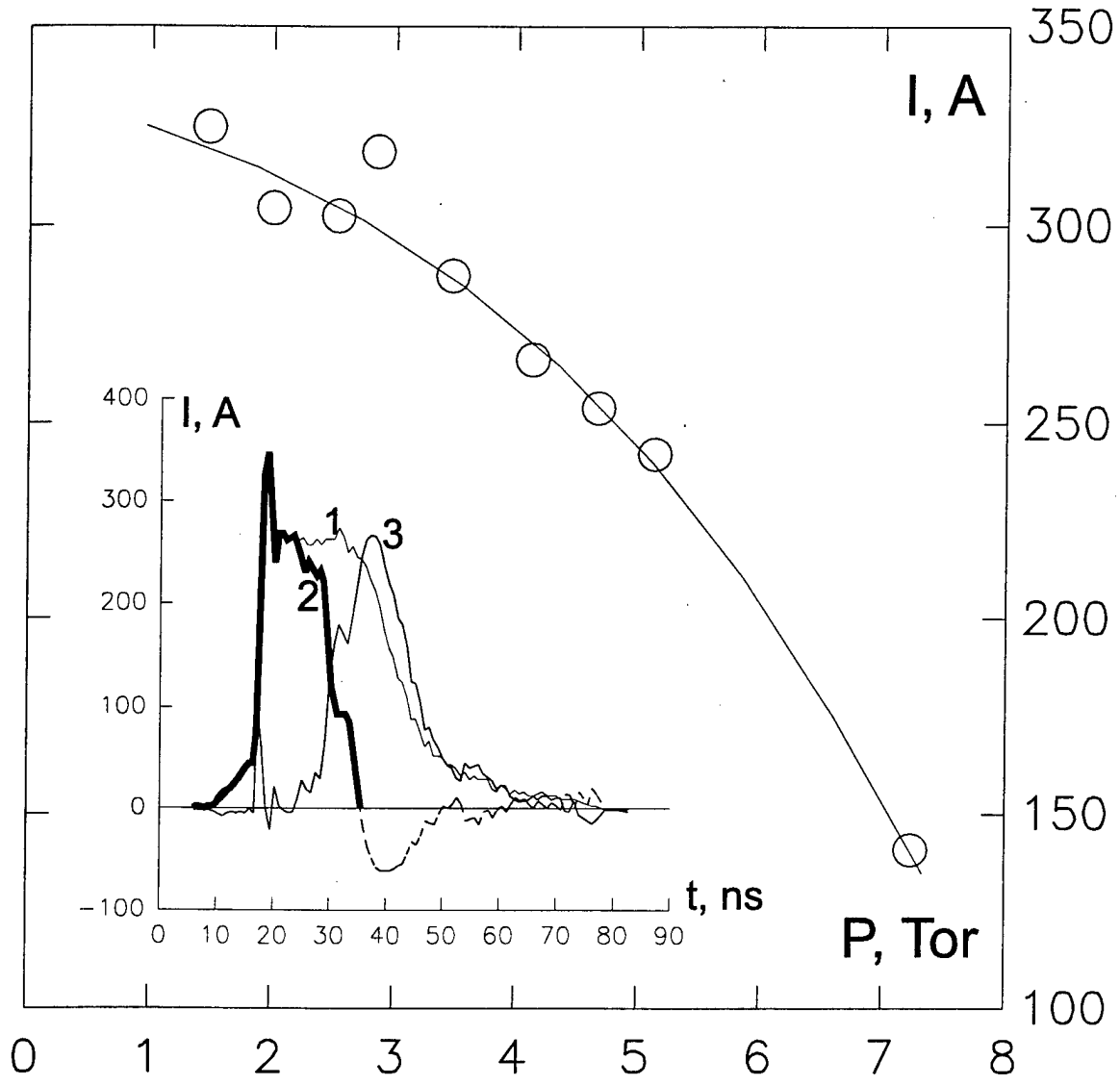

Figure 4.3: The dependence of peak current upon pressure and typical oscillogramms of coming *1*, reflected *2* and transmitted *3* currents. The part of the pulse, reflected from the ionization wave front, is marked with a thick line.

Chapter 5

N_2O decomposition by high-current nanosecond electric discharge.

To understand the main processes on the stage of ignition initiation of hydrocarbon-bearing fuels it is important to investigate the electric discharge influence on the large (threeatomic and polyatomic) molecules and radicals.

For this purposes decomposition of simple treeatomic molecule N_2O has been studied in the afterglow of nanosecond pulsed discharge developed in the form of the fast ionization wave (FIW) in the pressure range $1 - 8$ Torr at a room temperature.

5.1 Experimental

The experimental installation is shown in Fig.5.1. The discharge device consists of quartz tube of length $l = 200$ mm and internal diameter of 47 mm with conical high-voltage electrode and ringed low-voltage electrode at faces made of aluminum. To output radiation there is CaF_2 window in the low-voltage electrode that is shorted to a grounded shield of the supply cable with the help of eight thick brass buses. Impulses of negative polarity voltage of amplitude $|U_{gen}| = 13$ kV, 25 ns duration at half maximum of the amplitude and 2 ns rise time were fed with repetition frequency of $f = 40$ Hz from pulse voltage generator to the high-voltage electrode of the discharge tube.

The discharge tube was evacuated through a hole located in the low-voltage electrode by a vacuum pump to 2×10^{-3} Torr pressure which was monitored by thermocouple vacuumeter PMT-2, after which it was filled with the N_2O at the specified pressure. Gas pressure was controlled by the MD×4S pressure gauge.

The amplitude and form of the current impulse in the discharge section during the ionization wave propagation in it were recorded with the help of a calibrated broad band back current shunt which was built in braiding of the supply cable, so that incident and reflected from the discharge device pulses were not overlapped. Signals were recorded by digital oscillograph Tektronix TDS 380. The shunt was calibrated with the help of pulse generator I1-7 with the following parameters: impulse duration is 30 ns, rise time is 1 ns, impulse amplitude is $10 - 100$ V.

The discharge radiation was observed in the mode of signal accumulation at the discharge device face with the use of monochromator MDR-23 (1.2 nm/mm, 1.2 m, 1200 lines/mm, $\Delta\lambda = 2.4$ Å), photoelectronic multiplier FEU-100, RC-filter, and digital os-

cillograph S9-8, mated through interface card to a computer. The time constant of the integrating circuit was 0.25 s and provided for operations with the high spectral resolution and low noise level.

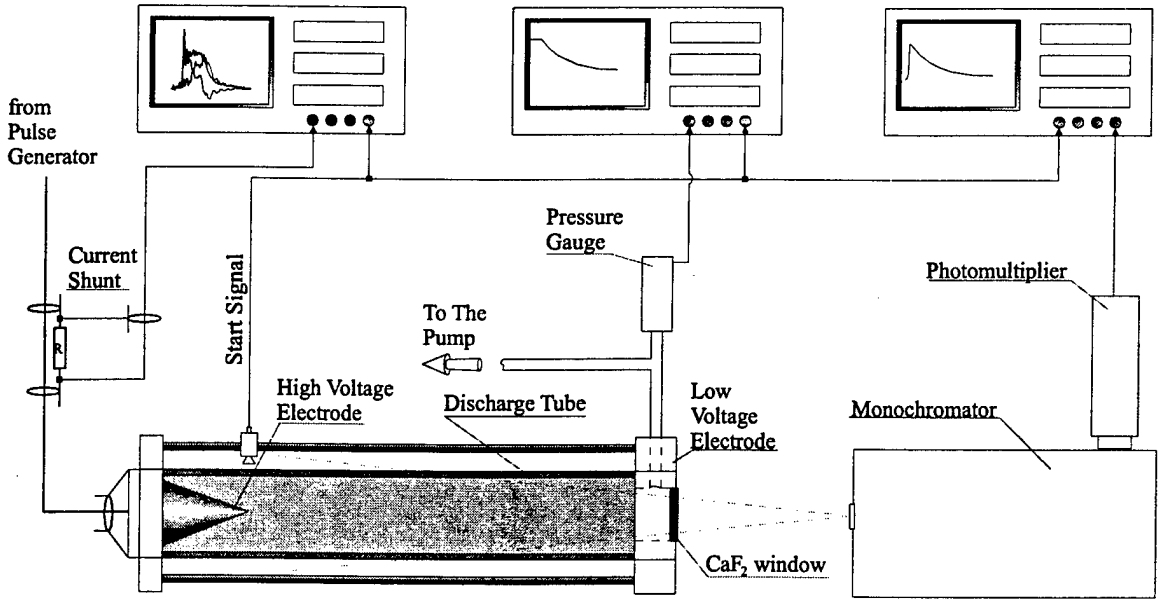

Figure 5.1: The experimental installation.

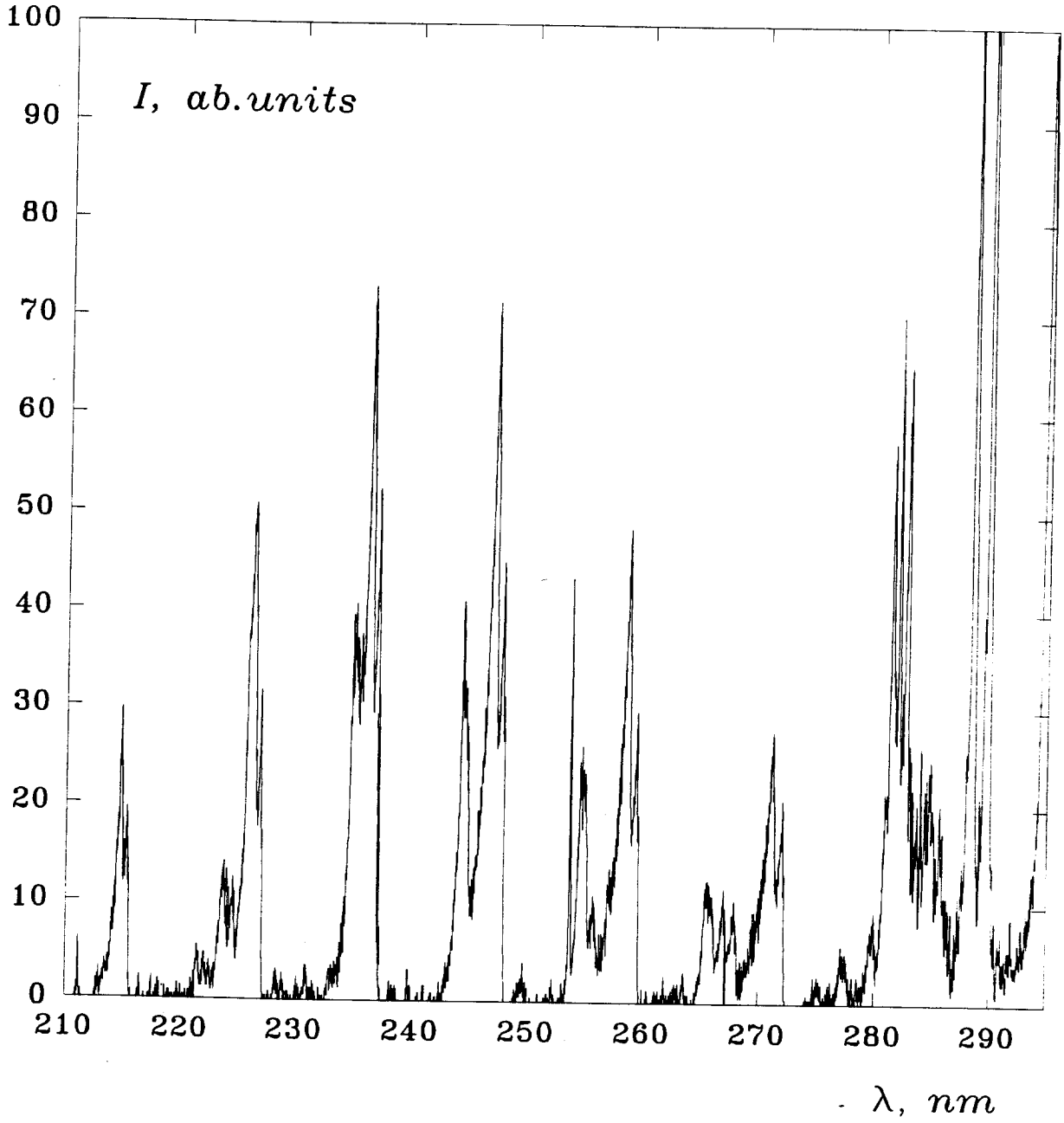

Figure 5.2: Spectrum of discharge at the pressure 4 Torr and 50 s after the start of process

5.2 Experimental results

5.2.1 Spectroscopic data

The part of integrated spectrum in the near UV region is shown in Fig.5.2. Transitions of γ-systems of NO are clearly seen.

The full set of experimental spectroscopic data and the pressure dynamics is presented in Fig.5.4. At the same pressures we measured the emission of second positive (λ = 337.1 nm, transition $C^3\Pi_u, v' = 0 \rightarrow B^3\Pi_g, v'' = 0$, Fig.5.3-1) and first negative (λ = 391.4 nm, transition $B^2\Sigma_u^+, v' = 0 \rightarrow X^2\Sigma_g^+, v'' = 0$, Fig.5.3-2) systems of nitrogen. This allows do determine characteristic time of production of N_2 molecules. The dynamics of relative NO concentration in the process of decay was measured on the wave length $\lambda = 237.02 \pm 0.02$ nm (transition $NO(A^3\Sigma^+) \rightarrow NO(X^2\Pi)$). The upper level of this transition is excited by an electron impact from the ground state of NO molecule and allow to control the rate of production and destruction of nitrogen monoxide (Figure 5.3-3 – time of half-production, Fig.5.3-4 – time of half-decrease of γ-system radiation after maximum). The measurements of pressure (Figure 5.3-5) give an information about the rate of conversion of threemolecular reagent (N_2O) into bimolecular reaction products.

5.2.2 Electron number dencity and electric field

The discharge electron number density and reduced electric field were determined with the use of time resolved measurements of the discharge gap current and voltage impulse amplitude.

The electric discharge gap current can be obtained as a sum of incident and reflected impulses. Fig.5.5 illustrates the *(1)* incident, *(2)* reflected and *I (3)* passing-over current impulses at initial $p = 4.06$ Torr. For convenience the reflected current impulse is shown with the opposite sign.

Figure 5.6 represents the pressure dependence of maximum conduction current I and its temporal length τ at half-maximum of the I-signal. It shows that in our pressure range discharge gap current amplitude varies from $I = 210$ A at $p = 3$ Torr to $I = 110$ A at $p = 7.5$ Torr.

Discharge current and voltage drop on the discharge gap allow to estimate an electron density and reduced electric field after closing the discharge gap (Fig.5.7).

Values of v_d calculated with consideration of the current chemical composition in the two-term approximation make it possible to obtain with the use of experimental data on the current density $j = I/S$ the evaluation of the maximum electron concentration in the discharge: $n_e = j/(ev_d)$, where e – elemental charge.

Fig.5.7 represents curves of reduced electric field E/n and electron concentration n_e dependencies at various pressures corresponding to initial composition of the mixture. In the parameters range under study the reduced electric field at the stage of the main current flow through the discharge cell varies from $E/n = 800$ to 300 Td, which is close to the limit of applicability of the two-term approximation of Boltzmann's equation to calculate rates of inelastic processes with participation of electrons. Below it is shown that at the lowest studied pressures this leads to remarkable discrepancy of the calculated and measured rates of the gas electron state excitation. At the same time in the pressure range

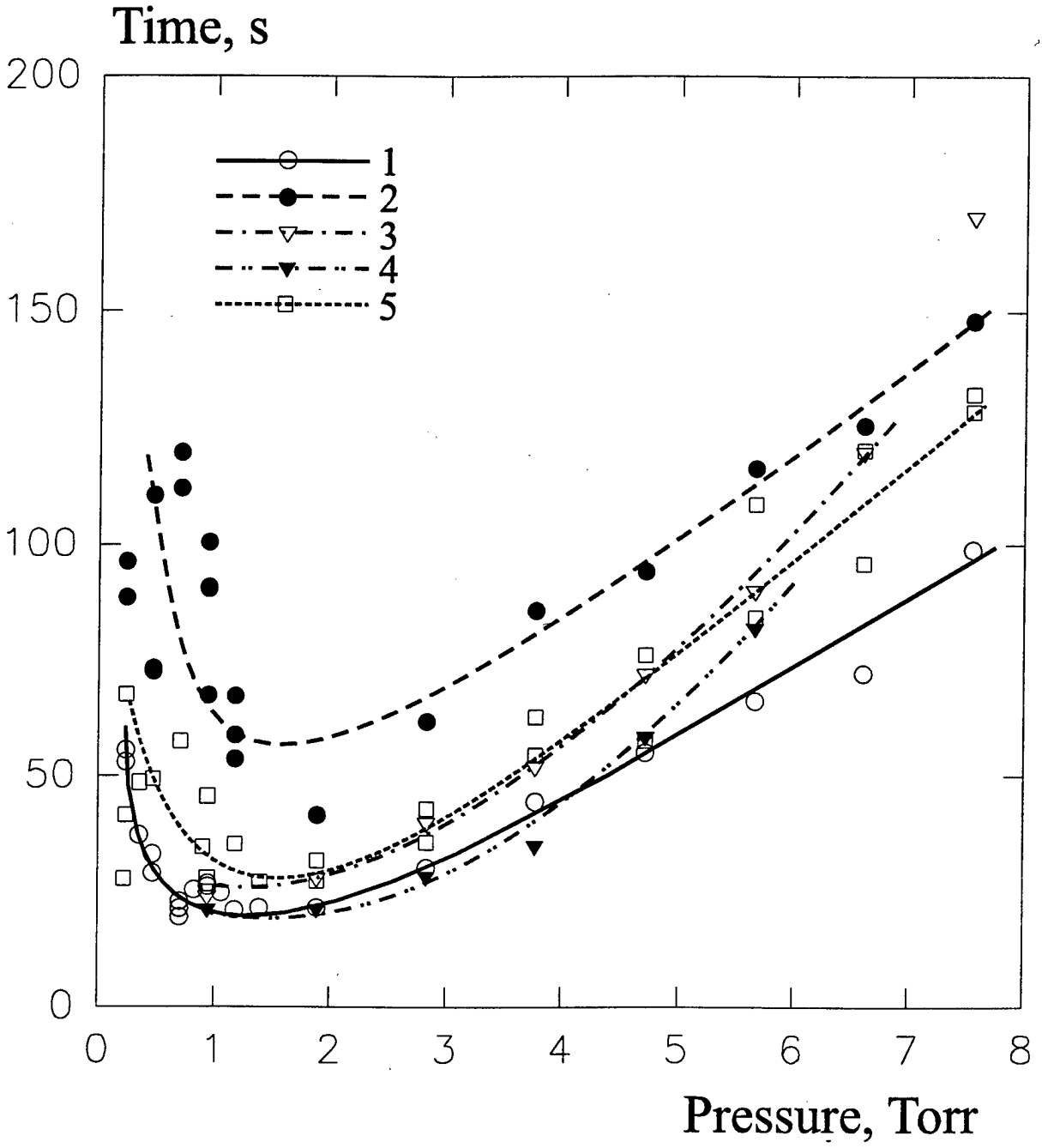

Figure 5.3: Times of decomposition (production) of main species. 1,2 – half-time of $N_2(C^3\Pi_u)$ and $N_2(B^2\Sigma_u^+)$ production, 3 – half-time of production and 4 – half-time of decrease of $NO(A^3\Sigma^+)$ after maximum, 5 -half-time of pressure growth.

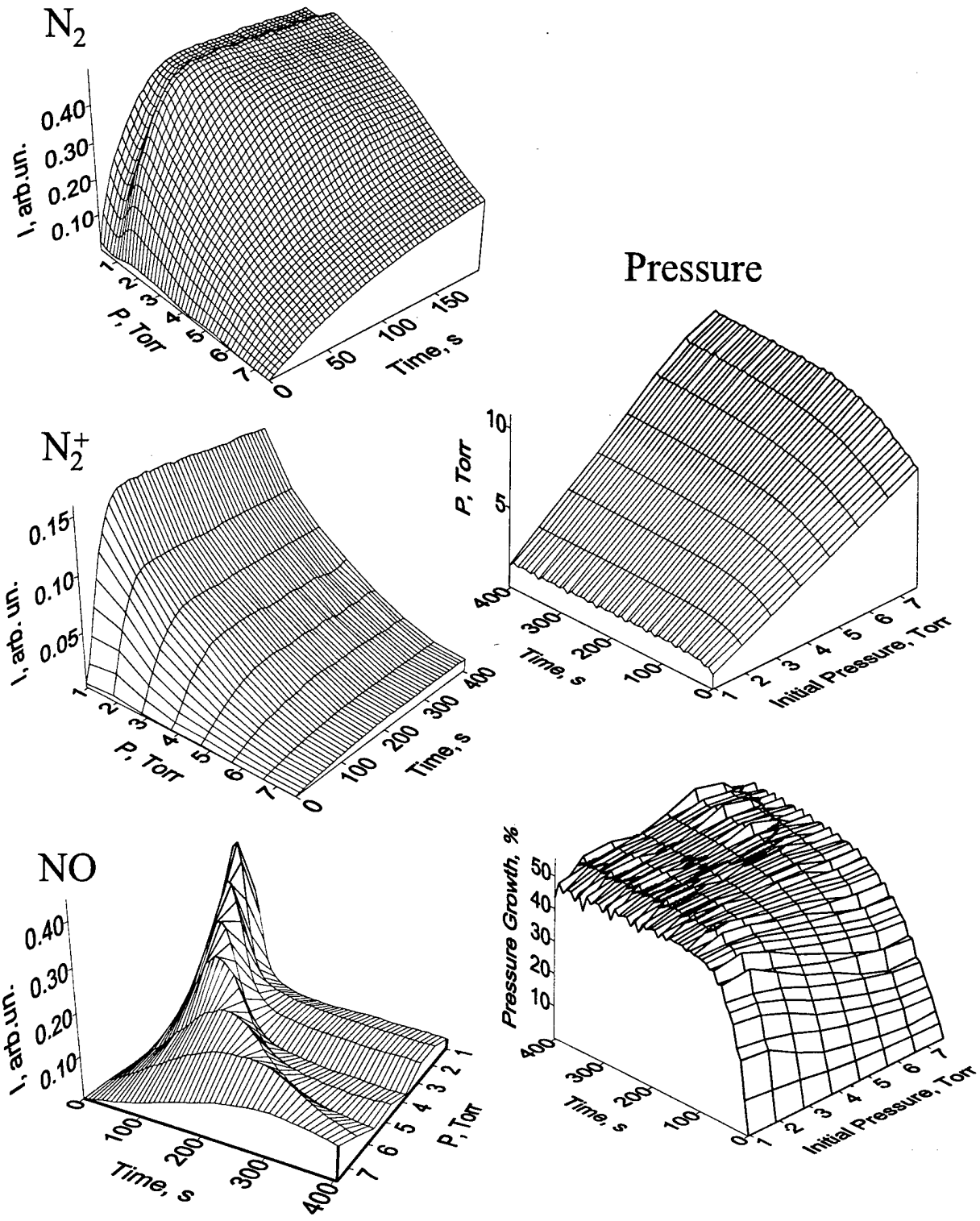

Figure 5.4: Experimental data. Temporal dynamics of $N_2(C^3\Pi_u)$, $N_2^+(B^2\Sigma_u^+)$, $NO(A^3\Sigma^+)$ and pressure *vs* initial pressure.

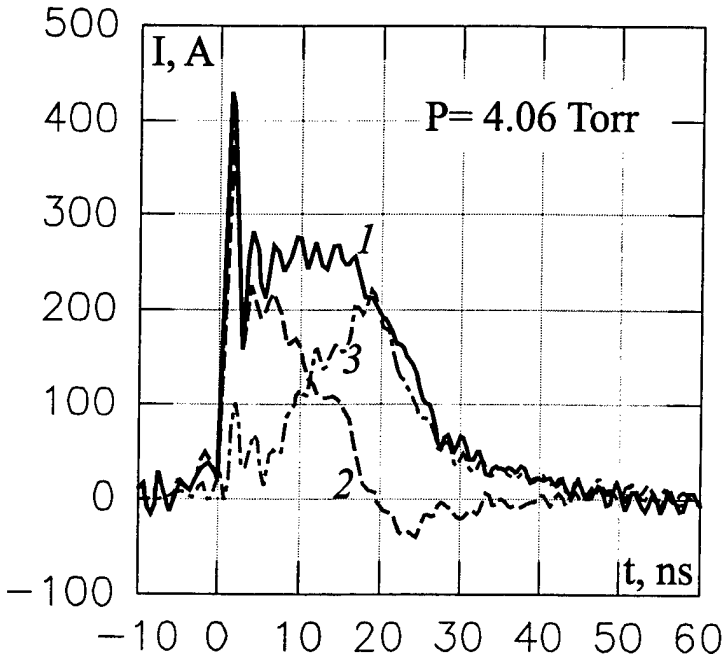

Figure 5.5: Incident *(1)*, inversed reflected *(2)* and passing-over I *(3)* current impulses. Initial pressure $p = 4.06$ Torr.

of $p = 3 \div 7.5$ Torr, as in paper [127], the discrepancy of calculated and experimentally measured excitation rates is minor.

The maximum discharge electron number density during the current impulse changes in the range of $n_e \simeq 0.9 - 2.2 \times 10^{12}$ cm^{-3} (Fig.5.7), which adequately corresponds to the measurement results [126, 32] at the similar conditions.

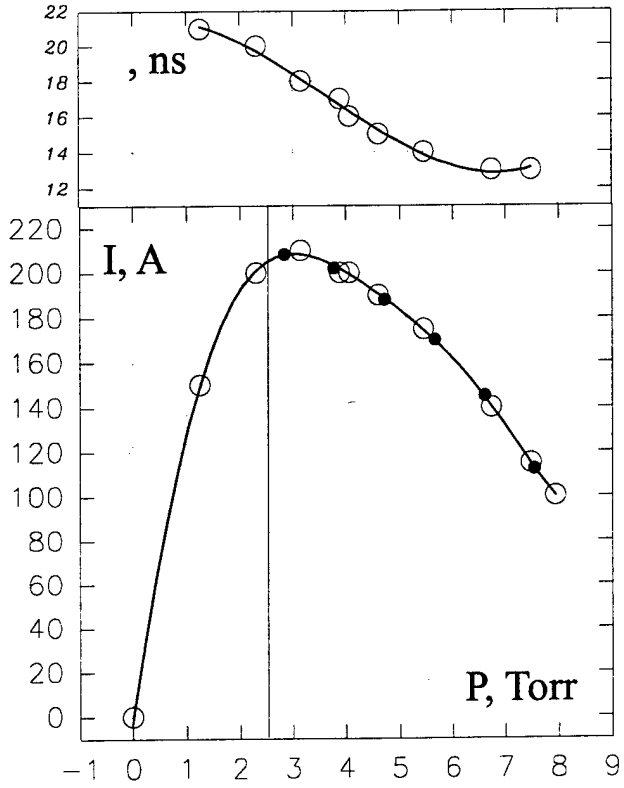

Figure 5.6: Average amplitude and duration of conduction current at different pressures.

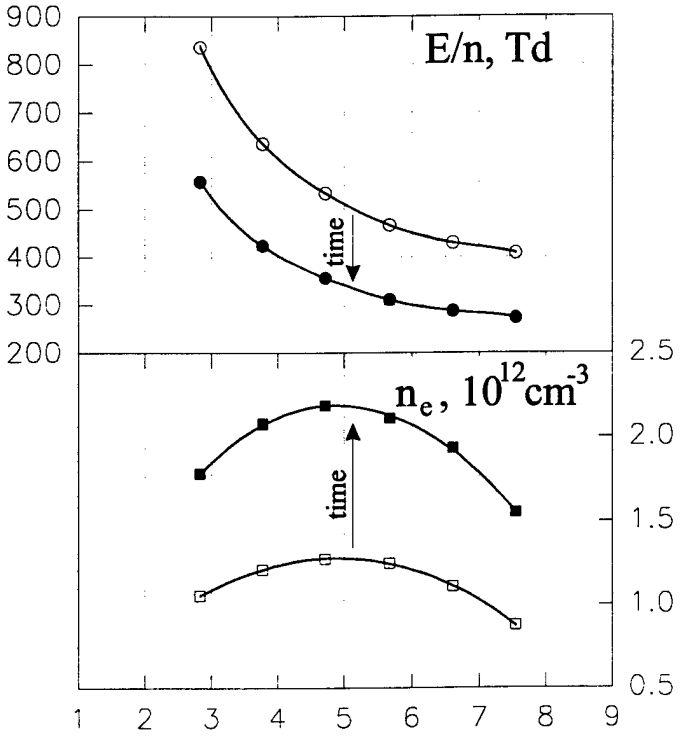

Figure 5.7: Reduced electric field and electron number density *vs* different pressures. Non-filled symbols – initial values, filled – values at the end of N_2O decomposition process.

Part IV

Numerical simulation of the plasma-chemical processes under nonequilibrium conditions

Chapter 6

Chemical reactions at thermally non-equilibrium conditions: reagents and products vibration excitation dependence of the rate constant

Models of description of chemical reactions at non-equilibrium energy distribution between vibration and translation-rotation degrees of freedom begin to play more important role [128]. This is caused by necessity to describe dynamic chemical processes which characteristic times are comparable with or less than the times of relaxation of vibration degrees of freedom of active molecules [129]. Chemical laser pumping [130], reactions involving molecules excited by discharge electrons [131], propagation of strong shock waves [132] can serve, as examples of such processes. Calculation of reaction kinetics at such conditions requires the insight into the nature of molecule and product distribution over vibrational degrees of freedom as well as knowledge of rate constants of reactions between reagents characterized by a certain vibrational energy. Owing to development of experimental methods and a number of computational studies, significant progress in qualitative insight of the vibrational energy role in reactions is gained at present [133, 134].

A great attention is drawn to development of theoretical models to describe reactions at non-equilibrium conditions.

A method of the vibrational energy usage factor which is developed in [135, 136, 137] should be emphasized; it reduces the reagent vibration energy role to the decrease of the reaction activation threshold by αE_{vib} and does not allow to calculate product distribution over vibration states. Vibration energy usage factor α is expressed with the use of activation energy and thermal effect of the reaction. Simplicity of such approach causes its broad application at present in actual calculations of multi-components thermally non-equilibrium active systems [138]. A model of bimolecular exchange reactions at conditions that vibrational temperature of active molecules differs from the translational one which has been recently developed by Macheret [132] is designed to estimate the rate constant and a factor of non-equilibrium of the simple exchange endothermic reaction. The model is characterized by simplicity of application but requires knowledge of energy release fraction in the reverse reaction which is directed to vibrational excitation and it is applicable only to a certain type of reactions [139].

It should be noted that virtually all analytical models available at present which describe reaction rate constants operate with term "vibrational temperature", which assumes that there is a beforehand specified distribution over vibrational levels of reagents; reaction product distribution over internal energy is disregarded at all in most cases. Such approach significantly decreases their value for modeling of the reaction kinetics at highly non- equilibrium conditions that molecule distribution over vibrational levels can be even inverse in a certain energy range [140].

Recently numerical calculations more frequently become an alternative to analytical models [141].

A great series of results of rate constant calculations and energy distribution of chemical reaction products with the use of Monte-Carlo method is given in [142]. However, it is necessary to note that despite the highly detailed pattern obtained by numerical calculations these calculations are extremely labor-consuming and their results highly depend on calculation approximations accepted [143]. Therewith, the use of these calculation results to simulate complicated active systems is problematic at present. Thereby, the problem to construct an analytical model that makes it possible to evaluate microconstants of reaction rates and a function of the level distribution of the product on the basis of experimentally measured values is going on to be actual.

6.1 Problem formulation

Let's treat a reaction of exchange type with energy release

$$\mathrm{AB} + \mathrm{C} \rightarrow \mathrm{A} + \mathrm{BC} + \Delta H \tag{6.1}$$

in which molecules AB and BC can by characterized by distribution over vibrational energy which differs from the equilibrium one. Let's assume that this reaction rate at reagent equilibrium distribution over energy is described by the law of mass action, and experimentally measurable rate constant is characterized by the Arrenius temperature dependence:

$$W = k[\mathrm{AB}][\mathrm{C}] \tag{6.2}$$

$$k = k_0 \exp\{-E_a/T\} \tag{6.3}$$

where W — process rate, [AB] and [C] — AB and C components concentrations, E_a — activation energy.

Integral reaction (6.1) proceeds through elementary channels of the following type:

$$\mathrm{AB}(v) + \mathrm{C} \rightarrow \mathrm{A} + \mathrm{BC}(w) \tag{6.4}$$

v, w — numbers of vibrational levels where molecules AB and C are located respectively. The rate of such process is determined by relation:

$$W^{v,w} = k^{v,w}[\mathrm{AB}(v)][\mathrm{C}] \tag{6.5}$$

where

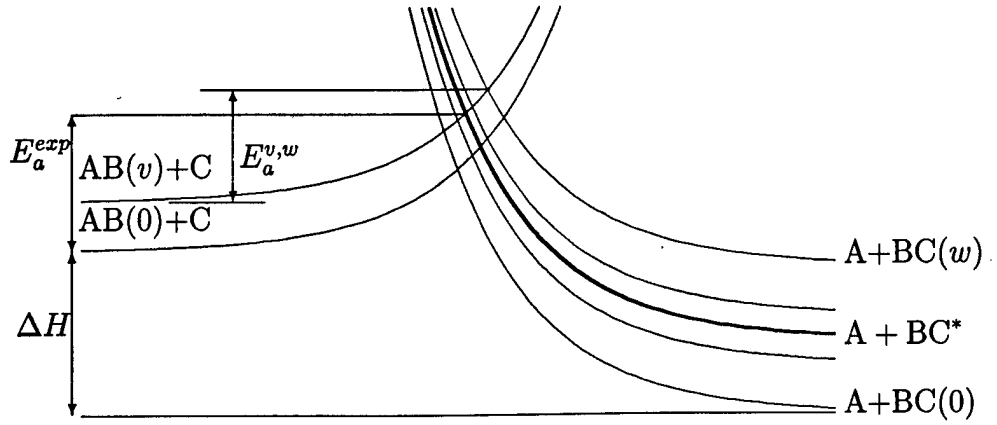

Figure 6.1: Structure of Model Curves of Potential Energy of Reaction AB + C → A + BC. Bold line marks a term that corresponds to the rate averaged over all vibration levels of reagents and products; for this term $E_a = E_a^{exp}$.

$$k^{v,w} = k_0^{v,w} \exp\{-E_a^{v,w}/T\} \tag{6.6}$$

a $E_a^{v,w}$ — process activation energy (6.4). For $k^{v,w}$ the condition of normalization is effective

$$\sum_{v,w} W^{v,w} = W \tag{6.7}$$

at equilibrium (Boltzmann) distribution of molecule AB over vibrational energy. To determine numerical values of $k_0^{v,w}$ and $E_a^{v,w}$ let's use a model of vibronic terms [129]. In this approximation the profile of a potential energy surface which corresponds to interaction AB(v)+C is obtained by parallel shift upward by E_{vib}^{AB} of the surface corresponding to state AB+C. In doing so, the form of the potential energy surface is constant (Fig. 6.1).

Allowing for interaction between states AB(v)+C and BC(w)+A, the form of the potential energy surface in the vicinity of the cross point changes in general. In this region the genuine potential energy surface is located below the initial surfaces and the value of the threshold decrease is determined by the matrix element of interaction [144]. Let's assume that the region of the state interaction is sufficiently small and located in the vicinity of the barrier top, i.e. the potential energy surfaces correspond to either AB(v)+C, or BC(w)+A everywhere except, probably, a narrow zone.

Application of this model is best justified for electron - non-adiabatic processes where allowing for interaction between states AB+C and A+BC affects potential curves of associated states only in a small region near a point of transition from one state to the other [129].

6.2 Changing of the reaction threshold and probability of transition with reagents excitation

Should the initial terms be approximated by exponential coordinate dependencies (r_{AB-C} and r_{A-BC}, with r_1 and r_2 parameters of decrease respectively), surfaces of potential energy of an exothermic reaction (6.4) can be represented in the form of:

$$U_1 = \Delta H + E_a^{00} \exp\{r/r_1\} \tag{6.8}$$

for reagents and

$$U_2 = (\Delta H + E_a^{00}) \exp\{-r/r_2\} \tag{6.9}$$

for products, where E_a^{00} — energy of the process activation.

$$\mathrm{AB}(v=0) + \mathrm{C} \rightarrow \mathrm{A} + \mathrm{BC}(w=0) \tag{6.10}$$

6.2.1 Evaluation of reaction threshold

Within the assumptions accepted, threshold $E_a^{v,w}$ of elementary process (6.4) is determined from equation system

$$E_{vib}^{\mathrm{AB}}(v) + \Delta H + E_a^{00} \exp\{r^*/r_1\} = E_{vib}^{\mathrm{BC}}(w) + (\Delta H + E_a^{00}) \exp\{-r^*/r_2\} \tag{6.11}$$

$$E_a^{v,w} = E_a^{00} \exp\{r^*/r_1\} \tag{6.12}$$

where r^* — coordinate of the cross point of vibronic terms, $E_{vib}^{\mathrm{AB}}(v)$ and $E_{vib}^{\mathrm{BC}}(w)$ — vibration energies of molecules AB and BC in states with vibration quantum numbers v and w respectively.

In most cases interaction radii of reagents r_1 and products r_2 are close values. If $r_1 = r_2$ is assumed, then solution of this system is of a simple form:

$$E_a^{v,w} = \frac{1}{2}\Big[\sqrt{(\Delta H + E_{vib}^{\mathrm{AB}}(v) - E_{vib}^{\mathrm{BC}}(w))^2 + 4E_a^{00}(E_a^{00} + \Delta H)} - \\ - (\Delta H + E_{vib}^{\mathrm{AB}}(v) - E_{vib}^{\mathrm{BC}}(w))\Big] \tag{6.13}$$

6.2.2 Estimation of transition probability for selected levels

Estimate of $k_0^{v,w}$ probability of transition for separated levels is the probability of electron - non-adiabatic transition that corresponds to rearrangement of electron structure of complex A-B-C from a state correlating with reagents to the state describing products of reaction and takes place in the vicinity of the barrier top. Together with $E_a^{v,w}$, the v and w dependence of this value determines reaction rate constant (6.4) and product distribution over vibration energy. To evaluate probability of this transition the semi-classical approximation [144] was used. Let's consider the non-stationary wave equation:

$$i\hbar \frac{d\Psi(r,t)}{dt} = H_e(r,R)\Psi(r,t) \tag{6.14}$$

where time dependence of electron hamiltonian $H_e(r,R)$ depends on time dependence of nucleus coordinates $R = R(t)$.

Let's find $\Psi(r,t)$ in the form of extension in terms of adiabatic electron functions $\varphi_m(r)$ in semi-classical approximation:

$$\Psi(r,t) = \sum_m a_m(t)\varphi_m(r)\exp\left[-\frac{i}{\hbar}\int^t U_m(R)dt\right] \tag{6.15}$$

where U_m – adiabatic electron therms of molecular system. Then, giving (6.15) into (6.14) and using the property of ortho-normalization of function φ_m, for coefficients $a_m(t)$ one can obtain [144]:

$$i\hbar\frac{\partial a_m(t)}{\partial t} = \sum_n \langle\varphi_m\left|-i\hbar\frac{\partial}{\partial t}\right|\varphi_n\rangle\exp\left[-\frac{i}{\hbar}\int^t (U_n - U_m)dt\right]a_n \tag{6.16}$$

Let's limit ourselves further by the two-state approximation, i.e. non- adiabatic bond only between two electron terms is taken into account. This allows to retain only two terms of the whole sum (6.15), approximating the non-adiabatic function by the following expression [144]:

$$\begin{aligned}\Psi(r,t) = a_1(t)\exp\left[-\frac{i}{\hbar}\int^t U_1(R)dt\right]\varphi_1(r,R) + \\ +a_2(t)\exp\left[-\frac{i}{\hbar}\int^t U_2(R)dt\right]\varphi_2(r,R)\end{aligned} \tag{6.17}$$

The hamiltonian matrix in the atomic basis φ_1^0 and φ_2^0 can be represented in the form of:

$$H_e = \begin{pmatrix} H_{11}(R) & H_{12}(R) \\ H_{21}(R) & H_{22}(R)\end{pmatrix} \tag{6.18}$$

with eigenvalues

$$\begin{gathered} U_{1,2} = \bar{U}(R) \pm \Delta U(R) \\ \bar{U}(R) = 1/2(H_{11}(R) + H_{22}(R)) \\ \Delta U = 1/2\{[H_{11}(R) - H_{22}(R)]^2 + 4\left|H_{12}(R)\right|^2\}^{1/2}\end{gathered} \tag{6.19}$$

If complete adiabatic hamiltonian H_e is represented in the form of a certain zero hamiltonian and slight disturbance $H_e = H_0 + V$, then diagonalizing matrix (6.18), the adiabatic functions of such hamiltonian can be expressed with the use of the adiabatic functions of the zero hamiltonian [144]:

$$\begin{aligned}\varphi_1 &= \varphi_1^0\cos\chi + \varphi_2^0\sin\chi \\ \varphi_2 &= -\varphi_1^0\sin\chi + \varphi_2^0\cos\chi\end{aligned} \tag{6.20}$$

where

$$\chi = \frac{1}{2} \cdot \mathrm{arctg}\left(\frac{2V_{12}}{E_1^0 + V_{11} - E_2^0 - V_{22}}\right) \tag{6.21}$$

Equations for probability amplitudes a_1 and a_2 which are obtained from (6.16) provided that all the states are neglected in it except the two considered are as follows [144]:

$$\begin{aligned} i\hbar\frac{da_1}{dt} &= i\hbar(\dot{\chi} + \langle\varphi_1^0|\dot{\varphi}_2^0\rangle)\exp\left[-\frac{i}{\hbar}\int_c^t (U_2 - U_1)dt\right]a_2 \\ i\hbar\frac{da_2}{dt} &= -i\hbar(\dot{\chi} + \langle\varphi_1^0|\dot{\varphi}_2^0\rangle)\exp\left[\frac{i}{\hbar}\int_c^t (U_2 - U_1)dt\right]a_1 \end{aligned} \tag{6.22}$$

It is shown in [145, 146] that equations (6.22) can be integrated in the complex plane and the following expression can be obtained for the probability of transition [147] (Landau - Zener model):

$$P_{12} = |a_2(+\infty)|^2 \simeq \exp\left[\frac{2}{\hbar}\mathrm{Im}\int_c^t \Delta U(t)dt\right] \tag{6.23}$$

Thereby, to evaluate probability P_{12} of transition into a state that correlates with the reaction products (probability of reaction provided that the energy of the system is sufficient to overcome the potential threshold) it is necessary to evaluate the t_c effective time of collision and characteristic value of the energy change in transition to a new state ΔU.

As stated in [148], probability of a non-adiabatic process is maximum in a region of maximum overlapping of translational wave functions in the vicinity of the turn point. Considering that the majority of active molecules are of the initial energy of translation motion which is only slightly more than reaction threshold $E_a^{v,w}$, let's suggest that the turn point of the system is located exactly at the top of the reaction threshold, i.e. at the cross point of vibronic terms. Let's evaluate the distance from the turn point to the region where probability of transition is maximum, as $r_0 \simeq \lambda/2$, where λ — de'Broglie wave length of the system. Value λ in the vicinity of the turn point in traveling on the surface U_1 in the coordinate system of the gravity center of the system can be evaluated from relation:

$$\lambda \simeq \frac{\hbar}{\bar{p}} = \frac{\hbar}{\mu\bar{u}} \tag{6.24}$$

where $\bar{u}$ — averaged rate in the interaction region, μ — reduced mass of the system. Allowing for the made suggestion that the cross point of vibronic terms is the turn point and relation $u = Ft/\mu$ [144], for $\bar{u}$ one can obtain:

$$\bar{u} = \frac{F}{2\mu}t_c \tag{6.25}$$

which together with (6.24) result in:

$$\lambda \simeq \frac{2\hbar}{Ft_c} \tag{6.26}$$

where t_c – characteristic time of interaction, λ – de'Broglie wave length that corresponds to the system in the vicinity of the turn point, $F = U'$ — tilt of the potential energy surface at this point.

As far as overlapping of the wave functions is determined by both λ_1 and λ_2, let's use the following estimate for r_0:

$$r_0 \simeq \bar{\lambda}/2 = \frac{\lambda_1 + \lambda_2}{4} = \frac{\hbar}{2t_c}\left\{\frac{F_1 + F_2}{F_1 F_2}\right\} \tag{6.27}$$

The energy difference between the potential energy surfaces corresponding to reagents and products at point $r = r_0$ is equal to:

$$\Delta U = |U_1(r) - U_2(r)| \simeq |F_1 - F_2|\, r_0 = \Delta F r_0 \tag{6.28}$$

where

$$F_1(r) = U_1'(r) = E_a^{00}/r_1 \exp(-r/r_1), \tag{6.29}$$

$$F_2(r) = U_2'(r) = (\Delta H + E_a^{00})/r_2 \exp(-r/r_2). \tag{6.30}$$

Considering that transitions between terms U_1 and U_2 in general take place in region $r \simeq r_0$ [148], let's disregard transitions in other regions. Therefore, for probability P_{12} of transition one can obtain:

$$P_{12} \simeq \exp\left[\frac{2}{\hbar}\mathrm{Im}\int_c^t \Delta U(t)\, dt\right] \simeq \exp\left[-\left|\frac{F_1}{F_2} - \frac{F_2}{F_1}\right|\right] \tag{6.31}$$

Thereby, in this case value $\left|\frac{F_1}{F_2} - \frac{F_2}{F_1}\right|$ plays the role of Messi parameter and determines probability of transition from reagents to reaction products. Taking into account relation (6.31) for value $k^{v,w}$ one can obtain:

$$k^{v,w} = A \exp\left\{-\left|\frac{F_1}{F_2} - \frac{F_2}{F_1}\right|\right\} \exp\left(-E_a^{v,w}/kT\right) \tag{6.32}$$

where

$$\frac{F_1}{F_2} = \frac{(E_a^{v,w})^2}{(E_a^{00} + \Delta H)E_a^{00}} \tag{6.33}$$

A — normalizing factor.

Thereby, equation system (6.13), (6.32) determines the value of the process rate constant (6.4) at known values A, E_a^{00} and ΔH, and allowing for other molecular constants explicitly is not required. Let's draw our attention to the problem of reconstruction of values A and E_a^{00} from reaction activation energy (6.1) E_a^{exp} measurable in quasi-stationary mode and pre-exponential factor k_0^{exp} which are the values averaged over all possible channels of the reaction (6.4). It is clear that the total process rate (6.4) with the Boltzmann

distribution of reagents over energy should correspond to the reaction rate (6.1) measured at thermally equilibrium conditions; their derivatives with respect to temperature should coincide as well. This results in two equations required to determine A and E_a^{00}:

$$\begin{aligned} \sum_{v,w} \{f_b^v(T) \times k_{v,w}\} &= k_0^{exp} \exp\left(-\frac{E_a^{exp}}{kT}\right) \\ \sum_{v,w} \{f_b^v(T) \times k_{v,w}\}' &= k_0^{exp} \left\{\exp\left(-\frac{E_a^{exp}}{kT}\right)\right\}' \end{aligned} \tag{6.34}$$

where "′" denotes the derivative with respect to temperature, $f_b^v(T)$ — Boltzmann function of reagent distribution over vibration levels at specified temperature $T_{vib} = T_{tr} = T$.

6.3 Model analysis

Thereby, equation (6.32), (6.34) makes it possible to evaluate rate constants values of reactions between vibration excited reagents with the use of known reaction rate constant and its temperature dependence at quasi-stationary conditions.

However, it is necessary to note that assumptions explicitly or implicitly made during construction of this model (model of vibronic terms, size of effective transition region, geometry of collision) introduce uncertainty in evaluation of the area of its applicability. Allowing for the above-stated it is necessary to treat the model (6.32), (6.34), as semi-empirical and to verify it for wide class of reactions at various ratios of translational and internal energy of reagents.

Let's separate for analysis several cases important for practical application:

- Monomolecular decomposition at $T_{tr} > T_{vib}$:

$$N_2(v) + M \rightarrow N + N + M \tag{6.35}$$

- Reactions in N_2-O_2 mixtures at $T_{tr} \neq T_{vib}$:

$$N_2(v) + O \rightarrow NO(w) + N \tag{6.36}$$

$$N + O_2(v) \rightarrow NO(w) + O \tag{6.37}$$

- Reactions in H_2-O_2 mixtures at $T_{tr} \ll T_{vib}$:

$$O + H_2(v) \rightarrow OH(w) + H \tag{6.38}$$

$$OH + H_2(v) \rightarrow H_2O(\nu_1, \nu_2, \nu_3) + H \tag{6.39}$$

- Distribution of exchange reaction products over vibration levels

$$H + BrCl \rightarrow HBr(w) + Cl \tag{6.40}$$

$$Cl + F_2 \rightarrow ClF(w) + F \tag{6.41}$$

It should be noted that the essential number of the above-listed reactions is not related with the electron - non-adiabatic processes and application of the model to them (6.32), (6.34) should be considered as analysis of possibility to construct empirical methods to calculate rates of processes involving vibration excited reagents for maximum wide class of reactions. The preliminary analysis has demonstrated that the best agreement with the available published data on dependence of the chemical reaction rate constants on the degree of non-equilibrium T_{vib}/T_{tr}, products distribution over vibration degrees of freedom and relation of reaction rates involving excited and non-excited reagents can be reached by introduction of correction to change the form of the potential energy surface with the growth of reagent and product vibration excitation.

In doing so, equation (6.11) transforms into:

$$E_{vib}^{AB}(v) + \Delta H + E_1 \exp\{r^*/r_1\} = E_{vib}^{BC}(w) + (\Delta H + E_2)\exp\{-r^*/r_2\} \tag{6.42}$$

$$E_a^{v,w} = E_1 \exp\{r^*/r_1\} \tag{6.43}$$

$$E_1 = \begin{cases} E_a^{00} - \gamma E_{vib}^{AB}(v), & \text{if} \quad E_a^{00} - \gamma E_{vib}^{AB}(v) > \Delta E \\ \Delta E, & \text{if} \quad E_a^{00} - \gamma E_{vib}^{AB}(v) \le \Delta E \end{cases} \tag{6.44}$$

$$E_2 = \begin{cases} E_a^{00} - \gamma E_{vib}^{BC}(w), & \text{if} \quad E_a^{00} - \gamma E_{vib}^{BC}(w) > \Delta E \\ \Delta E, & \text{if} \quad E_a^{00} - \gamma E_{vib}^{BC}(w) \le \Delta E \end{cases} \tag{6.45}$$

where terms $\gamma E_{vib}^{AB}(v)$, $\gamma E_{vib}^{BC}(w)$ allow to take into consideration the deviation from the vibronic term model at the great vibration excitation by specifying the relative decrease of reaction energy threshold at vibration excitation of reagents and products. Then, at $\gamma = 0$ equations (6.8)-(6.9) transform into the initial model of vibronic terms, and at $0 < \gamma < 1$ the relative height of the reaction energy threshold decreases with the growth of vibration level up to a certain minimum level of $\Delta E > 0$. Equation (6.13) transforms into:

$$E_a^{v,w} = \frac{1}{2}\left[\sqrt{(\Delta H + E_{vib}^{AB}(v) - E_{vib}^{BC}(w))^2 + 4E_1(E_2 + \Delta H)} - \right.$$
$$\left. - (\Delta H + E_{vib}^{AB}(v) - E_{vib}^{BC}(w))\right] \tag{6.46}$$

equations (6.29), (6.30)

$$F_1(r) = U_1'(r) = E_1/r_1 \exp(-r/r_1), \tag{6.47}$$

$$F_2(r) = U_2'(r) = (\Delta H + E_2)/r_2 \exp(-r/r_2). \tag{6.48}$$

and equations (6.32), (6.34) do not change.

Conditions $\Delta E > 0$ is required to provide intersection of the model terms that correlate with reagents and products. In this study the following is used in all the cases:

$$\Delta E = 0.005 \times (\theta^{\mathrm{AB}} + \theta^{\mathrm{BC}})$$

where θ^{AB}, θ^{BC} — vibration quantum of reagent and product respectively. In this choice of the ΔE values there is virtually no sensitivity of calculation results to its variation by several times in any direction.

The γ value that describes the relative decrease of the reaction energy threshold at high level of excitation can be considered as a parameter of the problem, and be chosen so that the best agreement of calculations by model (6.32), (6.34) with experimental data are provided. The choice of specific value of γ only slightly affects reactions between non-excited component and becomes essential for description of reactions with the great energy threshold between highly excited reagents.

As a result of analysis performed, it has been obtained that the best agreement of the calculation results by (6.32), (6.34) with the data of other authors is reached in wide range of parameters at:

$$\gamma = 0.3$$

This value is used in all the calculations.

Given below is results of model testing (6.32), (6.34) for several typical processes and their comparison with data of other authors. Therewith, to compare with the results of other studies which are represented as a vibration and translation temperatures function, convolution of $k_{v,w}$ with Boltzmann function of distribution over vibration levels at $T = T_{vib}$ is used:

$$k(T_{tr}, T_{vib}) = \sum_{v,w} \{f_b^v(T_{vib}) \times k_{v,w}(T_{tr})\} \tag{6.49}$$

where $f_b^v(T)$ — Boltzmann function of reagent distribution over vibration levels at temperature $T = T_{vib}$.

6.3.1 Monomolecular decomposition at $T_{tr} > T_{vib}$

Interest to reaction of monomolecular decomposition is related with problems of modeling of space craft entrance (re-entry regimes) into the atmosphere and chemical reactions behind strong shock waves.

A survey of numerical models developed by now to describe such processes is given, for instance, in [139].

One of the most intensively studied reactions of monomolecular decomposition at non-equilibrium conditions is the process of (6.35) $\mathrm{N_2}(v) + \mathrm{M} \rightarrow \mathrm{N} + \mathrm{N} + \mathrm{M}$.

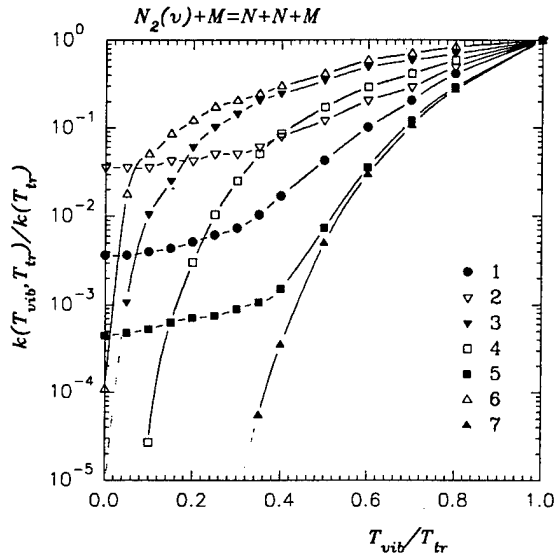

Figure 6.2: Dependence of the Rate Constant of Monomolecular Decay of N_2 on Non-Equilibrium Degree T_{vib}/T_{tr} at $T_{tr} = 2 \times 10^4$ K. 1 — [151], $U = D/6k$; 2 — [151], $U = D/3k$; 3 — [153]; 4 — [152]; 5 — [149, 150]; 6 — [154]; 7 — model (6.32),(6.34).

For modeling of the dependence of monomolecular decomposition rate constant on the degree of vibration non-equilibrium by model (6.32), (6.34) it should be noted that decomposition of molecule AB during collision with partner C can be formally described by scheme (6.4) with quasi-continuous spectrum for energy and zero life time for the product of reaction BC. Fig.6.2 gives results of calculations of the rate constant of reaction (6.35) at $T_{vib}/T_{tr} < 1$ which are obtained with the use of diverse models.

It is seen that up to value $T_{vib}/T_{tr} = 0.5$ of deviation from equilibrium the results of calculation by model (6.32), (6.34) are in good agreement with the data obtained by Macheret - Rich - Fridman model [149, 150]. At high values of deviation from the equilibrium the model [149, 150] predicts higher rates of the dissociation process than calculated by (6.32), (6.34). This relates to the fact that multi-quantum VT-transitions which form essentially non-Boltzmann distribution over high vibration levels due to decrease of vibration quantum and increase of the rate of energy exchange with the translation degree of freedom are taken into account in model [149, 150]. In this case the effective temperature of the upper level population can attain the value of translation temperature, which essentially accelerates the dissociation process (fig.6.2).

In principle this effect depends on prehistory of the process (particularly on the manner of production of non-equilibrium distribution) and is not universal. Therefore, Boltzmann distribution with $T = T_{vib}$ over all vibration levels was assumed in simulation by model (6.32), (6.34), which resulted in the decrease of the rate constant at $T_{vib}/T_{tr} \ll 1$ in comparison with data [149, 150]. In consideration of formation of Boltzmann distribution over vibration levels in upper range of the energy spectrum, model (6.32), (6.34) provides T_{vib}/T_{tr} dependence of the dissociation rate constant which is similar to [149, 150].

Deviation of results of calculation by [149, 150] and (6.32), (6.34) from more rough models of Treanor [151], Park [152, 153] and Brun [154] is sufficiently great in the whole range of parameters (Fig.6.2).

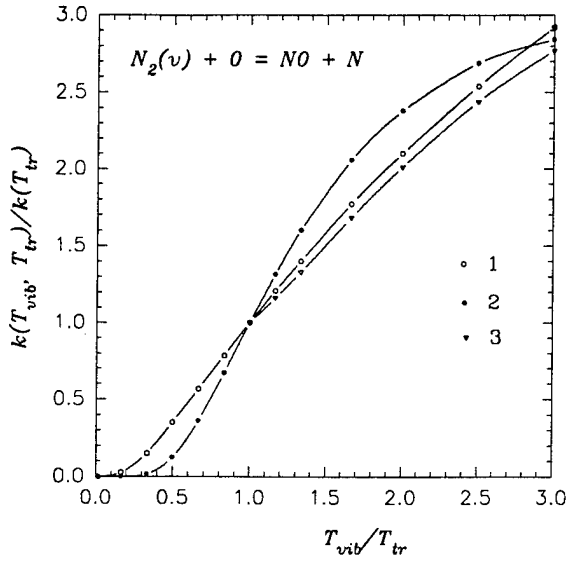

Figure 6.3: Dependence of the Rate Constant of Reaction $N_2(v)+O \rightarrow NO+N$ on Degree of Non-Equilibrium T_{vib}/T_{tr} at $T_{tr} = 1.5 \times 10^4$ K. 1 — model (6.32),(6.34); 2 — [156], $s = 0.5$; 3 — α-model, [139], $\alpha = 0.51$.

6.3.2 Reactions in N_2-O_2 mixtures

Reaction $N_2 + O \rightarrow NO + N$ is one of the crucial for description of the chemical reaction kinetics in strong shock waves in air. Experimentally obtained estimate for the factor of the vibration energy usage in this process is $\alpha \simeq 0.51$ [155].

Fig.6.3 shows results of calculation of the reaction rate constant (6.36) in dependence on ratio between vibration and translation temperatures T_{vib}/T_{tr} at fixed translation temperature $T_{tr} = 15000$ K for model (6.32), (6.34), α-model [129] at $\alpha = 0.51$ and Park model [156] with $s = 0.5$ which become the reference point for comparison of diverse models of high temperature kinetics description at thermally non-equilibrium conditions.

It is seen that model (6.32), (6.34) provides good agreement of the reagent vibration excitation dependence of the rate constant with calculations based on the experimental value of $\alpha \simeq 0.51$ in a wide range of conditions.

Along with this, more sharp vibration temperature dependence of results of calculation by (6.32), (6.34) at $T_{vib} < T_{tr}$ in comparison with data obtained by Park model (fig.6.3) is noted. It should be pointed out that the α-model in this range of parameters is not applicable [139].

Other reaction of great importance to describe non-equilibrium kinetics in air at high temperatures is process

$$N + O_2(v) \rightarrow NO + O$$

that is characterized by significantly less activation energy of ($\Theta_{6.37} = 3150$ K, $\Theta_{6.36} = 38370$ K) and less sensitivity to degree of reagent vibration excitation (experimentally measured value of factor of the vibration energy usage is $\alpha_{6.37} \simeq 0.24$ [155]). Fig.6.4 shows results of calculation of reaction rate constant (6.37) at translation temperature $T_{tr} = 300$ K with the essential overheating of reagents. Results obtained by the model (6.32), (6.34) are in good agreement with calculation using experimentally measured value

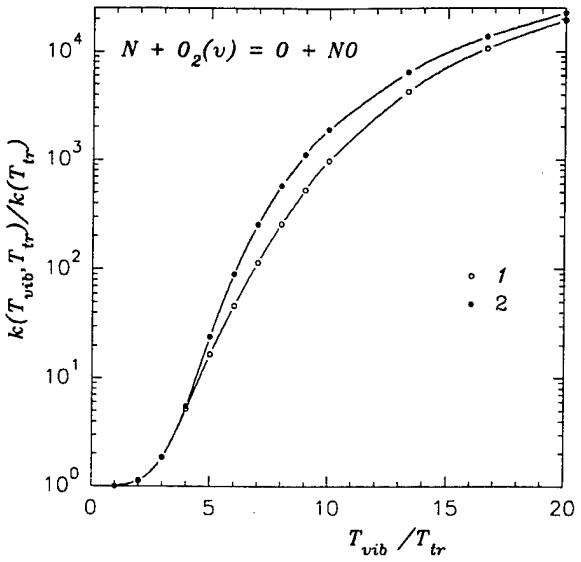

Figure 6.4: Dependence of the Rate Constant of Reaction $N+O_2(v) \rightarrow NO+O$ on Degree of Non-Equilibrium T_{vib}/T_{tr} at $T_{tr} = 300$ K. 1 — model (6.32),(6.34); 2 — α-model, [139], $\alpha = 0.24$.

of $\alpha = 0.24$ [129].

6.3.3 Reactions in H_2-O_2 system

Reactions between excited molecules of hydrogen $H_2(v)$ and radicals which rates highly depend on gas vibration excitation are of the greatest interest for description of processes of thermally non-equilibrium ignition.

One of the well-studied examples of such reactions is process $H_2(v)+O \rightarrow H+OH(w)$ [157].

It is shown in study [158] that ratio of specific constants of the reaction rates at $v = 1$ and $v = 0$ is $k(v = 1)/k(v = 0) = 2600$ at $T = 300$ K. A feature of this process is formation of radical OH which takes place mainly in vibration excited state [158]:

$$O(^3P) + H_2(v = 1) \rightarrow OH(v = 1) + H, \quad k = (1.0^{+0.4}_{-0.6}) \times 10^{-14}\ cm^3/s \qquad (6.50)$$

$$O(^3P) + H_2(v = 1) \rightarrow OH(v = 0) + H, \quad k \leq 4.7 \times 10^{-15}\ cm^3/s \qquad (6.51)$$

In accordance with results of experimental measurements the averaged factor of vibration energy usage in this reaction is $\alpha = 0.31$ [129]. Fig.6.5 shows results of calculation of the reaction rate constant (6.38) at translation temperature $T_{tr} = 300$ K for various vibration temperatures with the Boltzmann distribution of molecules over energy levels. The dependence calculated by (6.32), (6.34) is in good agreement with calculation by α-model at $\alpha = 0.31$ with the degree of overheating of $T_{vib}/T_{tr} < 5$ (Fig.6.5). At high values of T_{vib}/T_{tr} calculation by α-model predicts more sharp growth of the reaction rate constant.

At $T_{tr} = 300$ K calculation by model (6.32), (6.34) provides ration of specific constants of the reaction rate for $H_2(v = 1)$ and $H_2(v = 0)$ $k(v = 1)/k(v = 0) = 2795$, which is in perfect agreement with experiments [158]. Ratio of channels (6.50) and (6.51) at

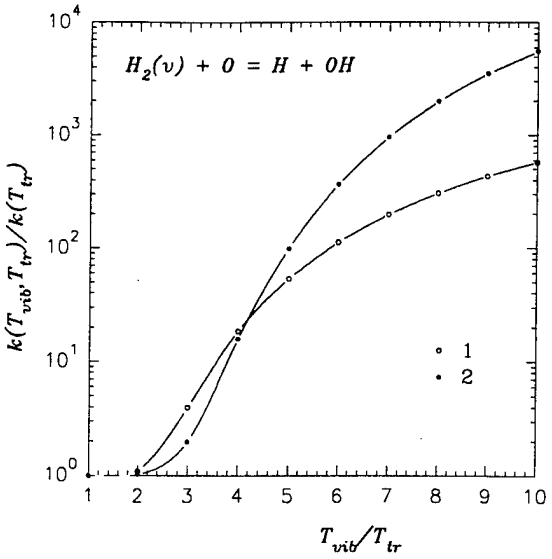

Figure 6.5: Dependence of the Rate Constant of Reaction $H_2(v)+O \rightarrow H+OH$ on Degree of Non-Equilibrium T_{vib}/T_{tr} at $T_{tr} = 300$ K. 1 — model (6.32),(6.34); 2 — α-model, [139], $\alpha = 0.31$.

$T_{tr} = 300$ K is equal to $k_{6.50}/k_{6.51} = 7.9$, which also is in good agreement with estimate [158].

In study [159] the Arrenius expression for the rate constant (6.50) was theoretically obtained. The activation energy calculated in this study was $\Theta_{6.50} = 1868$ K, which well correlates with results of calculation by models (6.32), (6.34); these results predict the value of $\Theta_{6.50} = 2160$ K.

Reactions involving multi-atomic molecules, as reagents or products, are more complicated for treatment. Models available at present do not make it possible to evaluate the relative efficiency of various vibration mode contribution to overcome of the reaction activation threshold and distribution of energy released, as a result of reaction, over various vibration modes. At this study the assumption that only deformation (lowest energy) vibration mode H_2O is excited, as a results of energy fraction release to internal degrees of freedom was made in this study for simulation of reaction $OH + H_2(v) \rightarrow H_2O + H$. Fig.6.6 shows the vibration overheating dependence of the reaction rate constants (6.39) which is obtained in this approximation. This dependence is in good agreement with calculations based on experimentally measured value of $\alpha = 0.24$ [129]. An estimate for ratio of the rate constants of processes was obtained in [160]:

$$OH + H_2(v = 0) \rightarrow H_2O + H$$

$$OH + H_2(v = 1) \rightarrow H_2O + H$$

$k_{v=1}/k_{v=0} \leq 1000$ at $T = 298$ K, which is in good agreement with the estimate of $k_{v=0} = 2.9 \times 10^{-15}$ cm^{-}3s^{-}1, $k_{v=1} = 1.8 \times 10^{-12}$ cm^{-}3s^{-}1 obtained by model (6.32), (6.34) which provides the value of $k_{v=1}/k_{v=0} = 620$ for ratio of these constants.

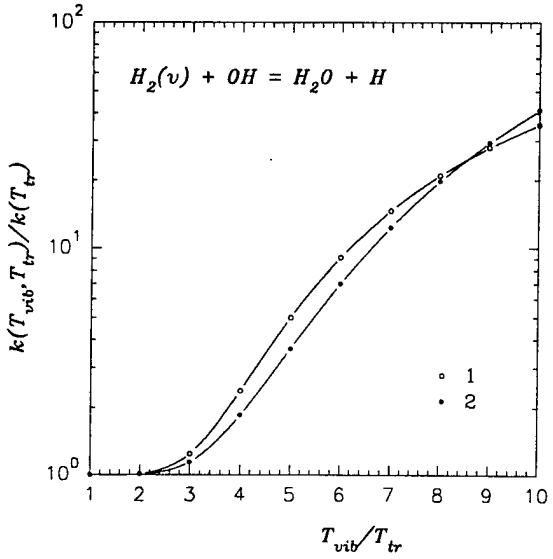

Figure 6.6: Dependence of the Rate Constant of Reaction $H_2(v) + OH \rightarrow H_2O + H$ on Degree of Non-Equilibrium T_{vib}/T_{tr} at $T_{tr} = 300$ K. 1 — model (6.32),(6.34); 2 — α-model, [139], $\alpha = 0.24$.

6.3.4 Distribution of exchange reaction products over vibration levels

To study possibility of description of distribution of energy that releases in the process of chemical reactions over the various degrees of freedom of products the following processes were treated

$$H + BrCl \rightarrow HBr(w) + Cl$$

$$Cl + F_2 \rightarrow ClF(w) + F$$

in which the reaction products are characterized by highly non-equilibrium non-Boltzmann distribution over vibration levels [142]. Results of calculation of function f_w of molecule-product distribution over vibration levels by model (6.32), (6.34) are given in Figures 6.7 and 6.8. Data [142] obtained during calculation of product energy distribution in chemical two-channel reactions with the use of trajectory calculations by Monte-Carlo methods and experimental results [161] are shown in the same Figures for comparison.

For all the processes studied the good agreement is obtained as to the vibration energy released into vibration degrees of freedom. The form of function of distribution over vibration levels in calculation by model (6.32),(6.34) is obtained more sharp than in experiments [161] and trajectory calculations [142], however, position of the population maximum is reproduced with high accuracy (Fig.6.7). With the decrease of the products vibration quantum (reaction (6.41)) selectivity of population decreases and the half width of the distribution function that is calculated by (6.32),(6.34) becomes close to results of the trajectory modeling [142].

It is interesting to analyze the transformation of function of the product distribution over vibration levels for a change of the reaction activation energy. The growth of activation energy results in more effective population of the lower vibration levels of reaction

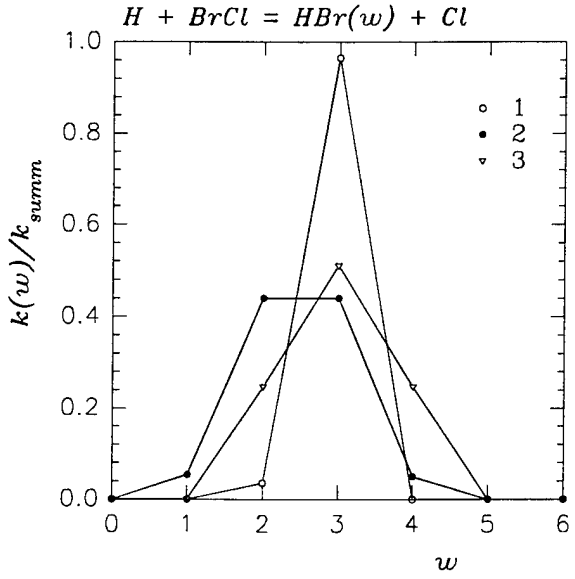

Figure 6.7: Vibration Level Distribution of Molecules HBr in Reaction H + BrCl $\rightarrow$ HBr(w) + Cl at T_{tr} = 300 K. 1 — calculation by model (6.32), (6.34); 2 — calculation by a method of classical trajectories [142]; 3 — experiment [161].

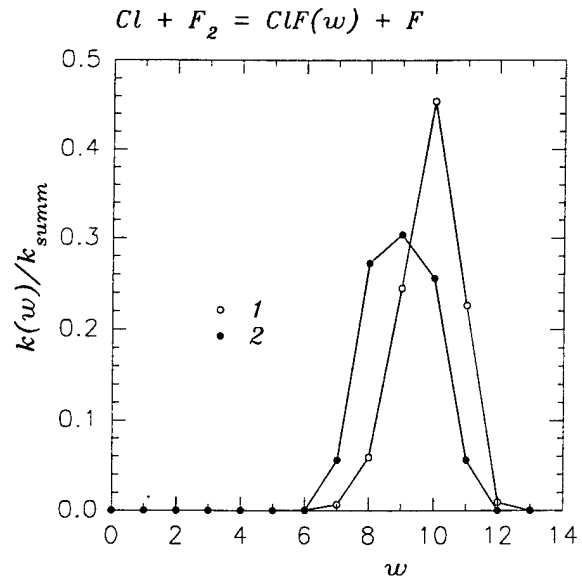

Figure 6.8: Vibration Level Distribution of Molecules ClF in Reaction Cl+F_2 $\rightarrow$ ClF(w)+ F at T_{tr} = 300 K. 1 — calculation by model (6.32), (6.34); 2 — calculation by a method of classical trajectories [142].

products and at sufficiently high values (comparable with ΔH) the maximum population falls on the zero vibrational level. On the contrary, the decrease of activation energy results in the fact that the most fraction of energy releasing in the reaction is directed to vibration degrees of freedom of products. Function of distribution over vibration energy levels acquires the prominent maximum that shifts to the level for which $E_{vib} \simeq \Delta H$, as the activation energy decreases.

Thereby, processes which activation energy E_a^{00} is low in comparison with translation temperature of reagents take place with the highest deviation of function of product distribution over vibration energy from the equilibrium value. Processes with high activation energy $E_a^{00} \gg T_{tr}$, virtually at any values of ΔH do not lead to remarkable energy release into vibration degrees of freedom of products and can not cause considerable deviation of energy of internal degrees of freedom from the equilibrium values.

Thereby, the thermally non-equilibrium reactions model suggested in this paper makes it possible to evaluate microconstants of process rates associated with certain vibration states of reagents AB(v) and products BC(w). Values of microconstants are completely determined by the value and temperature dependence of the experimentally measurable rate constant of reaction AB + C $\rightarrow$ A + BC under thermally equilibrium conditions and the value of energy release in reaction ΔH; and, along with this, allowing for other molecular constants explicitly is not required. Comparison of calculations by the suggested model with the available experimental data and other models demonstrates the possibility to use it for various processes.

Chapter 7

Numerical simulation of the hydrogen oxidation in high-voltage pulsed discharge

7.1 The stage of the discharge

The stage of quasi-steady-state electric current in discharge gap is characterized by two electrical parameters, namely by current I and voltage U. After closing the discharge gap, one may estimate the electric field as $E = U/l$, where l is a distance between the electrodes. Then, taking into account discharge uniformity in the cross-section S and relation

$$I = en_e v_d S \tag{7.1}$$

it is possible to estimate the density of electrons n_e. The drift velocity $v_d = f(E/n, \xi_i)$, where ξ_i — are particular concentrations of N_2, O_2, H_2 and H_2O, was calculated on the basis of Boltzmann equation for low-energy part of electron energy distribution function (EEDF) in the two-term approximation [14].

The equation for the quasi-steady-state EEDF for the mixture of l gases in electric field E may be written as follows [14]:

$$\begin{aligned} \frac{E^2\varepsilon}{3\sum\limits_l N_l\sigma_{m,l}(\varepsilon)} &+ \sum_l \frac{2m}{M_l}\cdot N_l\varepsilon^2\sigma_{m,l}(\varepsilon)\cdot\left\{f(\varepsilon)+\frac{T}{e}\frac{df(\varepsilon)}{d\varepsilon}\right\}+ \\ &+ \sum_l B_{el}\cdot N_l\varepsilon\sigma_{rot,l}(\varepsilon)\cdot\left\{f(\varepsilon)+\frac{T}{e}\frac{df(\varepsilon)}{d\varepsilon}\right\}= \\ &- \sum_l N_l\cdot\sum_{i,j}\int\limits_{\varepsilon}^{\varepsilon+\varepsilon_{ij}}\varepsilon\sigma_{l,i,j}(\varepsilon')\cdot\varepsilon' f(\varepsilon')d\varepsilon' \end{aligned} \tag{7.2}$$

where e, m, M are the charge, mass of electron and mass of neutrals; B_e is a rotational constant; $\sigma_m(\varepsilon)$, $\sigma_{rot}(\varepsilon)$ are the transport cross-section for electron scattering and cross-section for rotational levels excitation; ($\sigma_{ij}(\varepsilon)$ are th cross-section of nonequilibrium processes; T is a gas temperature.

It was necessary to take into account both change of the chemical composition of the mixture in the process of hydrogen conversion and change of the mixture pressure. It was supposed that the main components responsible for the EEDF formation are N_2, O_2, H_2 and H_2O. Processes taken into consideration for EEDF calculation are represented in the Table 7.1. Transport cross-sections were taken from [52, 44, 48].

On the basis of calculated v_d values and experimental data for the current density $j = I/S$ maximum density of electrons in the discharge was estimated: $n_e = j/(ev_d)$.

Reduced electric field values E/n and electron density n_e for initial mixture composition are plotted in Fig. 7.1 for different pressures. In the investigated range of parameters reduced electric field value after closing the discharge gap changes from $E/n = 800$ Td at low pressures to 400 Td at high ones.

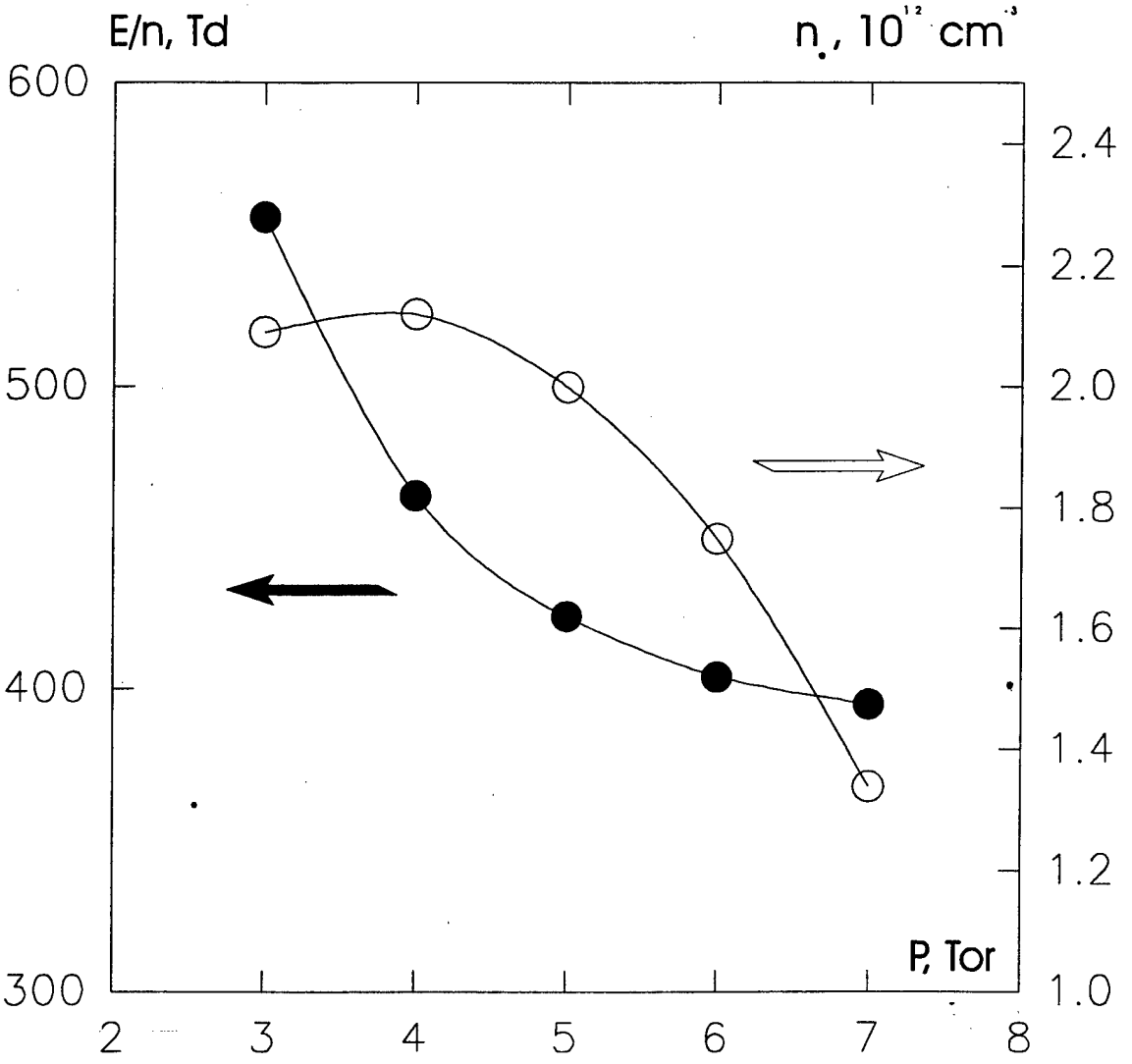

Figure 7.1: Maximum electron density and initial reduced electric field value in the discharge cell on the stage of a high-current discharge *vs* pressure.

Maximum electron density in the discharge lies in the range $n_e \simeq 1.3-2.2\times10^{12}$ cm^{-3}. This value is in a good agreement with the results of previous works [27, 32].

Energy branching in the mixture H_2-O_2-N_2 is shown in Fig. 7.2. The maximum energy

consumption at discharge electric field corresponds to the electronic degrees of freedom. This fact, as it will be shown below, defines the major role of process with electronically excited molecules in the process of hydrogen oxidation. Some smaller part of energy consumes for the dissociation and ionization, and the role of ionization increases with the reduced electric field. The excitation of the vibrational degrees of freedom in such a strong fields is quite poor.

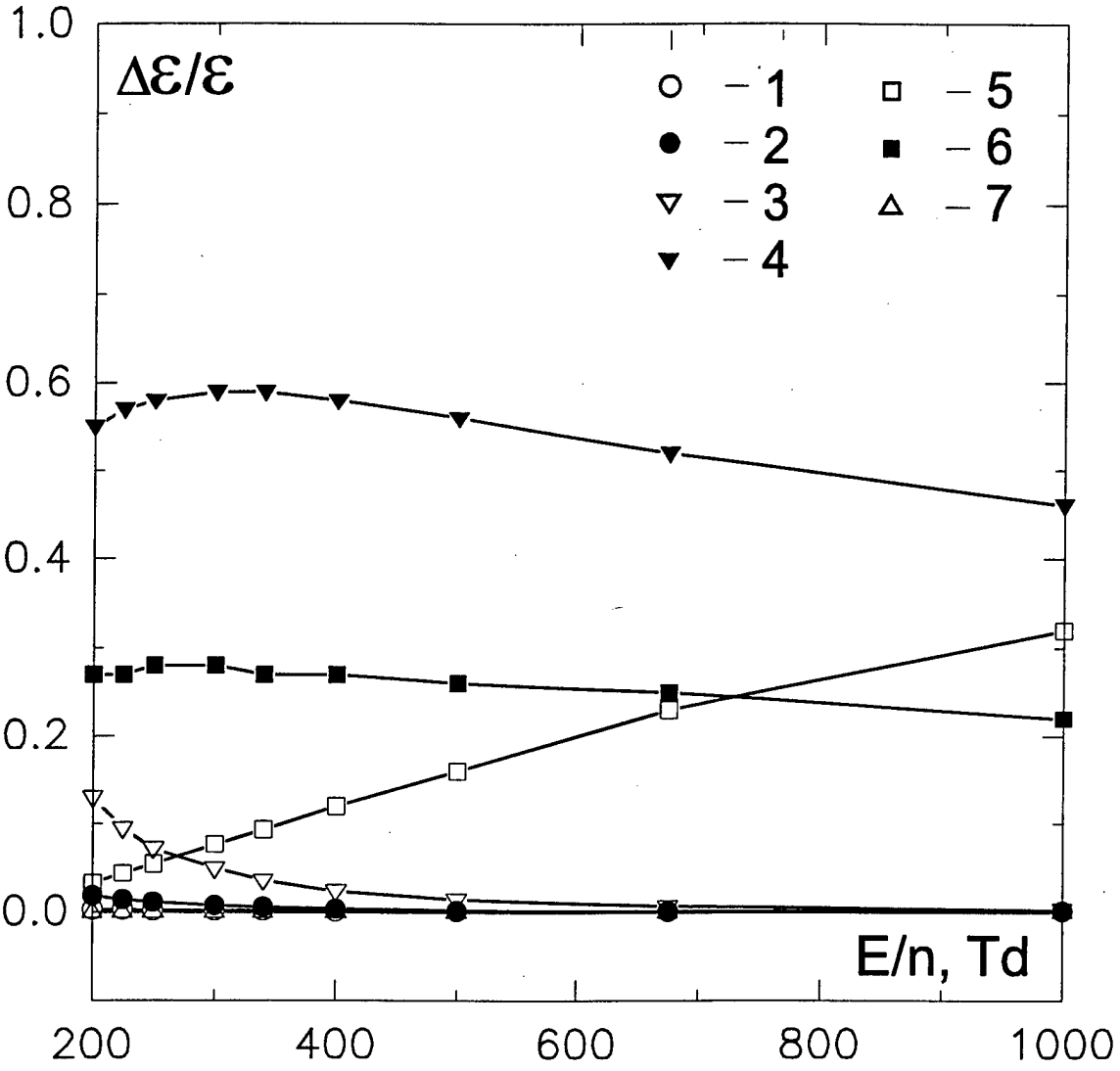

Figure 7.2: Energy branching in H_2-O_2-N_2 mixture. the numbers correspond to the energy consumption to different internal degrees of freedom: translational *1*, rotational *2*, vibrational *3*, electronic levels excitation *4*, ionization *5*, dissociation *6* and attachment *7*.

Table 7.1: Processes of a gas excitation by direct electron impact

Process			Ref.
H_2 excitation			
$e + H_2$	$\rightarrow$	$e + H_2(v = 1)$	[35]

Table 7.1: Processes of a gas excitation by direct electron impact

Process			Ref.
$e + H_2$	$\rightarrow$	$e + H_2(v = 2)$	[35]
$e + H_2$	$\rightarrow$	$e + H_2(v = 3)$	[35]
$e + H_2$	$\rightarrow$	$e + H_2(rot)$	[35]
$e + H_2$	$\rightarrow$	$e + H_2(d^3\Pi_u)$	[34]
$e + H_2$	$\rightarrow$	$e + H_2(a^3\Sigma_g^+)$	[34]
$e + H_2$	$\rightarrow$	$e + H_2(b^2\Sigma_g)$	[34]
$e + H_2$	$\rightarrow$	$e + H_2(c^3\Pi_u)$	[34]
$e + H_2$	$\rightarrow$	$e + H_2(B^{1\prime}\Sigma_u^+)$	[34]
$e + H_2$	$\rightarrow$	$e + H_2(B^1\Sigma_u^+)$	[34]
$e + H_2$	$\rightarrow$	$e + H_2(E^1\Sigma_g^+)$	[34]
$e + H_2$	$\rightarrow$	$e + H_2(C^1\Pi_u)$	[34]
$e + H_2$	$\rightarrow$	$e + H_2(e^3\Sigma_u^+)$	[34]
$e + H_2$	$\rightarrow$	$e + H + H$	[35]
$e + H_2$	$\rightarrow$	$e + e + H_2^+$	[35]
$e + H_2$	$\rightarrow$	$H^- + H$	[45]
N_2 excitation			
$e + N_2$	$\rightarrow$	$e + N_2(v = 1)$	[41]
$e + N_2$	$\rightarrow$	$e + N_2(v = 2)$	[41]
$e + N_2$	$\rightarrow$	$e + N_2(v = 3)$	[41]
$e + N_2$	$\rightarrow$	$e + N_2(v = 4)$	[41]
$e + N_2$	$\rightarrow$	$e + N_2(v = 5)$	[41]
$e + N_2$	$\rightarrow$	$e + N_2(v = 6)$	[41]
$e + N_2$	$\rightarrow$	$e + N_2(v = 7)$	[41]
$e + N_2$	$\rightarrow$	$e + N_2(v = 8)$	[41]
$e + N_2$	$\rightarrow$	$e + N_2(v = 9)$	[42]
$e + N_2$	$\rightarrow$	$e + N_2(v = 10)$	[42]
$e + N_2$	$\rightarrow$	$e + N_2(A^3\Sigma_u^+)$	[39]
$e + N_2$	$\rightarrow$	$e + N_2(B^3\Pi_g)$	[39]
$e + N_2$	$\rightarrow$	$e + N_2(C^3\Pi_u)$	[39]
$e + N_2$	$\rightarrow$	$e + N_2(W^1\Delta_u)$	[39]
$e + N_2$	$\rightarrow$	$e + N_2(W^3\Delta_u)$	[39]
$e + N_2$	$\rightarrow$	$e + N_2(a^{1\prime}\Sigma_u^-)$	[39]
$e + N_2$	$\rightarrow$	$e + N_2(a^1\Pi_g)$	[39]
$e + N_2$	$\rightarrow$	$e + N_2(a^{1\prime\prime}\Sigma_g)$	[39]
$e + N_2$	$\rightarrow$	$e + N_2(B^{13}\Sigma_u^-)$	[39]
$e + N_2$	$\rightarrow$	$e + N_2(B^1\Pi_u)$	[53]
$e + N_2$	$\rightarrow$	$e + N_2(E^3\Sigma_g^+)$	[39]
$e + N_2$	$\rightarrow$	$e + N_2(Rydber)$	[39]
$e + N_2$	$\rightarrow$	$N_2^- \rightarrow e + N(^4S^0) + N(^4S^0)$	[36]
$e + N_2$	$\rightarrow$	$N + N$	[37, 38]
$e + N_2$	$\rightarrow$	$e + e + N_2^+$	[57]
$e + N_2$	$\rightarrow$	$N(4s) + N^+(^3P) + e + e$	[55]

Table 7.1: Processes of a gas excitation by direct electron impact

Process			Ref.
$e + N_2(j=0)$	$\rightarrow$	$e + N_2(j=2,4,6,8)$	[40]
O_2 excitation			
$e + O_2(j_1)$	$\rightarrow$	$e + O_2(j_2)$	[43]
$e + O_2$	$\rightarrow$	$e + O_2(v=1)$	[45]
$e + O_2$	$\rightarrow$	$e + O_2(v=2)$	[45]
$e + O_2$	$\rightarrow$	$e + O_2(v=3)$	[45]
$e + O_2$	$\rightarrow$	$e + O_2(v=4)$	[45]
$e + O_2$	$\rightarrow$	$e + O_2(a^1\Delta_g)$	[43]
$e + O_2$	$\rightarrow$	$e + O_2(b^1\Sigma_g^+)$	[43]
$e + O_2$	$\rightarrow$	$e + O_2(B^3\Sigma_u^-)$	[43]
$e + O_2$	$\rightarrow$	$e + O_2(A^3\Sigma_u^+)$	[43]
$e + O_2$	$\rightarrow$	$e + O_2(C^3\Delta_u)$	[54]
$e + O_2$	$\rightarrow$	$e + O_2(9.9eV)$	[43]
$e + O_2$	$\rightarrow$	$e + O_2(Rydberg)$	[43]
$e + O_2$	$\rightarrow$	$O_2^-(X^2\Pi_g) \rightarrow O^-(^2P^0) + O(^3P)$	[56]
$e + O_2$	$\rightarrow$	$e + O + O$	[43]
$e + O_2$	$\rightarrow$	$e + O^+ + O^-$	[56]
$e + O_2$	$\rightarrow$	$e + e + O_2^+$	[57]
$e + O_2$	$\rightarrow$	$e + e + O(^3P) + O^+(^4S)$	[55]
H_2O excitation			
$e + H_2O$	$\rightarrow$	$H^- + OH$	[46]
$e + H_2O$	$\rightarrow$	$OH + H(^2P)$	[48, 49]
$e + H_2O$	$\rightarrow$	$e + H_2O(7\ eV)$	[48, 49]
$e + H_2O$	$\rightarrow$	$e + H_2O(14\ eV)$	[48, 49]
$e + H_20$	$\rightarrow$	$e + e + H_2O^+$	[57]
$e + H_2O$	$\rightarrow$	$e + e + OH^+ + H$	[47]
$e + H_2O$	$\rightarrow$	$e + H_2O(100+001)$	[48, 49]
$e + H_2O$	$\rightarrow$	$e + H_2O(010)$	[48, 49]

Table 7.2: Reactions between heavy particles included into kinetic scheme A – 1/s, cm^3/s, cm^6/s, E_a – K

Reaction			A^+	n^+	E_a^+, K	A^-	n^-	E_a^-, K	Ref$^+$	Ref$^-$
Ionization										
$N_2b(a'^1\Sigma_u^-)+N_2(A^3\Sigma_u^+)$	$\rightarrow$	$N_4^+ + e$	5.0-11	0.0	0.0	0.0	0.0	0.0	[58]	—
$N_2(a'^1\Sigma_u^-)+N_2(a'^1\Sigma_u^-)$	$\rightarrow$	$N_4^+ + e$	2.0-10	0.0	0.0	0.0	0.0	0.0	[58]	—
$N(^2D)+N(^2P)$	$\rightarrow$	$N_2^+ + e$	1.0-12	0.0	0.0	0.0	0.0	0.0	[58]	—
$N(^2P)+O$	$\rightarrow$	$NO^+ + e$	1.0-12	0.0	0.0	0.0	0.0	0.0	[58]	—
$N(^2P)+N(^2P)$	$\rightarrow$	$N_2^+ + e$	5.0-12	0.0	0.0	0.0	0.0	0.0	[45]	—
$N_2(a'^1\Sigma_u^-)+N_2(a'^1\Sigma_u^-)$	$\rightarrow$	$N_2+N_2^+ + e$	2.0-10	0.0	0.0	0.0	0.0	0.0	[59]	—
$N_2(a'^1\Sigma_u^-)+N_2(A^3\Sigma_u^+)$	$\rightarrow$	$N_2+N_2^+ + e$	5.0-11	0.0	0.0	0.0	0.0	0.0	[59]	—
Recombination										
$N_2^+ + e$	$\rightarrow$	N+N	6.06-6	-0.50	0.0	1.41-14	1.0	6.77+4	[60]	[61]
$NO^+ + e$	$\rightarrow$	N+O	2.54-15	0.37	3.20+3	1.10-12	0.0	3.19+4	[68]	[61]
$O_2^+ + e$	$\rightarrow$	O+O	4.29-6	-0.60	0.0	0.0	0.0	0.0	[69]	—
$N_4^+ + e$	$\rightarrow$	N_2+N_2	2.80-5	-0.50	0.0	0.0	0.0	0.0	[68]	—
$H_3^+ + e$	$\rightarrow$	$H+H_2$	4.0-6	-0.50	0.0	0.0	0.0	0.0	[68]	—
$H_2^+ + e$	$\rightarrow$	H+H	2.25-6	-0.40	0.0	0.0	0.0	0.0	[60]	—
$NH^+ + e$	$\rightarrow$	H+N	1.48-6	-0.50	0.0	0.0	0.0	0.0	[60]	—

Table 7.2: Reactions between heavy particles included into kinetic scheme A – 1/s, cm^3/s, cm^6/s, E_a – K

Reaction			A^+	n^+	E_a^+, K	A^-	n^-	E_a^-, K	Ref$^+$	Ref$^-$
$OH^+ + e$	→	$H + O$	1.30-6	-0.50	0.0	0.0	0.0	0.0	[60]	—
$H^+ + e$	→	H	2.28-10	-0.70	0.0	0.0	0.0	0.0	[69]	—
$N^+ + e$	→	N	1.73-10	-0.70	0.0	0.0	0.0	0.0	[69]	—
$N_2O_2^+ + e$	→	$NO + NO$	2.25-5	-0.50	0.0	0.0	0.0	0.0	[58]	—
$N_3O^+ + e$	→	$N_2 + NO$	2.25-5	-0.50	0.0	0.0	0.0	0.0	[58]	—
$NO_3^+ + e$	→	$NO + O_2$	2.25-5	-0.50	0.0	0.0	0.0	0.0	[58]	—
$N_2O_2^+ + e$	→	$N_2 + O_2$	2.25-5	-0.50	0.0	0.0	0.0	0.0	[58]	—
$NO_2^+ + e$	→	$NO + O$	3.46-6	-0.50	0.0	0.0	0.0	0.0	[58]	—
$N_2O^+ + e$	→	$N_2 + O$	3.46-6	-0.50	0.0	0.0	0.0	0.0	[58]	—
$N_3^+ + e$	→	$N + N_2$	3.46-6	-0.50	0.0	0.0	0.0	0.0	[58]	—
$N_2^+ + e + e$	→	$N_2 + e$	1.40-8	-4.50	0.0	0.0	0.0	0.0	[58]	—
$O_2^+ + e + e$	→	$O_2 + e$	1.40-8	-4.50	0.0	0.0	0.0	0.0	[58]	—
$NO^+ + e + e$	→	$NO + e$	1.40-8	-4.50	0.0	0.0	0.0	0.0	[58]	—
$N^+ + e + e$	→	$N + e$	1.40-8	-4.50	0.0	0.0	0.0	0.0	[58]	—
$O^+ + e + e$	→	$O + e$	1.40-8	-4.50	0.0	0.0	0.0	0.0	[58]	—
$N_2 + N_2^+ + e$	→	$N_2 + N_2$	9.35-21	-2.50	0.0	0.0	0.0	0.0	[58]	—
$N_2 + O_2^+ + e$	→	$N_2 + O_2$	9.35-21	-2.50	0.0	0.0	0.0	0.0	[58]	—
$N_2 + NO^+ + e$	→	$N_2 + NO$	9.35-21	-2.50	0.0	0.0	0.0	0.0	[58]	—
$N^+ + N_2 + e$	→	$N + N_2$	9.35-21	-2.50	0.0	0.0	0.0	0.0	[58]	—
$N_2 + O^+ + e$	→	$N_2 + O$	9.35-21	-2.50	0.0	0.0	0.0	0.0	[58]	—
$N_2^+ + O_2 + e$	→	$N_2 + O_2$	9.35-21	-2.50	0.0	0.0	0.0	0.0	[58]	—
$O_2 + O_2^+ + e$	→	$O_2 + O_2$	9.35-21	-2.50	0.0	0.0	0.0	0.0	[58]	—
$NO^+ + O_2 + e$	→	$NO + O_2$	9.35-21	-2.50	0.0	0.0	0.0	0.0	[58]	—
$N^+ + O_2 + e$	→	$N + O_2$	9.35-21	-2.50	0.0	0.0	0.0	0.0	[58]	—
$O^+ + O_2 + e$	→	$O + O_2$	9.35-21	-2.50	0.0	0.0	0.0	0.0	[58]	—
$H_3O^+ + e$	→	$H_2 + OH$	2.08-5	-0.50	0.0	0.0	0.0	0.0	[68]	—
$H_3^+ + e$	→	$H + H + H$	4.0-6	-0.50	0.0	0.0	0.0	0.0	[60]	—
$O_2^+ + e$	→	$O + O(^1S)$	1.93-7	-0.60	0.0	0.0	0.0	0.0	[69]	—
$O_2^+ + e$	→	$O + O(^1D)$	2.11-6	-0.60	0.0	0.0	0.0	0.0	[69]	—
$N_2^+ + e$	→	$N + N(^2D)$	3.46-6	-0.50	0.0	0.0	0.0	0.0	[58]	—
$NO^+ + e$	→	$N(^2D) + O$	9.0-5	-1.0	0.0	0.0	0.0	0.0	[58]	—
$N_2^+ + e$	→	$N + N_2(B^3\Pi_g)$	4.30-7	-0.50	0.0	0.0	0.0	0.0	[70]	—
$N_2^+ + e$	→	$N + N_2(A^3\Sigma_u^+)$	4.30-7	-0.50	0.0	0.0	0.0	0.0	[70]	—
Attachment										
$N_2 + O_2 + e$	→	$N_2 + O_2^-$	8.33-32	0.0	0.0	4.20-16	1.50	4.99+3	[61]	[61]
$O + O_2 + e$	→	$O + O_2^-$	2.76-32	0.0	0.0	1.0-16	1.50	5.33+3	[61]	[61]
$O_3 + e$	→	$O + O_2^-$	1.0-9	0.0	0.0	1.66-10	0.0	0.0	[58]	[61]
$O_3 + e$	→	$O^- + O_2$	1.0-11	0.0	0.0	5.0-15	0.0	0.0	[58]	[58]
$NO_2 + e$	→	$NO + O^-$	1.0-11	0.0	0.0	1.66-10	0.0	0.0	[58]	[61]
$N_2O + e$	→	$N_2 + O^-$	2.0-10	0.0	0.0	1.0-12	0.0	0.0	[58]	[71]
$O_2 + O_2 + e$	→	$O_2 + O_2^-$	4.0-30	0.0	0.0	9.0-15	1.50	4.99+3	[61]	[61]
$NO + NO + e$	→	$NO + NO^-$	7.80-26	-1.50	9.40+2	3.30-10	0.0	1.22+3	[72]	[72]
$N_2O + NO + e$	→	$N_2O + NO^-$	1.0-25	-1.50	9.70+2	4.30-10	0.0	1.24+3	[72]	[72]
$N_2 + O + e$	→	$N_2 + O^-$	5.51-30	-0.50	0.0	4.0-13	1.0	1.69+4	[61]	[61]
$H_2 + NO + e$	→	$H_2 + NO^-$	1.56-27	-1.50	6.80+2	6.30-12	0.0	9.60+2	[72]	[72]
$NH_4 + NO + e$	→	$NH_4 + NO^-$	5.20-26	-1.50	4.10+2	2.30-10	0.0	6.80+2	[72]	[72]
$NO + O_2 + e$	→	$NO + O_2^-$	2.76-32	0.0	0.0	1.0-16	1.50	5.33+3	[61]	[61]
$N_2 + N_2O + e$	→	$N_2 + N_2O^-$	3.50-39	2.0	0.0	0.0	0.0	0.0	[58]	—
$NO_2 + O_2 + e$	→	$NO_2^- + O_2$	3.0-28	0.0	0.0	0.0	0.0	0.0	[58]	—
$N_2 + NO_2 + e$	→	$N_2 + NO_2^-$	8.0-28	0.0	0.0	0.0	0.0	0.0	[58]	—
$N_2(A^3\Sigma_u^+) + O^-$	→	$N + NO + e$	1.0-10	0.0	0.0	0.0	0.0	0.0	[73]	—
$O^- + O_3$	→	$O_2 + O_2 + e$	5.0-10	0.0	0.0	0.0	0.0	0.0	[73]	—
$O + O_2 + e$	→	$O^- + O_2$	4.0-30	0.0	0.0	0.0	0.0	0.0	[61]	—
$O_2 + O_3 + e$	→	$O_2 + O_3^-$	3.97-30	0.0	0.0	0.0	0.0	0.0	[61]	—
$NO_2 + O + e$	→	$NO_2 + O^-$	8.33-31	0.0	0.0	0.0	0.0	0.0	[61]	—
$O + O + e$	→	$O + O^-$	8.33-31	0.0	0.0	0.0	0.0	0.0	[61]	—
$NO + O + e$	→	$NO + O^-$	8.33-31	0.0	0.0	0.0	0.0	0.0	[61]	—
Detachment										
$N + O^-$	→	$NO + e$	2.60-10	0.0	0.0	0.0	0.0	0.0	[58]	—
$NO_2^- + O$	→	$NO_3 + e$	1.0-12	0.0	0.0	0.0	0.0	0.0	[58]	—
$O + O^-$	→	$O_2 + e$	1.40-10	0.0	0.0	0.0	0.0	0.0	[61]	—
$N + O_2^-$	→	$NO_2 + e$	5.0-10	0.0	0.0	0.0	0.0	0.0	[71]	—
$H_2 + O^-$	→	$H_2O + e$	8.0-10	0.0	0.0	0.0	0.0	0.0	[71]	—
$H_2O + O^-$	→	$H_2O_2 + e$	6.0-13	0.0	0.0	0.0	0.0	0.0	[71]	—
$H + O_2^-$	→	$HO_2 + e$	1.20-9	0.0	0.0	0.0	0.0	0.0	[71]	—
$H^- + O_2$	→	$HO_2 + e$	1.20-9	0.0	0.0	0.0	0.0	0.0	[71]	—
$H + H^-$	→	$H_2 + e$	1.80-9	0.0	0.0	0.0	0.0	0.0	[71]	—
$OH^- + O$	→	$HO_2 + e$	1.80-9	0.0	0.0	0.0	0.0	0.0	[71]	—
$H + OH^-$	→	$H_2O + e$	1.0-9	0.0	0.0	0.0	0.0	0.0	[71]	—
$O^- + O_2(a^1\Delta_g)$	→	$O_3 + e$	4.0-9	0.0	0.0	0.0	0.0	0.0	[45]	—
$O_2(a^1\Delta_g) + O_2^-$	→	$O_2 + O_2 + e$	2.0-10	0.0	0.0	0.0	0.0	0.0	[72]	—
$O_2(b^1\Sigma_g^+) + O_2^-$	→	$O_2 + O_2 + e$	3.60-10	0.0	0.0	0.0	0.0	0.0	[72]	—
$N_2(A^3\Sigma_u^+) + O_2^-$	→	$N_2 + O_2 + e$	2.10-9	0.0	0.0	0.0	0.0	0.0	[72]	—
$N_2(a^1\Pi_g) + O_2^-$	→	$N_2 + O_2 + e$	2.50-9	0.0	0.0	0.0	0.0	0.0	[45]	—

Table 7.2: Reactions between heavy particles included into kinetic scheme A – 1/s, cm^3/s, cm^6/s, E_a – K

Reaction			A^+	n^+	E_a^+, K	A^-	n^-	E_a^-, K	Ref$^+$	Ref$^-$
$N_2(a'^1\Sigma_u^-)+O_2^-$	→	N_2+O_2+e	5.0-9	0.0	0.0	0.0	0.0	0.0	[45]	—
$N_2(B^3\Pi_g)+O_2^-$	→	N_2+O_2+e	2.50-9	0.0	0.0	0.0	0.0	0.0	[72]	—
$O^-+O_2(b^1\Sigma_g^+)$	→	$O+O_2+e$	6.90-10	0.0	0.0	0.0	0.0	0.0	[58]	—
$N_2(A^3\Sigma_u^+)+O^-$	→	N_2+O+e	2.20-9	0.0	0.0	0.0	0.0	0.0	[58]	—
$N_2(B^3\Pi_g)+O^-$	→	N_2+O+e	1.90-9	0.0	0.0	0.0	0.0	0.0	[58]	—
$O+O_3^-$	→	O_2+O_2+e	1.40-10	0.0	0.0	0.0	0.0	0.0	[61]	—
$N+O_2^-$	→	$NO+O+e$	4.0-10	0.0	0.0	0.0	0.0	0.0	[71]	—
Excitation	**and**	**Quenching**								
$O+O+O_2$	→	$O_2+O_2(a^1\Delta_g)$	2.45-31	-0.63	0.0	4.07	-2.50	4.80+4	[58]	[74]
$O+O+O_2$	→	$O_2+O_2(b^1\Sigma_g^+)$	2.45-31	-0.63	0.0	4.07	-2.50	4.03+4	[58]	[74]
N_2+O+O	→	$N_2+O_2(a^1\Delta_g)$	2.76-34	0.0	-7.20+2	4.07	-2.50	4.80+4	[58]	[74]
N_2+O+O	→	$N_2+O_2(b^1\Sigma_g^+)$	2.76-34	0.0	-7.20+2	4.07	-2.50	4.03+4	[58]	[74]
$N+N+O_2$	→	$N_2(A^3\Sigma_u^+)+O_2$	8.27-34	0.0	-5.0+2	3.80+5	-3.50	4.16+4	[58]	[74]
$N+N+N_2$	→	$N_2+N_2(A^3\Sigma_u^+)$	8.27-34	0.0	-5.0+2	3.80+5	-3.50	4.16+4	[58]	[74]
N_2+O+O	→	$N_2(A^3\Sigma_u^+)+O_2$	2.76-34	0.0	-7.20+2	2.54-12	0.0	0.0	[74]	[58]
$O_2(b^1\Sigma_g^+)+O_3$	→	$O_2(a^1\Delta_g)+O_3$	6.60-12	0.0	0.0	6.60-12	0.0	7.66+3	[75]	[70]
$N+N_2(A^3\Sigma_u^+)$	→	$N(^2P)+N_2$	5.0-11	0.0	0.0	4.0-11	0.0	0.0	[76]	[70]
$N_2+N_2(B^3\Pi_g)$	→	$N_2+N_2(A^3\Sigma_u^+)$	2.0-12	0.0	0.0	3.0-16	0.0	0.0	[77]	[76]
$N_2(B^3\Pi_g)+NO$	→	$N_2(A^3\Sigma_u^+)+NO$	2.40-10	0.0	0.0	2.40-10	0.0	1.37+4	[58]	[70]
$N_2+N_2(a'^1\Sigma_u^-)$	→	$N_2+N_2(B^3\Pi_g)$	2.0-13	0.0	0.0	2.0-13	0.0	1.22+4	[58]	[70]
N_2+O+O	→	$N_2(a'^1\Sigma_u^-)+O_2$	2.75-34	0.0	-7.20+2	2.80-11	0.0	0.0	[74]	[58]
$N+N_2+O$	→	$N_2(a'^1\Sigma_u^-)+NO$	1.76-31	-0.50	0.0	3.60-10	0.0	0.0	[74]	[58]
$N_2+N_2(C^3\Pi_u)$	→	$N_2+N_2(a'^1\Sigma_u^-)$	1.0-11	0.0	0.0	1.0-11	0.0	3.05+4	[58]	[70]
$O+O_2+O_2$	→	$O_2(b^1\Sigma_g^+)+O_3$	8.60-31	-1.25	0.0	1.80-11	0.0	0.0	[74]	[58]
$N_2+O_2(b^1\Sigma_g^+)$	→	$N_2+O_2(a^1\Delta_g)$	2.30-15	0.0	0.0	2.30-15	0.0	7.66+3	[58]	[70]
$O_2+O_2(b^1\Sigma_g^+)$	→	$O_2+O_2(a^1\Delta_g)$	1.50-16	0.0	0.0	1.50-16	0.0	7.66+3	[58]	[70]
$O+O_2(b^1\Sigma_g^+)$	→	$O+O_2(a^1\Delta_g)$	8.0-14	0.0	0.0	8.0-14	0.0	7.66+3	[58]	[70]
$NO+O_2(b^1\Sigma_g^+)$	→	$NO+O_2(a^1\Delta_g)$	5.0-15	0.0	0.0	5.0-15	0.0	7.66+3	[78]	[70]
$H_2+O_2(b^1\Sigma_g^+)$	→	$H_2+O_2(a^1\Delta_g)$	8.30-13	0.0	0.0	8.30-13	0.0	7.66+3	[78]	[70]
$N_2(A^3\Sigma_u^+)+N_2(A^3\Sigma_u^+)$	→	$N_2+N_2(B^3\Pi_g)$	1.10-9	0.0	0.0	1.10-9	0.0	5.79+4	[76]	[70]
$N_2(A^3\Sigma_u^+)+N_2(B^3\Pi_g)$	→	$N_2+N_2(C^3\Pi_u)$	4.60-10	0.0	0.0	4.60-10	0.0	2.89+4	[70]	[70]
$N_2+N_2(C^3\Pi_u)$	→	$N_2+N_2(B^3\Pi_g)$	3.30-11	0.0	0.0	3.30-11	0.0	4.27+4	[70]	[70]
$N(^2P)+N$	→	$N+N$	1.60-12	0.0	0.0	1.13-12	0.0	4.15+4	[70]	*
$N_2(B^3\Pi_g)+O_2$	→	$N_2(A^3\Sigma_u^+)+O_2(a^1\Delta_g)$	5.50-11	0.0	0.0	5.50-11	0.0	2.32+3	[79]	[70]
$N_2(B^3\Pi_g)+O_2$	→	$N_2(A^3\Sigma_u^+)+O_2$	5.50-11	0.0	0.0	5.50-11	0.0	1.37+4	[79]	[70]
$N+O_2(a^1\Delta_g)$	→	$NO+O$	2.0-14	0.0	6.0+2	0.0	0.0	0.0	[58]	—
$O+O_3$	→	$O_2+O_2(a^1\Delta_g)$	2.0-11	0.0	2.30+3	0.0	0.0	0.0	[58]	—
$N_2(A^3\Sigma_u^+)+NO$	→	N_2+NO	2.80-11	0.0	0.0	0.0	0.0	0.0	[76]	—
$N_2(B^3\Pi_g)+O_2$	→	N_2+O+O	3.0-10	0.0	0.0	0.0	0.0	0.0	[58]	—
$N_2(C^3\Pi_u)+O_2$	→	N_2+O+O	2.7-10	0.0	0.0	0.0	0.0	0.0	[102]	—
$N_2(A^3\Sigma_u^+)+O_2$	→	$N_2+O_2(b^1\Sigma_g^+)$	1.29-12	0.0	0.0	0.0	0.0	0.0	[58]	—
$N_2(C^3\Pi_u)+N_2$	→	N_2+N_2	9.0-12	0.0	0.0	0.0	0.0	0.0	[102]	—
$N_2(C^3\Pi_u)+H_2$	→	N_2+H_2	3.2-10	0.0	0.0	0.0	0.0	0.0	[102]	—
$N_2(C^3\Pi_u)+H_2O$	→	N_2+H_2O	3.9-10	0.0	0.0	0.0	0.0	0.0	[102]	—
$N_2(A^3\Sigma_u^+)+O$	→	N_2+O	2.10-11	0.0	0.0	0.0	0.0	0.0	[58]	—
$N+N_2(A^3\Sigma_u^+)$	→	$N+N_2$	5.0-11	0.0	0.0	0.0	0.0	0.0	[58]	—
$N_2+O_2(a^1\Delta_g)$	→	N_2+O_2	3.0-21	0.0	0.0	0.0	0.0	0.0	[78]	—
$O_2+O_2(a^1\Delta_g)$	→	O_2+O_2	3.0-18	0.80	0.0	0.0	0.0	0.0	[78]	—
$O+O_2(a^1\Delta_g)$	→	$O+O_2$	7.0-16	0.0	0.0	0.0	0.0	0.0	[58]	—
$NO+O_2(a^1\Delta_g)$	→	$NO+O_2$	2.50-11	0.0	0.0	0.0	0.0	0.0	[58]	—
$N_2(A^3\Sigma_u^+)+O_2$	→	N_2O+O	7.80-14	0.0	0.0	0.0	0.0	0.0	[58]	—
$N_2(A^3\Sigma_u^+)+O$	→	$N(^2D)+NO$	7.0-12	0.0	0.0	0.0	0.0	0.0	[58]	—
$N_2(A^3\Sigma_u^+)+N_2O$	→	$N+N_2+NO$	1.0-11	0.0	0.0	0.0	0.0	0.0	[58]	—
$N_2(A^3\Sigma_u^+)+N_2(A^3\Sigma_u^+)$	→	$N_2+N_2(C^3\Pi_u)$	5.54-4	-2.64	0.0	0.0	0.0	0.0	[80]	—
$N_2+N_2(A^3\Sigma_u^+)$	→	N_2+N_2	3.0-18	0.0	0.0	0.0	0.0	0.0	[58]	—
$N_2(A^3\Sigma_u^+)+O_2$	→	$N_2+O_2(a^1\Delta_g)$	1.29-12	0.0	0.0	0.0	0.0	0.0	[58]	—
$O_2+O_2(b^1\Sigma_g^+)$	→	O_2+O_2	4.0-17	0.0	0.0	0.0	0.0	0.0	[75]	—
$N_2(A^3\Sigma_u^+)+N_2^+$	→	$N+N_3^+$	3.0-10	0.0	0.0	0.0	0.0	0.0	[58]	—
$O_2(a^1\Delta_g)+O_4^+$	→	$O_2+O_2+O_2^+$	1.0-10	0.0	0.0	0.0	0.0	0.0	[58]	—
$O_2(b^1\Sigma_g^+)+O_4^+$	→	$O_2+O_2+O_2^+$	1.0-10	0.0	0.0	0.0	0.0	0.0	[58]	—
$O^-+O_2(a^1\Delta_g)$	→	$O+O_2^-$	1.0-10	0.0	0.0	0.0	0.0	0.0	[58]	—
$O_2(a^1\Delta_g)+O_4^-$	→	$O_2+O_2+O_2^-$	1.0-10	0.0	0.0	0.0	0.0	0.0	[58]	—
$O_2(b^1\Sigma_g^+)+O_4^-$	→	$O_2+O_2+O_2^-$	3.0-18	0.0	0.0	0.0	0.0	0.0	[78]	—
$H_2O+O_2(a^1\Delta_g)$	→	H_2O+O_2	4.50-18	0.0	0.0	0.0	0.0	0.0	[78]	—
$H_2+O_2(a^1\Delta_g)$	→	H_2+O_2	4.0-15	0.0	0.0	0.0	0.0	0.0	[78]	—
$O_2(a^1\Delta_g)+O_3$	→	O_2+O_3	2.0-17	0.0	0.0	0.0	0.0	0.0	[78]	—
$O_2(a^1\Delta_g)+O_2(a^1\Delta_g)$	→	$O_2+O_2(b^1\Sigma_g^+)$	3.40-11	0.0	0.0	0.0	0.0	0.0	[78]	—
$O(^1S)+O_2(a^1\Delta_g)$	→	$O+O+O$	2.30-15	0.0	0.0	0.0	0.0	0.0	[78]	—
$N_2+O_2(b^1\Sigma_g^+)$	→	N_2+O_2	6.70-12	0.0	0.0	0.0	0.0	0.0	[78]	—
$H_2O+O_2(b^1\Sigma_g^+)$	→	H_2O+O_2	7.90-13	0.0	0.0	0.0	0.0	0.0	[78]	—
$H_2+O_2(b^1\Sigma_g^+)$	→	H_2+O_2	1.80-11	0.0	0.0	0.0	0.0	0.0	[78]	—
$O_2(b^1\Sigma_g^+)+O_3$	→	O_2+O_3	8.0-14	0.0	0.0	0.0	0.0	0.0	[78]	—
$O+O_2(b^1\Sigma_g^+)$	→	$O+O_2$	1.30-10	0.0	0.0	0.0	0.0	0.0	[78]	—
$O(^1S)+O_2(a^1\Delta_g)$	→	$O+O_2(A^3\Sigma_u^+)$								

Table 7.2: Reactions between heavy particles included into kinetic scheme A – 1/s, cm^3/s, cm^6/s, E_a – K

Reaction			A^+	n^+	E_a^+, K	A^-	n^-	E_a^-, K	Ref$^+$	Ref$^-$
$N_2+N_2(a'^1\Sigma_u^-)$	→	N_2+N_2	6.0-14	0.0	0.0	0.0	0.0	0.0	[77]	—
$N+N+N_2$	→	$N_2+N_2(B^3\Pi_g)$	2.40-33	0.0	0.0	0.0	0.0	0.0	[77]	—
$N(^2D)+N+N_2$	→	$N_2+N_2(C^3\Pi_u)$	1.0-34	0.0	0.0	0.0	0.0	0.0	[70]	—
$N+N_2(B^3\Pi_g)$	→	$N(^2P)+N_2$	1.0-10	0.0	0.0	0.0	0.0	0.0	[70]	—
$N+N_2(C^3\Pi_u)$	→	$N(^2P)+N_2$	3.0-10	0.0	0.0	0.0	0.0	0.0	[70]	—
$N+N_2(a'^1\Sigma_u^-)$	→	$N(^2P)+N_2$	3.0-10	0.0	0.0	0.0	0.0	0.0	[70]	—
$O_2(a^1\Delta_g)+O_3$	→	$O+O_2+O_2$	5.20-11	0.0	2.84+3	0.0	0.0	0.0	[79]	—
$N_2(C^3\Pi_u)+O_2$	→	$N_2(A^3\Sigma_u^+)+O_2$	1.35-11	0.0	0.0	0.0	0.0	0.0	[79]	—
$N_2(C^3\Pi_u)+O_2$	→	$N_2+O+O(^1D)$	1.35-11	0.0	0.0	0.0	0.0	0.0	[79]	—
$O(^1S)+O_2(a^1\Delta_g)$	→	$O+O_2(a^1\Delta_g)$	2.75-10	0.0	0.0	0.0	0.0	0.0	[81]	—
$O(^1S)+O_2(a^1\Delta_g)$	→	$O(^2P)+O_2(a^1\Delta_g)$	2.75-10	0.0	0.0	0.0	0.0	0.0	[81]	—
$N_2+N_2(B^3\Pi_g)$	→	N_2+N_2	1.0-12	0.0	0.0	0.0	0.0	0.0	[76]	—
$N_2(C^3\Pi_u)$	→	$N_2(B^3\Pi_g)$	2.73+7	0.0	0.0	0.0	0.0	0.0	[82]	—
$N_2(B^3\Pi_g)$	→	$N_2(A^3\Sigma_u^+)$	1.25+5	0.0	0.0	0.0	0.0	0.0	[82]	—
$N_2(A^3\Sigma_u^+)$	→	N_2	5.26-1	0.0	0.0	0.0	0.0	0.0	[82]	—
$N_2(a'^1\Sigma_u^-)$	→	N_2	2.0	0.0	0.0	0.0	0.0	0.0	[82]	—
$N+N+N_2$	→	$N_2+N_2(A^3\Sigma_u^+)$	2.40-33	0.0	0.0	0.0	0.0	0.0	[83]	—
N_2+O+O	→	$N_2+O_2(A^3\Sigma_u^+)$	2.10-37	0.0	0.0	0.0	0.0	0.0	[84]	—
$N_2(A^3\Sigma_u^+)+O_2$	→	N_2+O_2	1.90-12	0.0	0.0	0.0	0.0	0.0	[76]	—
$N_2+N_2(C^3\Pi_u)$	→	N_2+N_2	5.0-11	0.0	0.0	0.0	0.0	0.0	[45]	—
$N_2(C^3\Pi_u)+O_2$	→	N_2+O_2	1.11-10	0.0	0.0	0.0	0.0	0.0	[45]	—
$N_2(C^3\Pi_u)+NO$	→	N_2+NO	2.0-11	0.0	0.0	0.0	0.0	0.0	[45]	—
$O(^1D)+O_2$	→	$O+O_2(a^1\Delta_g)$	1.0-12	0.0	0.0	0.0	0.0	0.0	[45]	—
O^-+O^+	→	$O+O(^5P)$	5.0-8	0.0	0.0	0.0	0.0	0.0	[69]	—
O^-+O^+	→	$O(^1D)+O(^5S)$	1.50-8	0.0	0.0	0.0	0.0	0.0	[69]	—
$N_2(A^3\Sigma_u^+)+NH_3$	→	N_2+NH_3	8.20-11	0.0	0.0	0.0	0.0	0.0	[76]	—
$N_2+N_2(a'^1\Sigma_u^-)$	→	$N_2+N_2(A^3\Sigma_u^+)$	2.0-13	0.0	0.0	0.0	0.0	0.0	[59]	—
$N+N+N_2$	→	$N_2+N_2(C^3\Pi_u)$	1.0-34	0.0	0.0	0.0	0.0	0.0	[70]	—
$N+N_2(B^3\Pi_g)$	→	$N+N_2(a'^1\Sigma_u^-)$	3.30-11	0.0	0.0	0.0	0.0	0.0	[85]	—
$N+N_2(B^3\Pi_g)$	→	$N+N_2(A^3\Sigma_u^+)$	1.0-10	0.0	0.0	0.0	0.0	0.0	[85]	—
$N+N_2(b^3\Sigma_u)$	→	$N+N_2(B^3\Pi_g)$	1.0-10	0.0	0.0	0.0	0.0	0.0	[85]	—
$N+N_2(C^3\Pi_u)$	→	$N+N_2(B^3\Pi_g)$	3.30-11	0.0	0.0	0.0	0.0	0.0	[85]	—
$N+N_2(W^3\Delta_u)$	→	$N+N_2(B^3\Pi_g)$	3.30-11	0.0	0.0	0.0	0.0	0.0	[85]	—
$N_2(B^3\Pi_g)$	→	$N_2(W^3\Delta_u)$	7.46+4	0.0	0.0	0.0	0.0	0.0	[53]	—
$N_2(b^3\Sigma_u)$	→	$N_2(B^3\Pi_g)$	2.20+4	0.0	0.0	0.0	0.0	0.0	[53]	—
$N_2(a^1\Pi_g)$	→	N_2	8.70+3	0.0	0.0	0.0	0.0	0.0	[53]	—
$N_2(w^1\Delta_u)$	→	N_2	4.0+3	0.0	0.0	0.0	0.0	0.0	[53]	—
$O(^1S)+O_2$	→	$O+O_2$	2.45-12	0.0	8.60+2	4.61-13	0.0	4.95+4	[81]	*
$O+O(^1S)$	→	$O+O$	2.50-11	0.0	3.10+2	8.49-12	0.0	4.88+4	[81]	*
$N(^2D)+O^+$	→	N^++O	1.30-10	0.0	0.0	6.39-11	0.0	1.76+4	[58]	*
$N_2O+O(^1D)$	→	$NO+NO$	7.20-11	0.0	0.0	1.06-12	0.0	4.09+4	[75]	*
$N_2O+O(^1D)$	→	N_2O+O	1.0-12	0.0	0.0	1.13-12	0.0	2.28+4	[75]	*
$H_2O+O(^1D)$	→	$OH+OH$	2.80-10	0.0	0.0	3.71-11	0.0	1.44+4	[86]	*
$H_2O+O(^1D)$	→	H_2O+O	2.80-10	0.0	0.0	3.16-10	0.0	2.28+4	[86]	*
$H_2+O(^1D)$	→	$H+OH$	1.10-10	0.0	0.0	5.30-11	0.0	2.18+4	[75]	*
$H_2+O(^1D)$	→	H_2+O	1.10-10	0.0	0.0	1.24-10	0.0	2.28+4	[75]	*
$H_2O+O(^1D)$	→	H_2+O_2	2.30-12	0.0	0.0	1.92-11	0.0	2.38+4	[75]	*
$O(^1S)+O_2(a^1\Delta_g)$	→	$O(^1D)+O_2(b^1\Sigma_g^+)$	3.60-11	0.0	0.0	3.60-11	0.0	1.80+3	[78]	[70]
$N(^2D)+O_2$	→	$NO+O$	4.30-13	0.50	0.0	2.85-13	0.50	4.37+4	[58]	*
$N(^2D)+NO$	→	N_2+O	7.0-11	0.0	0.0	3.64-10	0.0	6.55+4	[76]	*
$N(^2D)+N_2O$	→	N_2+NO	3.50-12	0.0	0.0	2.38-13	0.0	8.36+4	[76]	*
$N(^2D)+N_2$	→	$N+N_2$	6.0-15	0.0	0.0	7.33-15	0.0	2.77+4	[58]	*
$N(^2P)+O_2$	→	$NO+O$	2.60-12	0.0	0.0	9.96-13	0.0	5.75+4	[58]	*
$N(^2P)+NO$	→	N_2+O	3.40-11	0.0	0.0	1.02-10	0.0	7.93+4	[58]	*
$N(^2P)+N_2$	→	$N+N_2$	2.0-18	0.0	0.0	2.59-18	0.0	4.15+4	[58]	*
$N+N(^2P)$	→	$N+N(^2D)$	1.80-12	0.0	0.0	1.04-12	0.0	1.38+4	[58]	*
$O(^1D)+O_2$	→	$O+O_2(b^1\Sigma_g^+)$	1.70-5	-2.50	3.40+2	0.0	0.0	0.0	[45]	—
$O(^1D)+O_2$	→	$O+O_2$	3.20-11	0.0	-6.70+1	7.89-12	0.0	2.29+4	[87]	*
$N_2+O(^1D)$	→	N_2+O	3.20-11	0.0	1.07+2	3.61-11	0.0	2.29+4	[86]	*
$N_2O+O(^1D)$	→	N_2+O_2	7.40-11	0.0	0.0	8.53-12	0.0	6.27+4	[86]	*
$N_2(B'^3\Sigma_u^-)+N_2$	→	$N_2(B^3\Pi_g)+N_2$	1.0-11	0.0	0.0	0.0	0.0	0.0	[103, 104]	—
$H_2(d^3\Pi_u)$	→	$H_2(a^3\Sigma_g^+)$	1.5+7	0.0	0.0	0.0	0.0	0.0	[107]	—
$H_2(a^3\Sigma_g^+)$	→	$H+H$	9.6+7	0.0	0.0	0.0	0.0	0.0	[106]	—
$H_2(c^3\Pi_u)$	→	H_2	9.8+2	0.0	0.0	0.0	0.0	0.0	[108]	—
$H_2(B'^1\Sigma_u^+)$	→	H_2	1.0+8	0.0	0.0	0.0	0.0	0.0	[110]	—
$H_2(B^1\Sigma_u^+)$	→	H_2	1.2+9	0.0	0.0	0.0	0.0	0.0	[111]	—
$H_2(C^1\Pi_u^-)$	→	H_2	1.2+9	0.0	0.0	0.0	0.0	0.0	[111]	—
$O_2(B^3\Sigma_u^-)$	→	O_2	1.3+7	0.0	0.0	0.0	0.0	0.0	[106]	—
$H(^2P)$	→	H	2.0+8	0.0	0.0	0.0	0.0	0.0	[105]	—
$H(^4S)$	→	H	1.0+8	0.0	0.0	0.0	0.0	0.0	[105]	—
$N+O_2$	→	$NO+O$	1.59-12	0.50	3.70+3	5.31-15	1.	1.97+4	[61]	[61]
$N+O_3$	→	$NO+O_2$	3.32-14	0.0	2.93+2	2.21-15	0.0	6.34+4	[61]	*
$N+NO$	→	N_2+O	2.20-11	0.0	0.0	9.83-11	0.0	3.75+4	[61]	[61]
$N+NO_2$	→	N_2O+O	7.97-12	0.0	0.0	1.10-8	-1.0	2.11+4	[61]	[61]
$N+NO_2$	→	$NO+NO$	6.64-12	0.0	0.0	1.79-13	0.0	3.92+4	[61]	[61]
NO_2+O	→	$NO+O_2$	9.97-12	0.0	0.0	3.29-10	-0.50	2.36+4	[98]	[61]
$NO+O_3$	→	NO_2+O_2	8.0-13	0.0	1.20+3	1.10-12	0.0	2.51+4	[61]	[61]
$NO+NO_3$	→	NO_2+NO_2	1.70-11	0.0	0.0	4.50-10	0.0	1.85+4	[58]	[95]
$NO_2+NO_3+O_2$	→	$N_2O_5+O_2$	5.90-29	-1.27	0.0	1.74+8	-4.40	1.11+4	[58]	[75]

Table 7.2: Reactions between heavy particles included into kinetic scheme A – 1/s, cm^3/s, cm^6/s, E_a – K

Reaction	A^+	n^+	E_a^+, K	A^-	n^-	E_a^-, K	Ref$^+$	Ref$^-$
$N_2+NO_2+NO_3 \rightarrow N_2+N_2O_5$	5.90-29	-1.27	0.0	2.80+12	-6.10	1.11+4	[58]	[89]
$NO+NO_2+O_2 \rightarrow NO_2+NO_3$	0.0	0.0	-4.0+2	2.30-13	0.0	1.60+3	[89]	[58]
$N+N+N_2 \rightarrow N_2+N_2$	7.44-32	-0.50	0.0	8.17-7	-0.50	1.13+5	[61]	[61]
$NO+O+O_2 \rightarrow NO_2+O_2$	4.0-33	0.0	-9.70+2	2.61-7	0.0	3.63+4	[61]	[61]
$NO+NO_2+O \rightarrow NO_2+NO_2$	2.40-27	-1.80	0.0	7.30-8	0.0	3.30+4	[58]	[74]
$N+N+O_2 \rightarrow N_2+O_2$	3.0-32	-0.50	0.0	3.32-7	-0.50	1.13+5	[61]	[61]
$N+N+NO \rightarrow N_2+NO$	3.03-32	-0.50	0.0	3.32-7	-0.50	1.13+5	[61]	[61]
$N+N+N \rightarrow N+N_2$	3.31-27	-1.50	0.0	3.62-2	-1.50	1.13+5	[61]	[61]
$N+N+O \rightarrow N_2+O$	3.03-32	-0.50	0.0	3.32-7	-0.50	1.13+5	[61]	[61]
$N_2+O+O \rightarrow N_2+O_2$	9.18-31	-1.0	0.0	6.71-4	-1.50	5.95+4	[61]	[61]
$O+O+O_2 \rightarrow O_2+O_2$	4.08-30	-1.0	0.0	3.0-3	-1.50	5.95+4	[61]	[61]
$O+O+O \rightarrow O+O_2$	1.10-29	-1.0	0.0	8.0-3	-1.50	5.95+4	[61]	[61]
$N+O+O \rightarrow N+O_2$	8.27-33	-0.50	0.0	6.04-6	-1.0	5.95+4	[61]	[61]
$NO+O+O \rightarrow NO+O_2$	8.27-33	-0.50	0.0	6.04-6	-1.0	5.95+4	[61]	[61]
$N+N_2+O \rightarrow N_2+NO$	2.76-28	-1.50	0.0	6.74-4	-1.50	7.55+4	[61]	[61]
$N+O+O_2 \rightarrow NO+O_2$	2.76-28	-1.50	0.0	6.74-4	-1.50	7.55+4	[61]	[61]
$N+N+O \rightarrow N+NO$	5.51-27	-1.50	0.0	1.35-2	-1.50	7.55+4	[61]	[61]
$N+O+O \rightarrow NO+O$	5.51-27	-1.50	0.0	1.35-2	-1.50	7.55+4	[61]	[61]
$N+NO+O \rightarrow NO+NO$	5.51-27	-1.50	0.0	1.35-2	-1.50	7.55+4	[61]	[61]
$N_2+O+O_2 \rightarrow N_2+O_3$	3.50-35	0.0	-9.0+2	3.20-9	0.0	1.20+4	[61]	[61]
$O+O_2+O_3 \rightarrow O_3+O_3$	1.50-34	0.0	-7.50+2	7.70-9	0.0	1.20+4	[61]	[61]
$O+O_2+O_2 \rightarrow O_2+O_3$	4.10-35	0.0	-9.0+2	3.40-9	0.0	1.20+4	[61]	[61]
$O+O_3 \rightarrow O_2+O_2$	1.40-12	0.0	1.50+3	1.10-11	0.0	4.96+4	[61]	[61]
$N_2+NO+O \rightarrow N_2+NO_2$	4.0-33	0.0	-9.70+2	2.61-7	0.0	3.63+4	[61]	[61]
$NO+NO+NO \rightarrow N_2O+NO_2$	3.47-38	0.0	1.36+4	1.10-29	0.0	3.17+4	[89]	*
$HO_2+N_2+NO_2 \rightarrow HO_2NO_2+N_2$	2.10-31	0.0	0.0	5.0-6	0.0	1.0+4	[86]	[75]
$HO_2+NO \rightarrow OH+NO_2$	3.70-12	0.0	-2.40+2	3.0-11	0.0	3.36+3	[75]	[88]
$NH+NO \rightarrow OH+N_2$	4.20-12	0.0	0.0	1.70-11	0.0	4.69+4	[90]	*
$OH+NH \rightarrow H_2+NO$	2.60-12	0.60	7.55+2	8.44-11	0.60	3.53+4	[90]	*
$NH+O \rightarrow H+NO$	8.30-12	0.0	0.0	1.15-10	0.0	3.35+4	[90]	*
$NH+NH \rightarrow H_2+N_2$	6.60-13	0.55	9.57+2	8.69-11	0.55	8.24+4	[90]	*
$N+NH \rightarrow H+N_2$	1.77-11	0.0	0.0	5.69-10	0.0	7.13+4	[90]	*
$H+NH \rightarrow H_2+N$	1.70-12	0.68	9.57+2	6.96-12	0.68	1.11+4	[90]	*
$NH+O \rightarrow OH+N$	1.40-11	0.70	5.0+1	2.45-11	0.70	9.15+3	[90]	*
$OH+NH \rightarrow H_2O+N$	2.60-12	0.56	7.55+2	3.87-11	0.56	1.83+4	[90]	*
$OH+NH_2 \rightarrow H_2O+NH$	5.0-14	0.68	6.54+2	1.43-13	0.68	1.66+4	[90]	*
$NH_2+O \rightarrow OH+NH$	1.50-12	0.50	0.0	5.04-13	0.50	7.50+3	[90]	*
$H+NH_2 \rightarrow H_2+NH$	2.30-13	0.67	2.16+3	1.81-13	0.67	1.07+4	[90]	*
$NH_3+O \rightarrow OH+NH_2$	1.30-12	0.50	0.0	6.03-14	0.50	-2.88+3	[90]	*
$OH+NH_3 \rightarrow H_2O+NH_2$	6.60-14	0.68	5.54+2	2.60-14	0.68	6.07+3	[90]	*
$H+NH_3 \rightarrow H_2+NH_2$	3.20-13	0.67	1.72+3	3.48-14	0.67	-1.60+2	[90]	*
$NO+NO+O \rightarrow NO+NO_2$	2.40-27	-1.80	0.0	9.87-21	-1.80	3.62+4	[58]	*
$H_2+NO \rightarrow H+HNO$	2.30-11	0.0	2.84+4	3.0-11	0.0	5.0+2	[88]	[88]
$H+NO_2 \rightarrow OH+NO$	1.40-10	0.0	0.0	1.16-12	0.0	1.49+4	[88]	*
$HNO+O \rightarrow OH+NO$	3.0-11	0.0	0.0	9.69-12	0.0	2.67+4	[88]	*
$HNO+OH \rightarrow H_2O+NO$	8.0-11	0.0	5.0+2	2.20-10	0.0	3.56+4	[88]	*
$HNO+NO_2 \rightarrow HONO+NO$	1.0-12	0.0	1.0+3	1.25-12	0.0	1.59+4	[88]	*
$HNO+HNO \rightarrow H_2O+N_2O$	1.40-15	0.0	1.56+3	9.52-14	0.0	4.53+4	[88]	*
$HONO+O \rightarrow OH+NO_2$	2.0-11	0.0	3.0+3	5.18-12	0.0	1.48+4	[88]	*
$H+HONO \rightarrow H_2+NO_2$	2.10-14	1.0	6.80+1	1.27-14	1.0	1.29+4	[88]	*
$H+N_2O \rightarrow OH+N_2$	6.30-10	0.0	9.80+3	6.10-13	0.0	3.91+4	[99]	*
$OH+N_2O \rightarrow HO_2+N_2$	1.40-11	0.0	5.0+3	1.31-12	0.0	1.93+4	[88]	*
$H+NO \rightarrow OH+N$	4.40-10	0.0	2.54+4	4.90-11	0.0	0.0	[91]	[75]
$N_2+NO+O_2 \rightarrow N_2+NO_3$	1.41-26	-2.0	2.30+4	1.50-11	-2.0	2.32+4	[89]	[89]
$N_2O+N_2 \rightarrow N_2+O+N_2$	8.47-6	-1.12	3.00+4	5.02-38	0.0	0.0	[96, 101]	[112]
$N_2O+O \rightarrow N_2+O_2$	8.30-12	0.0	1.40+4	1.50-12	0.50	5.32+4	[97]	[61]
$N_2O+O \rightarrow NO+NO$	1.50-10	0.0	1.41+4	3.64-10	0.0	3.93+4	[97]	[61]
$NO+NO \rightarrow N_2+O_2$	5.64-3	-2.0	4.31+4	7.57	-2.50	6.46+4	[61]	[61]
$N_2O+NO \rightarrow N_2+NO_2$	4.17-10	0.0	2.52+4	1.91-10	0.0	4.19+4	[61]	*
$NO+NO+O_2 \rightarrow NO_2+NO_2$	2.0-38	0.0	0.0	3.32-12	0.0	1.36+4	[61]	[95]
$N_2O+NO+O \rightarrow N_2O+NO_2$	2.40-27	-1.80	0.0	9.87-21	-1.80	3.62+4	[58]	*
$N_2+NO_2+NO_2 \rightarrow N_2+N_2O_4$	9.0-28	-2.50	0.0	2.21-18	-2.50	6.45+3	[58]	*
$NO_2+NO_2+O_2 \rightarrow N_2O_4+O_2$	9.0-28	-2.50	0.0	2.21-18	-2.50	6.45+3	[58]	*
$N_2O_4+NO_2+NO_2 \rightarrow N_2O_4+N_2O_4$	9.0-28	-2.50	0.0	2.21-18	-2.50	6.45+3	[58]	*
$NO_2+NO_2+NO_2 \rightarrow N_2O_4+NO_2$	9.0-28	-2.50	0.0	2.21-18	-2.50	6.45+3	[58]	*
$N_2O_5+NO_2+NO_3 \rightarrow N_2O_5+N_2O_5$	5.90-29	-1.27	0.0	0.0	0.0	0.0	[58]	—
$NO+NO_2+NO_3 \rightarrow N_2O_5+NO$	5.90-29	-1.27	0.0	0.0	0.0	0.0	[58]	—
$N+NO_2 \rightarrow N_2+O_2$	7.0-13	0.0	0.0	0.0	0.0	0.0	[58]	—
$N+NO_2 \rightarrow N_2+O+O$	9.10-13	0.0	0.0	0.0	0.0	0.0	[58]	—
$NO_3+O \rightarrow NO_2+O_2$	1.0-11	0.0	0.0	0.0	0.0	0.0	[58]	—
$NO_2+O_3 \rightarrow NO_3+O_2$	1.20-13	0.0	2.45+3	0.0	0.0	0.0	[58]	—
$NO_3+NO_3 \rightarrow NO_2+NO_2+O_2$	5.0-12	0.0	3.0+3	0.0	0.0	0.0	[58]	—
$NO_2+O+O_2 \rightarrow NO_3+O_2$	7.10-27	-2.0	0.0	0.0	0.0	0.0	[58]	—
$N_2+NO_2+O \rightarrow N_2+NO_3$	7.10-27	-2.0	0.0	0.0	0.0	0.0	[58]	—
$N_3+O \rightarrow N_2+NO$	1.0-11	0.0	0.0	0.0	0.0	0.0	[89]	—
$N+N_3 \rightarrow N_2+N_2$	1.60-11	0.0	0.0	0.0	0.0	0.0	[89]	—
$N_3+N_3 \rightarrow N_2+N_2+N_2$	1.40-12	0.0	0.0	0.0	0.0	0.0	[89]	—
$OH+N_2+NO \rightarrow HONO+N_2$	5.73-25	-2.40	0.0	0.0	0.0	0.0	[86]	—
$OH+N_2+NO_2 \rightarrow HONO_2+N_2$	1.27-23	-2.70	0.0	0.0	0.0	0.0	[86]	—
$OH+HONO_2 \rightarrow H_2O+NO_3$	9.50-15	0.0	-7.78+2	0.0	0.0	0.0	[75]	—
$OH+NO_2+O_2 \rightarrow HONO_2+O_2$	3.36-23	-2.90	0.0	0.0	0.0	0.0	[75]	—
$HO_2NO_2+O_2 \rightarrow HO_2+NO_2+O_2$	3.60-6	0.0	1.0+4	0.0	0.0	0.0	[75]	—
$OH+O \rightarrow H+O_2$	8.47-12	0.0	-3.75+2	3.10-10	0.0	8.46+3	[99, 100]	[90]
$H+O_3 \rightarrow OH+O_2$	1.40-10	0.0	4.80+2	1.18-12	0.0	3.92+4	[86]	*
$H_2+OH \rightarrow H+H_2O$	4.20-10	0.0	5.03+3	1.58-10	0.0	1.02+4	[90]	[90]
$OH+OH \rightarrow H_2O+O$	4.20-12	0.0	2.40+2	2.49-14	1.14	8.69+3	[87]	[91]
$OH+OH+N_2 \rightarrow H_2O_2+N_2$	6.50-31	0.0	0.0	2.0-7	0.0	2.29+4	[86]	[91]
$OH+HO_2 \rightarrow H_2O+O_2$	4.60-11	0.0	-2.30+2	3.25-10	0.0	3.40+4	[87]	*
$OH+O_3 \rightarrow HO_2+O_2$	1.60-12	0.0	9.40+2	3.91-13	0.0	2.25+4	[87]	*

Table 7.2: Reactions between heavy particles included into kinetic scheme A – 1/s, cm^3/s, cm^6/s, E_a – K

Reaction			A^+	n^+	E_a^+, K	A^-	n^-	E_a^-, K	Ref$^+$	Ref$^-$
$OH+O_2+O_2$	→	HO_2+O_3	3.76-21	0.0	1.39+4	1.10-14	0.0	5.0+2	[70]	[58, 87]
H_2+O	→	$H+OH$	2.50-17	2.0	3.8+3	2.27-11	0.0	2.30+2	[92]	*
$H+H+H_2$	→	H_2+H_2	2.68-31	-0.60	0.0	2.14-26	-0.60	5.20+4	[91]	*
$H+H_2O+OH$	→	H_2O+H_2O	3.86-25	-2.0	0.0	1.12-19	-2.0	5.94+4	[91]	*
$H+OH+N_2$	→	H_2O+N_2	7.72-26	-2.0	0.0	3.30-8	0.0	5.29+4	[91]	[90]
$H+H_2+OH$	→	H_2+H_2O	7.72-26	-2.0	0.0	3.30-8	0.0	5.29+4	[91]	[90]
$H+N_2+O$	→	$OH+N_2$	1.66-31	0.0	-3.0+2	5.68-27	0.0	5.07+4	[91]	*
$H+H_2+O$	→	H_2+OH	6.64-32	0.0	-3.0+2	2.27-27	0.0	5.07+4	[91]	*
$H+H_2O+O$	→	H_2O+OH	4.32-31	0.0	-3.0+2	1.48-26	0.0	5.07+4	[91]	*
$H+HO_2$	→	$OH+OH$	4.15-10	0.0	9.50+2	1.69-11	0.0	1.82+4	[91]	*
H_2O_2+OH	→	H_2O+HO_2	3.30-12	0.0	2.0+2	9.69-12	0.0	1.79+4	[87]	*
$H+H_2O_2$	→	H_2O+OH	1.66-11	0.0	1.80+3	5.65-13	0.0	3.62+4	[91]	*
$H+O_2+O_2$	→	HO_2+O_2	1.77-29	-1.0	0.0	0.0	0.0	0.0	[75]	—
$H+HO_2$	→	H_2O+O	9.40-13	0.0	0.0	0.0	0.0	0.0	[86]	—
$H+N_2+O_2$	→	HO_2+N_2	1.80-29	-1.0	0.0	0.0	0.0	0.0	[86]	—
HO_2+O	→	$OH+O_2$	3.10-11	0.0	-2.0+2	0.0	0.0	0.0	[87]	—
H_2O_2+O	→	$OH+HO_2$	2.70-12	0.0	2.10+3	0.0	0.0	0.0	[86]	—
H_2O_2+O	→	H_2O+O_2	2.70-12	0.0	2.10+3	0.0	0.0	0.0	[86]	—
$H+H+N_2$	→	H_2+N_2	1.34-31	-0.60	0.0	0.0	0.0	0.0	[91]	—
$H+H+H_2O$	→	H_2+H_2O	1.34-30	-0.60	0.0	0.0	0.0	0.0	[91]	—
$H+HO_2$	→	H_2+O_2	4.15-11	0.0	3.50+2	0.0	0.0	0.0	[91]	—
$H+H_2O_2$	→	H_2+HO_2	2.82-12	0.0	1.90+3	0.0	0.0	0.0	[91]	—
HO_2+HO_2	→	$H_2O_2+O_2$	3.32-12	0.0	0.0	0.0	0.0	0.0	[91]	—
$H_2+H_2O_2$	→	$H_2+OH+OH$	5.0-7	0.0	2.29+4	0.0	0.0	0.0	[91]	—
$H_2O+H_2O_2$	→	$H_2O+OH+OH$	3.25-6	0.0	2.29+4	0.0	0.0	0.0	[91]	—
Charge transfer										
$N_2+N_2+N_2^+$	→	$N_2+N_4^+$	5.0-29	0.0	0.0	2.10-16	0.0	0.0	[58]	[58]
$O_2+O_2+O_2^+$	→	$O_2+O_4^+$	2.0-22	-3.20	0.0	2.67+4	-4.0	5.03+3	[58]	[58]
$N_2+N_2+O_2^+$	→	$N_2+N_2O_2^+$	8.10-26	-2.0	0.0	1.48+7	-5.30	2.36+3	[58]	[58]
$N_2+N_2+NO^+$	→	$N_2+N_3O^+$	1.60-20	-4.40	0.0	1.50+6	-5.40	2.45+3	[58]	[58]
N^++N_2+O	→	N_2+NO^+	1.0-29	0.0	0.0	1.58-23	0.0	1.37+5	[58]	**
N^++O+O_2	→	NO^++O_2	1.0-29	0.0	0.0	1.58-23	0.0	1.37+5	[58]	**
$N+N^++N_2$	→	$N_2+N_2^+$	1.0-29	0.0	0.0	1.40-11	0.0	0.0	[58]	[71]
$N+N^++O_2$	→	$N_2^++O_2$	1.0-29	0.0	0.0	5.68-24	0.0	1.01+5	[58]	**
N_2+O+O^+	→	$N_2+O_2^+$	1.0-29	0.0	0.0	3.92-24	0.0	7.77+4	[58]	**
$O+O^++O_2$	→	$O_2+O_2^+$	1.0-29	0.0	0.0	3.92-24	0.0	7.77+4	[58]	**
$N+N_2+O^+$	→	N_2+NO^+	1.0-29	0.0	0.0	3.45-24	0.0	1.27+5	[58]	**
$N+O^++O_2$	→	NO^++O_2	1.0-29	0.0	0.0	3.45-24	0.0	1.27+5	[58]	**
N^++O_2	→	$N+O_2^+$	2.30-10	0.0	0.0	4.49-10	0.0	2.84+4	[71]	**
N^++O_2	→	NO^++O	5.0-10	0.0	0.0	4.29-10	0.0	7.73+4	[71]	**
N^++O_2	→	$NO+O^+$	1.0-12	0.0	0.0	1.35-12	0.0	2.61+4	[71]	**
N^++O	→	$N+O^+$	5.0-10	0.0	0.0	2.20-9	0.0	1.09+4	[61]	[61]
N^++O_3	→	NO^++O_2	5.0-10	0.0	0.0	1.93-10	0.0	1.24+5	[58]	**
N^++NO	→	$N+NO^+$	8.0-10	0.0	0.0	4.65-9	0.0	6.13+4	[71]	**
N^++NO	→	N_2^++O	1.0-10	0.0	0.0	3.0-10	0.0	2.58+4	[61]	[61]
N^++NO	→	N_2+O^+	1.0-12	0.0	0.0	1.06-11	0.0	4.79+4	[71]	**
N_2+O^+	→	$N+NO^+$	3.0-12	0.0	0.0	1.10-12	0.0	1.22+4	[61]	[61]
O^++O_2	→	$O+O_2^+$	2.0-11	0.0	0.0	6.0-12	0.0	1.65+4	[61]	[61]
O^++O_3	→	$O_2+O_2^+$	1.0-10	0.0	0.0	9.63-12	0.0	6.54+4	[58]	**
$NO+O^+$	→	NO^++O	2.0-11	0.0	0.0	3.0-11	0.0	5.01+4	[61]	[61]
$NO+O^+$	→	$N+O_2^+$	3.0-12	0.0	0.0	4.34-12	0.0	2.30+3	[71]	**
N_2O+O^+	→	$NO+NO^+$	2.30-10	0.0	0.0	3.81-12	0.0	6.93+4	[58]	**
N_2O+O^+	→	$N_2+O_2^+$	2.0-11	0.0	0.0	8.74-13	0.0	5.82+4	[71]	**
$N_2^++O_2$	→	$N_2+O_2^+$	1.24-7	-1.35	0.0	2.68-7	-1.35	4.10+4	[71]	**
N_2^++O	→	$N+NO^+$	2.42-9	-0.50	0.0	6.71-9	-0.50	3.61+4	[93]	**
N_2^++O	→	N_2+O^+	7.0-12	0.0	0.0	3.54-11	0.0	2.27+4	[71]	**
N_2^++NO	→	N_2+NO^+	4.48-10	0.0	0.0	6.31-9	0.0	7.32+4	[61]	[61]
$N+N_2+NO^+$	→	$N_2^++N_2O$	1.24-16	0.0	1.66+4	4.0-10	0.0	0.0	[70]	[58, 71]
$N_2+O_2^+$	→	$NO+NO^+$	9.96-16	0.0	0.0	5.31-16	0.0	1.19+4	[61]	[61]
$N+O_2^+$	→	NO^++O	1.80-10	0.0	0.0	1.05-10	0.0	4.89+4	[71]	**
$NO+O_2^+$	→	NO^++O_2	9.13-10	0.0	0.0	7.31-9	0.0	3.36+4	[61]	[61]
$NO_2+O_2^+$	→	NO^++O_3	1.0-11	0.0	0.0	2.94-11	0.0	9.05+3	[71]	**
$N_2+O_4^+$	→	$N_2O_2^++O_2$	2.96-18	2.50	2.65+3	5.0-11	0.0	0.0	[58]	[58]
$O_2+O_2+O_2^-$	→	$O_2+O_4^-$	3.0-31	0.0	0.0	1.0-10	0.0	1.04+3	[71]	[58]
$N_2+O_2+O_2^-$	→	$N_2+O_4^-$	1.05-28	0.0	0.0	1.0-10	0.0	1.04+3	[58]	[58]
$O+O_2^-$	→	O^-+O_2	8.0-11	0.0	0.0	3.45-12	0.50	1.62+4	[61]	[61]
$NO_2+NO_2^-$	→	$NO+NO_3^-$	4.0-12	0.0	0.0	3.0-15	0.0	0.0	[58]	[58]
H^++O	→	$H+O^+$	3.80-10	0.0	0.0	2.30-11	0.50	0.0	[71]	[93]
$H_2+H_2^+$	→	$H+H_3^+$	2.10-9	0.0	0.0	6.63-9	0.0	2.0+4	[71]	**
$H^++H_2+H_2$	→	$H_2+H_3^+$	3.0-29	0.0	0.0	9.57-25	0.0	5.10+4	[71]	**
H^++NO	→	$H+NO^+$	1.90-9	0.0	0.0	2.62-9	0.0	5.09+4	[94]	**
N^++O^-	→	$N+O$	4.50-6	-0.50	0.0	5.78-6	-0.50	1.51+5	[69]	**
$O_2^-+O_2^+$	→	O_2+O_2	7.27-6	-0.50	0.0	1.25-5	-0.50	1.35+5	[69]	**
$N_2^++O_2^-$	→	N_2+O_2	2.77-6	-0.50	0.0	1.03-5	-0.50	1.76+5	[69]	**
O^-+O^+	→	$O+O$	4.68-6	-0.50	0.0	1.31-6	-0.50	1.41+5	[69]	**
$N^++N_2+O_2^-$	→	N_2+NO_2	3.10-19	-2.50	0.0	1.26-12	-2.50	2.15+5	[58]	**
H_2O+O^+	→	H_2O^++O	2.30-9	0.0	0.0	4.79-10	0.0	1.06+4	[71]	**

Table 7.2: Reactions between heavy particles included into kinetic scheme A – 1/s, cm^3/s, cm^6/s, E_a – K

Reaction			A^+	n^+	E_a^+, K	A^-	n^-	E_a^-, K	Ref$^+$	Ref$^-$
H_2+O^+	→	$H+OH^+$	2.0-9	0.0	0.0	4.46-10	0.0	8.0+3	[71]	**
H_2+OH^+	→	$H+H_2O^+$	1.50-9	0.0	0.0	2.17-9	0.0	9.0+3	[71]	**
$H_2^++H_2O$	→	$H_2+H_2O^+$	3.60-9	0.0	0.0	6.43-9	0.0	3.13+4	[71]	**
$H_2+N_2^+$	→	$H_2^++N_2$	2.0-11	0.0	0.0	1.18-11	0.0	2.0+3	[71]	**
$H_2O+N_2^+$	→	$H_2O^++N_2$	2.20-9	0.0	0.0	2.31-9	0.0	3.33+4	[71]	**
$N+N_2^+$	→	N^++N_2	1.0-11	0.0	0.0	1.11-11	0.0	1.26+4	[71]	**
N_2O+O^+	→	$N_2^++O_2$	2.0-11	0.0	0.0	4.05-13	0.0	1.72+4	[71]	**
N^++N_2O	→	N_2+NO^+	2.70-9	0.0	0.0	4.74-10	0.0	1.17+5	[71]	**
$NO+NO^+$	→	$N_2^++O_2$	1.83-13	0.0	5.15+4	3.0-14	0.0	0.0	[61]	[61]
$N+N_2+N_2^+$	→	$N_2+N_3^+$	9.0-30	0.0	4.0+2	0.0	0.0	0.0	[58]	—
$N^++N_2+N_2$	→	$N_2+N_3^+$	9.0-30	0.0	4.0+2	0.0	0.0	0.0	[58]	—
$N_2+NO^++O_2$	→	$N_2+NO_3^+$	3.0-31	0.0	0.0	0.0	0.0	0.0	[58]	—
$NO^++O_2+O_2$	→	$NO_3^++O_2$	9.0-32	0.0	0.0	0.0	0.0	0.0	[58]	—
NO_2+O^+	→	NO_2^++O	1.60-9	0.0	0.0	0.0	0.0	0.0	[58]	—
NO^++O_3	→	$NO_2^++O_2$	1.0-15	0.0	0.0	0.0	0.0	0.0	[58]	—
$NO+NO_2^+$	→	NO^++NO_2	2.90-10	0.0	0.0	0.0	0.0	0.0	[58]	—
$O+O_4^+$	→	$O_2^++O_3$	3.0-10	0.0	0.0	0.0	0.0	0.0	[58]	—
$N_2^++O_3$	→	$N_2+O+O_2^+$	1.0-10	0.0	0.0	0.0	0.0	0.0	[58]	—
$N_2O_5+NO^+$	→	$NO_2+NO_2+NO_2^+$	5.90-10	0.0	0.0	0.0	0.0	0.0	[58]	—
$N_3^++O_2$	→	$N+N_2+O_2^+$	2.30-11	0.0	0.0	0.0	0.0	0.0	[58]	—
N_3^++NO	→	$N+N_2+NO^+$	7.0-11	0.0	0.0	0.0	0.0	0.0	[58]	—
N_4^++O	→	$N_2+N_2+O^+$	2.50-10	0.0	0.0	0.0	0.0	0.0	[58]	—
$N+N_4^+$	→	$N^++N_2+N_2$	1.0-11	0.0	0.0	0.0	0.0	0.0	[58]	—
N_4^++NO	→	$N_2+N_2+NO^+$	4.0-10	0.0	0.0	0.0	0.0	0.0	[58]	—
$N_2O_5+O_2^+$	→	$NO_2^++NO_3+O_2$	8.80-10	0.0	0.0	0.0	0.0	0.0	[58]	—
$N_4^++O_2$	→	$N_2+N_2+O_2^+$	4.0-10	0.0	0.0	0.0	0.0	0.0	[71]	—
N_2O^++NO	→	N_2O+NO^+	2.90-10	0.0	0.0	0.0	0.0	0.0	[71]	—
$NO_2+O_2^+$	→	$NO_2^++O_2$	6.60-10	0.0	0.0	0.0	0.0	0.0	[71]	—
$N_2^++N_2O$	→	$N_2+N_2O^+$	5.0-10	0.0	0.0	0.0	0.0	0.0	[71]	—
$N_3^++O_2$	→	$N_2+NO_2^+$	6.0-11	0.0	0.0	0.0	0.0	0.0	[71]	—
$N+N_3^+$	→	$N_2+N_2^+$	2.70-12	0.0	0.0	0.0	0.0	0.0	[71]	—
N_3^++NO	→	$N_2+N_2O^+$	1.40-10	0.0	0.0	0.0	0.0	0.0	[71]	—
N_2O+O^+	→	N_2O^++O	1.60-9	0.0	0.0	0.0	0.0	0.0	[71]	—
$NO+O_4^+$	→	$NO^++O_2+O_2$	1.0-10	0.0	0.0	0.0	0.0	0.0	[58]	—
$O^-+O_2+O_2$	→	$O_2+O_3^-$	8.0-31	0.0	0.0	0.0	0.0	0.0	[71]	—
$N_2+O^-+O_2$	→	$N_2+O_3^-$	3.30-28	0.0	0.0	0.0	0.0	0.0	[58]	—
$N_2+N_2+O_3^-$	→	$N_2+N_2O_3^-$	1.50-31	0.0	0.0	0.0	0.0	0.0	[58]	—
$NO+O^-+O_2$	→	$NO_2^-+O_2$	3.97-29	0.0	0.0	0.0	0.0	0.0	[61]	—
N_2+NO+O^-	→	$N_2+NO_2^-$	2.04-32	0.0	0.0	0.0	0.0	0.0	[61]	—
$O_2^-+O_3$	→	$O_2+O_3^-$	4.0-10	0.0	0.0	0.0	0.0	0.0	[58]	—
$NO_2+O_2^-$	→	$NO_2^-+O_2$	7.16-10	0.0	0.0	0.0	0.0	0.0	[61]	—
$NO_3+O_2^-$	→	$NO_3^-+O_2$	5.0-10	0.0	0.0	0.0	0.0	0.0	[58]	—
$N_2O+O_2^-$	→	$N_2+O_3^-$	1.0-12	0.0	0.0	0.0	0.0	0.0	[58]	—
O^-+O_3	→	$O+O_3^-$	5.30-10	0.0	0.0	0.0	0.0	0.0	[58]	—
NO_2+O^-	→	NO_2^-+O	1.20-9	0.0	0.0	0.0	0.0	0.0	[58]	—
N_2O+O^-	→	$NO+NO^-$	2.0-10	0.0	0.0	0.0	0.0	0.0	[58]	—
N_2O+O^-	→	N_2O^-+O	2.0-12	0.0	0.0	0.0	0.0	0.0	[58]	—
$O+O_3^-$	→	$O_2+O_2^-$	3.20-10	0.0	0.0	0.0	0.0	0.0	[58]	—
$NO+O_3^-$	→	NO_3^-+O	1.0-11	0.0	0.0	0.0	0.0	0.0	[58]	—
$NO+O_3^-$	→	$NO_2^-+O_2$	9.96-12	0.0	0.0	0.0	0.0	0.0	[61]	—
$NO_2+O_3^-$	→	$NO_2^-+O_3$	7.0-10	0.0	0.0	0.0	0.0	0.0	[58]	—
$NO_2+O_3^-$	→	$NO_3^-+O_2$	2.0-11	0.0	0.0	0.0	0.0	0.0	[58]	—
$NO_3+O_3^-$	→	$NO_3^-+O_3$	5.0-10	0.0	0.0	0.0	0.0	0.0	[58]	—
NO^-+O_2	→	$NO+O_2^-$	5.0-10	0.0	0.0	0.0	0.0	0.0	[58]	—
NO^-+NO_2	→	$NO+NO_2^-$	7.40-16	0.0	0.0	0.0	0.0	0.0	[58]	—
N_2O+NO^-	→	$N_2+NO_2^-$	2.80-14	0.0	0.0	0.0	0.0	0.0	[58]	—
$NO_2^-+O_3$	→	$NO_3^-+O_2$	1.80-11	0.0	0.0	0.0	0.0	0.0	[58]	—
$NO_2^-+NO_3$	→	$NO_2+NO_3^-$	5.0-10	0.0	0.0	0.0	0.0	0.0	[58]	—
$N_2O_5+NO_2^-$	→	$NO+NO_3+NO_3^-$	7.0-10	0.0	0.0	0.0	0.0	0.0	[58]	—
$O+O_4^-$	→	$O_2+O_3^-$	4.0-10	0.0	0.0	0.0	0.0	0.0	[58]	—
$NO+O_4^-$	→	$NO_3^-+O_2$	2.50-10	0.0	0.0	0.0	0.0	0.0	[58]	—
$O+O_4^-$	→	$O^-+O_2+O_2$	3.0-10	0.0	0.0	0.0	0.0	0.0	[58]	—
$NO^-+NO_2^+$	→	$NO+NO_2$	8.83-6	-0.50	0.0	0.0	0.0	0.0	[69]	—
$NO_2^-+O_2^+$	→	NO_2+O_2	7.10-6	-0.50	0.0	0.0	0.0	0.0	[69]	—
$NO^++NO_3^-$	→	$NO+NO_3$	5.89-7	-0.50	0.0	0.0	0.0	0.0	[69]	—
$NO^++NO_2^-$	→	$NO+NO_2$	3.29-6	-0.50	0.0	0.0	0.0	0.0	[69]	—
H^-+H^+	→	$H+H$	6.75-6	-0.50	0.0	0.0	0.0	0.0	[69]	—
$N^++O_2^-$	→	$N+O_2$	3.46-6	-0.50	0.0	0.0	0.0	0.0	[58]	—
$O^++O_2^-$	→	$O+O_2$	3.46-6	-0.50	0.0	0.0	0.0	0.0	[58]	—
$NO^++O_2^-$	→	$NO+O_2$	3.46-6	-0.50	0.0	0.0	0.0	0.0	[58]	—

Table 7.2: Reactions between heavy particles included into kinetic scheme A – 1/s, cm^3/s, cm^6/s, E_a – K

Reaction			A^+	n^+	E_a^+, K	A^-	n^-	E_a^-, K	Ref$^+$	Ref$^-$
$NO_2^+ + O_2^-$	→	$NO_2 + O_2$	3.46-6	-0.50	0.0	0.0	0.0	0.0	[58]	—
$N_2O^+ + O_2^-$	→	$N_2O + O_2$	3.46-6	-0.50	0.0	0.0	0.0	0.0	[58]	—
$N_2^+ + O^-$	→	$N_2 + O$	3.46-6	-0.50	0.0	0.0	0.0	0.0	[58]	—
$O^- + O_2^+$	→	$O + O_2$	3.46-6	-0.50	0.0	0.0	0.0	0.0	[58]	—
$NO^+ + O^-$	→	$NO + O$	2.0-7	0.0	0.0	0.0	0.0	0.0	[61]	—
$NO_2^+ + O^-$	→	$NO_2 + O$	3.46-6	-0.50	0.0	0.0	0.0	0.0	[58]	—
$N_2O^+ + O^-$	→	$N_2O + O$	3.46-6	-0.50	0.0	0.0	0.0	0.0	[58]	—
$N_2^+ + O_3^-$	→	$N_2 + O_3$	3.46-6	-0.50	0.0	0.0	0.0	0.0	[58]	—
$O_2^+ + O_3^-$	→	$O_2 + O_3$	3.46-6	-0.50	0.0	0.0	0.0	0.0	[58]	—
$N^+ + O_3^-$	→	$N + O_3$	3.46-6	-0.50	0.0	0.0	0.0	0.0	[58]	—
$O^+ + O_3^-$	→	$O + O_3$	3.46-6	-0.50	0.0	0.0	0.0	0.0	[58]	—
$NO^+ + O_3^-$	→	$NO + O_3$	3.46-6	-0.50	0.0	0.0	0.0	0.0	[58]	—
$NO_2^+ + O_3^-$	→	$NO_2 + O_3$	3.46-6	-0.50	0.0	0.0	0.0	0.0	[58]	—
$N_2O^+ + O_3^-$	→	$N_2O + O_3$	3.46-6	-0.50	0.0	0.0	0.0	0.0	[58]	—
$N_2^+ + NO^-$	→	$N_2 + NO$	3.46-6	-0.50	0.0	0.0	0.0	0.0	[58]	—
$NO^- + O_2^+$	→	$NO + O_2$	3.46-6	-0.50	0.0	0.0	0.0	0.0	[58]	—
$N^+ + NO^-$	→	$N + NO$	3.46-6	-0.50	0.0	0.0	0.0	0.0	[58]	—
$NO^- + O^+$	→	$NO + O$	3.46-6	-0.50	0.0	0.0	0.0	0.0	[58]	—
$NO^- + NO^+$	→	$NO + NO$	3.46-6	-0.50	0.0	0.0	0.0	0.0	[58]	—
$N_2O^+ + NO^-$	→	$N_2O + NO$	3.46-6	-0.50	0.0	0.0	0.0	0.0	[58]	—
$N_2^+ + NO_2^-$	→	$N_2 + NO_2$	3.46-6	-0.50	0.0	0.0	0.0	0.0	[58]	—
$N^+ + NO_2^-$	→	$N + NO_2$	3.46-6	-0.50	0.0	0.0	0.0	0.0	[58]	—
$NO_2^- + O^+$	→	$NO_2 + O$	3.46-6	-0.50	0.0	0.0	0.0	0.0	[58]	—
$NO_2^- + NO_2^+$	→	$NO_2 + NO_2$	3.46-6	-0.50	0.0	0.0	0.0	0.0	[58]	—
$N_2O^+ + NO_2^-$	→	$N_2O + NO_2$	3.46-6	-0.50	0.0	0.0	0.0	0.0	[58]	—
$N_2^+ + NO_3^-$	→	$N_2 + NO_3$	3.46-6	-0.50	0.0	0.0	0.0	0.0	[58]	—
$NO_3^- + O_2^+$	→	$NO_3 + O_2$	3.46-6	-0.50	0.0	0.0	0.0	0.0	[58]	—
$N^+ + NO_3^-$	→	$N + NO_3$	3.46-6	-0.50	0.0	0.0	0.0	0.0	[58]	—
$NO_3^- + O^+$	→	$NO_3 + O$	3.46-6	-0.50	0.0	0.0	0.0	0.0	[58]	—
$NO_2^+ + NO_3^-$	→	$NO_2 + NO_3$	3.46-6	-0.50	0.0	0.0	0.0	0.0	[58]	—
$N_2O^+ + NO_3^-$	→	$N_2O + NO_3$	3.46-6	-0.50	0.0	0.0	0.0	0.0	[58]	—
$N_2^+ + N_2O^-$	→	$N_2 + N_2O$	3.46-6	-0.50	0.0	0.0	0.0	0.0	[58]	—
$N_2O^- + O_2^+$	→	$N_2O + O_2$	3.46-6	-0.50	0.0	0.0	0.0	0.0	[58]	—
$N^+ + N_2O^-$	→	$N + N_2O$	3.46-6	-0.50	0.0	0.0	0.0	0.0	[58]	—
$N_2O^- + O^+$	→	$N_2O + O$	3.46-6	-0.50	0.0	0.0	0.0	0.0	[58]	—
$N_2O^- + NO^+$	→	$N_2O + NO$	3.46-6	-0.50	0.0	0.0	0.0	0.0	[58]	—
$N_2O^- + NO_2^+$	→	$N_2O + NO_2$	3.46-6	-0.50	0.0	0.0	0.0	0.0	[58]	—
$N_2O^- + N_2O^+$	→	$N_2O + N_2O$	3.46-6	-0.50	0.0	0.0	0.0	0.0	[58]	—
$N_2 + O^+ + O_2^-$	→	$N_2 + O_3$	3.10-19	-2.50	0.0	0.0	0.0	0.0	[58]	—
$N_2 + NO^+ + O_2^-$	→	$N_2 + NO_3$	3.10-19	-2.50	0.0	0.0	0.0	0.0	[58]	—
$N^+ + O_2 + O_2^-$	→	$NO_2 + O_2$	3.10-19	-2.50	0.0	0.0	0.0	0.0	[58]	—
$O^+ + O_2 + O_2^-$	→	$O_2 + O_3$	3.10-19	-2.50	0.0	0.0	0.0	0.0	[58]	—
$NO^+ + O_2 + O_2^-$	→	$NO_3 + O_2$	3.10-19	-2.50	0.0	0.0	0.0	0.0	[58]	—
$N_2 + N_2^+ + O^-$	→	$N_2 + N_2O$	3.10-19	-2.50	0.0	0.0	0.0	0.0	[58]	—
$N_2 + O^- + O_2^+$	→	$N_2 + O_3$	3.10-19	-2.50	0.0	0.0	0.0	0.0	[58]	—
$N_2 + NO^+ + O^-$	→	$N_2 + NO_2$	3.10-19	-2.50	0.0	0.0	0.0	0.0	[58]	—
$N_2 + O^- + O^+$	→	$N_2 + O_2$	3.10-19	-2.50	0.0	0.0	0.0	0.0	[58]	—
$N^+ + N_2 + O^-$	→	$N_2 + NO$	3.10-19	-2.50	0.0	0.0	0.0	0.0	[58]	—
$N_2^+ + O^- + O_2$	→	$N_2O + O_2$	3.10-19	-2.50	0.0	0.0	0.0	0.0	[58]	—
$O^- + O_2 + O_2^+$	→	$O_2 + O_3$	3.10-19	-2.50	0.0	0.0	0.0	0.0	[58]	—
$NO^+ + O^- + O_2$	→	$NO_2 + O_2$	3.10-19	-2.50	0.0	0.0	0.0	0.0	[58]	—
$O^- + O^+ + O_2$	→	$O_2 + O_2$	3.10-19	-2.50	0.0	0.0	0.0	0.0	[58]	—
$N^+ + O^- + O_2$	→	$NO + O_2$	3.10-19	-2.50	0.0	0.0	0.0	0.0	[58]	—
$N_2^+ + O_4^-$	→	$N_2 + O_2 + O_2$	1.0-7	0.0	0.0	0.0	0.0	0.0	[58]	—
$O_2^+ + O_4^-$	→	$O_2 + O_2 + O_2$	1.0-7	0.0	0.0	0.0	0.0	0.0	[58]	—
$N^+ + O_4^-$	→	$N + O_2 + O_2$	1.0-7	0.0	0.0	0.0	0.0	0.0	[58]	—
$O^+ + O_4^-$	→	$O + O_2 + O_2$	1.0-7	0.0	0.0	0.0	0.0	0.0	[58]	—
$NO^+ + O_4^-$	→	$NO + O_2 + O_2$	1.0-7	0.0	0.0	0.0	0.0	0.0	[58]	—
$NO_2^+ + O_4^-$	→	$NO_2 + O_2 + O_2$	1.0-7	0.0	0.0	0.0	0.0	0.0	[58]	—
$N_2O^+ + O_4^-$	→	$N_2O + O_2 + O_2$	1.0-7	0.0	0.0	0.0	0.0	0.0	[58]	—
$N_2^+ + N_2O_3^-$	→	$N_2 + N_2 + O_3$	1.0-7	0.0	0.0	0.0	0.0	0.0	[58]	—
$N_2O_3^- + O_2^+$	→	$N_2 + O_2 + O_3$	1.0-7	0.0	0.0	0.0	0.0	0.0	[58]	—
$N^+ + N_2O_3^-$	→	$N + N_2 + O_3$	1.0-7	0.0	0.0	0.0	0.0	0.0	[58]	—
$N_2O_3^- + O^+$	→	$N_2 + O + O_3$	1.0-7	0.0	0.0	0.0	0.0	0.0	[58]	—
$N_2O_3^- + NO^+$	→	$N_2 + NO + O_3$	1.0-7	0.0	0.0	0.0	0.0	0.0	[58]	—
$N_2O_3^- + NO_2^+$	→	$N_2 + NO_2 + O_3$	1.0-7	0.0	0.0	0.0	0.0	0.0	[58]	—
$N_2O^+ + N_2O_3^-$	→	$N_2 + N_2O + O_3$	1.0-7	0.0	0.0	0.0	0.0	0.0	[58]	—
$N_2^+ + O_2^-$	→	$N + N + O_2$	1.0-7	0.0	0.0	0.0	0.0	0.0	[58]	—
$O_2^- + O_2^+$	→	$O + O + O_2$	1.0-7	0.0	0.0	0.0	0.0	0.0	[58]	—
$NO^+ + O_2^-$	→	$N + O + O_2$	1.0-7	0.0	0.0	0.0	0.0	0.0	[58]	—
$NO_2^+ + O_2^-$	→	$NO + O + O_2$	1.0-7	0.0	0.0	0.0	0.0	0.0	[58]	—

Table 7.2: Reactions between heavy particles included into kinetic scheme A – 1/s, cm^3/s, cm^6/s, E_a – K

Reaction			A^+	n^+	E_a^+, K	A^-	n^-	E_a^-, K	Ref$^+$	Ref$^-$
$N_2O^+ + O_2^-$	→	$N + NO + O_2$	1.0-7	0.0	0.0	0.0	0.0	0.0	[58]	—
$N_3^+ + O_2^-$	→	$N + N_2 + O_2$	1.0-7	0.0	0.0	0.0	0.0	0.0	[58]	—
$N_4^+ + O_2^-$	→	$N_2 + N_2 + O_2$	1.0-7	0.0	0.0	0.0	0.0	0.0	[58]	—
$O_2^- + O_4^+$	→	$O_2 + O_2 + O_2$	1.0-7	0.0	0.0	0.0	0.0	0.0	[58]	—
$N_3O^+ + O_2^-$	→	$N_2 + NO + O_2$	1.0-7	0.0	0.0	0.0	0.0	0.0	[58]	—
$NO_3^+ + O_2^-$	→	$NO + O_2 + O_2$	1.0-7	0.0	0.0	0.0	0.0	0.0	[58]	—
$N_2O_2^+ + O_2^-$	→	$NO + NO + O_2$	1.0-7	0.0	0.0	0.0	0.0	0.0	[58]	—
$N_2O_2^+ + O_2^-$	→	$N_2 + O_2 + O_2$	1.0-7	0.0	0.0	0.0	0.0	0.0	[58]	—
$N_2^+ + O^-$	→	$N + N + O$	1.0-7	0.0	0.0	0.0	0.0	0.0	[58]	—
$O^- + O_2^+$	→	$O + O + O$	1.0-7	0.0	0.0	0.0	0.0	0.0	[58]	—
$NO^+ + O^-$	→	$N + O + O$	1.0-7	0.0	0.0	0.0	0.0	0.0	[58]	—
$NO_2^+ + O^-$	→	$NO + O + O$	1.0-7	0.0	0.0	0.0	0.0	0.0	[58]	—
$N_2O^+ + O^-$	→	$N + NO + O$	1.0-7	0.0	0.0	0.0	0.0	0.0	[58]	—
$N_3^+ + O^-$	→	$N + N_2 + O$	1.0-7	0.0	0.0	0.0	0.0	0.0	[58]	—
$N_4^+ + O^-$	→	$N_2 + N_2 + O$	1.0-7	0.0	0.0	0.0	0.0	0.0	[58]	—
$O^- + O_4^+$	→	$O + O_2 + O_2$	1.0-7	0.0	0.0	0.0	0.0	0.0	[58]	—
$N_3O^+ + O^-$	→	$N_2 + NO + O$	1.0-7	0.0	0.0	0.0	0.0	0.0	[58]	—
$NO_3^+ + O^-$	→	$NO + O + O_2$	1.0-7	0.0	0.0	0.0	0.0	0.0	[58]	—
$N_2O_2^+ + O^-$	→	$NO + NO + O$	1.0-7	0.0	0.0	0.0	0.0	0.0	[58]	—
$N_2O_2^+ + O^-$	→	$N_2 + O + O_2$	1.0-7	0.0	0.0	0.0	0.0	0.0	[58]	—
$N_2^+ + O_3^-$	→	$N + N + O_3$	1.0-7	0.0	0.0	0.0	0.0	0.0	[58]	—
$O_2^+ + O_3^-$	→	$O + O + O_3$	1.0-7	0.0	0.0	0.0	0.0	0.0	[58]	—
$NO^+ + O_3^-$	→	$N + O + O_3$	1.0-7	0.0	0.0	0.0	0.0	0.0	[58]	—
$NO_2^+ + O_3^-$	→	$NO + O + O_3$	1.0-7	0.0	0.0	0.0	0.0	0.0	[58]	—
$N_2O^+ + O_3^-$	→	$N + NO + O_3$	1.0-7	0.0	0.0	0.0	0.0	0.0	[58]	—
$N_3^+ + O_3^-$	→	$N + N_2 + O_3$	1.0-7	0.0	0.0	0.0	0.0	0.0	[58]	—
$N_4^+ + O_3^-$	→	$N_2 + N_2 + O_3$	1.0-7	0.0	0.0	0.0	0.0	0.0	[58]	—
$O_3^- + O_4^+$	→	$O_2 + O_2 + O_3$	1.0-7	0.0	0.0	0.0	0.0	0.0	[58]	—
$N_3O^+ + O_3^-$	→	$N_2 + NO + O_3$	1.0-7	0.0	0.0	0.0	0.0	0.0	[58]	—
$NO_3^+ + O_3^-$	→	$NO + O_2 + O_3$	1.0-7	0.0	0.0	0.0	0.0	0.0	[58]	—
$N_2O_2^+ + O_3^-$	→	$NO + NO + O_3$	1.0-7	0.0	0.0	0.0	0.0	0.0	[58]	—
$N_2O_2^+ + O_3^-$	→	$N_2 + O_2 + O_3$	1.0-7	0.0	0.0	0.0	0.0	0.0	[58]	—
$N_2^+ + NO^-$	→	$N + N + NO$	1.0-7	0.0	0.0	0.0	0.0	0.0	[58]	—
$NO^- + O_2^+$	→	$NO + O + O$	1.0-7	0.0	0.0	0.0	0.0	0.0	[58]	—
$NO^- + NO^+$	→	$N + NO + O$	1.0-7	0.0	0.0	0.0	0.0	0.0	[58]	—
$NO^- + NO_2^+$	→	$NO + NO + O$	1.0-7	0.0	0.0	0.0	0.0	0.0	[58]	—
$N_2O^+ + NO^-$	→	$N + NO + NO$	1.0-7	0.0	0.0	0.0	0.0	0.0	[58]	—
$N_3^+ + NO^-$	→	$N + N_2 + NO$	1.0-7	0.0	0.0	0.0	0.0	0.0	[58]	—
$N_4^+ + NO^-$	→	$N_2 + N_2 + NO$	1.0-7	0.0	0.0	0.0	0.0	0.0	[58]	—
$NO^- + O_4^+$	→	$NO + O_2 + O_2$	1.0-7	0.0	0.0	0.0	0.0	0.0	[58]	—
$N_3O^+ + NO^-$	→	$N_2 + NO + NO$	1.0-7	0.0	0.0	0.0	0.0	0.0	[58]	—
$NO^- + NO_3^+$	→	$NO + NO + O_2$	1.0-7	0.0	0.0	0.0	0.0	0.0	[58]	—
$N_2O_2^+ + NO^-$	→	$NO + NO + NO$	1.0-7	0.0	0.0	0.0	0.0	0.0	[58]	—
$N_2O_2^+ + NO^-$	→	$N_2 + NO + O_2$	1.0-7	0.0	0.0	0.0	0.0	0.0	[58]	—
$N_2^+ + NO_2^-$	→	$N + N + NO_2$	1.0-7	0.0	0.0	0.0	0.0	0.0	[58]	—
$NO_2^- + O_2^+$	→	$NO_2 + O + O$	1.0-7	0.0	0.0	0.0	0.0	0.0	[58]	—
$NO^+ + NO_2^-$	→	$N + NO_2 + O$	1.0-7	0.0	0.0	0.0	0.0	0.0	[58]	—
$NO_2^- + NO_2^+$	→	$NO + NO_2 + O$	1.0-7	0.0	0.0	0.0	0.0	0.0	[58]	—
$N_2O^+ + NO_2^-$	→	$N + NO + NO_2$	1.0-7	0.0	0.0	0.0	0.0	0.0	[58]	—
$N_3^+ + NO_2^-$	→	$N + N_2 + NO_2$	1.0-7	0.0	0.0	0.0	0.0	0.0	[58]	—
$N_4^+ + NO_2^-$	→	$N_2 + N_2 + NO_2$	1.0-7	0.0	0.0	0.0	0.0	0.0	[58]	—
$NO_2^- + O_4^+$	→	$NO_2 + O_2 + O_2$	1.0-7	0.0	0.0	0.0	0.0	0.0	[58]	—
$N_3O^+ + NO_2^-$	→	$N_2 + NO + NO_2$	1.0-7	0.0	0.0	0.0	0.0	0.0	[58]	—
$NO_2^- + NO_3^+$	→	$NO + NO_2 + O_2$	1.0-7	0.0	0.0	0.0	0.0	0.0	[58]	—
$N_2O_2^+ + NO_2^-$	→	$NO + NO + NO_2$	1.0-7	0.0	0.0	0.0	0.0	0.0	[58]	—
$N_2O_2^+ + NO_2^-$	→	$N_2 + NO_2 + O_2$	1.0-7	0.0	0.0	0.0	0.0	0.0	[58]	—
$N_2^+ + NO_3^-$	→	$N + N + NO_3$	1.0-7	0.0	0.0	0.0	0.0	0.0	[58]	—
$NO_3^- + O_2^+$	→	$NO_3 + O + O$	1.0-7	0.0	0.0	0.0	0.0	0.0	[58]	—
$NO^+ + NO_3^-$	→	$N + NO_3 + O$	1.0-7	0.0	0.0	0.0	0.0	0.0	[58]	—
$NO_2^+ + NO_3^-$	→	$NO + NO_3 + O$	1.0-7	0.0	0.0	0.0	0.0	0.0	[58]	—
$N_2O^+ + NO_3^-$	→	$N + NO + NO_3$	1.0-7	0.0	0.0	0.0	0.0	0.0	[58]	—
$N_3^+ + NO_3^-$	→	$N + N_2 + NO_3$	1.0-7	0.0	0.0	0.0	0.0	0.0	[58]	—
$N_4^+ + NO_3^-$	→	$N_2 + N_2 + NO_3$	1.0-7	0.0	0.0	0.0	0.0	0.0	[58]	—
$NO_3^- + O_4^+$	→	$NO_3 + O_2 + O_2$	1.0-7	0.0	0.0	0.0	0.0	0.0	[58]	—
$N_3O^+ + NO_3^-$	→	$N_2 + NO + NO_3$	1.0-7	0.0	0.0	0.0	0.0	0.0	[58]	—
$NO_3^- + NO^+$	→	$NO + NO_3 + O_2$	1.0-7	0.0	0.0	0.0	0.0	0.0	[58]	—
$N_2O_2^+ + NO_3^-$	→	$NO + NO + NO_3$	1.0-7	0.0	0.0	0.0	0.0	0.0	[58]	—
$N_2O_2^+ + NO_3^-$	→	$N_2 + NO_3 + O_2$	1.0-7	0.0	0.0	0.0	0.0	0.0	[58]	—
$N_2^+ + N_2O^-$	→	$N + N + N_2O$	1.0-7	0.0	0.0	0.0	0.0	0.0	[58]	—
$N_2O^- + O_2^+$	→	$N_2O + O + O$	1.0-7	0.0	0.0	0.0	0.0	0.0	[58]	—

Table 7.2: Reactions between heavy particles included into kinetic scheme A – 1/s, cm^3/s, cm^6/s, E_a – K

Reaction			A^+	n^+	E_a^+, K	A^-	n^-	E_a^-, K	Ref$^+$	Ref$^-$
$N_2O^-+NO^+$	→	$N+N_2O+O$	1.0-7	0.0	0.0	0.0	0.0	0.0	[58]	—
$N_2O^-+NO_2^+$	→	$N_2O+NO+O$	1.0-7	0.0	0.0	0.0	0.0	0.0	[58]	—
$N_2O^-+N_2O^+$	→	$N+N_2O+NO$	1.0-7	0.0	0.0	0.0	0.0	0.0	[58]	—
$N_2O^-+N_3^+$	→	$N+N_2+N_2O$	1.0-7	0.0	0.0	0.0	0.0	0.0	[58]	—
$N_2O^-+N_4^+$	→	$N_2+N_2+N_2O$	1.0-7	0.0	0.0	0.0	0.0	0.0	[58]	—
$N_2O^-+O_4^+$	→	$N_2O+O_2+O_2$	1.0-7	0.0	0.0	0.0	0.0	0.0	[58]	—
$N_2O^-+N_3O^+$	→	N_2+N_2O+NO	1.0-7	0.0	0.0	0.0	0.0	0.0	[58]	—
$N_2O^-+NO_3^+$	→	$N_2O+NO+O_2$	1.0-7	0.0	0.0	0.0	0.0	0.0	[58]	—
$N_2O^-+N_2O_2^+$	→	$N_2O+NO+NO$	1.0-7	0.0	0.0	0.0	0.0	0.0	[58]	—
$N_2O^-+N_2O_2^+$	→	$N_2+N_2O+O_2$	1.0-7	0.0	0.0	0.0	0.0	0.0	[58]	—
N_2O+O^+	→	$N+NO^++O$	2.30-10	0.0	0.0	0.0	0.0	0.0	[71]	—
$NH_3+O_2^+$	→	$NH_3^++O_2$	2.40-9	0.0	0.0	0.0	0.0	0.0	[71]	—
H_2O+OH^+	→	H_2O^++OH	1.60-10	0.0	0.0	0.0	0.0	0.0	[71]	—
$O_2+O_2^+$	→	$O+O_3^+$	1.20-10	0.0	0.0	0.0	0.0	0.0	[71]	—
$H_2+O_2^+$	→	$H+HO_2^+$	4.0-11	0.0	0.0	0.0	0.0	0.0	[71]	—
$H_2O+O_4^+$	→	$H_2O_3^++O_2$	1.20-10	0.0	0.0	0.0	0.0	0.0	[71]	—
$N_2O+O_4^+$	→	$N_2O_3^++O_2$	2.50-10	0.0	0.0	0.0	0.0	0.0	[71]	—
$H_2^++O_2$	→	$H+HO_2^+$	1.90-9	0.0	0.0	0.0	0.0	0.0	[71]	—
$H_3^++O_2$	→	$H_2+HO_2^+$	1.30-10	0.0	0.0	0.0	0.0	0.0	[71]	—
$H_2O+O^-+O_2$	→	$H_2O_2^-+O_2$	1.30-28	0.0	0.0	0.0	0.0	0.0	[71]	—
$H_2O+O_2+O_2^-$	→	$H_2O_3^-+O_2$	2.20-28	0.0	0.0	0.0	0.0	0.0	[71]	—
$H+O_2^-$	→	OH^-+O	1.20-9	0.0	0.0	0.0	0.0	0.0	[71]	—
$H+O_2^-$	→	H^-+O_2	1.20-9	0.0	0.0	0.0	0.0	0.0	[71]	—
$H_2O+N_4^+$	→	$H_2O^++N_2+N_2$	1.90-9	0.0	0.0	0.0	0.0	0.0	[71]	—
$H_2O+H_3^+$	→	$H_2+H_3O^+$	5.90-9	0.0	0.0	0.0	0.0	0.0	[71]	—
H_2O+OH^+	→	H_3O^++O	1.50-9	0.0	0.0	0.0	0.0	0.0	[71]	—
$H_2+H_2O^+$	→	$H+H_3O^+$	1.40-9	0.0	0.0	0.0	0.0	0.0	[71]	—
$N_3^++O_2$	→	N_2+NO^++O	1.0-10	0.0	0.0	0.0	0.0	0.0	[71]	—
$NO_2+NO_2^+$	→	NO^++NO_3	4.60-10	0.0	0.0	0.0	0.0	0.0	[71]	—
$NO+NO+NO^+$	→	$N_2O_2^++NO$	5.0-30	0.0	0.0	0.0	0.0	0.0	[71]	—
$O+O_2+O_2^-$	→	$O_2+O_3^-$	1.50-31	0.0	0.0	0.0	0.0	0.0	[61]	—
$NO+NO+O^-$	→	$NO+NO_2^-$	2.04-31	0.0	0.0	0.0	0.0	0.0	[61]	—
$NO+O+O^-$	→	NO_2^-+O	2.04-31	0.0	0.0	0.0	0.0	0.0	[61]	—

)* – If it is not specified, the relative efficiency of collision partners in the three-body reactions was given as $k_{Ar} = 1.5 \times k_{N_2} = 1.5 \times k_{O_2} = 3 \times k_{H_2} = 20 \times k_{H_2O} = 3 \times k_{NO} = 5 \times k_O = 5 \times k_H = 5 \times k_N$ (see [92]).

** From the principle of detailed equilibrium.

7.2 The afterglow of the discharge

The kinetic scheme consists of 813 processes; 98 components are taken into account, including excited and charged particles, electrons, radicals and neutral components (see Table 7.2).

The processes included into kinetic scheme are associative and Penning ionization, recombination of positive ions and electrons, electron attachment and detachment, interaction between neutral unexcited components, interaction between neutral unexcited and neutral exited components, conversion of positive and negative ions, recombination of positive and negative ions.

It was assumed that reactions of excitation by an electron impact are important only for the time of discharge (first 25 ns).

To calculate reaction rates with a participation of vibrationally-excited reagents we use a model described in the chapter 6 of the Report.

For example, a reaction

$$H_2(v) + O \rightarrow OH + H,$$

like all other processes with vibrationally excited reagents, is represented as a set of elementary reactions of the type

$$H_2(v=0) + O \rightarrow OH(w=0) + H$$
$$H_2(v=1) + O \rightarrow OH(w=0) + H$$
$$H_2(v=0) + O \rightarrow OH(w=1) + H$$
$$\cdot$$
$$\cdot$$
$$\cdot$$
$$H_2(v=i) + O \rightarrow OH(w=j) + H$$

7.3 Reaction rates for VV and VT — relaxation in a reacting H_2-O_2-N_2 system

In the present work at a modelling of the chemical reactions in the H_2-O_2-N_2 system level-to level kinetics of vibrational energy exchange between H_2, O_2, N_2, OH and H_2O has been taken into account. Reaction rates $k_{n,n-1}^{n'-1,n'}(T)$ and $k_{n,n-1}(T)$ similarly to the reaction constant rate for the molecular nitrogen in the frameworks of the SSH theory.

For H_2O molecule relaxation of symmetrical, antisymmetrical and a deformation mode were assumed to be independent and were described by the same model. Energy exchange between the modes was described taken into account an anharmonism of the vibrations. At this mode mixing at high vibrational levels [162] may be taken as an effective increase of a VV'-exchange rate constant.

In such a consideration a hypothetical effect of a VT-relaxation acceleration on high vibrational levels because of anharmonicity of vibrations is not taken into account in principle. This effect may lead to a depletion of H_2O molecules vibrational distribution function on upper levels. But as far as H_2O molecule is a main product of practically irreversible at $T = 300$ K reaction, some increase in H_2O decay connected with possible understated value of VT-relaxation of upper levels does not influence on the results.

In this case the total energy exchange diagram may be represented as an energy flux due to eV, VT, VV, EV, VV'-exchanges, active particle loss in dissociation process, recombination flux on the highest vibrational levels, and vibrational energy release/loss in bimolecular exchange reactions (Fig.7.3).

The constant rates of a vibrational relaxation (for low levels) from reviews [176, 179, 117, 180] which are used in the present work are represented below (Tables 7.3,7.4,7.5).

Table 7.3: VT-processes

Process			$\lg(k, [\mathrm{cm}^3/\mathrm{s}])$
$H_2O(100)+O_2$	$\rightarrow$	H_2O+O_2	-13.24
$H_2O(100)+N_2$	$\rightarrow$	H_2O+N_2	-13.24
$H_2O(100)+H_2O$	$\rightarrow$	H_2O+H_2O	-8.84
$H_2O(100)+H_2$	$\rightarrow$	H_2O+H_2	-5.82
$H_2O(010)+O_2$	$\rightarrow$	H_2O+O_2	-8.76
$H_2O(010)+N_2$	$\rightarrow$	H_2O+N_2	-8.76
$H_2O(010)+H_2O$	$\rightarrow$	H_2O+H_2O	-5.84
$H_2O(010)+H_2$	$\rightarrow$	H_2O+H_2	-5.06
$H_2O(010)+OH$	$\rightarrow$	H_2O+OH	-5.84
$H_2O(010)+H$	$\rightarrow$	H_2O+H	-4.72
$H_2O(010)+O$	$\rightarrow$	H_2O+O	-6.84
$H_2O(001)+O_2$	$\rightarrow$	H_2O+O_2	-14.38
$H_2O(001)+N_2$	$\rightarrow$	H_2O+N_2	-14.38
$H_2O(001)+H_2O$	$\rightarrow$	H_2O+H_2O	-9.95
$H_2O(001)+H_2$	$\rightarrow$	H_2O+H_2	-6.66
$H_2(1)+H_2$	$\rightarrow$	H_2+H_2	-18.12
$H_2(1)+H_2O$	$\rightarrow$	H_2+H_2O	-18.76
$H_2(1)+OH$	$\rightarrow$	H_2+OH	-18.76
$H_2(1)+N_2$	$\rightarrow$	H_2+N_2	-19.22
$H_2(1)+O_2$	$\rightarrow$	H_2+O_2	-19.22
$H_2(1)+O$	$\rightarrow$	H_2+O	-11.65
$H_2(1)+H$	$\rightarrow$	H_2+H	-12.52
$N_2(1)+N_2$	$\rightarrow$	N_2+N_2	-26.49
$N_2(1)+N$	$\rightarrow$	N_2+N	-28.60
$N_2(1)+O_2$	$\rightarrow$	N_2+O_2	-26.49
$N_2(1)+H_2$	$\rightarrow$	N_2+H_2	-15.88
$N_2(1)+OH$	$\rightarrow$	N_2+OH	-15.88
$N_2(1)+H$	$\rightarrow$	N_2+H	-15.38
$N_2(1)+O$	$\rightarrow$	N_2+O	-14.48
$N_2(1)+H_2O$	$\rightarrow$	N_2+H_2O	-14.17
$O_2(1)+O_2$	$\rightarrow$	O_2+O_2	-16.92
$O_2(1)+H_2$	$\rightarrow$	O_2+H_2	-15.56
$O_2(1)+H$	$\rightarrow$	O_2+H	-15.33
$O_2(1)+O$	$\rightarrow$	O_2+O	-17.33
$O_2(1)+H_2O$	$\rightarrow$	O_2+H_2O	-16.22
$O_2(1)+OH$	$\rightarrow$	O_2+OH	-16.22
$O_2(1)+N_2$	$\rightarrow$	O_2+N_2	-16.82
$OH(1)+H_2$	$\rightarrow$	$OH+H_2$	-15.91
$OH(1)+H_2O$	$\rightarrow$	$OH+H_2O$	-15.91

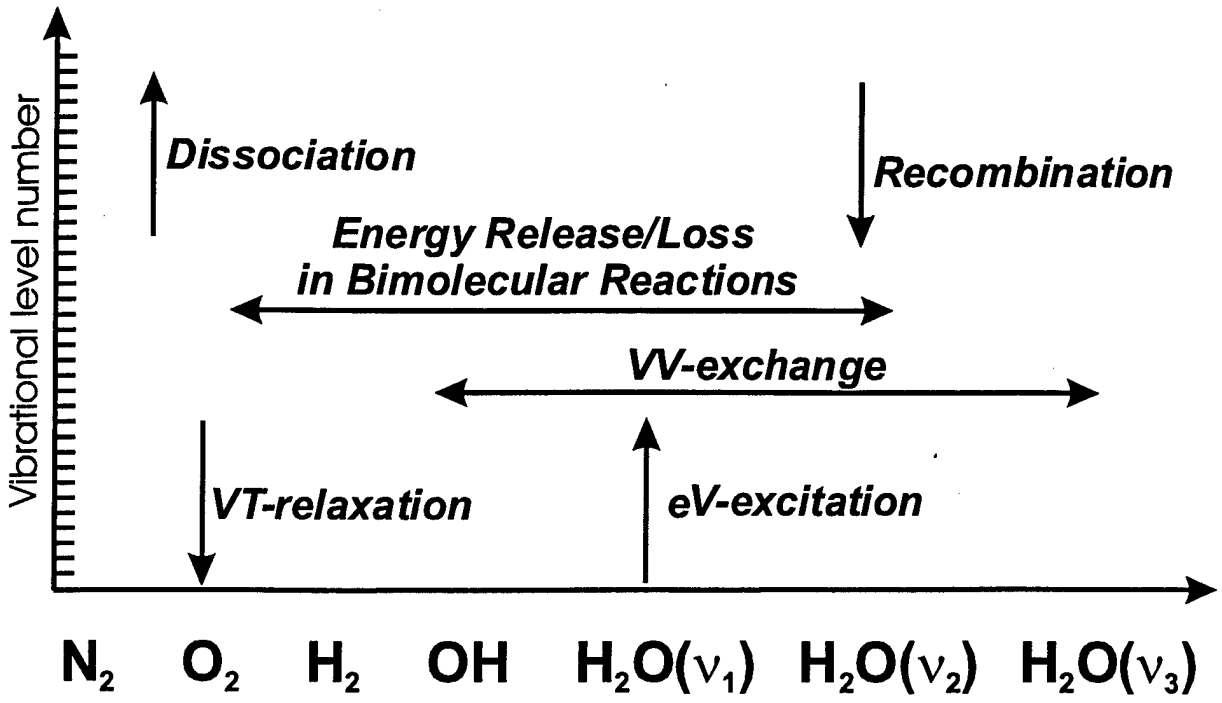

Figure 7.3: Vibrational energy exchange diagram. H_2-air mixture.

Table 7.4: VV-processes

Process			$\lg(k, [\mathrm{cm}^3/\mathrm{s}])$
$N_2(1)+N_2$	$\rightarrow$	$N_2+N_2(1)$	-13.06
$O_2(1)+O_2$	$\rightarrow$	$O_2+O_2(1)$	-12.58
$H_2(1)+H_2$	$\rightarrow$	$H_2+H_2(1)$	-12.56
$OH(1)+OH$	$\rightarrow$	$OH+OH(1)$	-12.57
$N_2(1)+H_2O$	$\rightarrow$	$N_2+H_2O(010)$	-15.30
$O_2+H_2O(010)$	$\rightarrow$	$O_2(1)+H_2O$	-12.09
$OH+H_2O(001)$	$\rightarrow$	$OH(1)+H_2O$	-11.59
$H_2(1)+H_2O$	$\rightarrow$	$H_2+H_2O(001)$	-11.59
$H_2(1)+OH$	$\rightarrow$	$H_2+OH(1)$	-11.59
$N_2+H_2(1)$	$\rightarrow$	$N_2(1)+H_2$	-14.68
$N_2(1)+O_2$	$\rightarrow$	$N_2+O_2(1)$	-17.70

Table 7.5: VV'-processes

Process			$\lg(k, [\mathrm{cm}^3/\mathrm{s}])$
$H_2O(100)+H_2O$	$\rightarrow$	$H_2O+H_2O(100)$	-7.50
$H_2O(010)+H_2O$	$\rightarrow$	$H_2O+H_2O(010)$	-7.50
$H_2O(001)+H_2O$	$\rightarrow$	$H_2O+H_2O(001)$	-7.50
$H_2O(100)+H_2O$	$\rightarrow$	$H_2O+H_2O(020)$	-7.20
$H_2O+H_2O(001)$	$\rightarrow$	$H_2O(100)+H_2O$	-6.41

Table 7.6: Electron detachment processes with a participation of vibrationally excited molecules

$O^- + N_2(v)$	$\rightarrow$	$O + N_2(w) + e$
$O_2^- + O_2(v)$	$\rightarrow$	$O_2 + O_2(w) + e$
$O_2^- + N_2(v)$	$\rightarrow$	$O_2 + N_2(w) + e$

Table 7.7: Electron-vibrational conversion

$H_2(v) + O_2(a^1\Delta_g)$	$\rightarrow$	$H_2 + O_2(b^1\Sigma_g^+)$
$N_2(v) + N_2(n)$	$\rightarrow$	$N_2 + N_2(a^{1\prime}\Sigma_u^-)$
$N_2(A^3\Sigma_u^+) + N_2(v)$	$\rightarrow$	$N_2(B^3\Pi_g) + N_2$
$N_2(B^3\Pi_g) + N_2(v)$	$\rightarrow$	$N_2(A^3\Sigma_u^+) + N_2(w)$
$N_2(v) + N_2(n)$	$\rightarrow$	$N_2(A^3\Sigma_u^+) + N_2$
$N_2(v) + N_2(n)$	$\rightarrow$	$N_2(B^3\Pi_g) + N_2$

7.4 Numerical modelling of a chemical kinetics in the pulsed nanosecond discharge afterglow with a consideration of vibrationally nonequilibrium processes

At modelling of the H_2 oxidization processes in an air under the pulsed nanosecond discharge following processes with vibrationally excited components were taken into account: (Tables. 7.6, 7.7, 7.8, 7.9, 7.10). The inverse processes were also considered.

7.5 Analysis of the main processes in the discharge and in the afterglow

Calculations were performed directly for each pulse taking into account changes in chemical composition of the mixture from pulse to pulse.

The comparison of kinetic curves for concentration of $H_2(a^3\Sigma_g^+)$ molecule at different pressures obtained from the experiment and from the calculation is represented in Fig. 7.4. Data in Fig. 7.4.1 correspond to the pressure $p = 3$ Torr and, consequently, to the maximum reduced electric field value. It is clearly seen that calculated concentration of excited hydrogen molecules nearly 1.5 times lower than experimentally measured one,

Table 7.8: Ionization processes

$N_2(a^{1\prime\prime}\Sigma_g) + N_2(v)$	$\rightarrow$	$N_4^+ + e$
$N_2(A^3\Sigma_u^+) + N_2(v)$	$\rightarrow$	$N_4^+ + e$

Table 7.9: Exchange reactions

$H_2(v) + N$	$\rightarrow$	$NH + H$
$H_2(v) + O_2(n)$	$\rightarrow$	$HO_2 + H$
$H_2(v) + O_2(n)$	$\rightarrow$	$OH(w) + OH(m)$
$H_2(v) + O$	$\rightarrow$	$OH(w) + H$
$H_2(v) + OH(n)$	$\rightarrow$	$H_2O(w_1, w_2, w_3) + H$
$N_2(v) + O$	$\rightarrow$	$NO + N$
$O_2(v) + H$	$\rightarrow$	$OH(w) + O$
$O_2(v) + N$	$\rightarrow$	$NO + O$
$OH(v) + H$	$\rightarrow$	$H_2(w) + O$
$OH(v) + N$	$\rightarrow$	$NH + O$
$OH(v) + NO$	$\rightarrow$	$NO_2 + H$
$OH(v) + O$	$\rightarrow$	$O_2(w) + H$
$OH(v) + OH(n)$	$\rightarrow$	$H_2O + O(^1D)$
$OH(v) + OH(n)$	$\rightarrow$	$H_2O(w_1, w_2, w_3) + O$
$OH(v) + OH(n)$	$\rightarrow$	$HO_2 + H$

Table 7.10: Reactions of a monomolecular destruction

$H_2O(v_1, v_2, v_3) + M$	$\rightarrow$	$H + OH + M$
$H_2(v) + M$	$\rightarrow$	$H + H + M$
$OH(v) + M$	$\rightarrow$	$H + O + M$
$O_2(v) + M$	$\rightarrow$	$O + O + M$
$N_2(v) + M$	$\rightarrow$	$N + N + M$

in spite of the fact that time of hydrogen conversion is in a good agreement with the measured time (see Fig.4.1). Really, in high fields the accuracy of Boltzmann equation solution is violated. This especially reflects on the constant rates of high-energy electron levels population ($H_2(a^3\Sigma_g^+)$). At the same time we can describe correctly the population of low-energy level $N_2(B^3\Pi_g)$, and, consequently, atomic oxygen conversion in reaction

$$N_2(B^3\Pi_g) + O_2 \rightarrow N_2 + O + O \tag{7.3}$$

which is responsible for molecular hydrogen conversion in the system.

Beginning from the pressure $p = 4$ Torr quite a good coincidence both for absolute value of $H_2(a^3\Sigma_g^+)$ -level concentration (Fig. 4.2) and for the conversion time (Fig. 4.1) is demonstrated. A good agreement of calculated and measured profiles of the $H_2(a^3\Sigma_g^+)$ concentration (Fig. 7.4.2-7.4.5) allows to conclude that the process of excitation may be described with the aid of proposed kinetic scheme using the two-term approximation of the Boltzmann equation on the stage of the electric breakdown.

7.6 The excitation of vibrational levels of molecules in the discharge and an energy exchange in conditions of chemically-nonequilibrium H_2-O_2-N_2 mixtures

Vibrational distributions for different molecules in the discharge afterglow are represented in Figures 7.5 – 7.6.

A nonequilibrium character of distributions is clearly seen. So, the H_2 molecules distribution up to $\tau \simeq 1$ μs has a local maximum at $n \simeq 10$, which is connected with an intensive population of these states at a radiative depopulation of singlet levels of a molecular hydrogen excited by a discharge (Fig. 7.5).

Vibrational distribution for a deformation mode of $H_2O(\nu_2)$ molecule has clear inverse population near the dissociation limit because of intense recombination flow on upper levels in the reaction

$$H_2 + O + M \rightarrow H_2O + M$$

On the contrary, vibrational distribution for OH radical is characterized by a significant depletion near the levels $n > 5$ due to their fast consumption in the reaction

$$OH(v) + OH \rightarrow HO_2 + H$$

The scale of an influence of vibrationally excited components on the total rate of the H_2 consumption and H_2O production is demonstrated in Figure 7.7. It is clearly seen that the consideration of the vibrationally nonequilibrium kinetics leads to a strong (more then 5 times) increase of the reactions rate. Thus, vibrationally nonequilibrium kinetics is very important in the present conditions and lead to a sharp change in processes rates in the chemically-reactive afterglow plasma.

In the connection with points which are represented above the sensitivity analysis of the kinetic scheme to the choice of the main process rates becomes especially important.

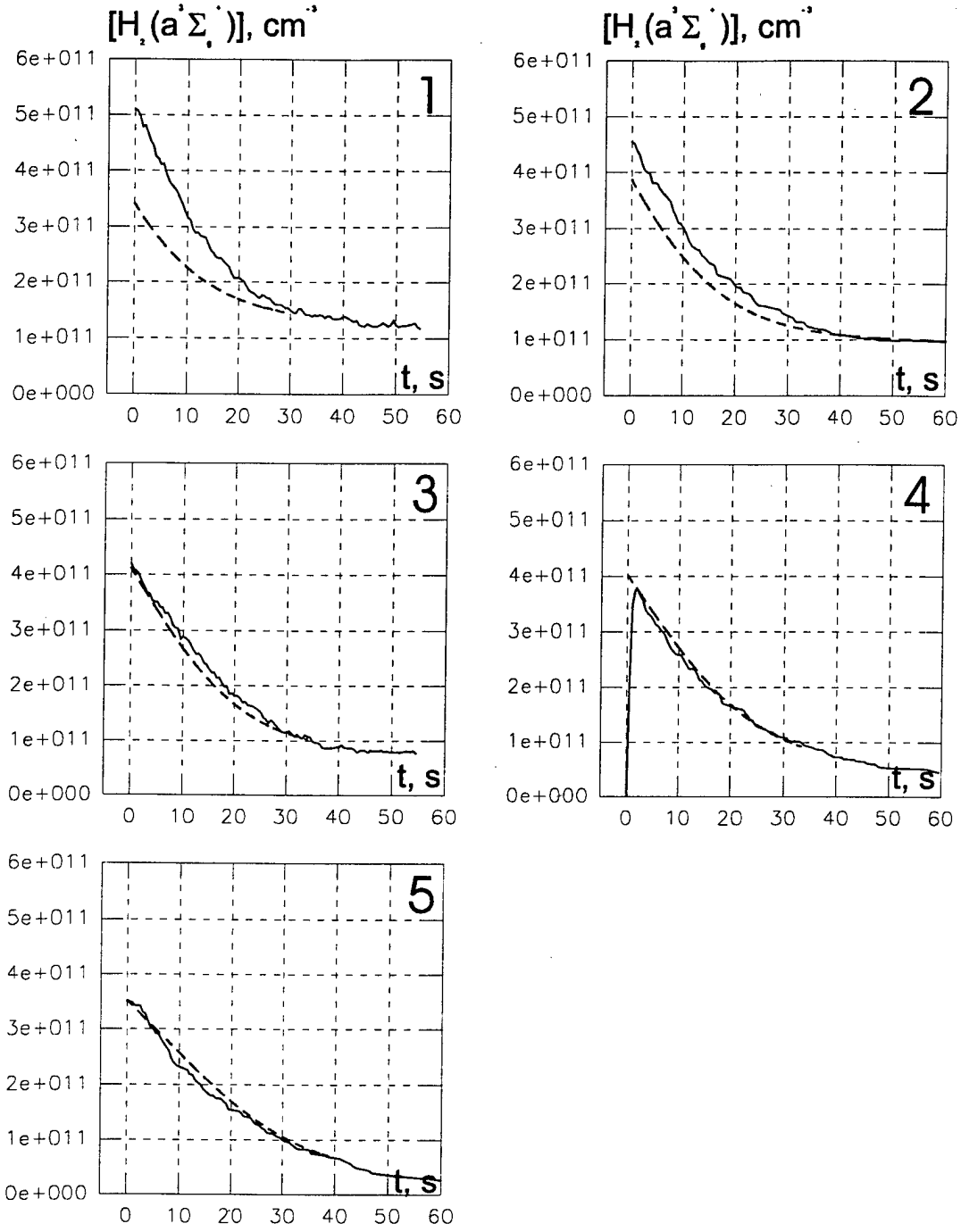

Figure 7.4: Absolute concentrations of the molecular hydrogen in electronically excited $a^3\Sigma_g^+$ - state *vs* pressure. 1-5 — initial pressure of the mixture is $p = 3, 4, 5, 6$ and 7 Torr, respectively. Solid lines — experiment, dashed ones — calculation.

As follows form the calculations performed the most important processes for the hydrogen oxidization acceleration is

$$H_2(v) + O \rightarrow OH + H$$

with an energetic threshold of $E_a = 4410$ K at $v = 0$. This threshold value decreases

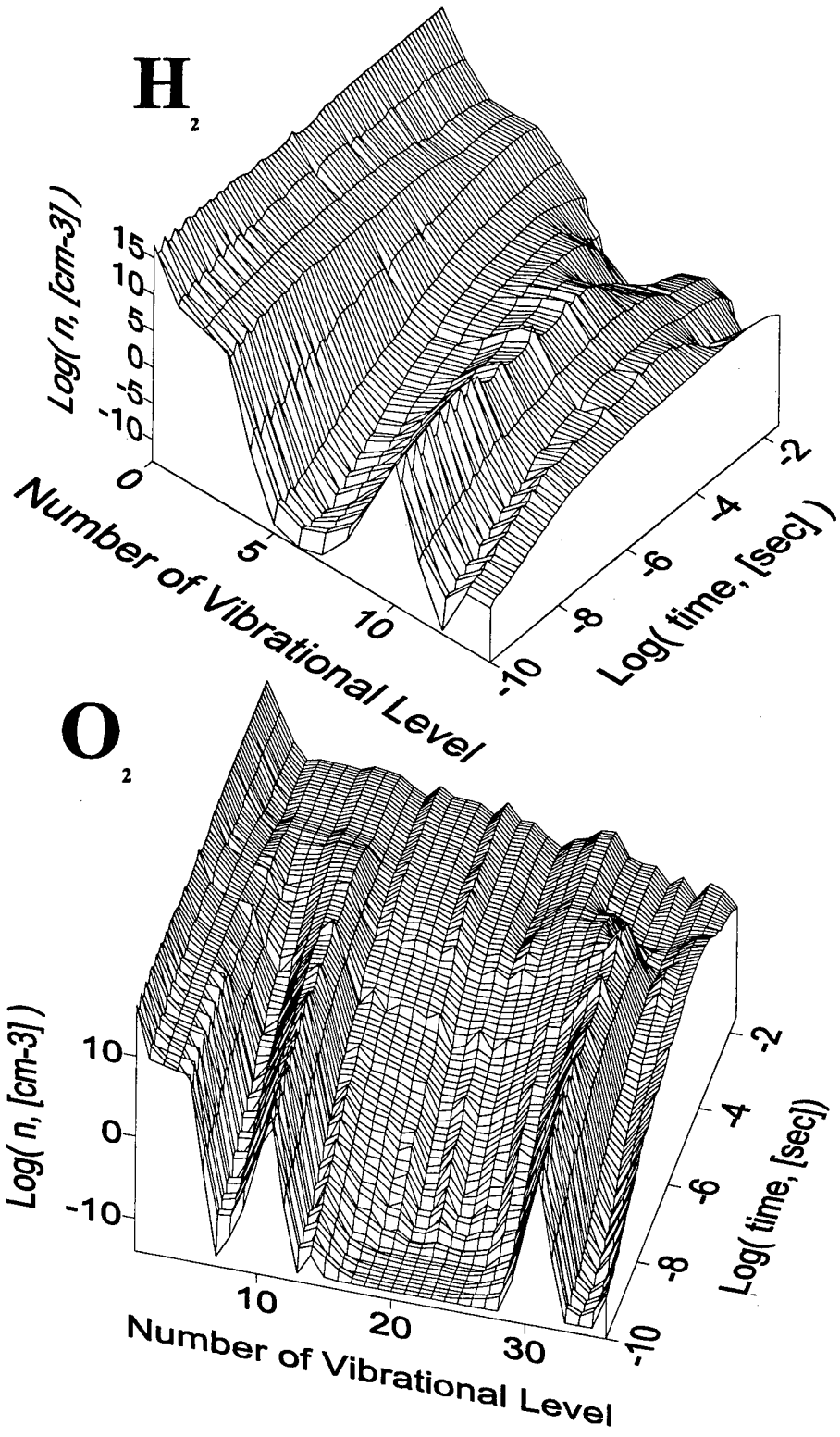

Figure 7.5: Vibrational distributions for H_2 and O_2 molecules

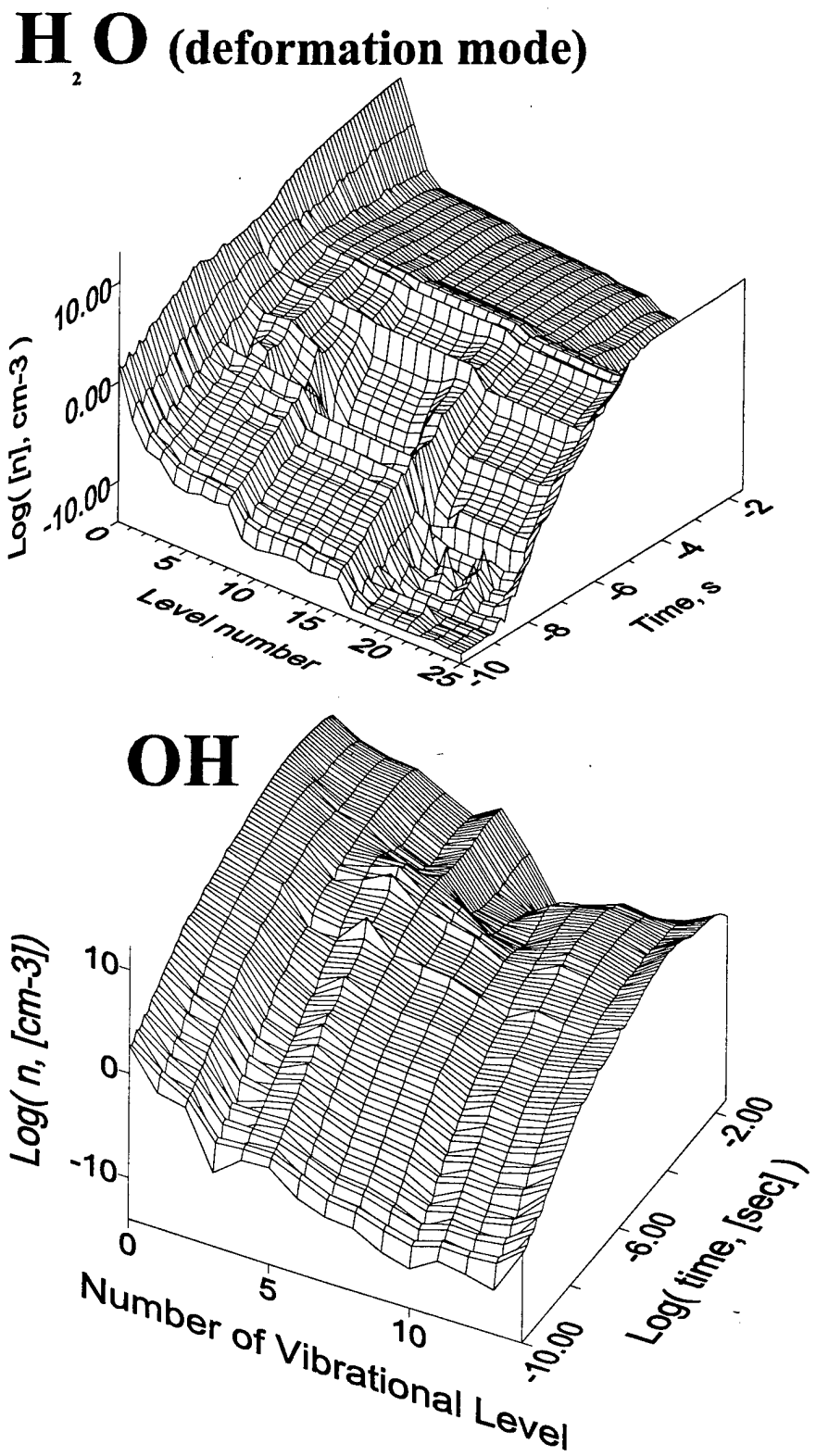

Figure 7.6: Vibrational distributions for H_2O molecule and OH radical

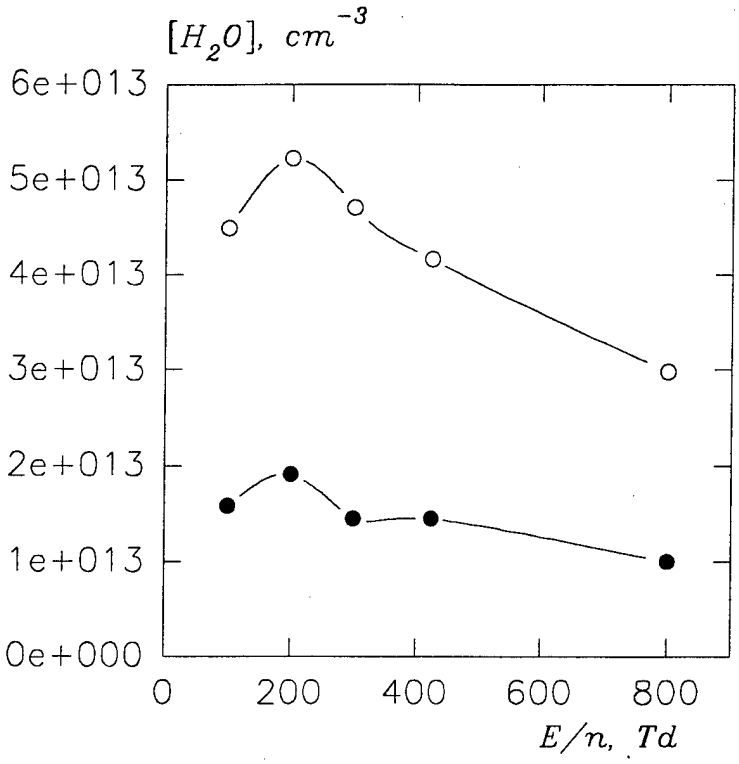

Figure 7.7: Water molecules, which are produced at the moment second pulse comes on a discharge tube. Open symbols are correspond to the calculations taking into account vibrationally excited molecules; filled ones – without taking vibrationally nonequilibrium processes into account

sharply at the conditions of the vibrational excitation of H_2 ($\Theta_{H_2} = 6326$ K) molecule, at that experimentally measured increase in the reaction rate at $T = 300$ K is equal to $k_{v=1}/k_{v=0} = 2600$ [157].

The model for the description of kinetics of vibrationally excited components used in this work provides an excellent coincidence in constant rate of the processes mentioned and in its dependence upon a vibrational excitation (see discussion above).

The total effect of a vibrational excitation depends also upon the rates of VT, VV and VV'-relaxation of H_2 molecule and upon the rate of population of vibrationally excited levels of H_2 in discharge by an electron impact.

Because of a relatively low rate of the vibrational relaxation in the range of pressures and temperatures used in this work the choice of the particular rates for these processes does not very decisive. Data scattering in the literature (see, for example, review in [179]) does not exceed 3 times even for the slow process of the VT-relaxation, which does not influence on the results of the work.

The sensitivity of the kinetic scheme for the rate of population of H_2 vibrational levels is also small, because it defines only linear (that is proportional to the population of appropriate levels) dependence of H_2 molecule oxidization.

It should be noted that the rates of eV-processes depend only slightly upon the reduced electric field in this range of parameters ($E/n = 400 - 800$ Td) and may be calculated with a high degree of accuracy from the solution of the Boltzmann equation. To calculate the constant rates $k_{eV}(H_2)$ we used cross sections represented in [181].

To analyze the role of different processes in the discharge afterglow we perform the rate analysis of the kinetic scheme for the conditions of the first pulse propagation through the discharge gap at the pressure 5 Torr (the initial mixture composition is $H_2 : O_2 : N_2 = 0.296 : 0.148 : 0.556$).

Kinetic curves for the main components in the afterglow of the first pulse are represented in Fig. 7.8. Time interval between two pulses may be divided into 4 parts: the first one — from 0 to 10^{-7} s, the second one — from 10^{-7} to 10^{-5} s, the third one — from 10^{-5} to 10^{-3} s and the fourth — from 10^{-3} to 25×10^{-3} s.

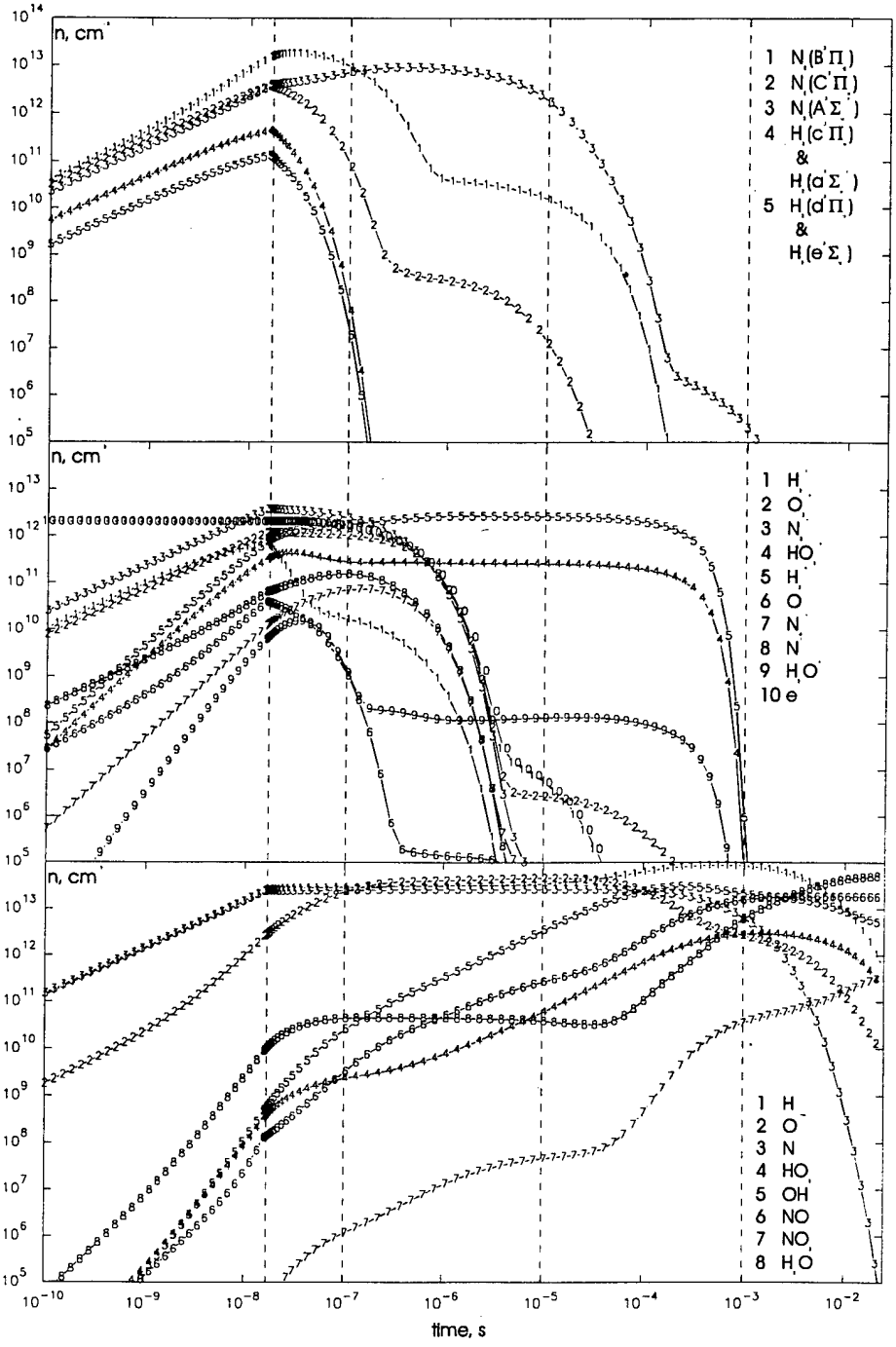

Figure 7.8: Calculated kinetic curves for the main components at the pressure $p = 5$ Torr.

The first time interval corresponds to the stage of discharge and its early afterglow, where the majority of excited particles, ions and radicals is generated, radiative depopulation and collisional quenching of excited electronic states take place.

The second stage is characterized by an active ion recombination; from the electronically excited molecules the only $N_2(A^3\Sigma_u^+)$ - state remains significant.

For the third time interval the most significant process is a conversion of the rest of ions and excited molecules to the active radicals.

And, finally, on the fourth stage (time interval $10^{-3} - 25\ 10^{-3}$ s) chemical processes with free radicals are predominate.

Diagrams of the active particles flow are represented for each of time intervals in Fig. 7.9, 7.10. Let us consider the most principal processes for each of the time interval.

1. The most fast process during first 10^{-7} s after current pulse is off is a dissociative quenching of electronically excited level $N_2(B^3\Pi_g)$ by the O_2 molecule with the creation of atomic oxygen. The next is the reaction of H_2^+ conversion to H_3^+ and H. The main channel of the water production on this stage is a reaction of molecular hydrogen with the ion O^-, created in discharge in the reaction $O_2+e^- \rightarrow O+O^-$.

2. Atomic oxygen concentration continues to growth due to dissociative quenching of $N_2(B^3\Pi_g)$ and $N_2(A^3\Sigma_u^+)$ molecules. Destruction of the ions H_2^+, O_2^+ and N_2^+ takes place, the most fast process is a destruction of O_2^+ with a production of O and O_3^+; the last one create atomic oxygen in reaction with an electron. Another channel of O_2^+ ion destruction is its reaction with H_2 with a production of HO_2^+ and H. Up to this moment the accumulation of O-atoms took place, and now its reaction with hydrogen leads to the production of H and OH radicals.

3. The process ($O+H_2 \rightarrow H+OH$) predominates up to the beginning of the next pulse. Metastable nitrogen $N_2(A^3\Sigma_u^+)$ in reaction with oxygen gives additional O-atoms, which lead to the production of H and OH. As a result of a three-body conversion of H-atoms with O_2 we obtain HO_2, which, in reaction with OH gives H_2O molecules.

4. On the final stage atomic oxygen in the reaction with H_2 gives H and OH radicals. Atomic hydrogen gives HO_2, which, in reaction with OH, gives H_2O. Another channel of the water creation is a OH+OH reaction.

Thus, it may be concluded that the excitation of the gas in the conditions of these experiments takes place behind the front of nanosecond gas breakdown in relatively small electric fields $E/n \simeq 300 - 600$ Td and electron densities $n_e \simeq (1-2) \times 10^{12}$ cm^{-3} during a time interval $\simeq 10$ ns. The description of the gas excitation with the help of two-term approximation of Boltzmann equation gives a good correlation with the experimental data up to electric field $E/n = 600$ Td in a stoichiometric hydrogen-air mixture.

Up to 100 ns the main role belong to the processes with electronically excited particles, in the microsecond time scale – to the molecular - ion reactions, in the time interval 100 μs – 25 ms – to the reaction with radicals.

The proposed mechanism of chemical kinetics description in essentially nonequilibrium conditions gives a possibility of the quantitative analysis of vibrationally nonequilibrium processes and their influence of a whole chemical kinetics in the system. It was shown

that in the conditions of a pulsed high-current nanosecond discharge the role of the processes with participation of vibrationally excited components is principal an significantly influences the kinetics in the system.

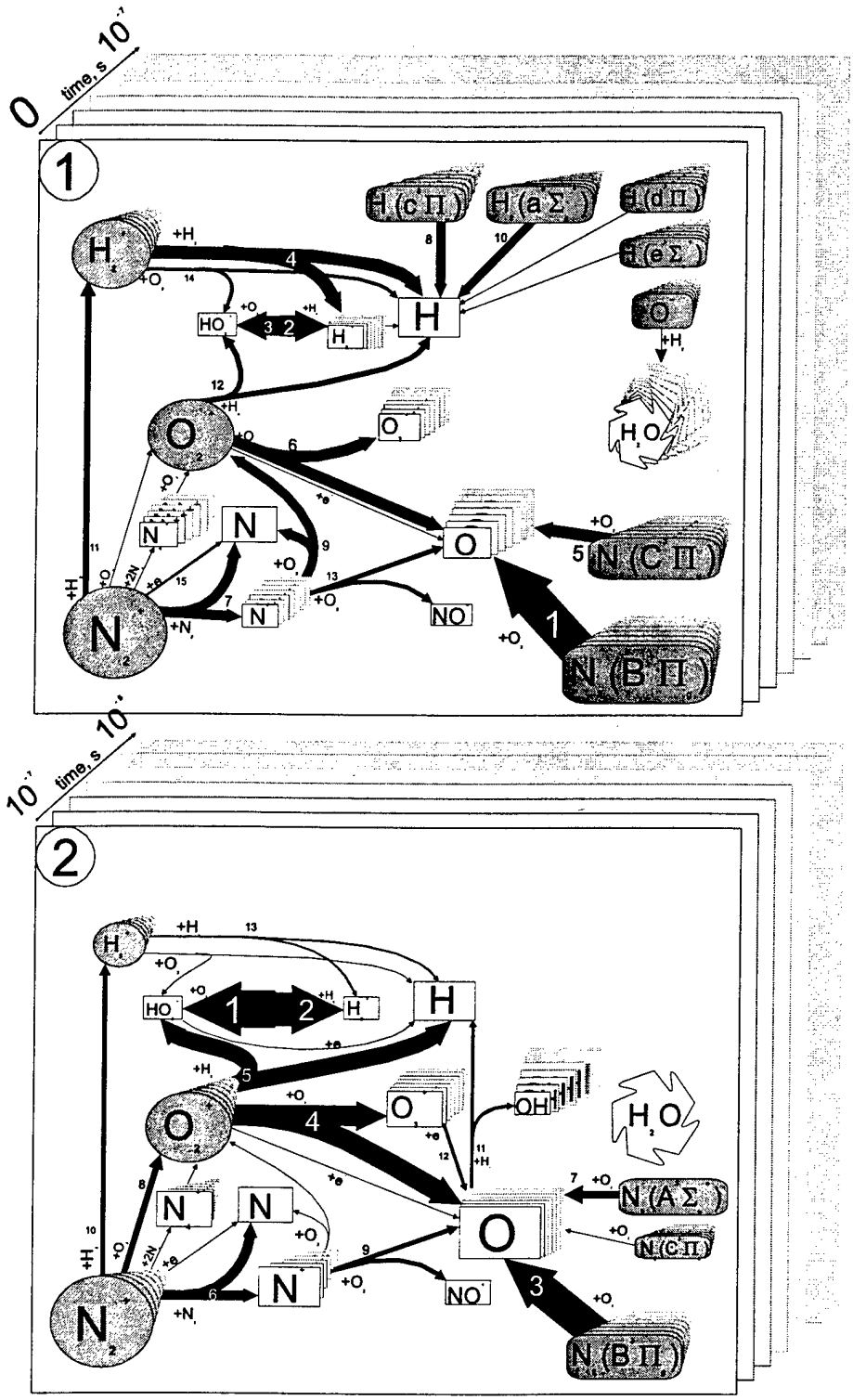

Figure 7.9: Diagrams for the active particles flow. The thickness of the line corresponds to the velocity of the appropriate process, and a figure near the process – to its significance in the manifold of the reactions. The dynamics of the concentration of the appropriate chemical component during the certain time interval is represented as a level-to-level increase or decrease of the appropriate field. 1) — time interval $\tau = 0 - 1 \times 10^{-7}$ s, 2) — $\tau = 1 \times 10^{-7} - 1 \times 10^{-5}$ s.

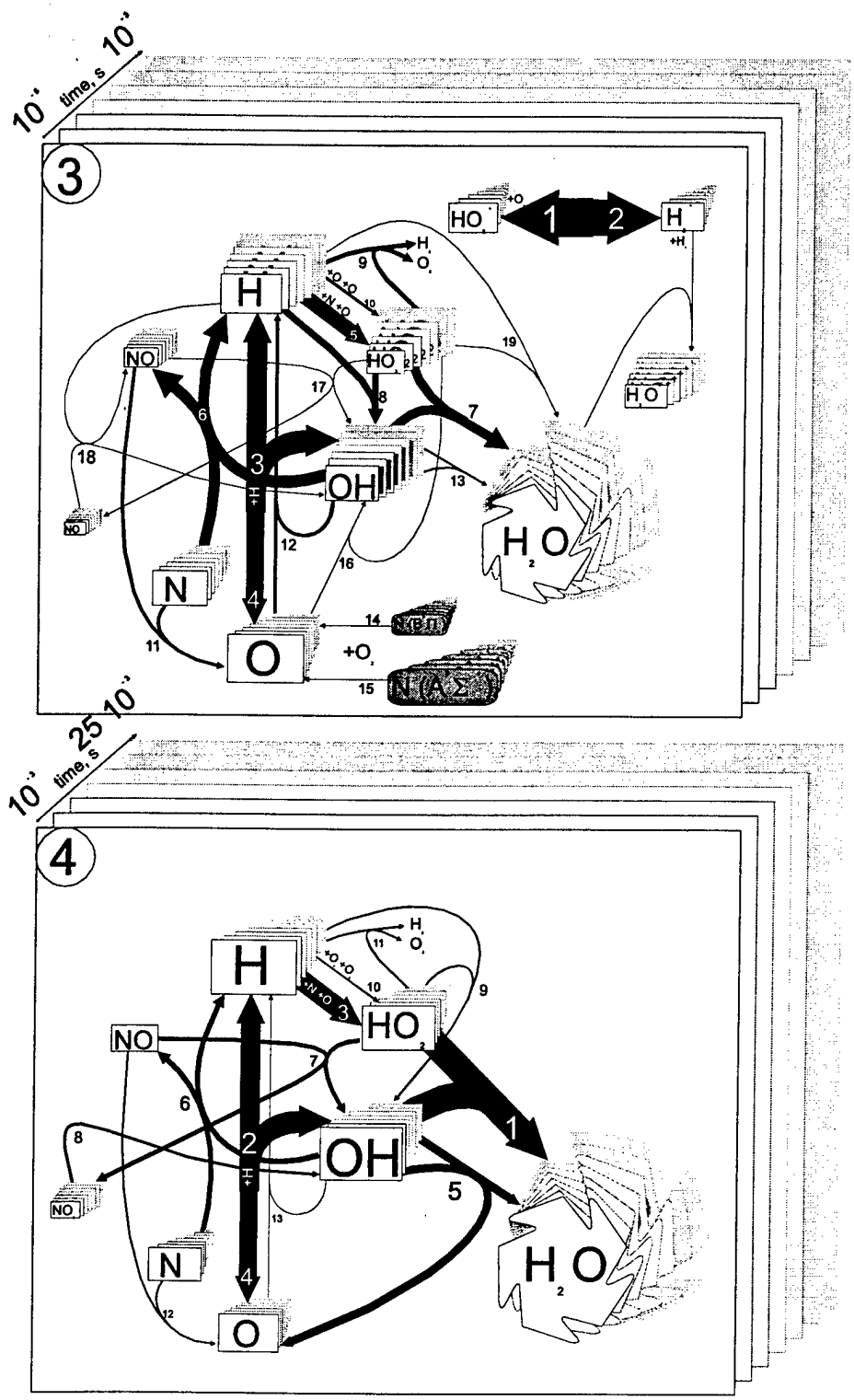

Figure 7.10: Diagrams for the active particles flow. 3) — $\tau = 1 \times 10^{-5} - 1 \times 10^{-3}$ s, 4) — $\tau = 1 \times 10^{-3} - 25 \times 10^{-3}$ s.

Chapter 8

Numerical simulation of N_2O Decomposition in High-Current Nanosecond Electric Discharge.

Calculations were performed, as in the case of H_2-air mixture, directly for each pulse taking into account changes in chemical composition of the mixture from pulse to pulse.

8.1 Electron energy distribution

It was suggested that main components determine EEDF shape and rate constants of all processes with electrons participation are N_2O, O_2 and N_2. Momentum-transfer and inelastic cross-sections were taken from [52, 44, 48, 50].

Kinetic scheme was the same as for H_2-air non-thermal oxidation modelling.

8.2 Vibrational excange rate constants in N-O-H-C system

In the table 8.1 it was shown the full set of vibrational energy exchange processes for simulation of N_2O decomposition under non-equilibrium conditions, which was used in this work. Rate constants for this processes and its temperature dependence are shown it the table 8.2.

Table 8.1: Vibrational energy exchange processes in the C, N, O, H system

Process	Label
$CO_2(00^01) + N_2(v=0) \leftrightarrow CO_2(00^00) + N_2(v=1)$	$W_{3,4}$
$CO_2(00^01) + M \leftrightarrow CO_2(11^10, 03^10) + M$	$W^M_{3,\Sigma}$
$CO_2(00^01) + CO(v=0) \leftrightarrow CO_2(00^00) + CO(v=1)$	$W_{3,9}$
$CO_2(00^01) + N_2O(00^00) \leftrightarrow CO_2(00^00) + N_2O(00^01)$	$W_{3,13}$
$CO_2(00^00) + N_2(v=1) \leftrightarrow CO_2(11^10, 03^10) + N_2(v=0)$	$W_{4,\Sigma}$
$CO_2(00^00) + CO(v=1) \leftrightarrow CO_2(11^10, 03^10) + CO(v=0)$	$W_{9,\Sigma}$

Table 8.1: Vibrational energy exchange processes in the C, N, O, H system

Process	Label
$CO_2(00^00) + O_2(v=1) \leftrightarrow CO_2(10^00, 03^10) + O_2(v=0)$	$W_{5,1}$
$CO_2(10^00) + N_2O(00^00) \leftrightarrow CO_2(00^00) + N_2O(10^00)$	$W_{1,11}$
$CO_2(00^00) + N_2O(00^01) \leftrightarrow CO_2(11^10) + N_2O(00^00)$	$W_{13,\Sigma}$
$CO_2(10^00) + M \leftrightarrow CO_2(02^00) + M$	$W^M_{1,2}$
$CO_2(01^10) + M \leftrightarrow CO_2(00^00) + M$	$W^M_{2,0}$
$N_2(v=1) + CO(v=0) \leftrightarrow N_2(v=0) + CO(v=1)$	$W_{4,9}$
$N_2(v=1) + O_2(v=0) \leftrightarrow N_2(v=0) + O_2(v=1)$	$W_{4,5}$
$N_2(v=1) + H_2O(000) \leftrightarrow N_2(v=0) + H_2O(010)$	$W_{4,7}$
$N_2(v=1) + N_2O(00^00) \leftrightarrow N_2(v=0) + N_2O(00^01)$	$W_{4,13}$
$N_2(v=1) + NO(v=0) \leftrightarrow N_2(v=0) + NO(v=1)$	$W_{4,10}$
$N_2(v=1) + M \leftrightarrow N_2(v=0) + M$	$W^M_{4,0}$
$NO(v=1) + O_2(v=0) \leftrightarrow NO(v=0) + O_2(v=1)$	$W^M_{10,5}$
$H_2O(010) + O_2(v=0) \leftrightarrow H_2O(000) + O_2(v=1)$	$W^M_{7,5}$
$O_2(v=1) + N_2O(00^00) \leftrightarrow O_2(v=0) + N_2O(10^00)$	$W^M_{5,11}$
$O_2(v=1) + M \leftrightarrow O_2(v=0) + M$	$W^M_{5,0}$
$H_2O(001) + M \leftrightarrow H_2O(100) + M$	$W^M_{8,6}$
$H_2O(001) + M \leftrightarrow H_2O(020) + M$	$W^M_{8,7}$
$H_2O(100) + M \leftrightarrow H_2O(020) + M$	$W^M_{6,7}$
$H_2O(010) + M \leftrightarrow H_2O(000) + M$	$W^M_{7,0}$
$CO(v=1) + H_2O(000) \leftrightarrow CO(v=0) + H_2O(010)$	$W_{9,7}$
$NO(v=1) + H_2O(000) \leftrightarrow NO(v=0) + H_2O(010)$	$W_{10,7}$
$H_2(v=1) + H_2O(000) \leftrightarrow H_2(v=0) + H_2O(001)$	$W_{14,8}$
$OH(v=1) + H_2O(000) \leftrightarrow OH(v=0) + H_2O(100)$	$W_{15,6}$
$CO(v=1) + NO(v=0) \leftrightarrow CO(v=0) + NO(v=1)$	$W_{9,10}$
$CO(v=1) + O_2(v=0) \leftrightarrow CO(v=0) + O_2(v=1)$	$W_{9,5}$
$N_2O(00^01) + CO(v=0) \leftrightarrow N_2O(00^00) + CO(v=1)$	$W_{13,9}$
$CO(v=1) + M \leftrightarrow CO(v=0) + M$	$W^M_{9,0}$
$N_2O(00^01) + NO(v=0) \leftrightarrow N_2O(00^00) + NO(v=1)$	$W_{13,10}$
$NO(v=1) + M \leftrightarrow NO(v=0) + M$	$W^M_{10,0}$
$N_2O(00^01) + M \leftrightarrow N_2O(11^10, 03^10) + M$	W^M_{13,Σ_1}
$N_2O(00^01) + M \leftrightarrow N_2O(12^00, 20^00, 04^00) + M$	W^M_{13,Σ_2}
$N_2O(10^00) + M \leftrightarrow N_2O(02^00) + M$	$W^M_{11,12}$
$N_2O(01^10) + M \leftrightarrow N_2O(00^00) + M$	$W^M_{12,0}$
$H_2(v=1) + OH(v=0) \leftrightarrow H_2(v=0) + OH(v=1)$	$W^M_{14,15}$
$H_2(v=1) + M \leftrightarrow H_2(v=0) + M$	$W^M_{14,0}$

Table 8.2: Vibrational energy exchange rate constants in C, N, O, H system

Process	$W_{p,q}$, cm^3/s	Ref.
$W^{CO_2}_{3,\Sigma}$	$1.36T \times 10^{-16} / \exp(9.456 - 218.23T^{-1/3} + 1687.7T^{-2/3} - 3909.27T^{-1})$	[62]

Table 8.2: Vibrational energy exchange rate constants in C, N, O, H system

Process	$W_{p,q}$, cm^3/s	Ref.
$W_{3,\Sigma}^{N_2}$	$1.36T \times 10^{-16} / \exp(15.456 - 424.03T^{-1/3} + 3852.67T^{-2/3} - 10672T^{-1})$	[62]
$W_{3,\Sigma}^{O_2}$	$0.141T \times 10^{(-6.303-122.27T^{-1/3}+384T^{-2/3})\theta}$	[67]
$W_{3,\Sigma}^{H_2O}$	$4 \times 10^{-15} T\theta$	[62]
$W_{3,\Sigma}^{CO}$	$0.141T \times 10^{(-9.143-84.23T^{-1/3}+271.7T^{-2/3})\theta}$	[67]
$W_{3,\Sigma}^{NO}$	$\exp(-16.234 - 171.359T^{-1/3} + 453.455T^{-2/3}), \quad T > 400\ K$	[62]
	$W_{3,\Sigma}^{NO}(T = 400\ K), \quad T \leq 400\ K$	
$W_{3,\Sigma}^{H_2}$	$0.141T \times 10^{(-14.363-3.73T^{-1/3}+32T^{-2/3})\theta}$	[67]
$W_{3,\Sigma}^{OH}$	$W_{3,\Sigma}^{H_2O}$	[62]
$W_{3,\Sigma}^{O}$	$0.141T \times 10^{(-7.956-122.2T^{-1/3}+384T^{-2/3})\theta}$	[67]
$W_{3,\Sigma}^{H}$	$0.8 \cdot W_{3,\Sigma}^{H_2}$	[62]
$W_{3,\Sigma}^{He}$	$103.36T \times 10^{(-7.69T^{-1/3}-16.1)\theta}$	[67]
$W_{3,\Sigma}^{N_2O}$	$W_{3,\Sigma}^{CO_2}$	[62]
$W_{2,0}^{CO_2}$	$0.141T \times 10^{(-10.673-57.31T^{-1/3}+156.7T^{-2/3})}$	[65]
$W_{2,0}^{N_2}$	$0.141T \times 10^{(-9.987-68.78T^{-1/3}+188.5T^{-2/3})}$	[65]
$W_{2,0}^{O_2}$	$0.141T \times 10^{(-24.458+35.957T^{-1/3}-32.4623T^{-2/3})}$	[65]
$W_{2,0}^{Ar}$	$1.36 \cdot 10^{-10} \times T / 10^{(10.011-49.4T^{-1/3}+77.3T^{-2/3})}$	[65]
$W_{2,0}^{H_2O}$	$0.141T \times 10^{(-11.864-2.1\times10^{-3}T+0.705\times10^{-6}T^2)}$	[65]
$W_{2,0}^{CO}$	$0.141T \times 10^{(-11.04-51.65T^{-1/3}+121.8T^{-2/3})}$	[65]
$W_{2,0}^{NO}$	$0.141T \times 10^{(-14.57+2.8T^{-1/3})}$	[65]
$W_{2,0}^{H_2}$	$0.141T \times 10^{(-12.097-28.46T^{-1/3}+144.5T^{-2/3})}$	[65]
$W_{2,0}^{OH}$	$W_{2,0}^{H_2O}$	[62]
$W_{2,0}^{O}$	$0.141T \times 10^{(-10.989-49.4T^{-1/3}+77.3T^{-2/3})}$	[67]
$W_{2,0}^{H}$	$0.9 \cdot W_{2,0}^{H_2}$	[62]
$W_{2,0}^{He}$	$0.141T \times 10^{(-12.289+14.75T^{-1/3})}$	[65]
$W_{3,4}$	$4.16 \times 10^{-14} \sqrt{T} \exp(8.842 \times 10^{-7} T^2 - 2.072 \times 10^{-3} T)$	[62]
$W_{3,9}$	$0.141T \times 10^{(-11.856-31.91T^{-1/3}+103.5T^{-2/3})}$	[67]
$W_{3,13}$	$103.36T \times 10^{-21} \exp(-10.773 + 10.814T^{-1/3} - 11.128T^{-2/3})$	[62]
$W_{13,\Sigma}$	$W_{4,\Sigma}$	[62]
$W_{4,\Sigma}$	$0.28 \cdot W_{3,\Sigma}^{N_2}$	[62]
$W_{9,\Sigma}$	$0.141T \times 10^{(-10.292-69.94T^{-1/3}+203.3T^{-2/3})}$	[67]
$W_{4,9}$	$0.141T \times 10^{(-15.2+0.0865(T^{-1/3}-0.1)^2)}$	[62]
$W_{1,11}$	$W_{3,13}$	[62]
$W_{4,5}$	$\exp(-15.397 - 281.451T^{-1/2} + 902.709T^{-2/3} - 638.17T^{-1})$	[62]
$W_{4,7}$	$\exp(-17.658 - 149.023T^{-1/3} + 347.214T^{-2/3} - 881.093T^{-1})$	[62]
$W_{4,10}$	$\exp(-25.894 - 41.416T^{-1/3} - 166.29T^{-2/3})$	[62]
$W_{4,13}$	$103.36T \times 10^{(-2.094T^{-1/3}+0.732T^{-2/3}-16.559)}$	[63]
$W_{4,0}^{CO_2}$	$\exp(-19.414 - 134.727T^{-1/3} + 253.19T^{-2/3} + 2551.7T^{-1})$	[62]
$W_{4,0}^{N_2}$	$0.141T \times 10^{(-9.079-142.84T^{-1/3}+431.4T^{-2/3})}$	[67]
$W_{4,0}^{CO}$	$0.141T \times 10^{-21} \exp(24.81 - 220T^{-1/3})$	[62]
$W_{4,0}^{O_2}$	$W_{4,0}^{N_2}$	[67]

Table 8.2: Vibrational energy exchange rate constants in C, N, O, H system

Process	$W_{p,q}$, cm^3/s	Ref.
$W_{4,0}^{H_2O}$	$0.141T \times 10^{(-14.4-9.2T^{-1/3})}$	[67]
$W_{4,0}^{H_2}$	$0.141T \times 10^{(-10.44-72.63T^{-1/3}+171.3T^{-2/3})}$	[67]
$W_{4,0}^{NO}$	$9.2 \times 10^{-12} T \exp(-221T^{-1/3})$	[62]
$W_{4,0}^{He}$	$0.141T \times 10^{(-9.913-85.16T^{-1/3}+171.1T^{-2/3})}$	[67]
$W_{4,0}^{N_2O}$	$W_{4,0}^{CO_2}$	[62]
$W_{4,0}^{OH}$	$W_{4,0}^{H_2}$	[62]
$W_{4,0}^{H}$	$3.1 \cdot W_{4,0}^{H_2}$	[62]
$W_{4,0}^{O}$	$0.141T \times 10^{(-13.929-14.38T^{-1/3})}$	[67]
$W_{10,5}$	$\exp(-15.397 - 281.451T^{-1/3} + 902.709T^{-2/3} - 638.17T^{-1})$	[62]
$W_{7,5}$	$1.39 \times 10^{-11} T^{-1/2}$	[62]
$W_{5,11}$	$0.141T \times 10^{(-15.003-11.71T^{-1/3})}$	[64]
$W_{5,0}^{CO_2}$	$1.34 \times 10^{-12} T \exp(-146.5T^{-1/3})$	[62]
$W_{5,0}^{N_2}$	$6.8 \times 10^{-13} \exp(-132T^{-1/3})$	[62]
$W_{5,0}^{O_2}$	$1.11 \times 10^{-8} \exp(-157T^{-1/3})$	[62]
$W_{5,0}^{Ar}$	$1.36 \cdot 10^{-16} \times T/10^{(-4.04+69.7T^{-1/3})}$	[66]
$W_{5,0}^{H_2O}$	$100.0 \cdot W_{5,0}^{O_2}$	[62]
$W_{5,0}^{CO}$	$6.8 \times 10^{-13} T \exp(-131.6T^{-1/3})$	[62]
$W_{5,0}^{NO}$	$7.5 \times 10^{-13} T \exp(-134T^{-1/3})$	[62]
$W_{5,0}^{H_2}$	$10^{-17} \exp(17.1 - 91.5T^{-1/3})$	[62]
$W_{5,0}^{OH}$	$W_{5,0}^{H_2O}$	[62]
$W_{5,0}^{N_2O}$	$W_{5,0}^{CO_2}$	[62]
$W_{5,0}^{He}$	$0.454 \times 10^{-13} \exp(-60.85T^{-1/3})$	[62]
$W_{5,0}^{H}$	$1.7 \cdot W_{5,0}^{H_2}$	[62]
$W_{5,0}^{O}$	$2.9T \times 10^{-13} \exp(-111T^{-1/3})$	[62]
$W_{7,0}^{CO_2}$	$0.5 \cdot W_{7,0}^{O_2}$	[62]
$W_{7,0}^{N_2}$	$0.141T \times 10^{(-14.407-8.065T^{-1/3}+20.51T^{-2/3})}$	[65]
$W_{7,0}^{Ar}$	$1.36 \cdot 10^{-10} \times T/10^{(0.8935-10.657T^{-1/3}+31.339T^{-2/3})}$	[65]
$W_{7,0}^{O_2}$	$0.141T \times 10^{(-17.38-42.036T^{-1/3}+116.515T^{-2/3})}$	[65]
$W_{7,0}^{H_2O}$	$0.141T \times 10^{(-6.627-99.092T^{-1/3}+404.127T^{-2/3})}$	[65]
$W_{7,0}^{CO}$	$W_{7,0}^{N_2}$	[62]
$W_{7,0}^{NO}$	$0.141T \times 10^{-21} \exp(10.85 + 36.8T^{-1/3} + 2300T^{-1})$	[62]
$W_{7,0}^{N_2O}$	$W_{7,0}^{CO_2}$	[62]
$W_{7,0}^{H_2}$	$W_{7,0}^{H_2O} \exp(-19.8 + 280T^{-1/3} - 1117T^{-2/3})$	[65]
$W_{7,0}^{OH}$	$W_{7,0}^{H_2O}$	[62]
$W_{7,0}^{He}$	$0.35 \cdot W_{7,0}^{H_2O}$	[65]
$W_{7,0}^{O}$	2.2×10^{-12}	[62]
$W_{7,0}^{H}$	$1.4 \cdot W_{7,0}^{H_2}$	[62]
$W_{9,7}$	$W_{4,7}$	[62]
$W_{10,7}$	$W_{7,5}$	[62]
$W_{14,8}$	$1/N_A \exp(35.6 - 67T^{-1/3} + 62.1T^{-2/3})$	[62]

Table 8.2: Vibrational energy exchange rate constants in C, N, O, H system

Process	$W_{p,q}$, cm^3/s	Ref.
$W_{9,10}$	$1.62 \times 10^{-11}\sqrt{T}\exp(1.7 \times 10^{-3}T - 9.7)$	[62]
$W_{9,5}$	$1.72 \times 10^{-11}\sqrt{T}\exp(-1.56 - 106T^{-1/3})$	[62]
$W_{13,9}$	$103.36T \times 10^{(-15.34-1.32T^{-1/3}+0.489T^{-2/3})}$	[63]
$W_{9,0}^{CO_2}$	$0.141T \times 10^{(-8.18-155.91T^{-1/3}+450.5T^{-2/3})}$	[67]
$W_{9,0}^{N_2}$	$W_{9,0}^{CO}$	[67]
$W_{9,0}^{CO}$	$0.141T \times 10^{(-7.335-155.91T^{-1/3}+450.3T^{-2/3})}$	[67]
$W_{9,0}^{O_2}$	$W_{9,0}^{CO}$	[67]
$W_{9,0}^{H_2O}$	$0.141T \times 10^{-14.3}$	[67]
$W_{9,0}^{H_2}$	$0.141T \times 10^{(-10.711-64.35T^{-1/3}+153.8T^{-2/3})}$	[67]
$W_{9,0}^{N_2O}$	$W_{9,0}^{CO_2}$	[62]
$W_{9,0}^{NO}$	$W_{9,0}^{CO}$	[62]
$W_{9,0}^{OH}$	$W_{9,0}^{H_2O}$	[62]
$W_{9,0}^{He}$	$0.141T \times 10^{(-11.032-65.35T^{-1/3}+113.6T^{-2/3})}$	[67]
$W_{9,0}^{O}$	$0.141T \times 10^{(-11.83-23.45T^{-1/3})}$	[67]
$W_{9,0}^{H}$	$0.141T \times 10^{(-13.34-1.3T^{-1/3})}$	[67]
$W_{13,10}$	$0.141T \times 10^{(-12.75-18.3T^{-1/3})}$	[66]
$W_{10,0}^{CO_2}$	$0.141T \times 10^{(-16.08+T^{-1/3})}$	[62]
$W_{10,0}^{N_2}$	$1.8T \times 10^{-12}\exp(-165T^{-1/3})$	[62]
$W_{10,0}^{O_2}$	$2.2 \times 10^{-12}T\exp(-171T^{-1/3})$	[62]
$W_{10,0}^{Ar}$	$1.36 \cdot 10^{-16} \times T^2/10^{(-5.69+47.3T^{-1/3})}$	[66]
$W_{10,0}^{H_2O}$	$0.141T \times 10^{(-14.7+T^{-1/3})}$	[62]
$W_{10,0}^{CO}$	$0.141T \times 10^{(-16.7+T^{-1/3})}$	[62]
$W_{10,0}^{N_2O}$	$W_{10,0}^{CO_2}$	[62]
$W_{10,0}^{H_2}$	$W_{9,0}^{H}$	[62]
$W_{10,0}^{OH}$	$W_{10,0}^{H_2O}$	[62]
$W_{10,0}^{NO}$	$0.141T \times 10^{(-14.7+T^{-1/3})}$	[62]
$W_{10,0}^{He}$	$0.141T \times 10^{(-16.4+T^{-1/3})}$	[62]
$W_{10,0}^{O}$	3.6×10^{-11}	[62]
$W_{10,0}^{H}$	$W_{9,0}^{H}$	[62]
$W_{12,0}^{CO_2}$	$W_{12,0}^{N_2O}$	[62]
$W_{12,0}^{N_2}$	$0.141T\Psi \times 10^{(-12.62-16.7T^{-1/3})}$	[65]
$W_{12,0}^{Ar}$	$1.36 \cdot 10^{-10} \times T/10^{(7.584-8.619T^{-1/3}-47.62T^{-2/3})}$	[65]
$W_{12,0}^{O_2}$	$0.141T\Psi \times 10^{(-12.545-17.55T^{-1/3})}$	[65]
$W_{12,0}^{H_2O}$	$0.141T\Psi \times 10^{(-12.15-2.04\times10^{-3}T+0.892T^2\times10^{-6})}$	[65]
$W_{12,0}^{CO}$	$0.141T\Psi \times 10^{(-9.601-65.345T^{-1/3}+196.47T^{-2/3})}$	[65]
$W_{12,0}^{N_2O}$	$0.141T\Psi \times 10^{(-12.036-32.88T^{-1/3}+88.954T^{-2/3})}$	[65]
$W_{12,0}^{H_2}$	$10^{-14}T\Psi$	[65]
$W_{12,0}^{NO}$	$0.141T\Psi \times 10^{(-13.92-1.6T^{-1/3})}$	[65]
$W_{12,0}^{OH}$	$W_{12,0}^{H_2O}$	[62]

Table 8.2: Vibrational energy exchange rate constants in C, N, O, H system

Process	$W_{p,q}$, cm^3/s	Ref.
$W^{He}_{12,0}$	$0.141T\Psi \times 10^{(-13.15-5.75T^{-1/3})}$	[65]
$W^{O}_{12,0}$	$4.9 \times 10^{-12}\sqrt{T}\exp(-1820/T)$	[62]
$W^{H}_{12,0}$	$0.9 \cdot W^{H_2}_{6,0}$	[62]
$W^{CO_2}_{13,\Sigma_1}$	$W^{N_2O}_{13,\Sigma_1}$	[62]
$W^{N_2}_{13,\Sigma_1}$	$W^{O_2}_{13,\Sigma_1}$	[63]
$W^{O_2}_{13,\Sigma_1}$	$103.36T \times 10^{(-13.99-45.34T^{-1/3}+96.81T^{-2/3})} \cdot \phi$	[63]
$W^{H_2O}_{13,\Sigma_1}$	$3.1 \times 10^{-15}T\exp(190T^{-1}) \cdot \phi$	[63]
W^{CO}_{13,Σ_1}	$103.36T \times 10^{(-15.549-18.14T^{-1/3})} \cdot \phi$	[63]
W^{NO}_{13,Σ_1}	$103.36T \times 10^{(-13.291-643T^{-1/3}+224.28T^{-2/3})} \cdot \phi$	[63]
W^{Ar}_{13,Σ_1}	$1.36 \cdot 10^{-16} \times T/10^{(-2.68+26.2T^{-1/3})}$	[66]
$W^{H_2}_{13,\Sigma_1}$	$103.36T \times 10^{(-16.53-4.8T^{-1/3})} \cdot \phi$	[63]
W^{OH}_{13,Σ_1}	$W^{H_2O}_{7,\Sigma_1}$	[62]
W^{O}_{13,Σ_1}	$W^{CO_2}_{13,\Sigma_1}(W^{O}_{3,\Sigma}/W^{CO_2}_{3,\Sigma})$	[62]
W^{H}_{13,Σ_1}	$W^{CO_2}_{13,\Sigma_1}(W^{H}_{3,\Sigma}/W^{CO_2}_{3,\Sigma})$	[62]
W^{He}_{13,Σ_1}	$103.36T \times 10^{(-12.086-82.26T^{-1/3}+260.27T^{-2/3})} \cdot \phi$	[63]
$W^{CO_2}_{14,0}$	$0.07 \cdot W^{H_2}_{14,0}$	[62]
$W^{N_2}_{14,0}$	$0.08 \cdot W^{H_2}_{14,0}$	[62]
$W^{O_2}_{14,0}$	$0.08 \cdot W^{H_2}_{14,0}$	[62]
$W^{H_2O}_{14,0}$	$0.23 \cdot W^{H_2}_{14,0}$	[62]
$W^{CO}_{14,0}$	$0.08 \cdot W^{H_2}_{14,0}$	[62]
$W^{NO}_{14,0}$	$0.08 \cdot W^{H_2}_{14,0}$	[62]
$W^{N_2O}_{14,0}$	$W^{CO_2}_{14,0}$	[62]
$W^{H_2}_{14,0}$	$2.18 \times 10^{-9}\exp(-144.9T^{-1/3})$	[62]
$W^{OH}_{14,0}$	$W^{H_2O}_{14,0}$	[62]
$W^{O}_{14,0}$	2.2×10^{-12}	[62]
$W^{H}_{14,0}$	$1.73 \times 10^{-14}\sqrt{T}$	[62]
$W^{He}_{14,0}$	$1.363 \times 10^{-22}\exp(8.958 - 45.09T^{-1/3})$	[62]

8.3 Results

8.3.1 Dymanics of vibrational levels population

Calculated vibrational distribution functions for main molecules are represented in Fig.8.1. It is obvious that all distributions are non-Boltzmann with overpopulated high-energy levels. The presence of maxima may be explained by a selective depopulation of electronically excited states and by recombination flows.

8.3.2 Dymanics of pressure and $N_2(C^3\Pi_u)$ population growth

Figures 8.2, 8.3 represent comparison between calculated and measured profiles of $N_2(C^3\Pi_u)$ number density and total mixture pressure at initial pressure $p_0 = 4.72$ Torr.

8.4 Kinetic scheme analysis

For the main processes underlining the kinetic scheme analysis was performed. This analysis depends on the reaction stage. We perform the analysis for the first stage of the reaction (100% N_2O in the mixture), and for the final stage, corresponded to the 50% N_2O decomposition.

Figures 8.4, 8.5 represent kinetic curves for most important components.

It was clearly seen the characteristic deviations of the kinetics during initial stage of the N_2O decomposition, when concentrations of N_2 and O_2 in the mixture are small, and during final stages, when processes of collisional dissociative deactivation with participation of electronically-excited N_2 molecules became dominant.

It was clearly seen the difference of the kinetics on the initial stage of the N_2O decomposition, when concentrations of molecular nitrogen and oxygen in the mixture are relatively small, and during final stage, when the processes with collisional dissociative deactivation of electronically-excited N_2 states became dominant (Fig.8.4, 8.5).

Time interval between two pulses may be divided into 4 parts: the first one — from 0 to 10^{-7} s, the second one — from 10^{-7} to 10^{-5} s, the third one — from 10^{-5} to 10^{-3} s and the fourth — from 10^{-3} to 25×10^{-3} s.

The first time interval corresponds to the stage of discharge and its early afterglow, where the majority of excited particles, ions and radicals is generated, radiative depopulation and collisional quenching of excited electronic states take place. The second stage is characterized by an active ion recombination. For the third time interval the most significant process is a conversion of the rest of ions and excited molecules to the active radicals. And, finally, on the fourth stage (time interval $10^{-3} - 25\ 10^{-3}$ s) chemical processes with free radicals are predominate.

8.4.1 Active particle flow diagrams

For this time intervals active particle flow diagrams were constructed. Diagrams of the active particles flow are represented for each of time intervals in Fig. 8.6, 8.7. Let us consider the most principal processes for each of the time interval.

1. The most significant processes during first stage 10^{-7} seconds after current pulse (Fig. 8.6,1) are processes of the charge transfer

$$e^- + (N_2O) \rightarrow O^- + (N_2O) \rightarrow NO^- + (N_2O) \rightarrow e^-, \tag{8.1}$$

This cycle leads to the fast N_2O decomposition.

N_2O decomposition takes place in the process of dissociative quenching of $N_2(A^3\Sigma_u^+)$ and in the reaction $N(2d)+(N_2O) \rightarrow NO+N_2$.

2. During the second time interval — from 10^{-7} to 10^{-5} s (Fig.8.6,2) — cycle (8.1) accelerates dye to NO^- number density increase. Nevertheless, the main role in N_2O decomposition during this stage plays the process $N_2(A^3\Sigma_u^+) + N_2O$.

3. Third subinterval — from 10^{-5} to 10^{-3} s (Fig.8.6,3) — is characterized by excited nitrogen concentration reduction and the relative role of the ionic mechanism increase.

4. From 10^{-3} to 25×10^{-3} s (Fig.8.6,4) rate of the processes with NO participation increases:

$$NO + O + M \rightarrow NO_2 + M$$

$$NO_2 + O \rightarrow NO + O_2$$

and

$$NO + N \rightarrow N_2 + O$$

The overall picture of N_2O decomposition significantly changes during N_2O concentration decrease. The set of main processes remains the same, but accents is transferred on the reactions with electronically-excited molecular nitrogen and oxygen ions (Fig.8.7).

The analysis performed shows that processes with participation of ions and electronically-excited components during N_2O-decomposition in high-current pulse discharge play principal role.

A relative role of processes with the participation of O-atoms is not significant because of a high energy threshold of the reaction

$$N_2O + O \rightarrow NO + NO$$

Despite of H_2-air system, where vibrational excitation of the gas resulted in sharp acceleration of the oxidation, in the process of N_2O-decomposition the vibrational excitation of the gas doesn't show strongly pronounced effect.

The influence of vibrational excitation on the N_2O decomposition by pure vibrational mechanism of acceleration of monomolecular decay, which was proposed in [51], doesn't play some noticeable role because of high relaxation rates of the energy distribution function at high values of vibrational numbers (within deformational mode).

A decrease of the reaction threshold of the process $N_2O + O \rightarrow NO + NO$ ($\Theta \simeq$ 14000 K), also does not lead to noticeable increase (compared with other mechanisms) of the rate of N_2O-decomposition.

The influence of vibrational non-equilibrium is revealed on another way.

On the one hand, due to the vibrational excitation of the gas processes of collisional detachment of electrons from ions O^-, O_2^- and NO^- are sharply accelerated. It leads to some acceleration of recombination processes of charged particles and, thus, to decrease of the rate of circle (8.1).

On the other hand, excitation of the gas leads to some increase of average electron energy in the discharge due to superelastic collisions, and, accordingly, to the increase of

$N_2(A^3\Sigma_u^+)$ population rate. This leads to the increase of rate of dissociation of N_2O in the quenching reaction. The rate of N_2O dissociation by direct electron impact also increases.

Both of this processes influence indirectly on overall rate of N_2O decomposition and practically do not change the whole rate of this process.

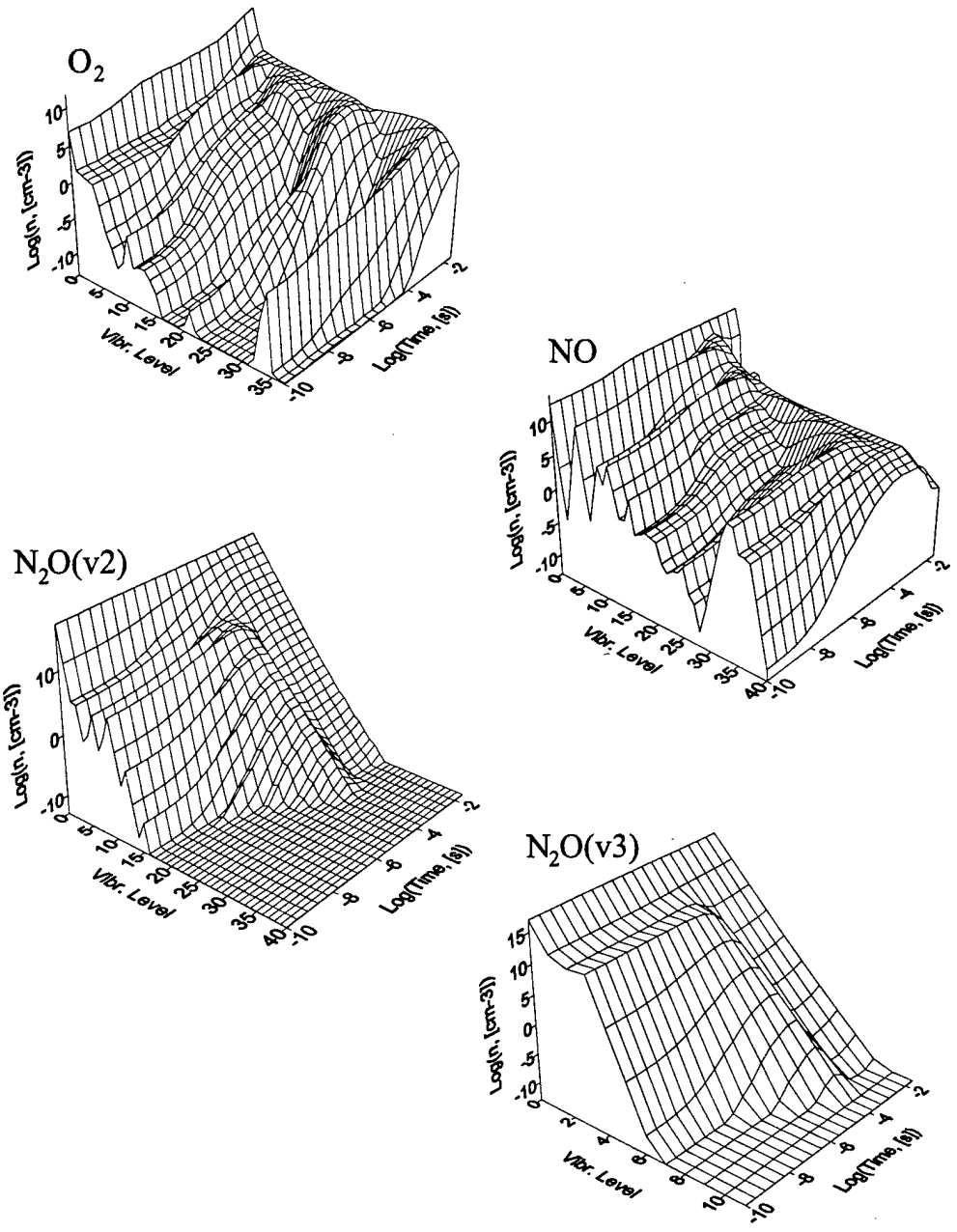

Figure 8.1: Vibrational energy distribution function for O_2, NO, $N_2O(\nu_2)$ (deformation mode) and $N_2O(\nu_3)$ (antisymmetric mode). $p = 2.8$ Torr, $U_{gen} = -13$ kV.

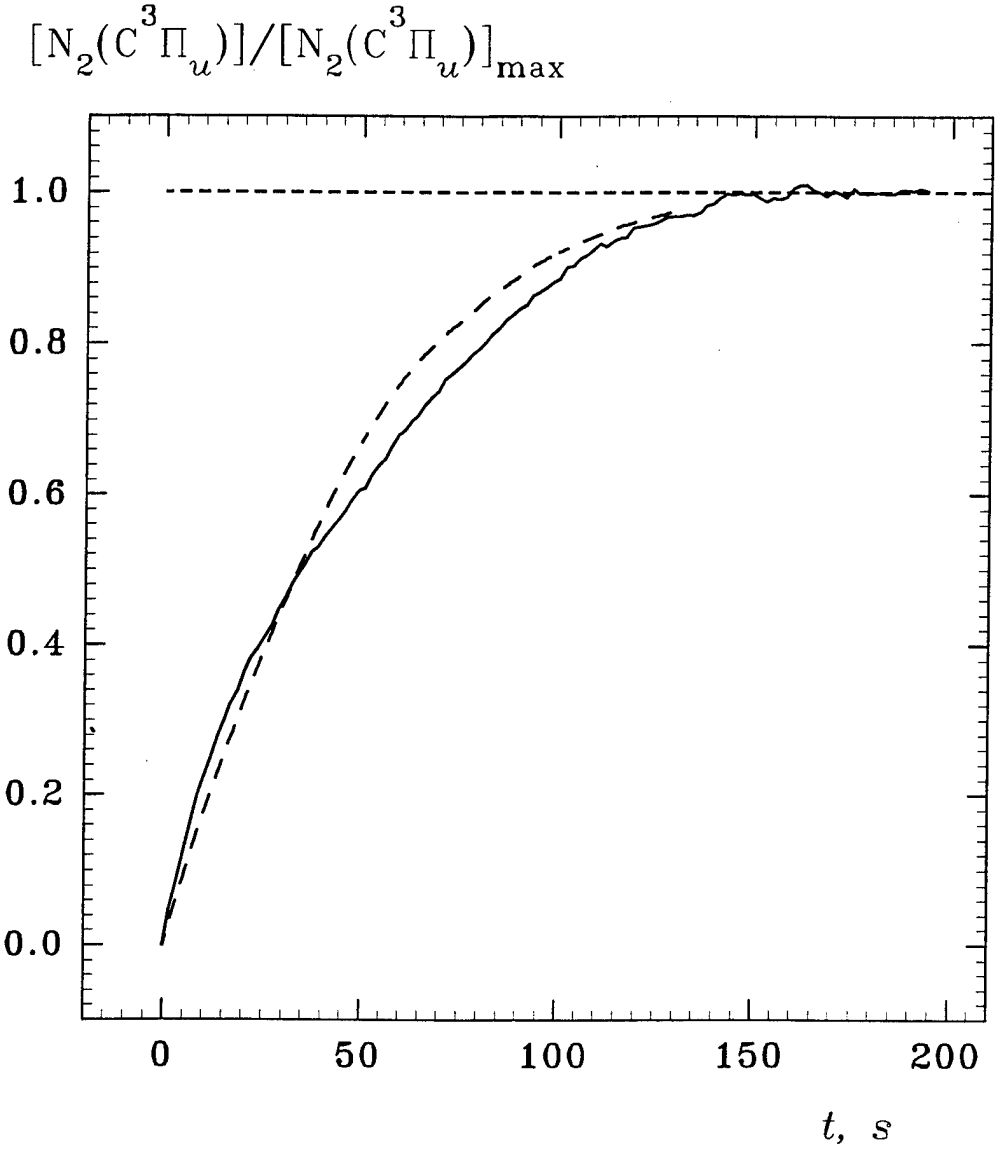

Figure 8.2: Calculated (dashed line) and measured (solid line) concentration of $N_2(C^3\Pi_u)$ at initial pressure of N_2O $p = 4.72$ Torr. $U_{gen} = -13$ kV.

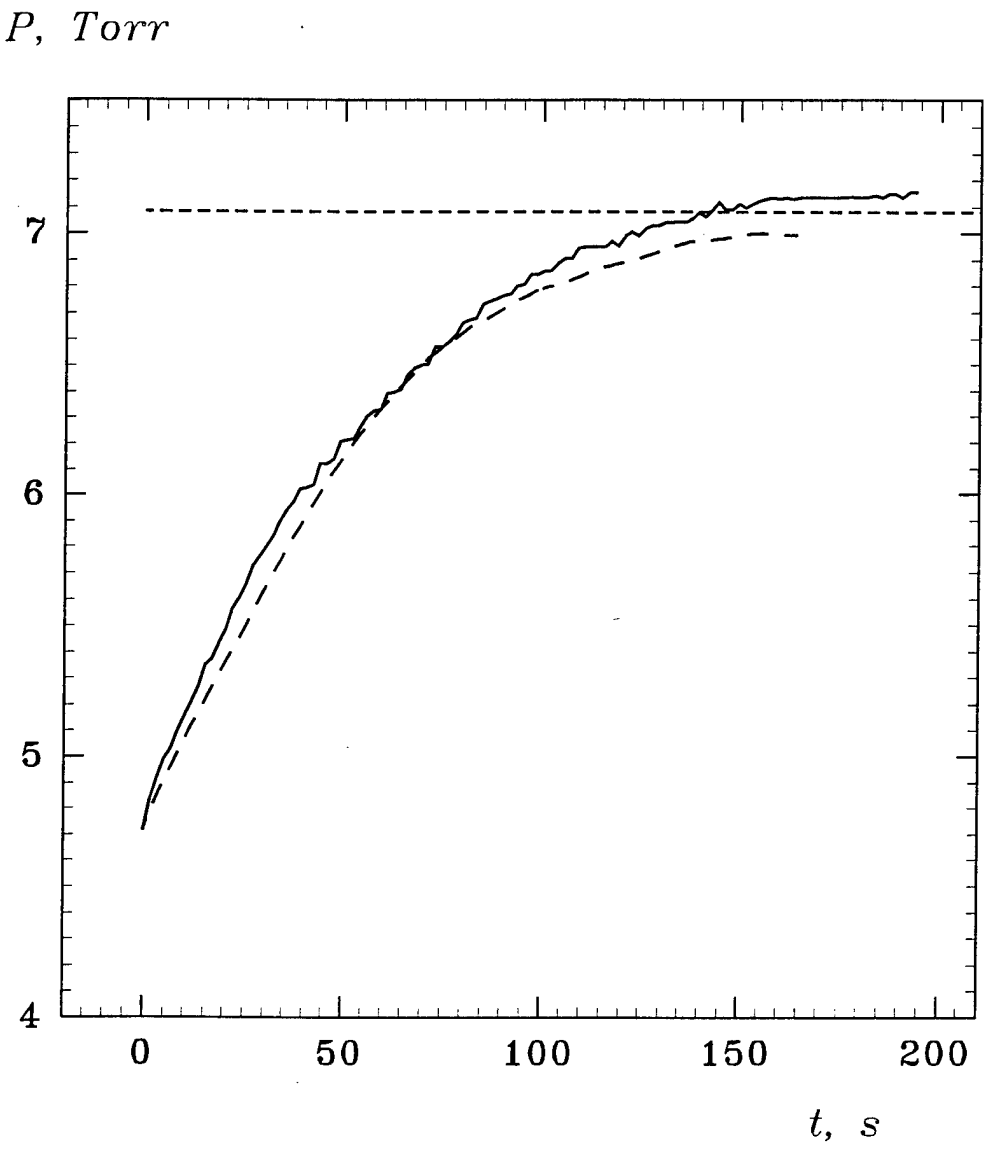

Figure 8.3: Calculated (dashed line) and measured (solid line) total mixture pressure at initial pressure of N_2O $p = 4.72$ Torr. $U_{gen} = -13$ kV.

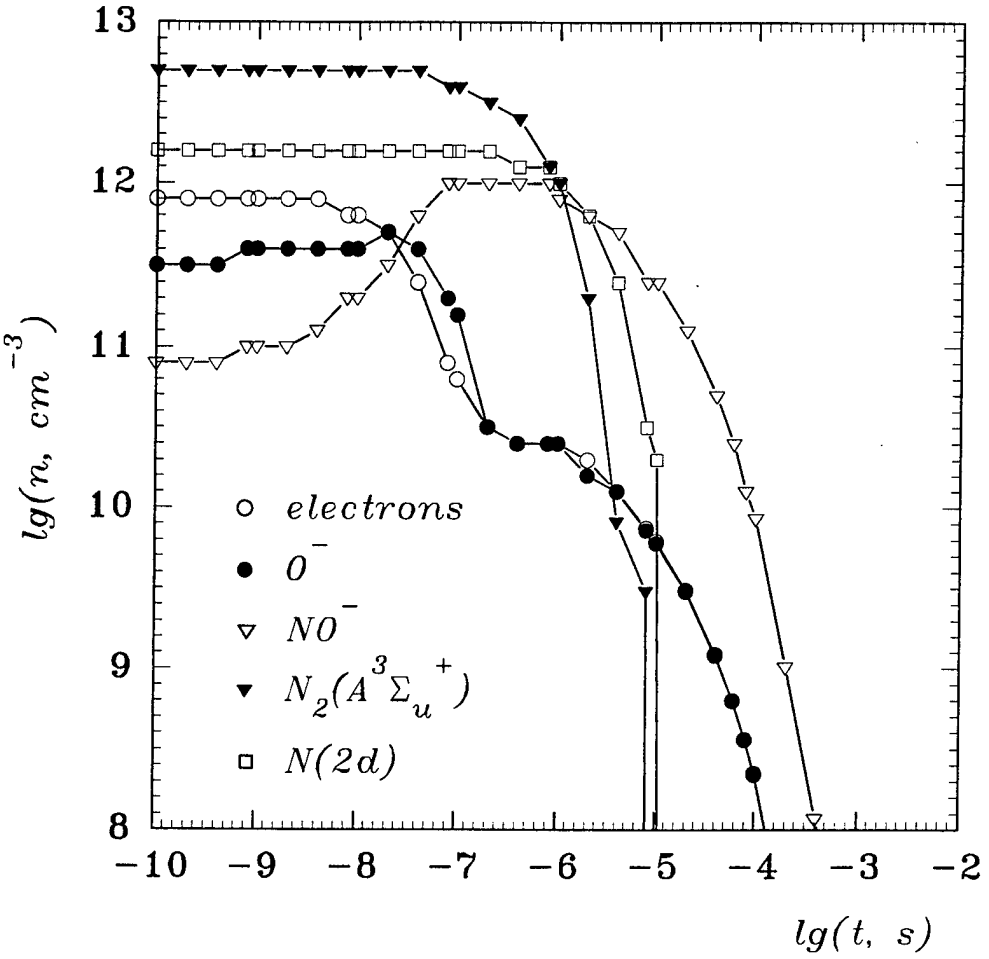

Figure 8.4: Main components number density dynamics. Initial stage of the decomposition ($[N_2O]/[N_2O]_0 \sim 1$). Initial pressure of N_2O $p = 4.72$ Torr. $U_{gen} = -13$ kV.

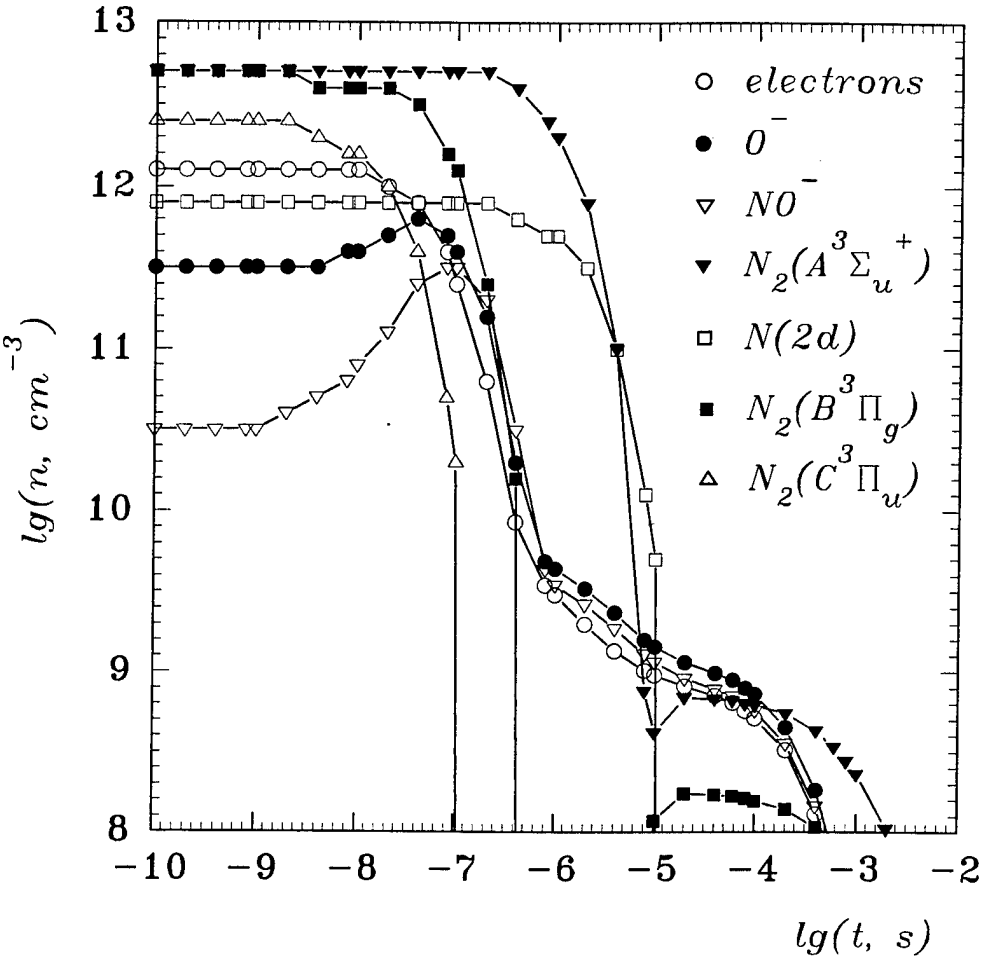

Figure 8.5: Main components number density dynamics. Final stage of the decomposition ($[N_2O]/[N_2O]_0 \sim 0.5$). Initial pressure of N_2O $p = 4.72$ Torr. $U_{gen} = -13$ kV.

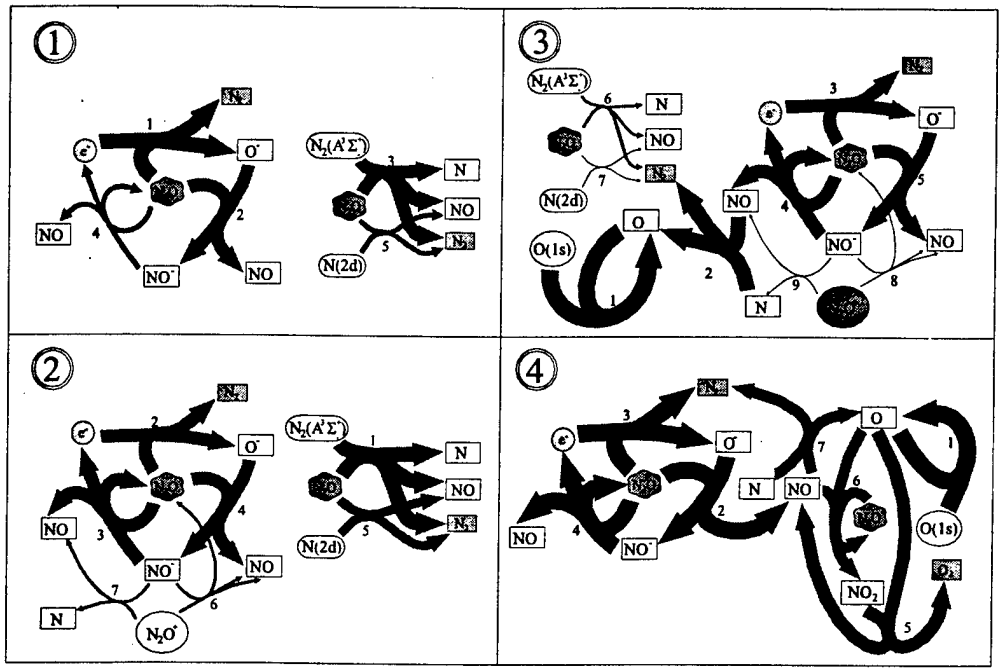

Figure 8.6: Active particles flow diagram. Initial stage of the decomposition ($[N_2O]/[N_2O]_0 \sim 1$). Initial pressure of N_2O $p = 4.72$ Torr. $U_{gen} = -13$ kV.

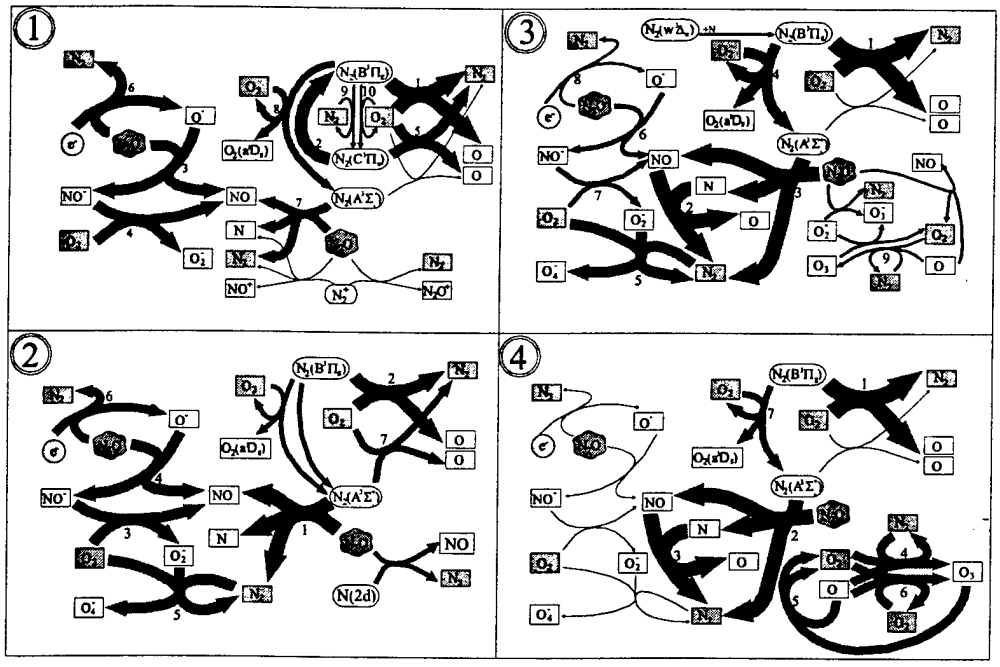

Figure 8.7: Active particles flow diagram. Final stage of the decomposition ($[N_2O]/[N_2O]_0 \sim 0.5$). Initial pressure of N_2O $p = 4.72$ Torr. $U_{gen} = -13$ kV.

Chapter 9

Numerical modeling of ignition of combustible mixtures by pulsed nanosecond discharge

In [113] we demonstrated the fundamental possibility of the FIW application for homogeneous ignition of chemically active mixtures. There was reviewed the problem of ignition of the preliminary heated mixture H_2 - O_2 when the initial active particle concentration is created by the nanosecond pulsed discharge. The main objective of this stage of research was a numerical evaluation of efficiency of the FIW application to initiate the H_2 – air and CH_4 – air mixture combustion.

9.1 Kinetic scheme

Kinetics scheme, designed by the purpose the subsequent identification of a set of chemical reactions, should, whenever possible, include the most complete list of those elementary processes, which in given conditions though potentially can render influence to process as a whole.

The selection of reactions and the optimization of model (spent with the help of the analysis of speeds and sensitivity spectrum of a system to change of constants of speeds of separate reactions) permit to identify as the most important stages and to exclude from consideration immaterial.

As far as the modelling of chemical processes under our conditions should be conducted in a wide range of concentration and temperatures, in kinetics scheme were included as reactions with the participation HO_2, essential only at the lowest temperatures, as reactions with participation of atoms N, which can introduce some contribution at temperatures above 3000 K. The model was completed by the set of reactions, which describe free radicals appearing due to the ionization wave development.

It is necessary to note a distinction between hydrogen- and methane- containing mixtures. In the case of the mixtures containing hydrogen a significant part of the energy stored in discharge is directed on the dissociation of molecular hydrogen. Relatively high dissociation degree leads to an active reaction development. In the mixtures containing methane, a cross-section of dissociation of CH_4 by an electron impact is mediocre, and the main radical produced is an atomic oxygen.

On the basis of great difference between characteristic times ($\sim 10^{-9}$ for FIW and $\sim 10^{-6}$ for combustion processes) the problems of active particles formation in the discharge and ignition/combustion were separately regarded.

The kinetic system including 83 reagents was used for analysis: H, H^-, H^+, H_2, H_2^+, H_3^+, HO, HO^-, HO^+, HO_2, HO_2^+, H_2O, H_2O^+, H_2O_2, $H_2O_2^-$, $H_2O_3^-$, $H_2O_3^+$, H_3O^+, HNO, HONO, $HONO_2$, HO_2NO_2, N, $N(^2D^0)$, $N(^2P^0)$, N^+, N_2, $N_2(a^{1\prime}\Sigma_u^-)$, $N_2(a^1\Pi_g)$, $N_2(A^3\Sigma_u^+)$, $N_2(B^3\Pi_g)$, $N_2(B^3\Sigma_u^-)$, $N_2(C^{1,3}\Pi_u)$, $N_2(C^3\Pi_u)$, $N_2(W^1\Delta_u)$, N_2^+, $N_2(w^3\Delta_u)$, N_3, N_3^+, N_3O^+, N_4^+, NH, NH^+, NH_2, NH_3, NH_3^+, NH_4, NO, NO^-, NO^+, NO_2, NO_2^-, NO_2^+, NO_3, NO_3^-, NO_3^+, N_2O, N_2O^-, N_2O^+, $N_2O_2^+$, $N_2O_3^-$, $N_2O_3^+$, N_2O_4, N_2O_5, O, $O(^1D)$, $O(^1S)$, $O^-(^2P^0)$, $O(^3P)$, O^-, O^+, O_2, $O_2(a^1\Delta_g)$, $O_2(A^3\Sigma_u^+)$, $O_2(b^1\Sigma_g^+)$, O_2^-, O_2^+, O_3, O_3^-, O_3^+, O_4^-, O_4^+, electrons.

For CH_4 bearing mixtures reactions of C and C_2 hydrocarbons were included.

9.2 Initial conditions

To solve the ignition problem FIW was assumed to be defined as an instantaneous source of the O, H, N, C atoms, ions and excited molecules of concentrations taken on the basis of the available experimental data and numerical calculations of excitation by an electron impact. The ignition of mixture H_2:O_2:N_2 = 5 : 19 : 76 was calculated for initiation of the ionization wave of amplitude $U \simeq 250$ kV.

9.3 Results of calculations

9.3.1 H_2-Air mixture

Calculated values of ignition times for pressures $P = 1, 0.1, 0.01, 0.001$ atm are given in Fig. 9.1 respectively. Curves "5-8" in the figure are the dependence for thermal excitation, and curves "1-4" — dependence at instantaneous exposure to a thermal excitation and an ionization wave. In the whole temperature range from 2500 to 800 K the induction time essentially decreases if a minor preliminary atom concentration is created.

Under all temperature range from 2500 to 800 K induction time under the ionization wave affect much more smaller, than under thermal excitation only. At high temperatures (2500 K) induction times differ from each other by 1.5 times. This difference monotonically increases with temperature decreasing and becomes an order of magnitude at $T = 1150$ K ($P = 1$ atm) and $T = 1100$ K ($P = 0.5$ atm). At more lower temperatures mechanism of ignition is changed.

The calculations show an additional increasing of the discrepancy between different ignition regimes with the translational temperature decrease ($\tau_{ind}^1/\tau_{ind}^2 \simeq 10$ and 1000 at $T = 1100$ and 1000 K, respectively).

The sensitivity of the induction time of the mixture at $T = 1250$ K, $p = 1$ atm in the condition of thermal (histograms "2") and combined (histograms "1") excitation is shown in Fig. 9.2. It is obvious that for the both cases the maximum sensitivity corresponds to the processes of the chain propagation:

$H + O_2 \rightarrow O + OH$

$O + H_2 \rightarrow H + OH$

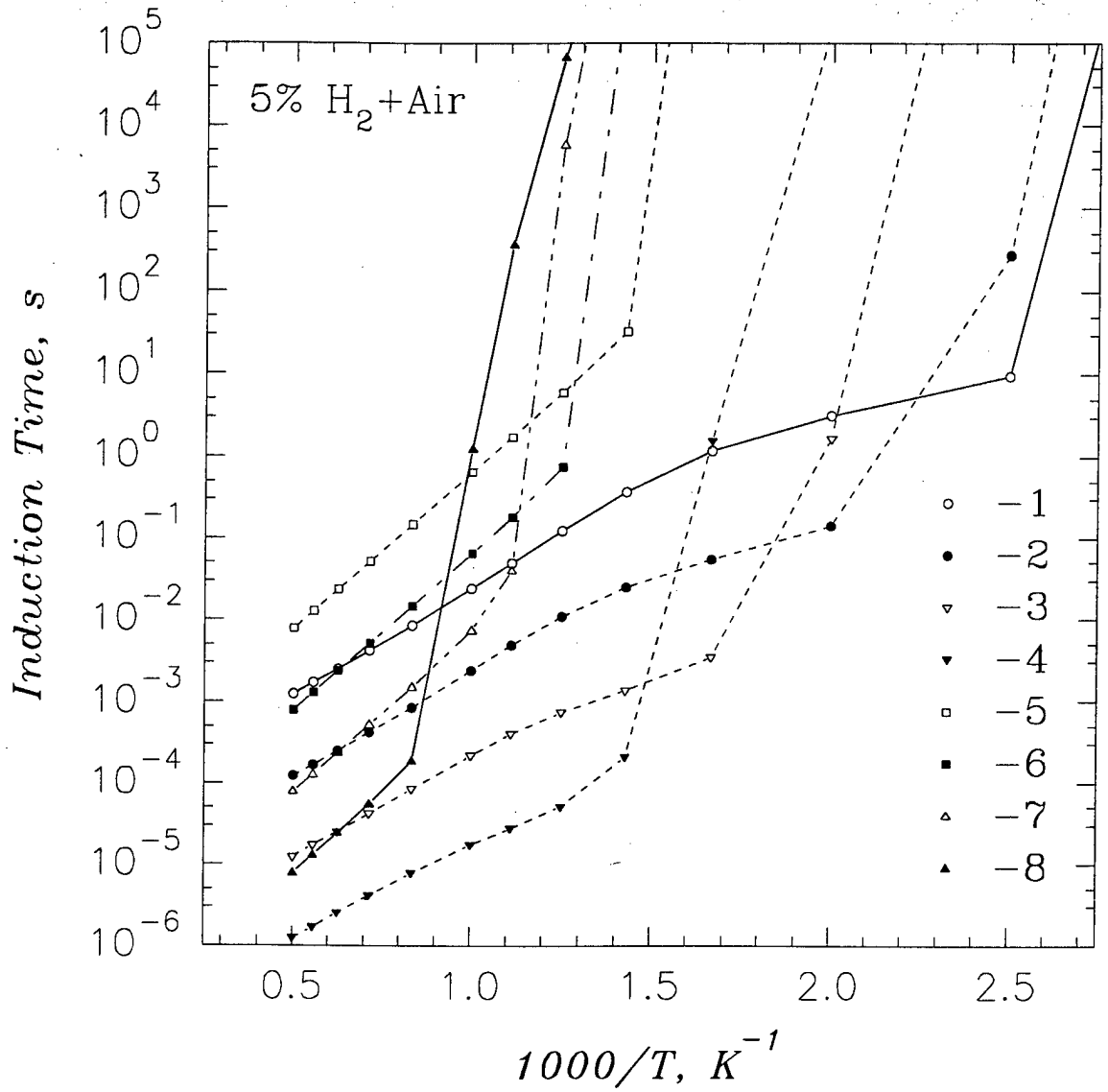

Figure 9.1: Temperature dependence of ignition delay time for thermal (5-8) and combined (1-4) initiation. Mixture 5% H_2 + Air. $P = 0.001, 0.01, 0.1, 1$ atm for 1-4 and 5-8, respectively.

and reaction of the chain break off:

$H + O_2 + M \rightarrow HO_2 + M$

The dependence of the sensitivity upon rate constants of different processes at combined excitation at $T = 820$, 925 and 1250 K is represented in Fig. 9.3 (curves 1, 2 and 3, respectively). The dynamics of the process as a whole is defined by the same stages at all temperatures considered. An abrupt rise of sensitivity coefficients should be noted at $T = 925$ K. It corresponds to the point of transition of an ignition mechanism (Fig. 9.1) and to the increase of the role of processes with HO_2 as temperature decrease.

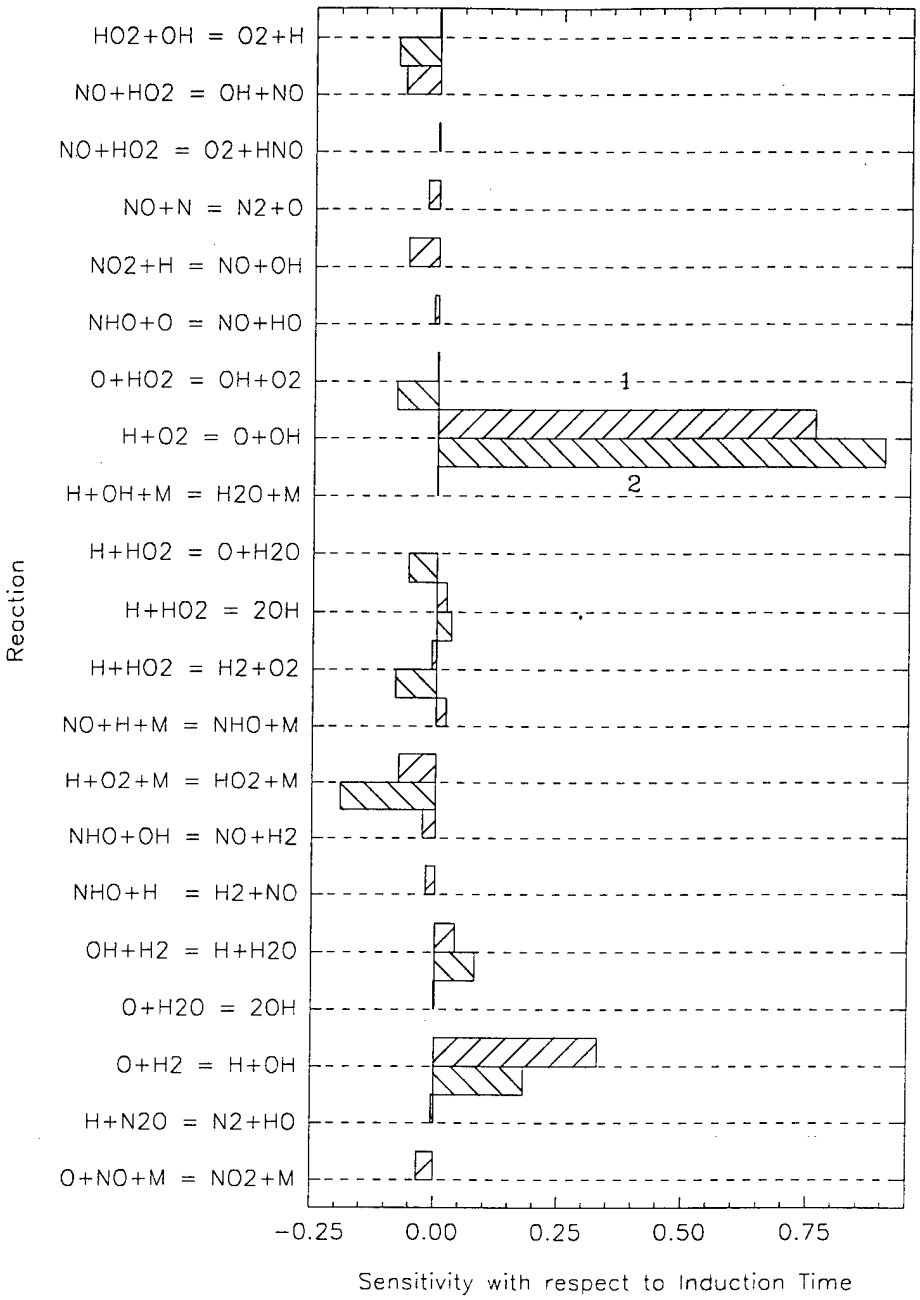

Figure 9.2: The sensitivity of the induction time of the mixture at $T = 1250$ K, $p = 1$ atm in the condition of thermal (histograms 2) and combined (histograms 1) excitation. Mixture 5% H_2 + Air.

9.3.2 CH_4-Air mixture

Inasmuch as dissociation degree of CH_4 in discharge substantially smaller then it is for hydrogen, an ignition of an air-methane mixture is much more difficult. The difference between thermal excitation and non-equilibrium initiation of process in methane is not so strong as in hydrogen-containing mixtures (Fig. 9.4, 9.5, 9.6, 9.7).

It is necessary to note that with the decrease of fuel concentration on the mixture the process transfers from chain-thermal to simple chain propagation mechanism. On further

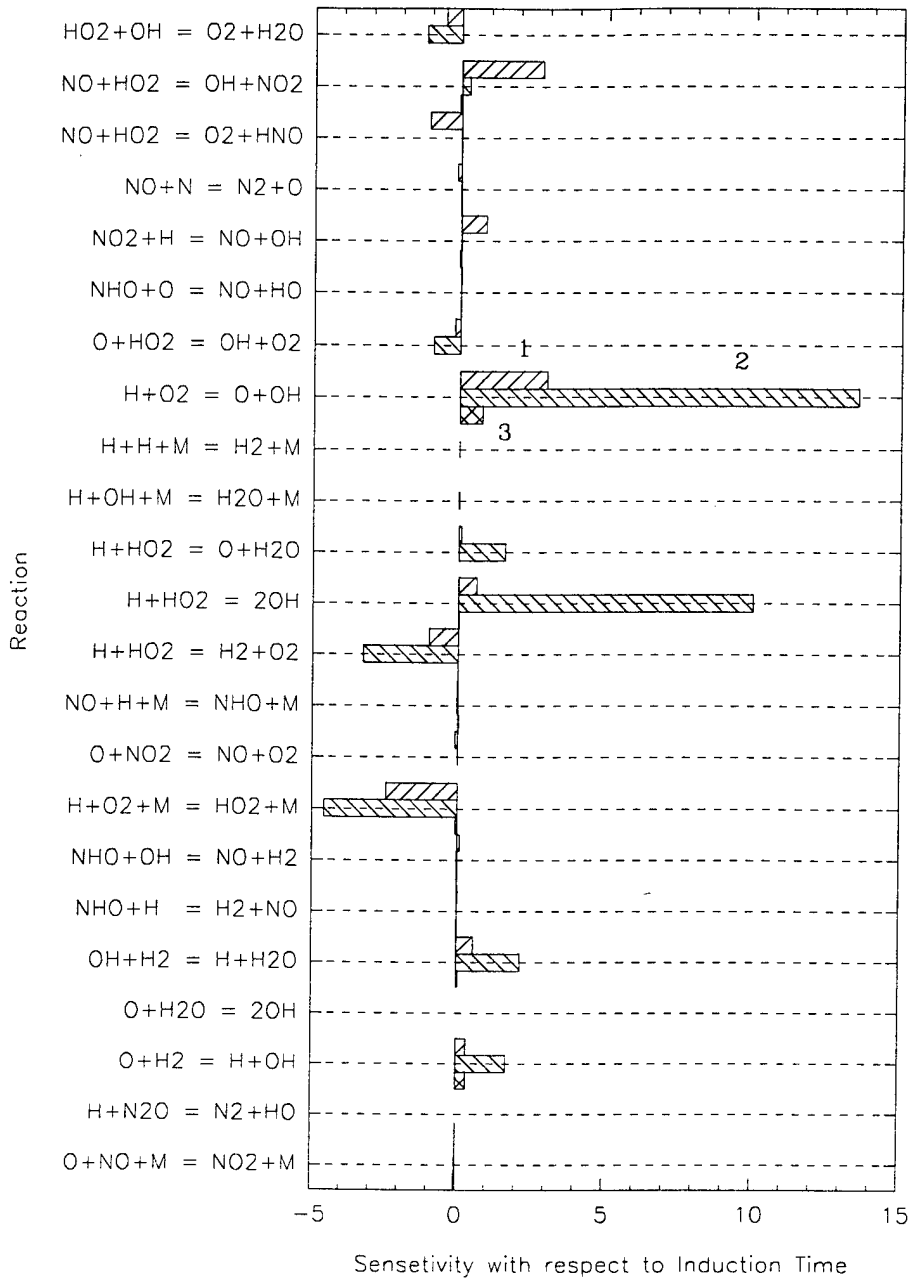

Figure 9.3: The dependence of the sensitivity upon rate constants of different processes at combined excitation at $T = 820$, 925 and 1250 K (histograms 1, 2 and 3, respectively). Mixture 5% H_2 + Air.

decrease of H_2 or CH_4 concentration the propagation of reaction comes to a stop. In such a case an influence of the pulsed discharge leads to the production of free radicals and electronically-excited molecules. The following evolution of created nonequilibrium plasma is described by the processes of recombination, redistribution of an internal energy and radiation of metastable states.

An analogous conclusion may be made for the high-temperature boundary of ignition. In fact, for the flame propagation a significant heating of the mixture is needed. At low temperatures the development of the process is bounded by a process of radicals

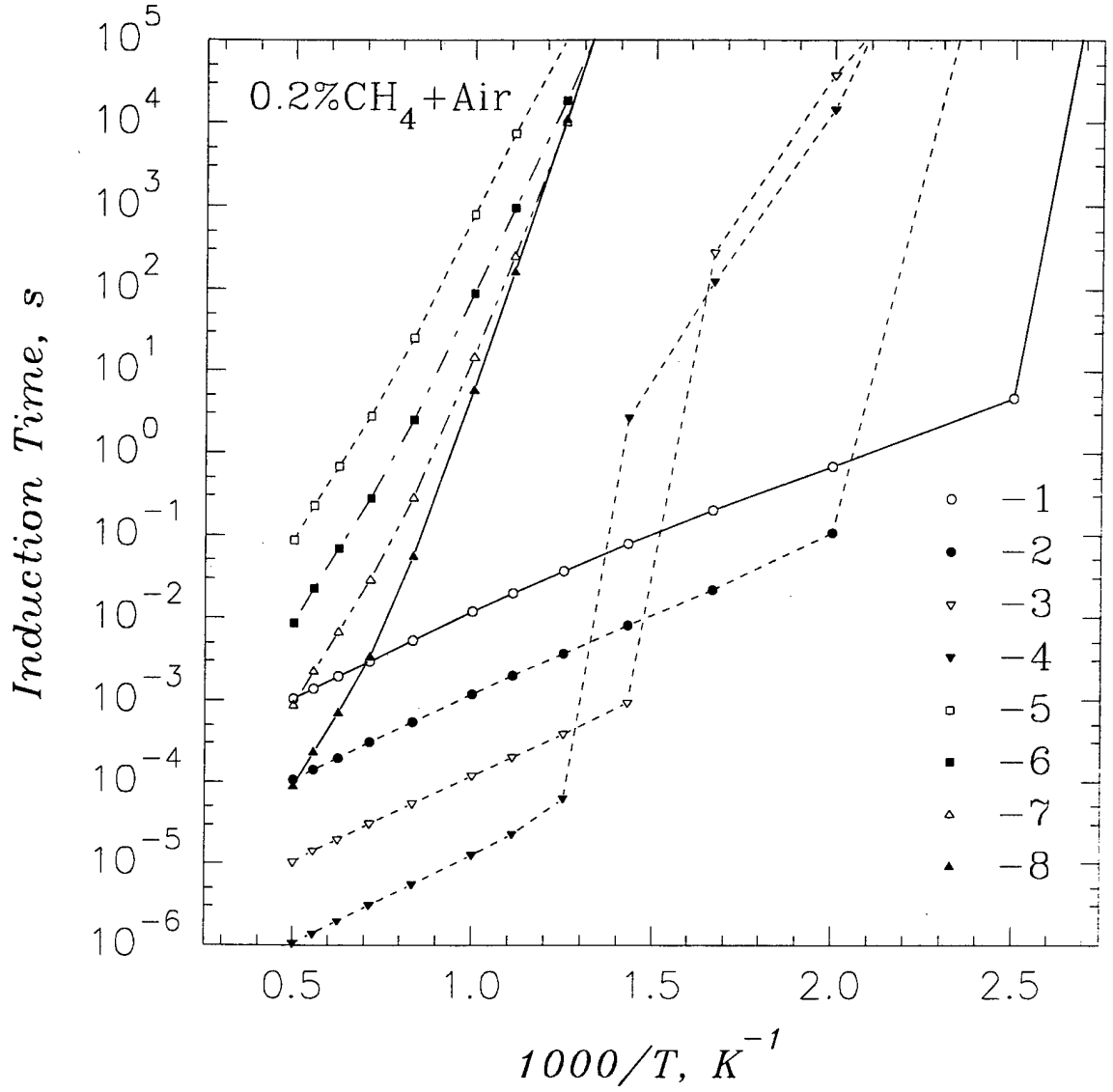

Figure 9.4: Temperature dependence of ignition delay time for thermal (5-8) and combined (1-4) initiation. Mixture 0.2% CH_4 + Air. $P = 0.001, 0.01, 0.1, 1$ atm for 1-4 and 5-8, respectively.

recombination because of relatively high energetic barrier of bimolecular processes of the chain development.

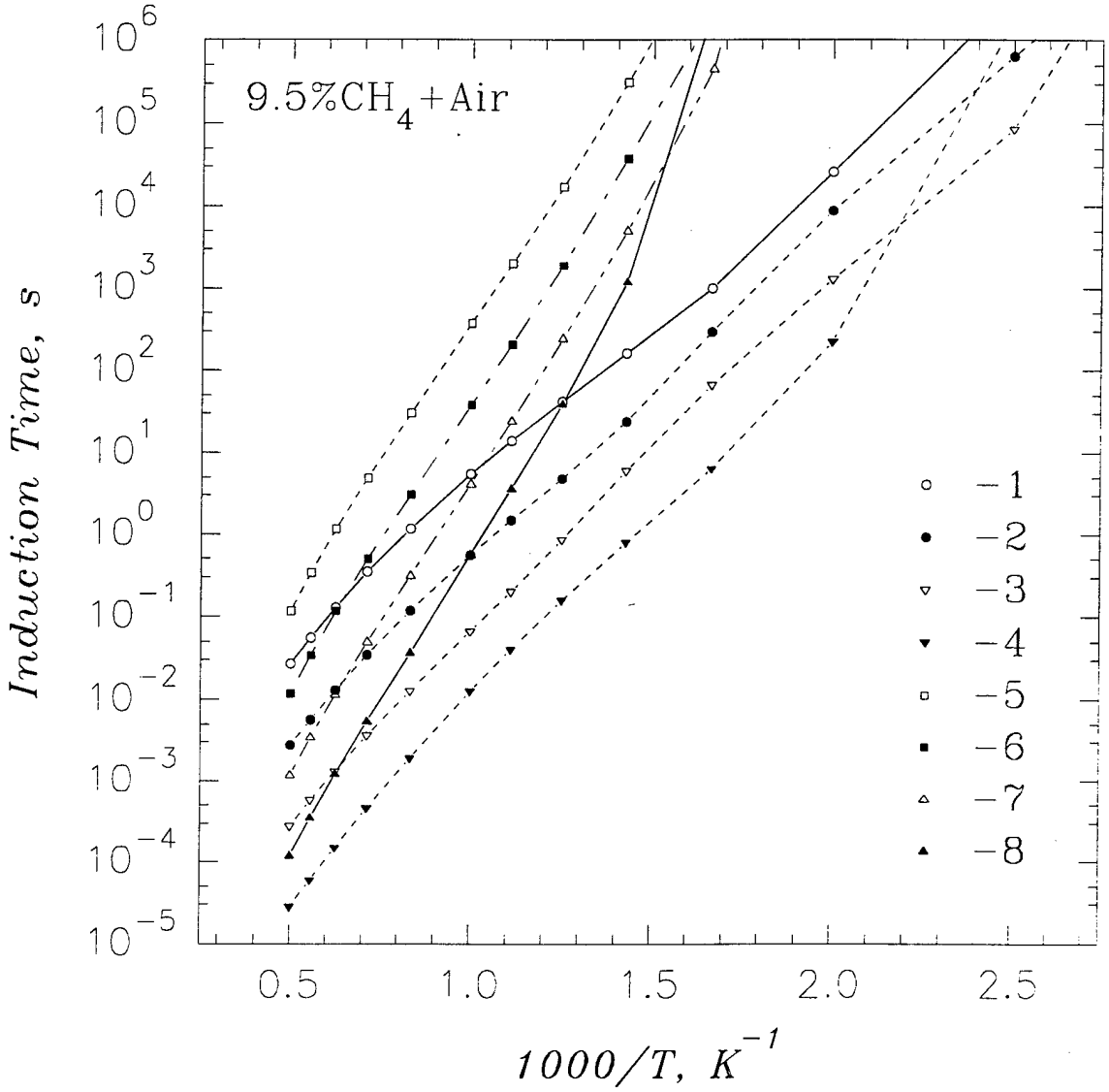

Figure 9.5: Temperature dependence of ignition delay time for thermal (5-8) and combined (1-4) initiation. Mixture 9.5% CH_4 + Air. $P = 0.001, 0.01, 0.1, 1$ atm for 1-4 and 5-8, respectively.

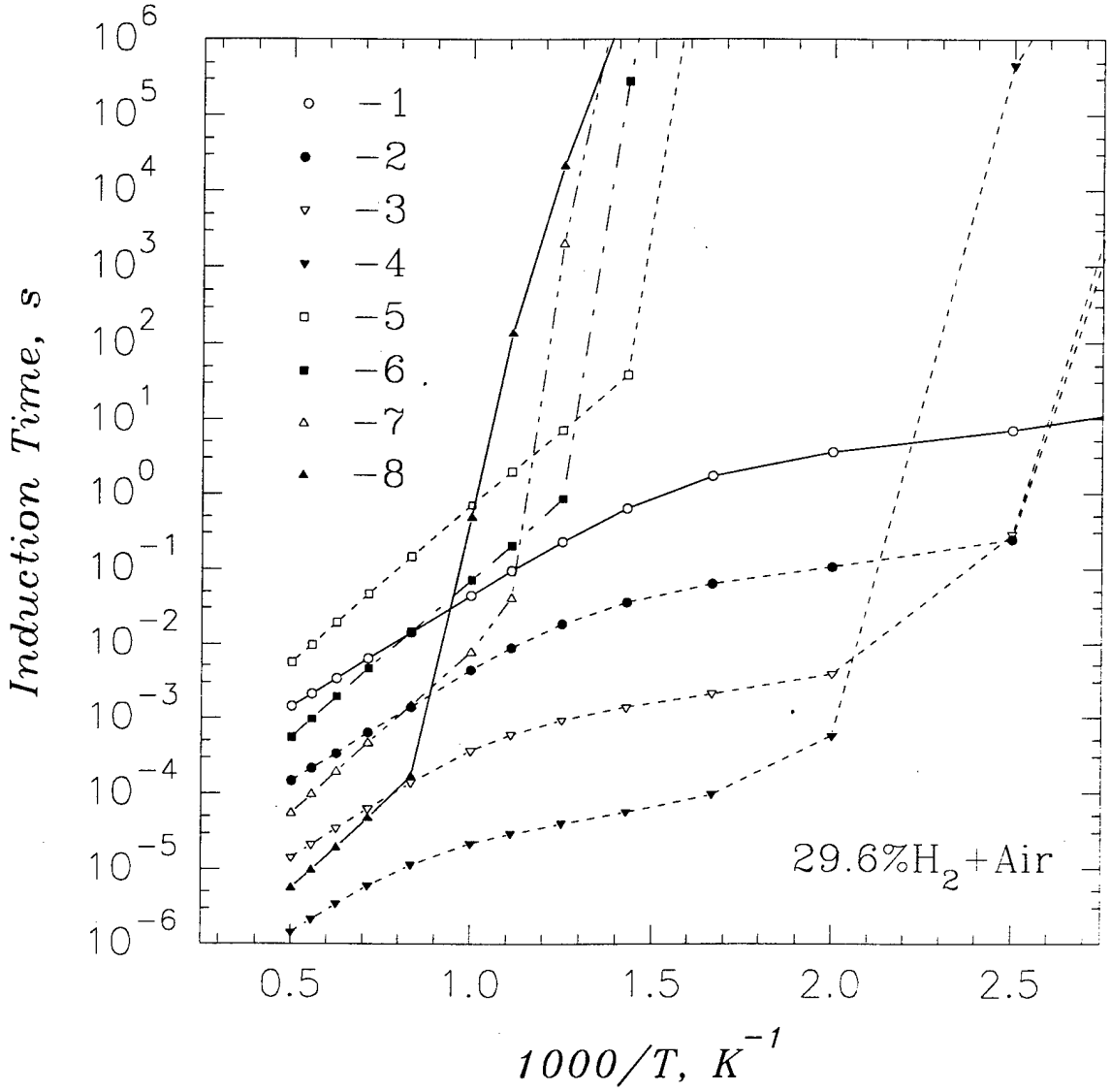

Figure 9.6: Temperature dependence of ignition delay time for thermal (5-8) and combined (1-4) initiation. Mixture 29.6%H_2 + Air. $P = 0.001, 0.01, 0.1, 1$ atm for 1-4 and 5-8, respectively.

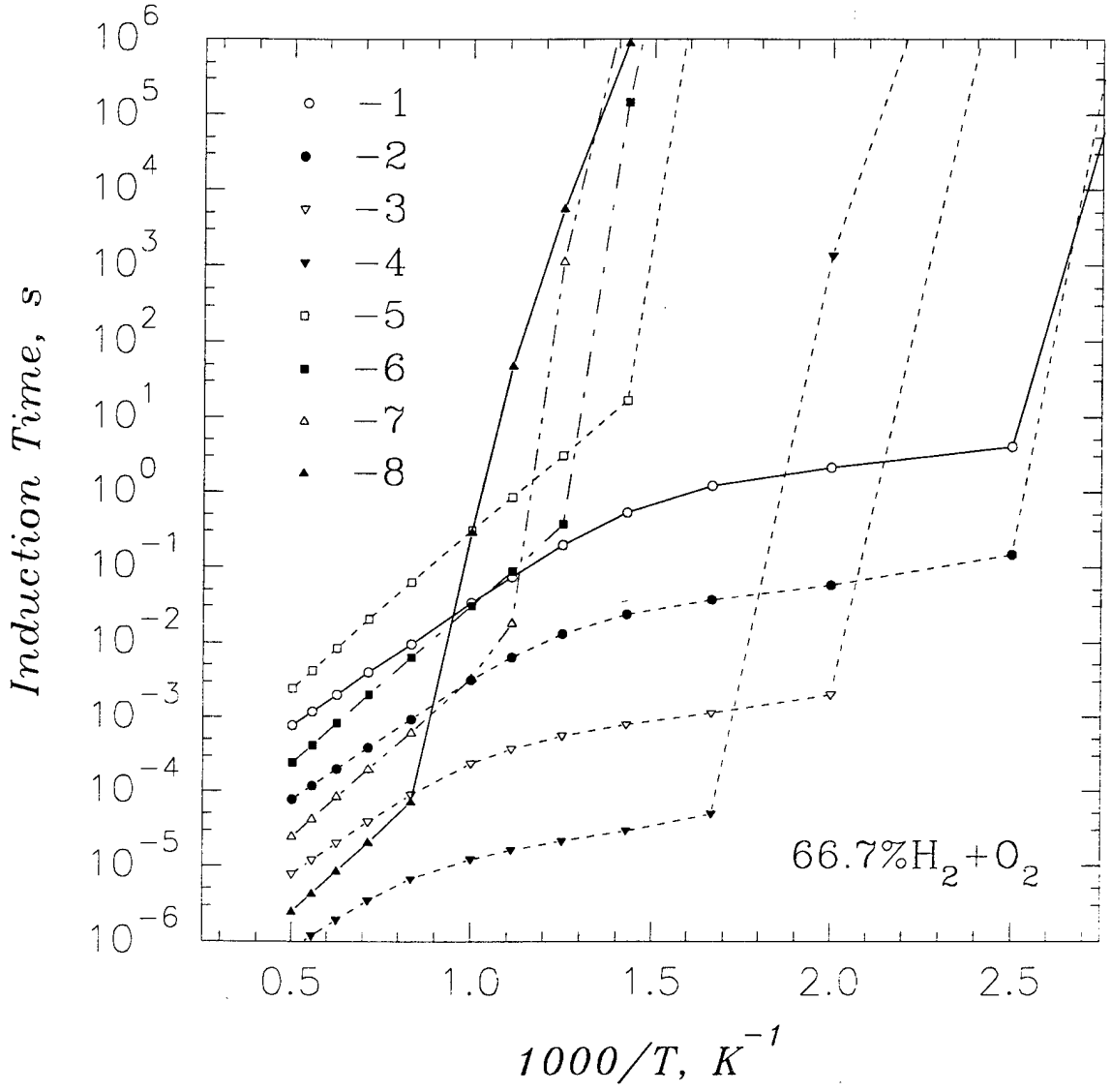

Figure 9.7: Temperature dependence of ignition delay time for thermal (5-8) and combined (1-4) initiation. Mixture 66.7% H_2 + O_2. $P = 0.001, 0.01, 0.1, 1$ atm for 1-4 and 5-8, respectively.

Chapter 10

Numerical Simulation of Active Species Production by a Positive Streamer and Streamer Ignition Initiation

10.1 Numerical modeling of streamer development and propagation

A possibility to propagate even in the discharge gaps with an external field less than breakdown one is a characteristic feature of a streamer breakdown [182]. Increasing interest for this type of discharge nowadays is explained by its technical applications, particularly for the production of atoms, ions and active radicals gases at high pressures.

Streamer development and propagation is governed by processes of a photoionization, ionization by an electron impact and drift of charged particles in the region of high electric fields in a streamer head. Streamer velocity range is $10^7 - 10^8$ cm/s at a typical radius of a streamer channel $10^{-2} - 1$ cm.

10.1.1 Numerical Modelling

Numerical calculations of the last decade [191]-[192] has been demonstrated the possibility of a modelling of streamer breakdown in uniform over-breakdown fields in 2-dimensional statement of the problem. All these papers were based on a hydrodynamic model of electron motion description solved together with a Poisson equation to calculate a self-consistent electric field.

There are a few papers [193, 194, 195] where the Monte-Carlo technique was used to calculate an electron motion and heating by electric field. In spite of the fact that this technique is applicable in extremely wide region of parameters and allows to obtain correct result even at very high electric fields and gradients where the hydrodynamic approach is not valid their computational complexity is so high that up to now only initial stages of the avalanche – streamer transition were calculated using Monte-Carlo technique [193].

In [196] for the description of a streamer propagation electron impulse and electron energy conservation laws were taken into account. Electrons were considered as a mass-

less particles in the local equilibrium with an electric field. Results of the calculations were close to results obtained in diffusion-drift approximation [191, 197, 198, 199, 192].

To solve the problem of a streamer propagation in the long discharge gaps so called 1.5D models were proposed [200]. These models include 1-dimensional conservation laws for charged particles and 2-dimensional equations for electric field calculation. Such models were used to describe streamer propagation and plasmachemical processes in weak fields [201]-[202]. Unfortunately these models need a fitting parameter. It is a diameter of a streamer channel, which influences strongly on a streamer dynamics and properties.

Taking this parameter from the experiment it is possible to fit calculations and experimental results. At the same time in complex gas mixtures and at experimental conditions where this parameter is unknown results will not be very reliable.

Models which take into account ionization expansion of a streamer channel represent an interesting development of the model mentioned [203, 204]. The dependence of initial choice of a channel radius is not so dramatic here. The main disadvantage of this method is an averaging of all plasma parameters across a diameter of a streamer channel.

10.1.2 Streamer propagation in air

Streamer modelling was held in 2D geometry in a diffusion-drift approximation. The numerical model includes a balance equations for charged particles (10.1,10.2) and equation for the distribution of electric fields in a discharge gap (10.3):

$$\frac{\mathrm{d}n_e}{\mathrm{d}t} + \mathrm{div}\left(\mathbf{v}_e \cdot n_e\right) = S_{ion} + S_{photo} - S_{att} \tag{10.1}$$

$$\frac{\mathrm{d}n_i}{\mathrm{d}t} = S_{ion} + S_{photo} - S_{att} \tag{10.2}$$

$$\mathrm{div}\mathbf{E} = \frac{e}{\varepsilon_0}\left(n_i - n_e\right) \tag{10.3}$$

Here n_e and n_i are electron and positive ion densities, $\mathbf{v_e}$ is a drift velocity in a local electric field $\mathbf{E}$, S_{ion} and S_{photo} are ionization and photoionization rates correspondingly, S_{att} is a velocity of an electron attachment.

$$S_{ion} = \left(k_{ion}^{N_2}[\mathrm{N_2}] + k_{ion}^{O_2}[\mathrm{O_2}]\right) n_e \tag{10.4}$$

$$S_{att} = k_{att}^{O_2}[\mathrm{O_2}] n_e \tag{10.5}$$

$$S_{photo} = \frac{1}{4\pi}\frac{p_q}{p+p_q}\int_V \mathrm{d}^3\mathbf{r}_1 \frac{S_{ion}(\mathbf{r}_1)}{|\mathbf{r}-\mathbf{r}_1|^2}\Psi(|\mathbf{r}-\mathbf{r}_1|\cdot p) \tag{10.6}$$

Here $[\mathrm{N_2}]$ and $[\mathrm{O_2}]$ are molecular nitrogen and oxygen concentrations in air, [M] is a total density of neutral particles, p is a gas pressure, p_q is pressure of quenching of the photoionizing states, $\Psi(|\mathbf{r}-\mathbf{r}_1|\cdot p)$ is a coefficient of ionizing radiation absorption.

The problem was solved in an axial geometry in a cylindrical coordinate system (z, r). The basic equations were projected on an adaptive mesh in a finite-difference approximation. An anode was given as a hyperboloid. A cathode was placed at a distance $L = 24$ mm from a top of a hyperboloid. The region near a streamer head was calculated

on a uniform mesh with a size 400x200 cell each one $\delta z_{min} = \delta r_{min} = 0.01$ mm. Outside the detailed mesh space step increased monotonically up to $\delta z_{max} = \delta r_{max} = 1.0$ mm. The total number of cells increased with a streamer propagation and reached value of 1000x500. A typical time step was $\delta t \sim 10^{-12}$ s and was corrected with every new iteration.

The equations (10.1-10.3) were solved numerically using final difference schemes which approximate initial equations to order Δt and $(\Delta x)^2$. The conservatism of an initial system of equations was kept. Equation (10.3) was transformed to a Poisson equation with known boundary conditions. To solve the equation standard method of Gauss-Seidel with an upper relaxation was used.

Because of computational complexity of photoionization calculation we calculated photoionization rate once per a several steps and in those cells only where electron density was less than threshold value $n_e \leq 10^{10}$ cm^{-3}.

Rates of elementary processes: ionization ($k_{ion}^{N_2}$, $k_{ion}^{O_2}$) and dissociative attachment O_2 ($k_{att}^{O_2}$) were taken from [205]. The photoionization rate S_{photo} was recalculated according to the constant rates and functional dependencies taken from [206, 207].

Approximating formulas for constant rates of processes with electrons and photoionization are represented below (here and further $\gamma = 10^{16}$ V·cm^2=10 Td; $\xi = 1$ cm·Torr). To calculate the constant rates authors [205] used stationary solution of the Boltzmann equation in two-term approximation.

- $e + N_2 \xrightarrow{k_{ion}^{N_2}} 2e + N_2^+$

$$\lg k_{ion}^{N_2} = \begin{cases} -8.09 - 40.29/\gamma, & 8 \leq \gamma \leq 30 \\ -7.37 - 61.81/\gamma, & 30 < \gamma \leq 100 \end{cases} \tag{10.7}$$

- $e + O_2 \xrightarrow{k_{ion}^{O_2}} 2e + O_2^+$

$$\lg k_{ion}^{O_2} = \begin{cases} -8.31 - 28.57/\gamma, & 6 \leq \gamma \leq 26 \\ -7.54 - 48.57/\left(\gamma + \lg(1 + 4 \cdot 10^{-7}\gamma^3)\right), & 26 < \gamma \leq 100 \end{cases} \tag{10.8}$$

- $e + O_2 \xrightarrow{k_{att}^{O_2}} O^- + O$

$$\lg k_{att}^{O_2} = \begin{cases} -9.42 - 12.7/\gamma, & 3 \leq \gamma \leq 9 \\ -10.21 - 5.7/\gamma, & 9 < \gamma \leq 30 \\ -10.33 - 2.7 \cdot 10^{-3}\gamma, & 30 < \gamma \leq 100 \end{cases} \tag{10.9}$$

- $h\nu + O_2 \xrightarrow{\Psi} O_2^+ + e$

$$\Psi(\xi) = \begin{cases} 7.145 \cdot 10^{-4} \exp(-0.05961\xi), & \xi \leq 100 \\ 5.463\xi^{-2.23619}, & 100 < \xi \leq 300 \\ 21.469\xi^{-3.30483}, & 300 < \xi \end{cases} \tag{10.10}$$

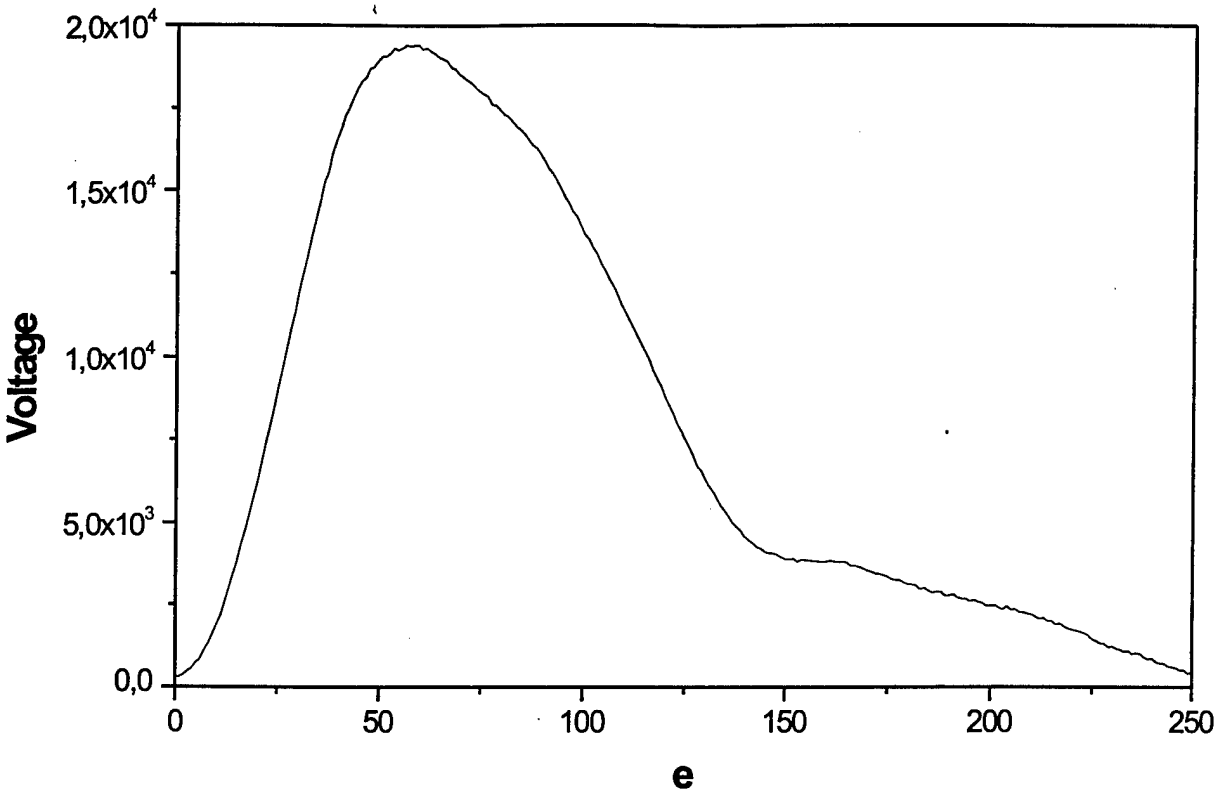

Figure 10.1: The shape of a voltage pulse

All other processes may be neglected in the time interval interested (up to 100 ns).

When modelling a streamer development in a "needle-plate" geometry high voltage electrode geometry was given as hyperboloid of revolution:

$$\left(\frac{z}{b}\right)^2 - \left(\frac{r}{a}\right)^2 = 1 \tag{10.11}$$

where $a = 1.8$ mm, $b = 10$ mm. The radius of curvature of an electrode tip in this case equal $a^2/b = 0.324$ mm. Such a shape of a high-voltage electrode looks like a real anode shape used in experiments.

Initial pre-ionization $n_e^0 = 10^{12}$ cm^{-3} was given in the close vicinity to the high-voltage electrode in a volume given by $\delta x = \delta r = 0.01$ mm.

Results of a numerical modelling

A strong dependence of streamer parameters upon a rise time of a high-voltage pulse on a high-voltage electrode has been demonstrated in [208] in the frameworks of a 1.5D-modelling of a streamer discharge in air in 1 cm gap. So, to be careful with the shape of initial voltage we used the high-voltage pulse with the same shape as it was in experiments [209] (Fig.10.1).

Typical streamer parameters at the time 50 ns after beginning of the voltage growth are represented in Fig.10.2, 10.3.

The dynamics of a streamer propagation is represented in Figures 10.4,10.5,10.6.

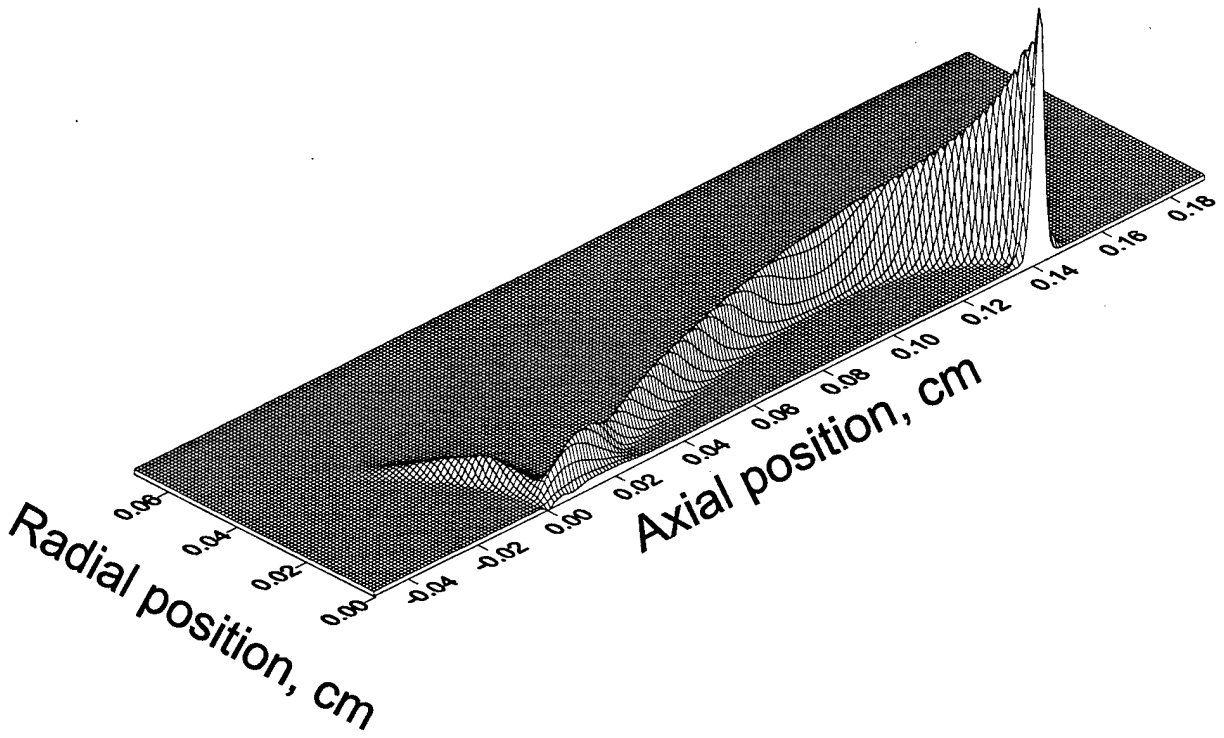

Figure 10.2: Graph of the electric charge in the discharge gap. $t = 50$ ns

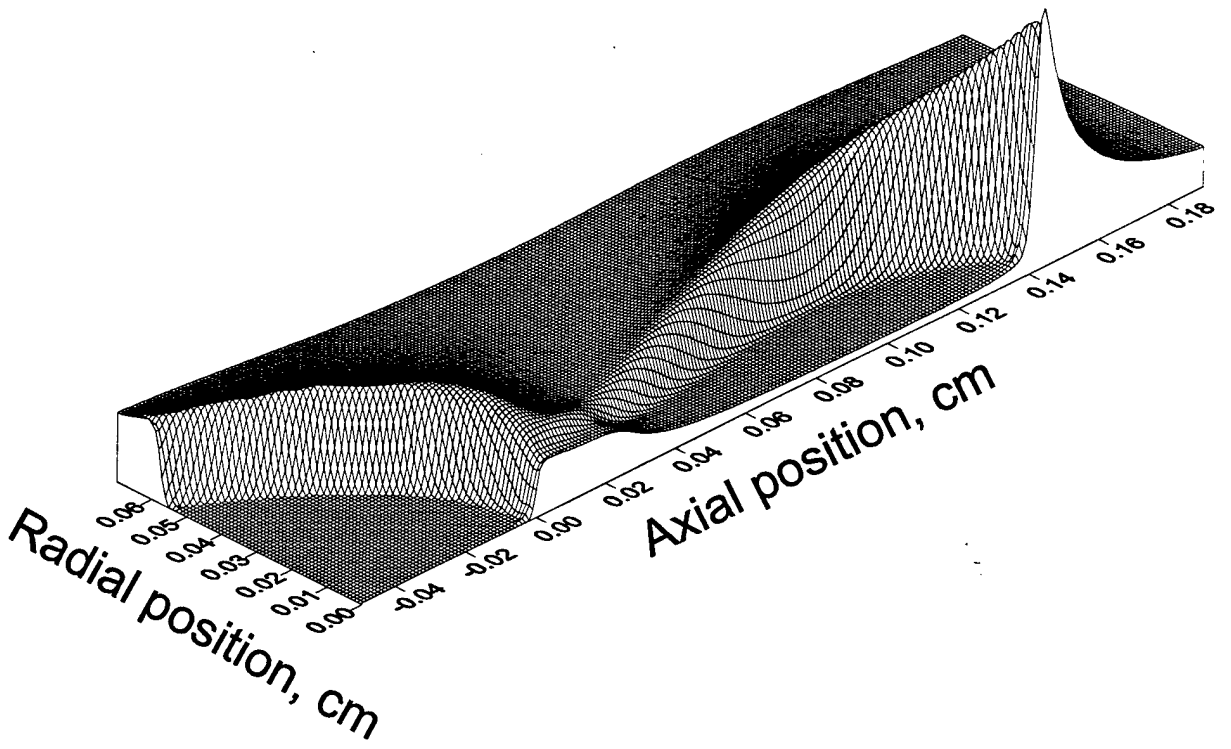

Figure 10.3: Graph of the absolute value of reduced electric field in the discharge gap. $t = 50$ ns

In all figures the isolines of a non-compensated charge, electron density, total electric field, ionization rate by an electron impact and photoionization rate are represented, correspondingly:

- **A** – logarithm of the space charge:
  - positive (blue) $3 \cdot 10^{-6} - 10^{-10}$ Kl/cm^3,
  - negative (red) $3 \cdot 10^{-7} - 10^{-10}$ Kl/cm^3;
- **B** – absolute reduced electric field value up to 600 Td with the step 50 Td;
- **C** – logarithm of the electron number density; *minimum* $= 10^{12}$, *maximum* $= 5 \cdot 10^{14}$ cm^{-3};
- **D** – logarithm of the ionization rate:
  - positive (blue) $2 \cdot 10^{12} - 10^{7}$ cm^{-3}/s,
  - negative (red) $10^{11} - 10^{7}$ cm^{-3}/s;
- **E** – the photoionization rate up to $2 \cdot 10^{8}$ cm^{-3}/s with the step size 10^{7} cm^{-3}/s.

Streamer channel length and radius change with time are represented in Fig.10.7. An initial acceleration and expansion of the channel are due to voltage rise on the anode.

Peak electric fields dynamic is represented in Fig.10.8. Practically in all the gap peak values of an electric fields do not change and equal $E_z = 530 \pm 10$ Td, $E_r = 350 \pm 5$ Td.

Comparison with the results of experiments

To compare with the experimentally studied intensities of emission of 2^+ and 1^- nitrogen systems the dynamics of population of $N_2(C^3\Pi_u, v = 0)$ and $N_2^+(B^2\Sigma_u^+, v = 0)$ excited states was calculated. Taking into account calculated electron density $n_e(z, r, t)$ and reduced electric field $E/N(z, r, t)$ the equation for the excited state balance were solved:

$$\frac{d[N^*]}{dt} = k_{ex} \cdot n_e \cdot [N_2(X^1\Sigma_g^+)] - \frac{[N^*]}{\tau}, \tag{10.12}$$

where k_{ex} is a constant rate of the level excitation by a direct electron impact, n_e is an electron density, τ is a total lifetime of the level taking into account radiative lifetime and collisional quenching:

$$\begin{aligned} \tau_c &= (1/\tau_0^c + k_c^{N_2}[N_2] + k_c^{O_2}[O_2])^{-1} \\ \tau_b &= (1/\tau_0^b + k_b^{N_2}[N_2] + k_b^{O_2}[O_2] + k_b^{M}[N_2][M])^{-1} \end{aligned} \tag{10.13}$$

The structure of the streamer head at a time moment $t = 62$ ns is represented in Fig.10.9. Profiles of the electric fields and electron density on the axis, profiles of the space charge per unit length and excitation rates of $N_2(C^3\Pi_u, v = 0)$ and $N_2^+(B^2\Sigma_u^+, v = 0)$ states are demonstrated in the Figure. It is obviously seen that the region of an intensive excitation of the electron states follows immediately after a front of the non-compensated charge. It is, in fact, a superposition of an electric field and electron density profiles.

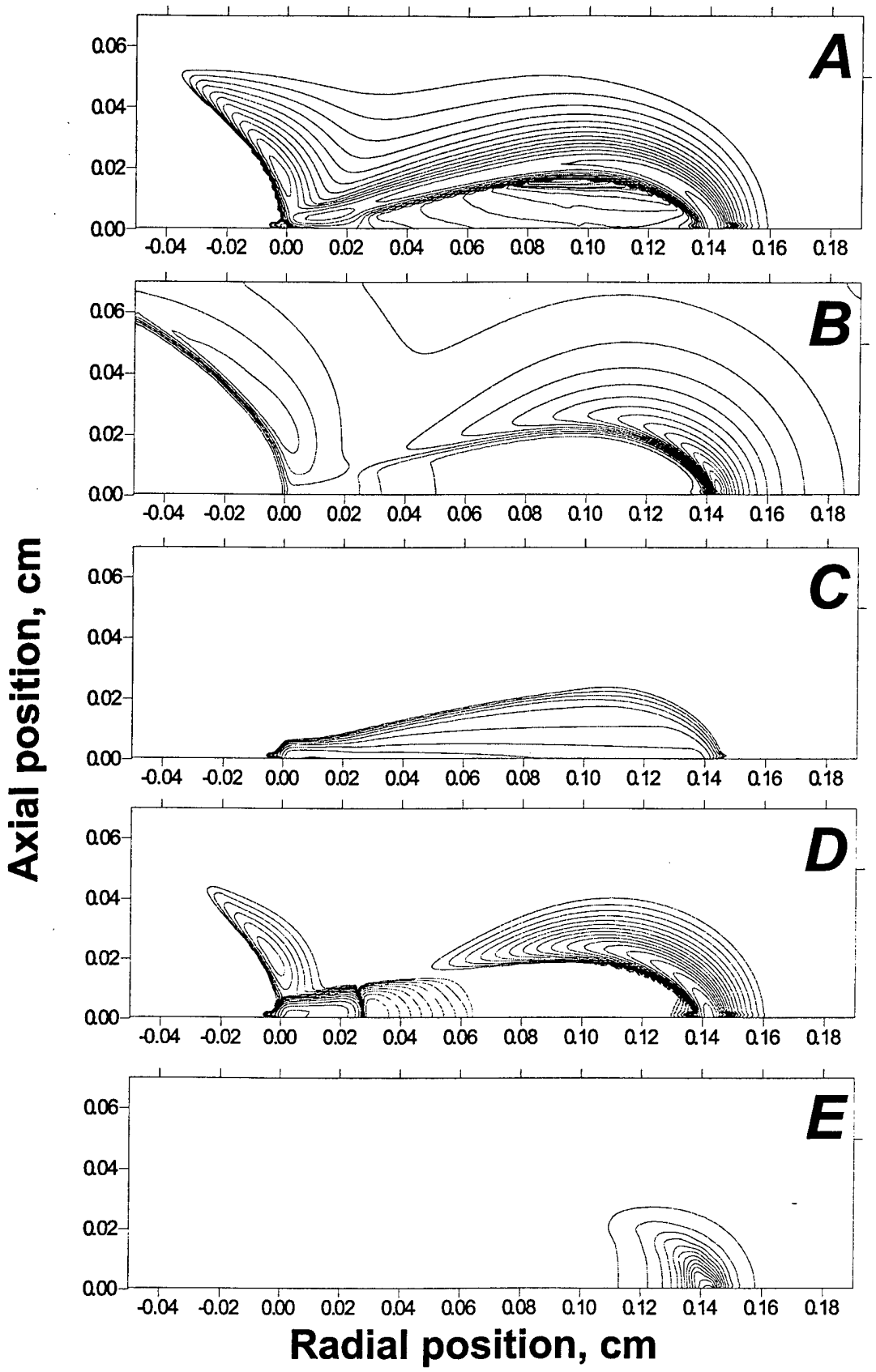

Figure 10.4: The isolines of a non-compensated charge, electron density, total electric field, ionization rate by an electron impact and photoionization rate at $t = 50$ ns.

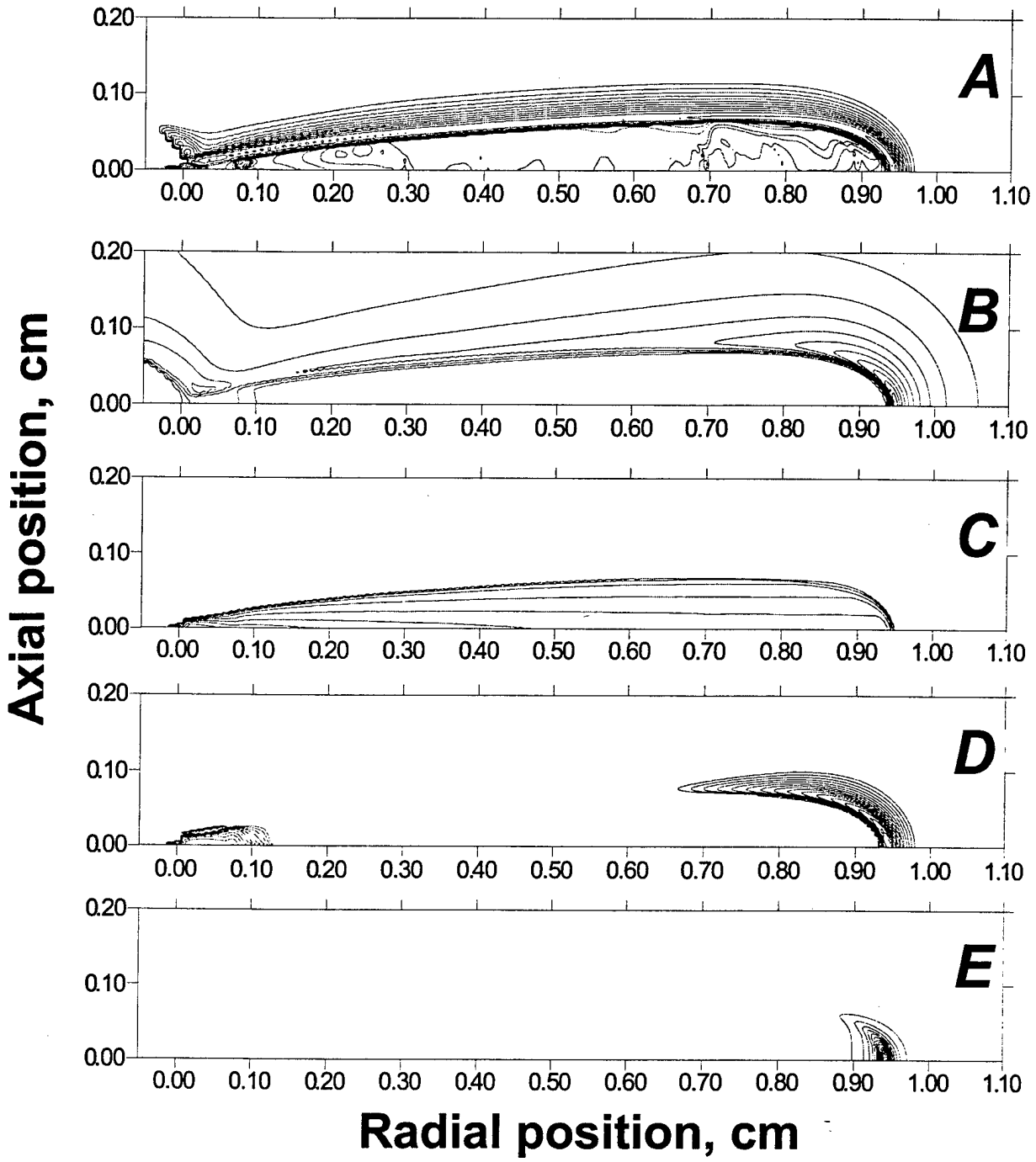

Figure 10.5: The isolines of a non-compensated charge, electron density, total electric field, ionization rate by an electron impact and photoionization rate at $t = 75$ ns.

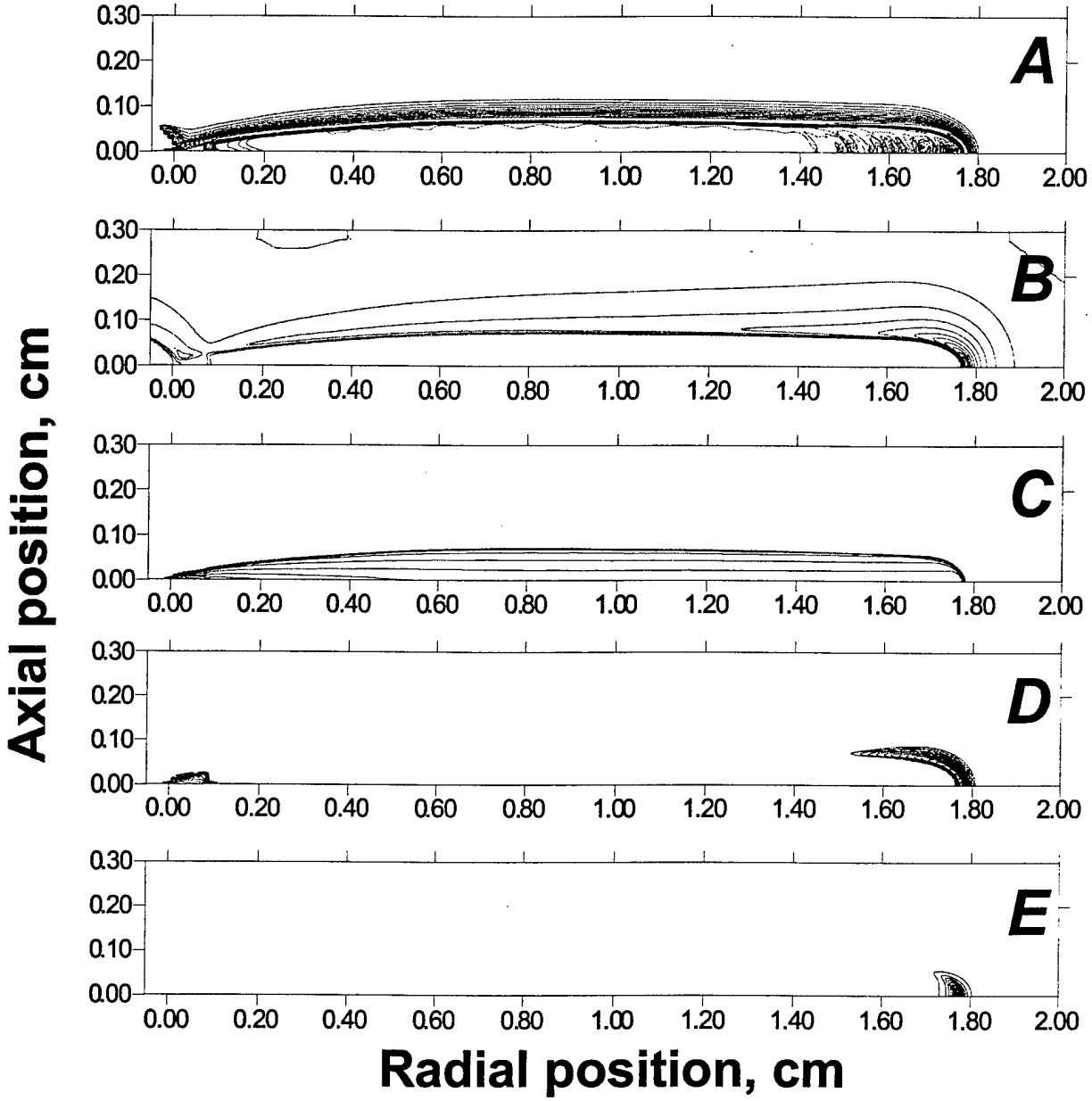

Figure 10.6: The isolines of a non-compensated charge, electron density, total electric field, ionization rate by an electron impact and photoionization rate at $t = 100$ ns.

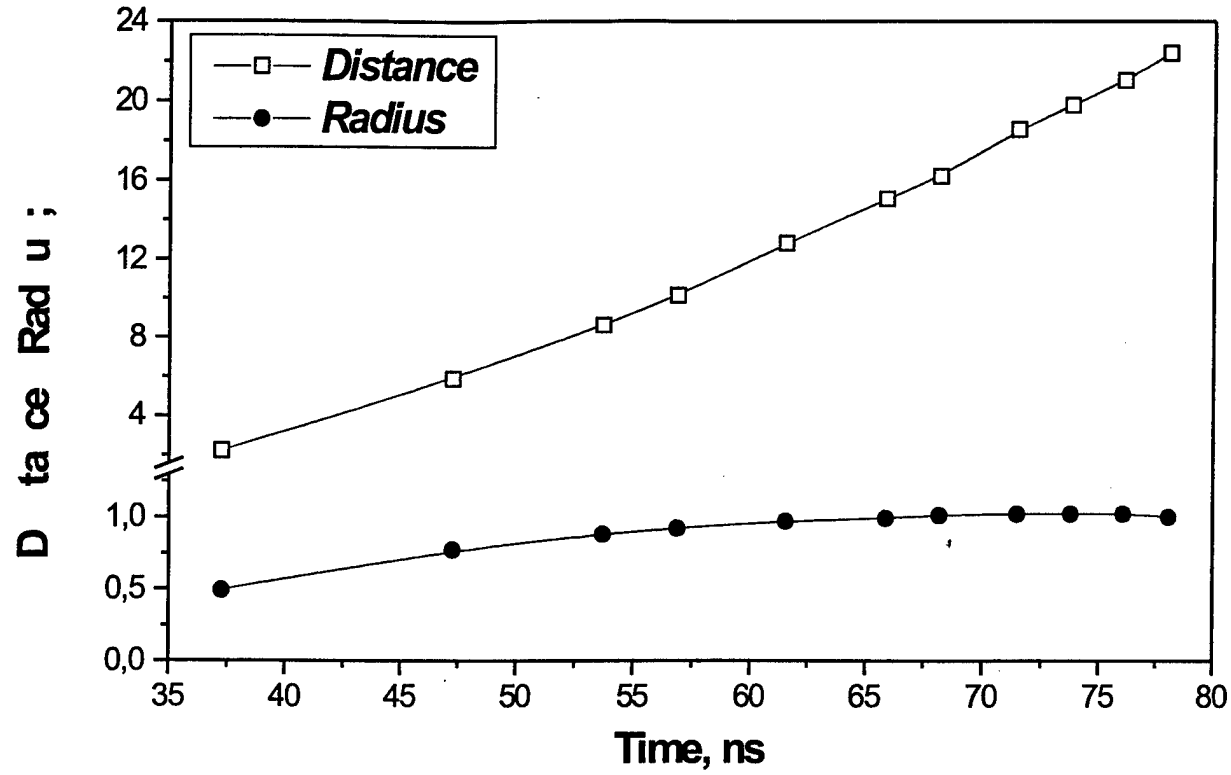

Figure 10.7: Streamer length and radius *vs* time.

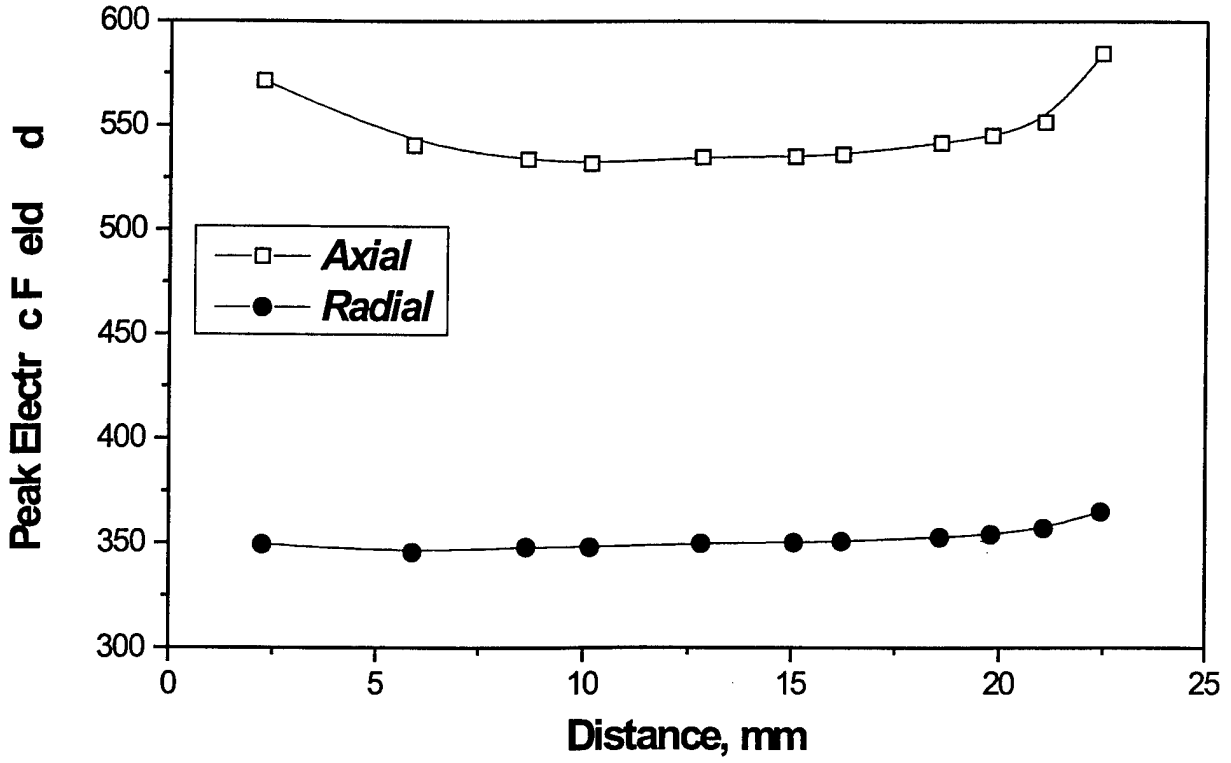

Figure 10.8: Peak values of the radial and axial electric fields *vs* a streamer length.

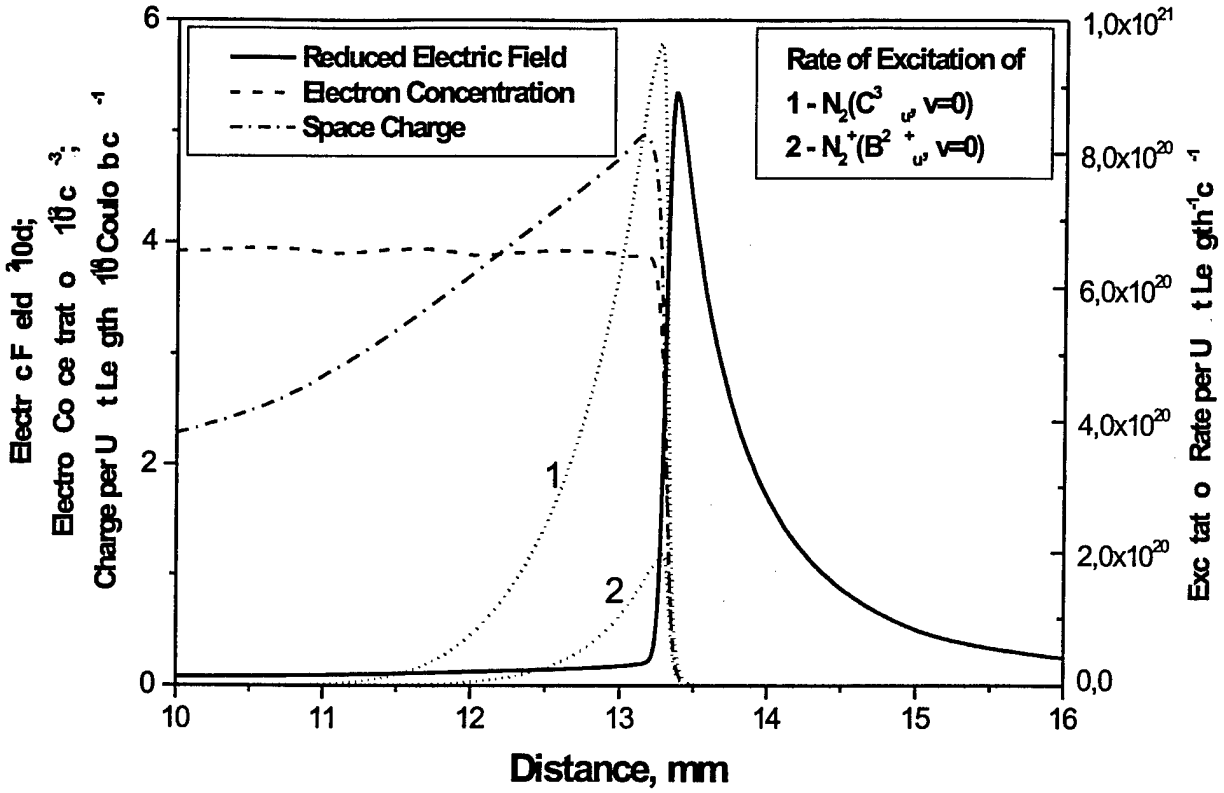

Figure 10.9: Streamer head structure at a time moment $t = 62$ ns.

Dependencies of production of $N_2(C^3\Pi_u, v = 0)$ and $N_2^+(B^2\Sigma_u^+, v = 0)$ per unit length of the channel – states along a discharge gap integrated in time is represented in Fig.10.10,10.11. A quite good coincidence of data may be considered as a validation of streamer description in a diffusion-drift approximation.

The comparison of experimental and calculated peak reduced electric fields along a discharge axis is represented in Fig.10.12. In the region of relatively weak electric field (up to 600 Td) we obtain a quite good coincidence. At small distances (less than 4-5 mm) difference may be explained by the fact that two-term approximation of the Boltzmann equation is not valid in this region because of strong electric fields near the electrode.

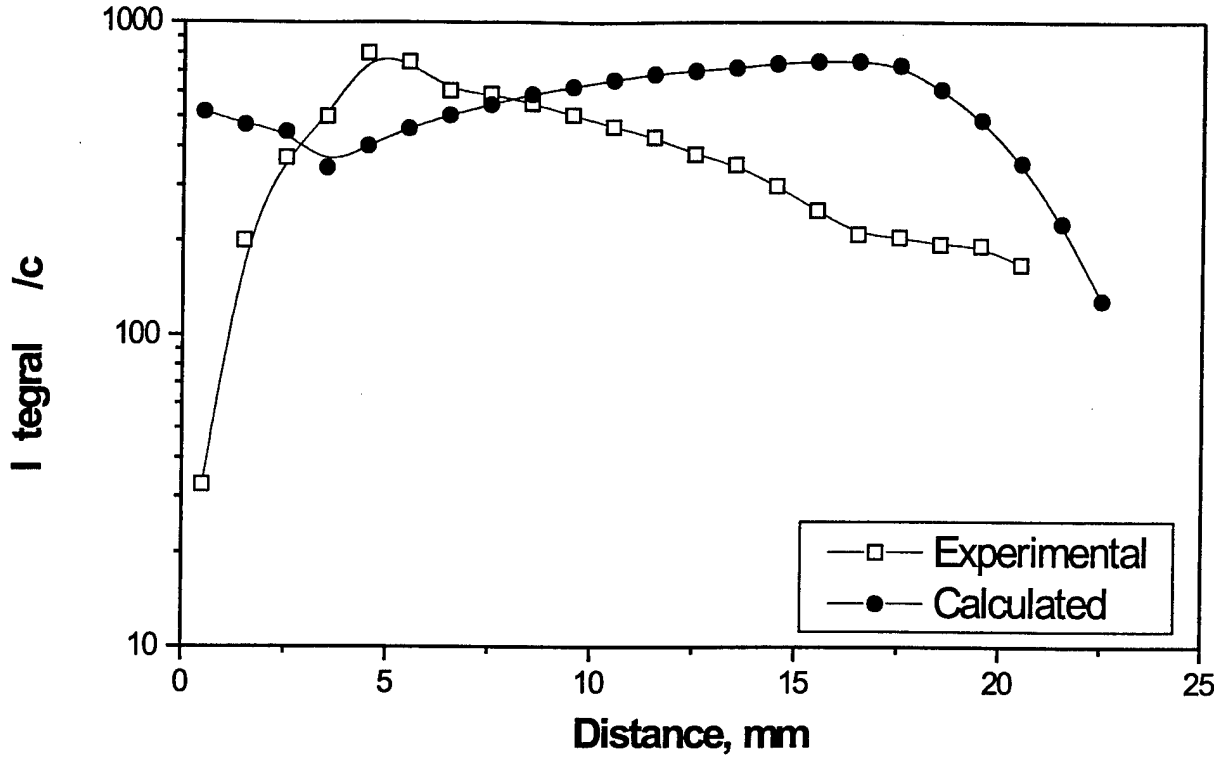

Figure 10.10: Production of the $N_2(C^3\Pi_u, v = 0)$ -state per unit length of the channel along a discharge axis.

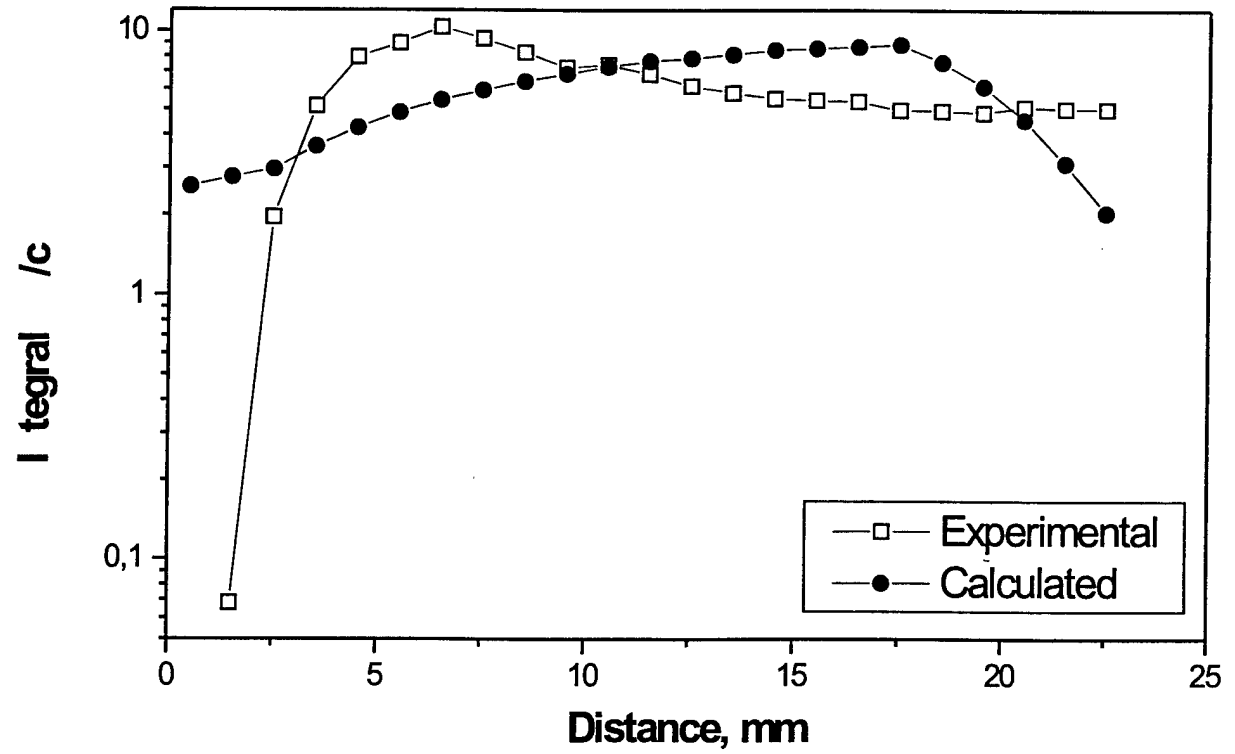

Figure 10.11: Production of the $N_2^+(B^2\Sigma_u^+, v = 0)$ -state per unit length of the channel along a discharge axis.

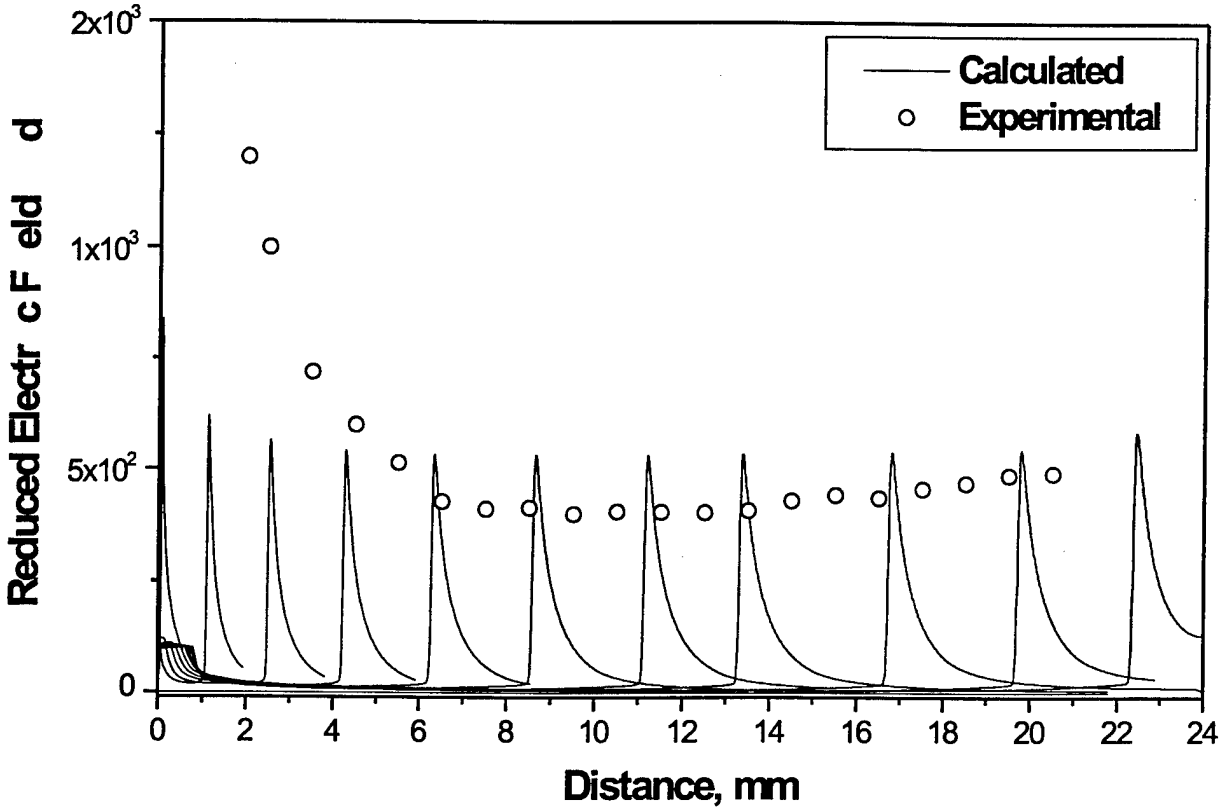

Figure 10.12: Peak electric field propagation. Comparison of experimental data and calculations. Numerical profiles are represented for time moments $t = 28 - 78$ ns with a time step $\Delta t = 5$ ns.

10.2 Simulation of active species production in CH_4:Air mixtures and ignition initiation

In this part, we simulate the properties of a positive streamer in CH_4-air mixtures in a nonuniform electric field. The production of the active particles including atoms, radicals and electronically excited molecules by a long positive streamer is calculated versus gas composition, pressure, and temperature. The results are used to estimate the efficiency of the streamer-corona ignition of the combustion in the considered gaseous mixtures.

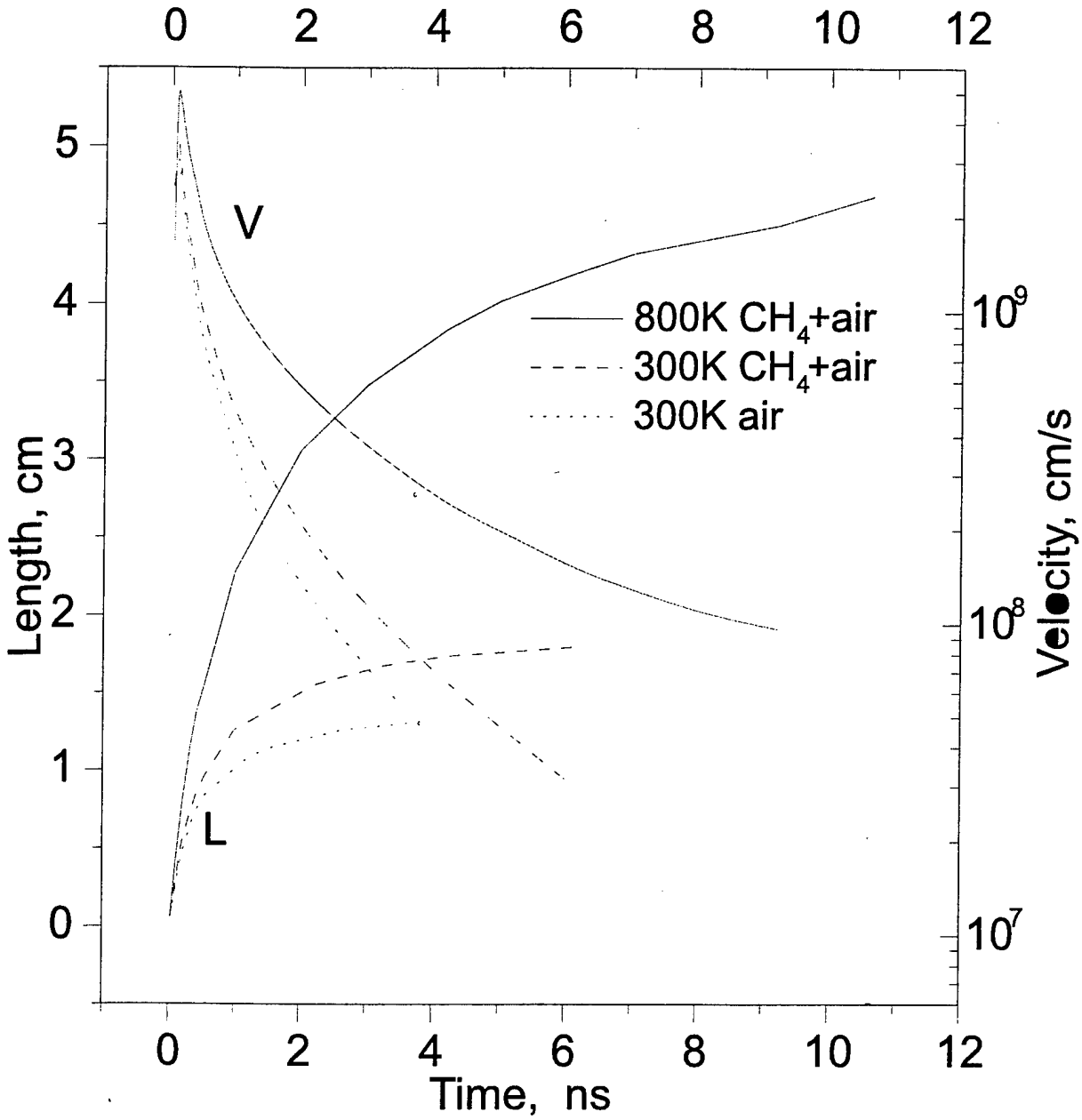

Figure 10.13: Streamer velocity and length

10.2.1 The simulation model

The 1.5D simulation model and numerical method used in the present calculation are essentially the same as those used by the authors to simulate a long-streamer propagation in atmospheric pressure air [58, 89]. That is, the radius of the streamer channel was assumed to be fixed. The basic dynamic equations for the streamer propagation are the continuity equations for electrons, ions and active species and Poisson's equation for the electric field. These equations were solved numerically.

10.3 Dependence of the rate constants on the reduced electric field value for numerical modelling of the streamer propagation in the stoichiometric mixture CH_4 - air.

All rate constants are in units cm^3/s. Reduced electric field is represented as a parameter $\gamma = |\vec{E}| \cdot 10^{16}/[N]$, where E in V/cm, N — in cm^{-3}; drift velocity is in cm/s.

10.3.1 Electrons drift velocity

$$\begin{cases} \text{if } \gamma \le 1 & \text{then} \quad v_{dr} = 2.31 \cdot 10^6 \cdot \gamma^{0.35} \cdot |\vec{E}|_x \\ \text{if } \gamma > 1 \text{ and } \gamma \le 30 & \text{then} \quad v_{dr} = 2.08 \cdot 10^6 \cdot \gamma^{0.74} \cdot |\vec{E}|_x \\ \text{if } \gamma > 30 & \text{then} \quad v_{dr} = 1.1 \cdot 10^5 \cdot \gamma^{1.7} \cdot |\vec{E}|_x \end{cases} \tag{10.14}$$

10.3.2 Processes rate constants with participation of N_2 and O_2

$$N_2 + e = N_2(A^3\Sigma_u^+) + e \tag{10.15}$$

$$k_{10.15} = 10^{-8.43-13.44/\gamma}$$

$$N_2 + e = N_2(B^3\Pi_g) + e \tag{10.16}$$

$$k_{10.16} = 10^{-8.25-14.32/\gamma}$$

$$N_2 + e = N_2(a'^1\Sigma_u^-) + e \tag{10.17}$$

$$k_{10.17} = 10^{-8.27-17.65/\gamma}$$

$$O_2 + e = O_2(a^1\Delta_g) + e \tag{10.18}$$

$$\begin{cases} \text{if } \gamma \le 4.5 & \text{then} \quad k_{10.18} = 10^{-10.26-0.79/\gamma} \\ \text{if } \gamma > 4.5 \text{ and } \gamma \le 20 & \text{then} \quad k_{10.18} = 10^{-8.74-7.68/\gamma} \\ \text{if } \gamma > 20 & \text{then} \quad k_{10.18} = 10^{-8.68-7.7/\gamma} - \gamma \cdot 3.1 \cdot 10^{-3} \end{cases}$$

$$O_2 + e = O_2(b^1\Sigma_g^+) + e \tag{10.19}$$

$$\begin{cases} \text{if } \gamma \le 5 & \text{then} \quad k_{10.19} = 10^{-12.06} + \gamma^2 \cdot 3.97 \cdot 10^{-2} \\ \text{if } \gamma > 5 \text{ and } \gamma \le 10 & \text{then} \quad k_{10.19} = 10^{-9.13-9.7/\gamma} \\ \text{if } \gamma > 10 & \text{then} \quad k_{10.19} = 10^{-9.4-7.05/\gamma} - \gamma \cdot 1.7 \cdot 10^{-3} \end{cases}$$

$$O_2 + e = O + O + e \tag{10.20}$$

$$\begin{cases} \text{if } \gamma \le 60 & \text{then} \quad k_{10.20} = 10^{-8.55-13.24/\gamma} \\ \text{if } \gamma > 60 & \text{then} \quad k_{10.20} = 10^{-8.96+9/\gamma} \end{cases}$$

$$O_2 + e = O + O(^1D_2) + e \tag{10.21}$$

$$\begin{cases} \text{if } \gamma \le 30 & \text{then} \quad k_{10.21} = 10^{-7.6-15.19/\gamma} \\ \text{if } \gamma > 30 & \text{then} \quad k_{10.21} = 10^{-7.18-29.65/\gamma} \end{cases}$$

$$O_2 + e = O + O(^1S_0) + e \tag{10.22}$$

$$k_{10.22} = k_{10.20}$$

$$N_2 + e = e + e + N_2^+ \tag{10.23}$$

$$\begin{cases} \text{if } \gamma \le 30 & \text{then} \quad k_{10.23} = 10^{-8.08-37.57/\gamma} \\ \text{if } \gamma > 30 & \text{then} \quad k_{10.23} = 10^{-6.57-80.76/\gamma} \end{cases}$$

$$N_2(A^3\Sigma_u^+) + e = N_2^+ + e + e \tag{10.24}$$

$$k_{10.24} = 10^{-8.2-20.4/\gamma}$$

$$O_2 + e = e + e + O_2^+ \tag{10.25}$$

$$\begin{cases} \text{if } \gamma \le 30 & \text{then} \quad k_{10.25} = 10^{-8.44-26.11/\gamma} \\ \text{if } \gamma > 30 & \text{then} \quad k_{10.25} = 10^{-6.43-81.46/\gamma} \end{cases}$$

$$O_2 + e + O_2 = O_2^- + O_2 \tag{10.26}$$

$$k_{10.26} = (4.7 - 0.25 \cdot \gamma) \cdot 10^{-31}$$

$$O_2 + e = O^- + O \tag{10.27}$$

$$\begin{cases} \text{if } \gamma \le 10 & \text{then} \quad k_{10.27} = 10^{-9.47-11.29/\gamma} \\ \text{if } \gamma > 10 \text{ and } \gamma \le 60 & \text{then} \quad k_{10.27} = 10^{-10.28-3.75/\gamma} \\ \text{if } \gamma > 60 & \text{then} \quad k_{10.27} = 10^{-10.87+13.96/\gamma} \end{cases}$$

$$O_3 + e = O_2 + O + e \tag{10.28}$$

$$k_{10.28} = 10 \cdot (k_{10.20} + k_{10.21} + k_{10.22})$$

$$N_2 + e = N_2(C^3\Pi_u) + e \tag{10.29}$$

$$k_{10.29} = 10^{-8.23-21.28/\gamma}$$

$$N_2(C^3\Pi_u) + e = e + e + N_2^+ \tag{10.30}$$

$$k_{10.30} = k_{10.104}$$

$$O_2^- + O_2 = e + O_2 + O_2 \tag{10.31}$$

$$\begin{aligned} k_{10.31} &= 10^{-10} \cdot (1 - \exp(-1570/T)) \times \\ &\times (0.73 \cdot \exp(-6030/T_{eff}) \\ &+ 1.75 \cdot \exp(-1540/T - 4490/T_{eff}) \\ &+ 2.63 \cdot \exp(-3060/T - 2970/T_{eff}) \\ &+ 3.50 \cdot \exp(-4560/T - 1470/T_{eff})) \end{aligned}$$

$$T_{eff} = T + 9.83 \cdot \gamma^2$$

$$N_4^+ + e = N_2 + N_2 \tag{10.32}$$

$$k_{10.32} = 2.0 \cdot 10^{-7} \cdot (300/T_e)^{0.7}$$

$$O_4^+ + e = O_2 + O_2 \tag{10.33}$$

$$k_{10.33} = 1.4 \cdot 10^{-6} \cdot \sqrt{T_e}$$

$$O_2N_2^+ + e = O_2 + N_2 \tag{10.34}$$

$$k_{10.34} = 1.5 \cdot 10^{-6} \cdot \sqrt{T_e}$$

$$N_2^+ + e = N + N \tag{10.35}$$

$$k_{10.35} = 2.8 \cdot 10^{-7} \cdot \sqrt{T_e}$$

$$O_2^+ + e = O + O\cdot \tag{10.36}$$

$$k_{10.36} = 2.0 \cdot 10^{-7} \cdot (300/T_e)^{0.7}$$

$$O + O_3 = O_2 + O_2 \tag{10.37}$$

$$k_{10.37} = 2 \cdot 10^{-11} \cdot \exp(-2300/T)$$

$$O + N_2 + O_2 = O_3 + N_2 \tag{10.38}$$

$$k_{10.38} = (6.2 \cdot 10^{-34}) \cdot \left(\frac{300}{T}\right)^2$$

$$O + O_2 = O_3 \tag{10.39}$$

$$k_{10.39} = (6.9 \cdot 10^{-34}) \cdot \frac{300}{T}$$

$$O_2(b^1\Sigma_g^+) + N_2 = O_2(a^1\Delta_g) + N_2 \tag{10.40}$$
$$k_{10.40} = \exp(-253/T) \cdot 4.9 \cdot 10^{-15}$$

$$O(^1S_0) + O_2 = O + O_2 \tag{10.41}$$
$$k_{10.41} = \exp(-850/T) \cdot 2.97 \cdot 10^{-12}$$

$$O(^1S_0) + O_2 = O(^1D_2) + O_2(v) \tag{10.42}$$
$$k_{10.42} = \exp(-850/T) \cdot 1.33 \cdot 10^{-12}$$

$$O(^1S_0) + O = O(^1D_2) + O \tag{10.43}$$
$$k_{10.43} = \exp(-\frac{300}{T}) \cdot 5 \cdot 10^{-11}$$

$$N_2^+ + N_2 + N_2 = N_4^+ + N_2 \tag{10.44}$$
$$k_{10.44} = (5 \cdot 10^{-29}) \cdot \left(\frac{300}{T}\right)^2$$

$$O_2^+ + O_2 + O_2 = O_4^+ + O_2 \tag{10.45}$$
$$k_{10.45} = (2.4 \cdot 10^{-30}) \cdot \left(\frac{300}{T}\right)^3$$

$$O_2^+ + N_2 + N_2 = O_2N_2^+ + N_2 \tag{10.46}$$
$$k_{10.46} = (0.9 \cdot 10^{-30}) \cdot \left(\frac{300}{T}\right)^2$$

$$O_4^+ + O_2 = O_2^+ + O_2 + 02 \tag{10.47}$$
$$k_{10.47} = 3.3 \cdot 10^{-6} \cdot \left(\frac{300}{T}\right)^4 \cdot \exp(-5030/T)$$

$$O_2N_2^+ + N_2 = O_2^+ + N_2 + N_2 \tag{10.48}$$
$$k_{10.48} = (1.1 \cdot 10^{-6}) \cdot \left(\frac{300}{T}\right)^2 \cdot \left(\frac{300}{T}\right)^3 \cdot \exp(-2357/T)$$

$$O_2^- + O_2 + M = O_4^- + M \tag{10.49}$$
$$k_{10.49} = (3.5 \cdot 10^{-31}) \cdot \frac{300}{T}$$

$$O^- + O_2 + M = O_3^- + M \tag{10.50}$$
$$k_{10.50} = (1.1 \cdot 10^{-30}) \cdot \frac{300}{T}$$

$$O_4^- + M = O_2^- + O_2 + M \tag{10.51}$$
$$k_{10.51} = \exp(-1044/T) \cdot 10^{-10}$$

$$O^- + N_2^+ = O + N_2 \tag{10.52}$$
$$k_{10.52} = 2 \cdot 10^{-7} \cdot \sqrt{300/T_{pr}}$$

$$O_2^- + N_2^+ = O_2 + N_2 \tag{10.53}$$
$$k_{10.53} = 2 \cdot 10^{-6} \cdot (300/T_{pr})^{3/2}$$

$$T_{pr} = T + 10 \cdot \gamma^2 \cdot \frac{300}{T}$$

$$O^- + O_2 = O + O_2^- \tag{10.54}$$

$$\begin{cases} \text{if } \gamma < 8 & \text{then} \quad k_{10.54} = 0 \\ \text{if } \gamma \geq 8 \text{ and } \gamma \leq 20 & \text{then} \quad k_{10.54} = \gamma^3 \cdot 1.7 \cdot 10^{-15} \\ \text{if } \gamma > 20 & \text{then} \quad k_{10.54} = \gamma \cdot 6.8 \cdot 10^{-13} \end{cases}$$

$$N_2(a'^1\Sigma_u^-) + N_2(a'^1\Sigma_u^-) = N_4^+ + e \tag{10.55}$$
$$k_{10.55} = 2 \cdot 10^{-10}$$

$$N_2(A^3\Sigma_u^+) + N_2(a'^1\Sigma_u^-) = N_4^+ + e \tag{10.56}$$
$$k_{10.56} = 5 \cdot 10^{-11}$$

$$O_3 + e = O_2^- + O \tag{10.57}$$
$$k_{10.57} = 1 \cdot 10^{-9}$$

$$O_2^- + O_2(a^1\Delta_g) = e + O_2 + O_2 \tag{10.58}$$
$$k_{10.58} = 2 \cdot 10^{-10}$$

$$O_2^- + O_2(b^1\Sigma_g^+) = e + O_2 + O_2 \tag{10.59}$$
$$k_{10.59} = 3.6 \cdot 10^{-10}$$

$$O_2^- + N_2(A^3\Sigma_u^+) = e + N_2 + O_2 \tag{10.60}$$
$$k_{10.60} = 2.1 \cdot 10^{-9}$$

$$O_2^- + N_2(B^3\Pi_g) = e + N_2 + O_2 \tag{10.61}$$
$$k_{10.61} = 2.5 \cdot 10^{-9}$$

$$O^- + O_2(a^1\Delta_g) = e + O_3 \tag{10.62}$$
$$k_{10.62} = 3 \cdot 10^{-10}$$

$$O^- + O_2(b^1\Sigma_g^+) = e + O + O_2 \tag{10.63}$$
$$k_{10.63} = 6.9 \cdot 10^{-10}$$

$$O^- + N_2(A^3\Sigma_u^+) = e + O + N_2 \tag{10.64}$$
$$k_{10.64} = 2.2 \cdot 10^{-9}$$

$$O^- + N_2(B^3\Pi_g) = e + O + N_2 \tag{10.65}$$
$$k_{10.65} = 1.9 \cdot 10^{-9}$$

$$O_2^- + O = e + O_3 \tag{10.66}$$
$$k_{10.66} = 1.5 \cdot 10^{-10}$$

$$O^- + O = e + O_2 \tag{10.67}$$
$$k_{10.67} = 5 \cdot 10^{-10}$$

$$O_3^- + O = e + O_2 + O_2 \tag{10.68}$$
$$k_{10.68} = 3 \cdot 10^{-10}$$

$$O^- + O_2 = e + O_3 \tag{10.69}$$
$$k_{10.69} = 5 \cdot 10^{-15}$$

$$N_2(A^3\Sigma_u^+) + O_2 = N_2 + O + O \tag{10.70}$$
$$k_{10.70} = 2.54 \cdot 10^{-12}$$

$$N_2(A^3\Sigma_u^+) + O_2 = N_2 + O_2(a^1\Delta_g) \quad \text{or} \quad O_2(b^1\Sigma_g^+) \tag{10.71}$$
$$k_{10.71} = 1.29 \cdot 10^{-12}$$

$$N_2(A^3\Sigma_u^+) + O = N_2 + O(^1S_0) \tag{10.72}$$
$$k_{10.72} = 2.1 \cdot 10^{-11}$$

$$N_2(B^3\Pi_g) + N_2 = N_2 + N_2 \tag{10.73}$$
$$k_{10.73} = 5 \cdot 10^{-11}$$

$$N_2(B^3\Pi_g) = h\nu \tag{10.74}$$
$$k_{10.74} = 1.5 \cdot 10^5$$

$$N_2(B^3\Pi_g) + O_2 = N_2 + O + O \tag{10.75}$$
$$k_{10.75} = 3 \cdot 10^{-10}$$

$$N_2(a'^1\Sigma_u^-) + N_2 = N_2(B^3\Pi_g) + N_2 \tag{10.76}$$
$$k_{10.76} = 2 \cdot 10^{-13}$$

$$N_2(a'^1\Sigma_u^-) + O_2 = N_2 + O + O \tag{10.77}$$
$$k_{10.77} = 2.8 \cdot 10^{-11}$$

$$O_3 + O_2(b^1\Sigma_g^+) = O_2 + O_2 + O \tag{10.78}$$
$$k_{10.78} = 1.8 \cdot 10^{-11}$$

$$O(^1D_2) + N_2 = O + N_2 \tag{10.79}$$
$$k_{10.79} = 2.57 \cdot 10^{-11}$$

$$O(^1D_2) + O_2 = O + O_2 \tag{10.80}$$
$$k_{10.80} = 3.20 \cdot 10^{-11}$$

$$O(^1D_2) + O_2 = O + O_2(v) \tag{10.81}$$
$$k_{10.81} = 8.0 \cdot 10^{-12}$$

$$O(^1D_2) + O_3 = O + O + O_2 \tag{10.82}$$
$$k_{10.82} = 1.2 \cdot 10^{-10}$$

$$O(^1D_2) + O_3 = O_2 + O_2(v) \tag{10.83}$$
$$k_{10.83} = 1.2 \cdot 10^{-10}$$

$$O(^1S_0) + O_3 = O(^1D_2) + O + O_2(v) \tag{10.84}$$
$$k_{10.84} = 2.9 \cdot 10^{-10}$$

$$O(^1S_0) + O_2(a^1\Delta_g) = O(^1D_2) + O_2(b^1\Sigma_g^+) \tag{10.85}$$
$$k_{10.85} = 3.6 \cdot 10^{-11}$$

$$O(^1S_0) + O_2(a^1\Delta_g) = O + O + O \tag{10.86}$$
$$k_{10.86} = 3.4 \cdot 10^{-11}$$

$$O(^1S_0) + O_2(a^1\Delta_g) = O + O_2(a^1\Delta_g) \tag{10.87}$$
$$k_{10.87} = 1.3 \cdot 10^{-10}$$

$$N_2^+ + O_2 = O_2^+ + N_2 \tag{10.88}$$
$$k_{10.88} = 6 \cdot 10^{-11}$$

$$N_2^+ + O_3 = O_2^+ + O + N_2 \tag{10.89}$$
$$k_{10.89} = 10^{-10}$$

$$N_4^+ + O_2 = O_2^+ + N_2 + N_2 \tag{10.90}$$
$$k_{10.90} = 2.5 \cdot 10^{-10}$$

$$N_2(B^3\Pi_g) + e = e + e + N_2^+ \tag{10.91}$$
$$k_{10.91} = 10^{-8.2-18.1/\gamma}$$

$$O_4^+ + O = O_2^+ + O_3 \tag{10.92}$$
$$k_{10.92} = 3 \cdot 10^{-10}$$

$$O_2N_2^+ + O_2 = O_2^+ + 2O_2 \tag{10.93}$$
$$k_{10.93} = 10^{-9}$$

$$O_2^- + O = O_2 + O^- \tag{10.94}$$
$$k_{10.94} = 3.3 \cdot 10^{-10}$$

$$O_2^- + O_3 = O_3^- + O_2 \tag{10.95}$$
$$k_{10.95} = 4 \cdot 10^{-10}$$

$$O^- + O_2(a^1\Delta_g) = O_2^- + O \tag{10.96}$$
$$k_{10.96} = 10^{-10}$$

$$O^- + O_3 = O + O_3^- \tag{10.97}$$
$$k_{10.97} = 5.3 \cdot 10^{-10}$$

$$O_3^- + O = O_2^- + O_2 \tag{10.98}$$
$$k_{10.98} = 3.2 \cdot 10^{-10}$$

$$O_4^- + O = O_3^- + O_2 \tag{10.99}$$
$$k_{10.99} = 4 \cdot 10^{-10}$$

$$O_4^- + O = O^- + 2O_2 \tag{10.100}$$
$$k_{10.100} = 3 \cdot 10^{-10}$$

$$O_3^- + N_2^+ = O_3 + N_2 \tag{10.101}$$
$$k_{10.101} = 3 \cdot 10^{7}$$

$$O_4^- + N_2^+ = O_4 + N_2 \tag{10.102}$$
$$k_{10.102} = 10^{-11}$$

$$O^- + O_2^+ = O + O_2 \tag{10.103}$$
$$k_{10.103} = 3 \cdot 10^{-10}$$

$$N_2(a'^1\Sigma_u^-) + e = e + e + N_2^+ \tag{10.104}$$
$$k_{10.104} = 10^{-7.72-18.9/\gamma}$$

$$O_3^- + O_2^+ = O_3 + O_2 \tag{10.105}$$
$$k_{10.105} = 0$$

10.3.3 Water vapor influence

$$e + O_2 + H_2O = O_2^- + H_2O \tag{10.106}$$
$$k_{10.106} = 3.16 \cdot 10^{-30}/(\gamma)^{0.54}$$

$$O^- + H_2O = OH^- + OH \tag{10.107}$$
$$k_{10.107} = 1.4 \cdot 10^{-9}$$

$$OH^- + O = H_2O + e \tag{10.108}$$
$$k_{10.108} = 2 \cdot 10^{-10}$$

$$O_2^- + H_2O + (M) = O_2^-(H_2O) + (M) \tag{10.109}$$

$$k_{10.109} = 2.8 \cdot 10^{-9}$$

$$O_2^-(H_2O) + H_2O + (M) = O_2^-(H_2O)_2 + (M) \tag{10.110}$$
$$k_{10.110} = 2.6 \cdot 10^{-9}$$

$$OH^- + H_2O + (M) = OH^-(H_2O) + (M) \tag{10.111}$$
$$k_{10.111} = 3.2 \cdot 10^{-9}$$

$$OH^-(H_2O) + H_2O + (M) = OH^-(H_2O) + (M) \tag{10.112}$$
$$k_{10.112} = 2.8 \cdot 10^{-9}$$

$$H^- + O_2 = HO_2 + e \tag{10.113}$$
$$k_{10.113} = 1.2 \cdot 10^{-9}$$

$$H^- + H_2O = OH^- + H_2 \tag{10.114}$$
$$k_{10.114} = 3.8 \cdot 10^{-9}$$

$$O_2^+ + H_2O + (M) = O_2^+(H_2O) + (M) \tag{10.115}$$
$$k_{10.115} = 0.93 \cdot 10^{-9}$$

$$O_2^+(H_2O) + H_2O = H_3O^+ + OH + O_2 \tag{10.116}$$
$$k_{10.116} = 10^{-10}$$

$$O_4^+ + H_2O = O_2^+(H_2O) + O_2 \tag{10.117}$$
$$k_{10.117} = 0.5 \cdot 10^{-9}$$

$$N_2^+ + H_2O = N_2 + H_2O^+ \tag{10.118}$$
$$k_{10.118} = 2.2 \cdot 10^{-9}$$

$$H_2O^+ + O_2 = H_2O + O_2^+ \tag{10.119}$$
$$k_{10.119} = 4.3 \cdot 10^{-10}$$

$$H_2O^+ + H_2O = H_3O^+ + OH \tag{10.120}$$
$$k_{10.120} = 0.57 \cdot 10^{-9}$$

$$H_3O^+ + H_2O + (M) = H_3O^+(H_2O) + (M) \tag{10.121}$$

$$k_{10.121} = 1.03 \cdot 10^{-9}$$

$$\mathrm{H_3O^+(H_2O) + H_2O + (M) = H_3O^+(H_2O)_2 + (M)} \tag{10.122}$$
$$k_{10.122} = 0.93 \cdot 10^{-9}$$

$$\mathrm{H_3O^+(H_2O)_2 + H_2O + (M) = H_3O^+(H_2O)_3 + (M)} \tag{10.123}$$
$$k_{10.123} = 0.87 \cdot 10^{-9}$$

$$\mathrm{e + H_2O^+ = H + OH} \tag{10.124}$$
$$k_{10.124} = 2.0 \cdot 10^{-7} \cdot (300/T_e)^{0.7} \cdot 3.15 \cdot 10^{-7} \cdot \sqrt{T_e}$$

$$\mathrm{e + H_3O^+ = H_2O + H} \tag{10.125}$$
$$k_{10.125} = 2.0 \cdot 10^{-7} \cdot (300/T_e)^{0.7} \cdot 5 \cdot 10^{-7} \cdot \sqrt{T_e}$$

$$\mathrm{e + O_2^+(H_2O) = O_2 + H_2O} \tag{10.126}$$
$$k_{10.126} = 2.0 \cdot 10^{-7} \cdot (300/T_e)^{0.7} \cdot 4.2 \cdot 10^{-6} \cdot (300/T_e)^{0.48}$$

$$\mathrm{e + H_3O^+(H_2O) = H + 2H_2O} \tag{10.127}$$
$$k_{10.127} = 2.0 \cdot 10^{-7} \cdot (300/T_e)^{0.7} \cdot 2.5 \cdot 10^{-6} \cdot \sqrt{T_e}$$

$$\mathrm{e + H_3O^+(H_2O)_2 = H + 3H_2O} \tag{10.128}$$
$$k_{10.128} = 2.0 \cdot 10^{-7} \cdot (300/T_e)^{0.7} \cdot 4.5 \cdot 10^{-6} \cdot \sqrt{T_e}$$

$$\mathrm{e + H_3O^+(H_2O)_3 = H + 4H_2O} \tag{10.129}$$
$$k_{10.129} = 2.0 \cdot 10^{-7} \cdot (300/T_e)^{0.7} \cdot 6.5 \cdot 10^{-6} \cdot \sqrt{T_e}$$

$$\mathrm{e + H_2O = O^- + OH} \tag{10.130}$$
$$k_{10.130} = k_{10.27}$$

$$\mathrm{e + H_2O = e + e + H_2O^+} \tag{10.131}$$
$$k_{10.131} = k_{10.25}$$

10.3.4 Processes with hydrocarbons participation

$$CH_4 + e = CH_4^+ + e + e \tag{10.132}$$

$$\begin{cases} \text{if } \gamma \le 30 \quad \text{then} \quad k_{10.132} = 10^{-8.01-26.39/\gamma} \\ \text{if } \gamma > 30 \quad \text{then} \quad k_{10.132} = 10^{-6.47-68.67/\gamma} \end{cases}$$

$$CH_4 + e = CH_4^* + e \tag{10.133}$$

$$\begin{cases} \text{if } \gamma \le 30 \quad \text{then} \quad k_{10.133} = 10^{-7.64-17.07/\gamma} \\ \text{if } \gamma > 30 \quad \text{then} \quad k_{10.133} = 10^{-6.78-40.66/\gamma} \end{cases}$$

$$CH_4 + e = CH_3 + H + e \tag{10.134}$$

$$k_{10.134} = 60 \cdot k_{10.133}/73$$

$$CH_4 + e = CH_2 + H_2 \tag{10.135}$$

$$k_{10.135} = 10 \cdot k_{10.133}/73$$

$$CH_4 + e = CH + H_2 + H \tag{10.136}$$

$$k_{10.136} = 3 \cdot k_{10.133}/73$$

10.3.5 Temperature correction for dissociative attachement

$$k_{10.27} = k_{10.27} \cdot (1 - z) \cdot (1 + 3.2 \cdot z + 7.9 \cdot z^2 + 15.8 \cdot z^3 + 28.2 \cdot z^4)$$

$$z = \exp(-2270/T)$$

10.3.6 Temperature correction for tree-body attachement

If $\gamma > 18.8 \quad k_{10.26} = 0.$
If $\gamma \le 18.8$:

$$k_{10.26} = k_{10.26} \cdot (300/T)^{0.33} \cdot (1 - z) \cdot (1 + 0.5 \cdot z + 0.45 \cdot z^2 + 0.32 \cdot z^3)$$

where

$$z = exp(-2270/T)$$

10.3.7 Secondary collisions correction

Processes (10.20), (10.22), (10.23), (10.25), (10.27)

If $\gamma \geq 14$:

$$\begin{cases} \text{if} \quad T_{vib} < 0.431 & \begin{cases} B_{corr} = 10^{C_{E/n} \cdot Z} \\ Z = \exp(-0.29/T_{vib}) \end{cases} \\ \text{if} \quad T_{vib} \geq 0.431 & \begin{cases} B_{corr} = T_{vib}/0.431 \cdot 10^{C_{E/n} \cdot Z} \\ Z = \exp(-0.29/0.431) \end{cases} \end{cases}$$

$$k_{10.20} = k_{10.20} \cdot B_{corr}$$

$$k_{10.22} = k_{10.22} \cdot B_{corr}$$

$$k_{10.23} = k_{10.23} \cdot B_{corr}$$

$$k_{10.25} = k_{10.25} \cdot B_{corr}$$

$$k_{10.27} = k_{10.27} \cdot B_{corr}$$

For $\gamma \leq 1.5$ parameter $C_{E/n} = 12.57$, for $\gamma > 1.5$ $C_{E/n} = 28.275/(\gamma^2)$.

Process (10.24)

For $\gamma \geq 14$:
If $T_{vib} < 0.431$, then

$$k_{10.24} = k_{10.24} \cdot A_{corr}$$

where

$$A_{corr} = \exp(5.57 \cdot Z \cdot ((1-\tau)^2)/\tau/(1-Z)) \cdot 10^{C_{E/n} \cdot Z}$$

$$Z = \exp(-0.2275/T_{vib})$$

If $T_{vib} \geq 0.431$,

$$k_{10.24} = k_{10.24} \cdot T_{vib}/0.431 \cdot A_{corr}$$

where

$$A_{corr} = \exp(5.57 \cdot Z \cdot ((1-\tau)^2)/\tau/(1-Z)) \cdot 10^{C_{E/n} \cdot Z}$$

$$Z = \exp(-0.2275/0.431)$$

$$\tau = \exp(-0.2275/U_e)$$

Process (10.91)

For $\gamma \geq 14$:
If $T_{vib} < 0.431$, then

$$k_{10.91} = k_{10.91} \cdot A_{corr}$$

where

$$A_{corr} = \exp(1.925 \cdot Z \cdot ((1-\tau)^2)/\tau/(1-Z)) \cdot 10^{C_{E/n} \cdot Z}$$

$$Z = \exp(-0.244/T_{vib})$$

If $T_{vib} \geq 0.431$,

$$k_{10.91} = k_{10.91} \cdot T_{vib}/0.431 \cdot A_{corr}$$

where

$$A_{corr} = \exp(1.925 \cdot Z \cdot ((1-\tau)^2)/\tau/(1-Z)) \cdot 10^{C_{E/n} \cdot Z}$$

$$Z = \exp(-0.244/0.431)$$

$$\tau = \exp(-0.244/U_e)$$

Process (10.104)

For $\gamma \geq 14$:
If $T_{vib} < 0.431$, then

$$k_{10.104} = k_{10.104} \cdot A_{corr}$$

where

$$A_{corr} = \exp(4.905 \cdot Z \cdot ((1-\tau)^2)/\tau/(1-Z)) \cdot 10^{C_{E/n} \cdot Z}$$

$$Z = \exp(-0.232/T_{vib})$$

If $T_{vib} \geq 0.431$,

$$k_{10.104} = k_{10.104} \cdot T_{vib}/0.431 \cdot A_{corr}$$

where

$$A_{corr} = \exp(4.905 \cdot Z \cdot ((1-\tau)^2)/\tau/(1-Z)) \cdot 10^{C_{E/n} \cdot Z}$$

$$Z = \exp(-0.232/0.431)$$

$$\tau = \exp(-0.232/U_e)$$

10.4 Simulation results

Figure 10.2 shows the calculated evolution with time of the streamer velocity and length in humid air (2% H_2O) and in a N_2:O_2:H_2O:CH_4=71:18:2:9 mixture.

The simulation was performed at a pressure of P=10 atm and T=300 and 800 K for a spherical anode of R_a=0.1 cm, an infinitely distant cathode and an applied voltage of U=180 kV (T=300 K) and 100 kV (T=800 K). The radius of the streamer channel was assumed to be r_s=0.03 cm. Our calculation shows that the effect of CH_4 admixture on the streamer properties is less pronounced than that of the gas temperature. The temperature effect is due to a change in the composition of positive ions in the streamer channel and as a result due to decelerating electron-ion recombination [86].

Figure 10.4 shows the axial profiles of densities of atoms, excited molecules and radicals in the streamer plasma in a N_2:O_2:H_2O:CH_4=71:18:2:9 mixture at the instant at which the streamer is 1.15 cm in length. The dominant neutral active species are O, N2($A^3\Sigma_u^+$), CH_3 and H.

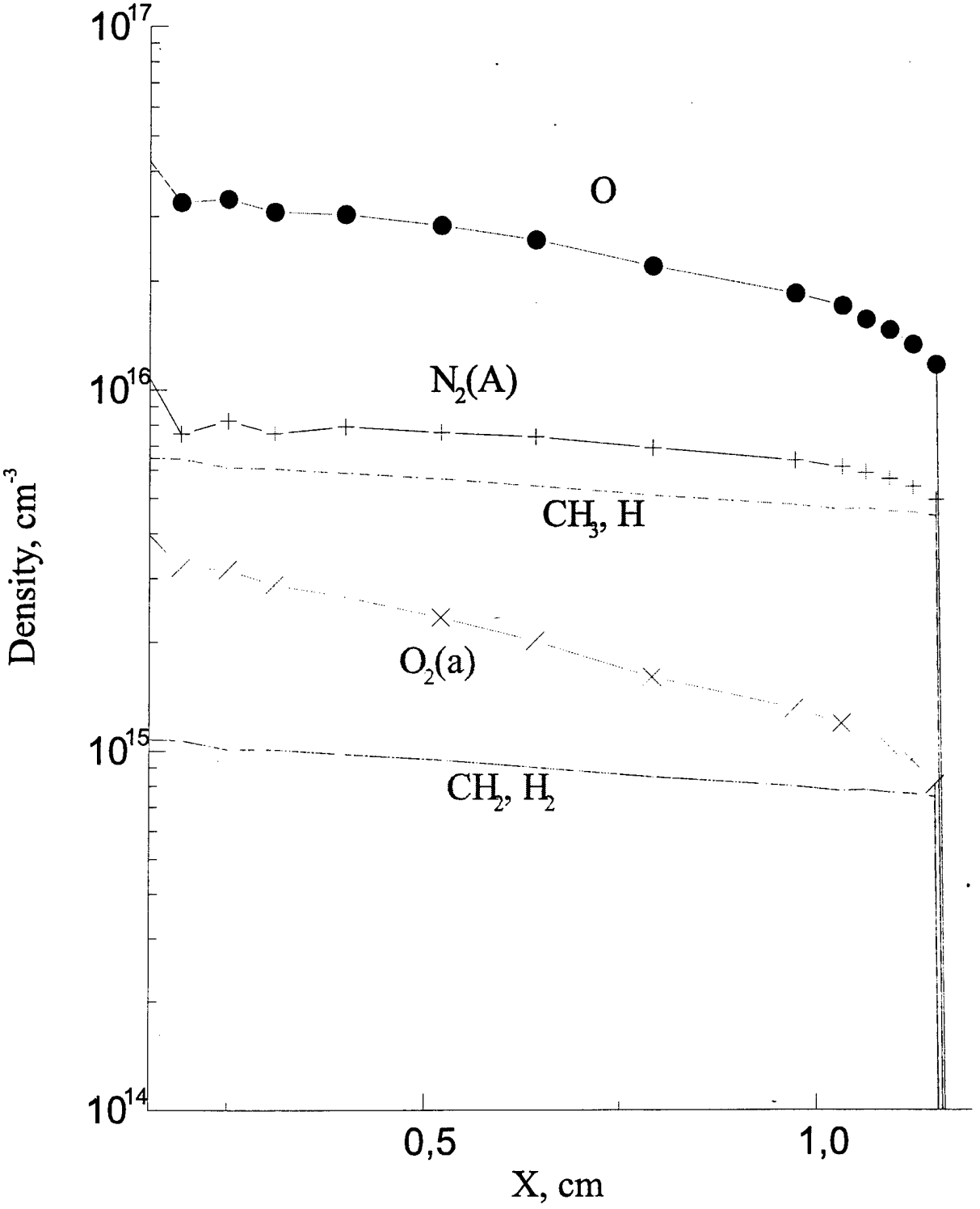

Figure 10.14: Axial profiles of densities

10.5 Initiation of ignition

The densities of active species in the streamer channel at 800 K and 10 atm were considered as initial conditions for the numerical modelling of ignition.

The kinetic scheme including 113 reagents was used for the analysis. For CH_4 — bearing mixtures reactions of C and C_2 hydrocarbons were included:

H, H^-, H^+, H_2, H_2^+, H_3^+, HO, HO^-, HO^+, HO_2, HO_2^+, H_2O, H_2O^+, H_2O_2, $H_2O_2^-$, $H_2O_3^-$, $H_2O_3^+$, H_3O^+,

HNO, HONO, $HONO_2$, HO_2NO_2,

N, $N(^2D^0)$, $N(^2P^0)$, N^+, N_2, $N_2(a^{1\prime}\Sigma_u^-)$, $N_2(a^1\Pi_g)$, $N_2(A^3\Sigma_u^+)$, $N_2(B^3\Pi_g)$, $N_2(B^3\Sigma_u^-)$, $N_2(C^{1,3}\Pi_u)$, $N_2(C^3\Pi_u)$, $N_2(W^1\Delta_u)$, N_2^+, $N_2(w^3\Delta_u)$, N_3, N_3^+, N_3O^+, N_4^+, NH, NH^+, NH_2, NH_3, NH_3^+, NH_4, NO, NO^-, NO^+, NO_2, NO_2^-, NO_2^+, NO_3, NO_3^-, NO_3^+, N_2O, N_2O^-, N_2O^+, $N_2O_2^+$, $N_2O_3^-$, $N_2O_3^+$, N_2O_4, N_2O_5,

O, $O(^1D)$, $O(^1S)$, $O^-(^2P^0)$, $O(^3P)$, O^-, O^+, O_2, $O_2(a^1\Delta_g)$, $O_2(A^3\Sigma_u^+)$, $O_2(b^1\Sigma_g^+)$, O_2^-, O_2^+, O_3, O_3^-, O_3^+, O_4^-, O_4^+,

electrons,

C, CO, CO_2, C^+, C_2^+, CO^+, CO_2^+, $C_2O_2^+$,

CH, CH_2, CH_3, CH_4, C_2H, C_2H_2, C_2H_3, C_2H_4, CH^+, CH_3^+, CH_4^+, C_2H^+, $C_2H_2^+$, $C_2H_3^+$,

HCHO, HCO, HCOOH, CH_3OOH, CH_3O_2, CH_3O, CH_3OOCH_3, CH_3OH.

Figures 3-5 shows the evolution in time of the mole fraction of a) electronically excited particles (fig.10.5); b) positive ions (fig.10.5) and c) dominant radicals and products of chemical reactions (fig.10.5).

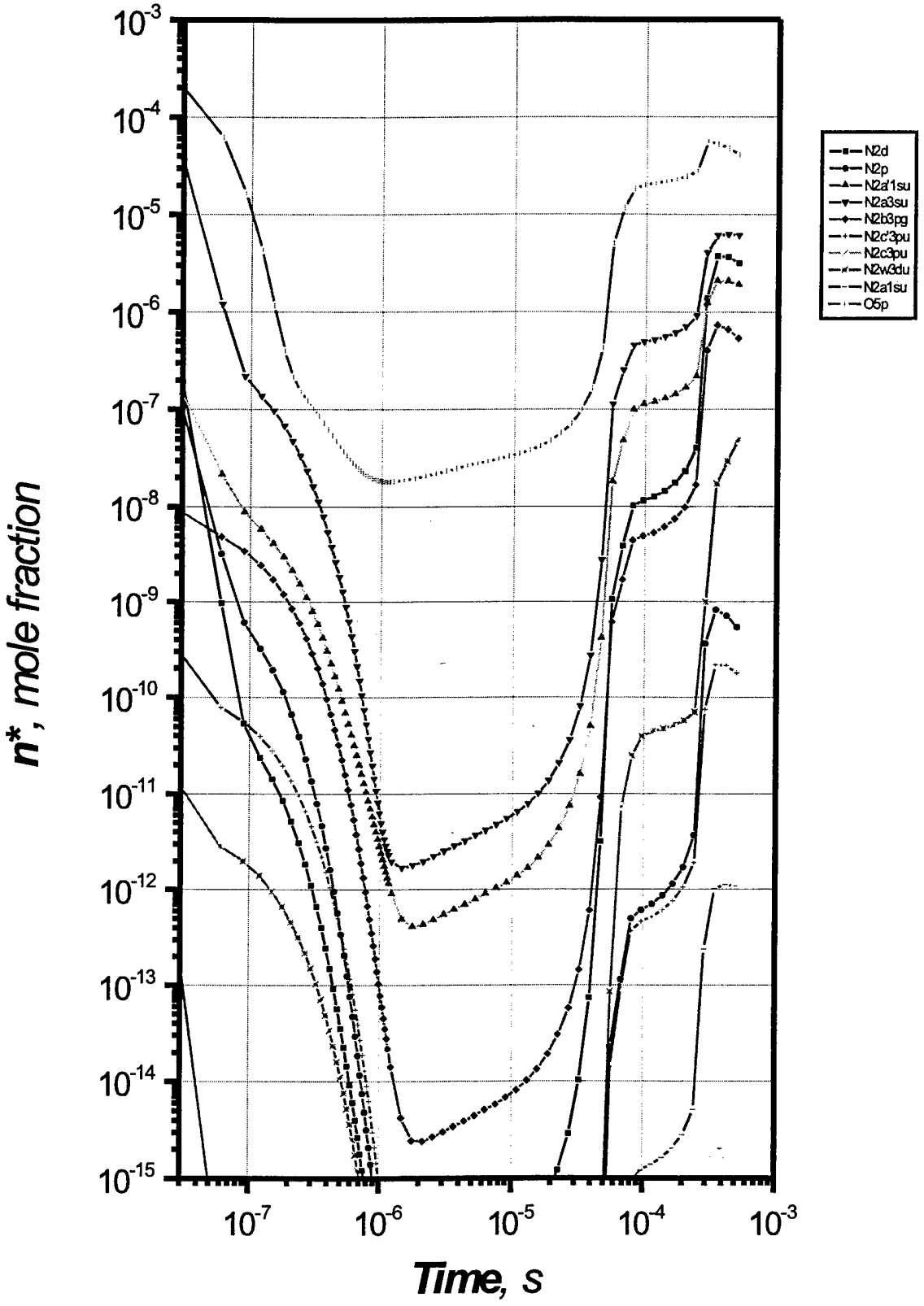

Figure 10.15: Time evolution of the mole fractions of electronically excited particles

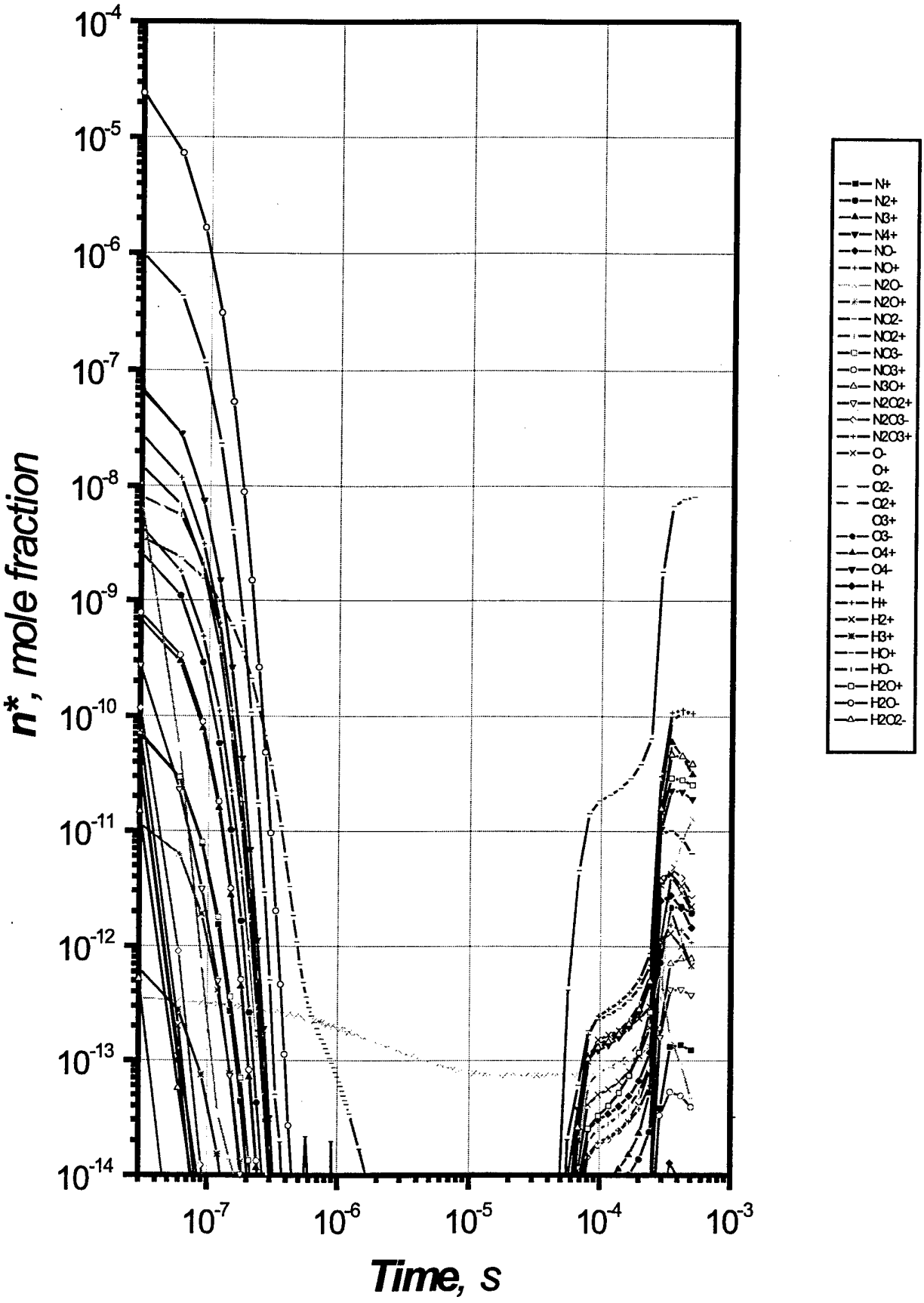

Figure 10.16: Time evolution of the mole fractions of positive ions

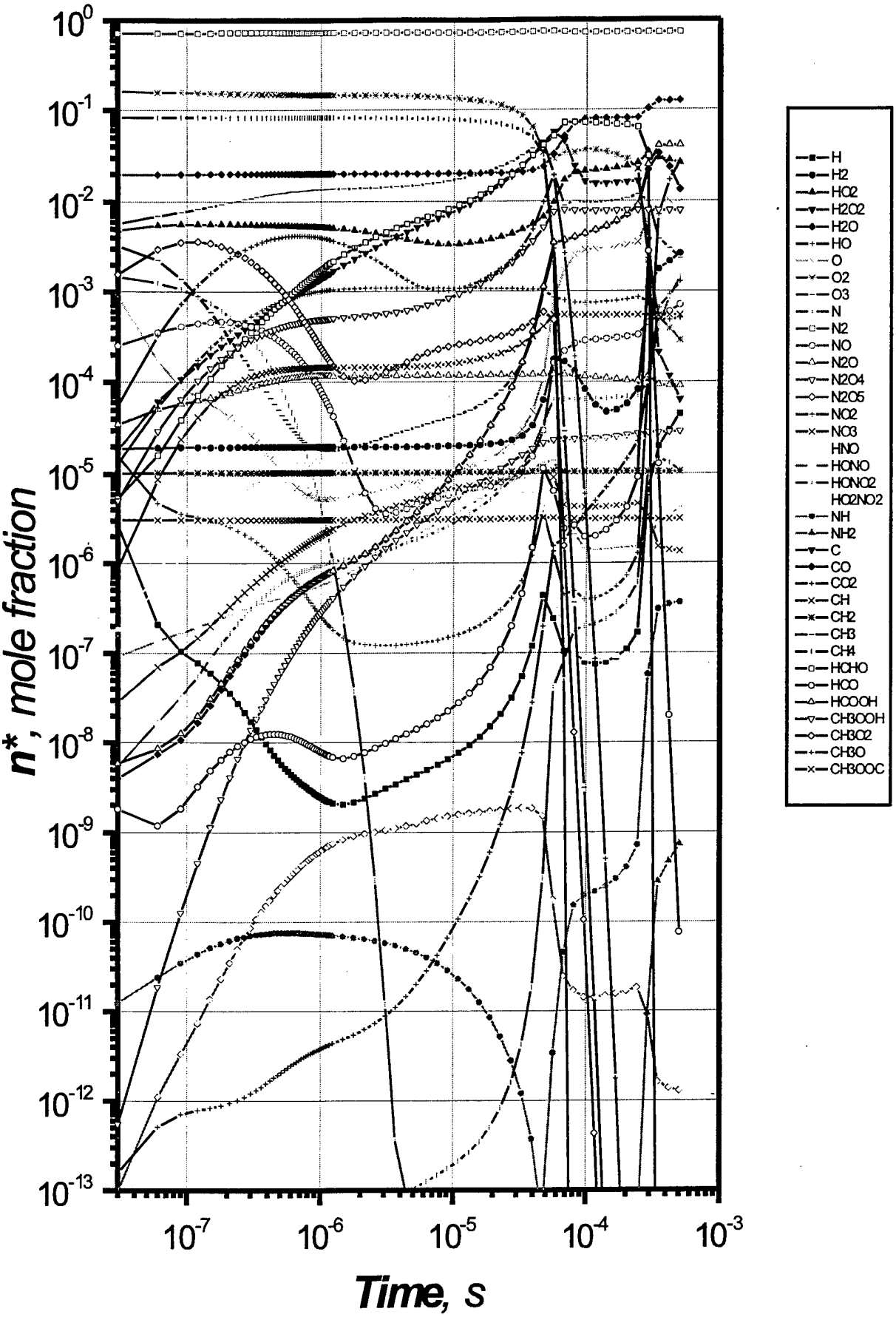

Figure 10.17: Time evolution of the mole fractions of dominant radicals and products

Four characteristic periods of the system evolution may be pointed out. The first one is a recombination of ions and electrons. At high pressures both dissociative recombination to form atoms and radicals and three-body recombination are important.

The relaxation of electronically excited states is mainly dominated by collisional quenching. This leads to an increase in the density of active species (see, for instance, the process $N_2(B^3\Pi_g) + O_2 \rightarrow N_2 + O + O$). Excited molecules (excluding $O_2(a^1\Delta_g)$) and ions disappear for a fraction of a millisecond.

The second stage corresponds to the initiation period of ignition. The possibility of ignition initiation depends strongly upon processes in this stage. A necessary condition for the development of combustion is the maintenance of the chain mechanism of reaction which is determined by the relation between the rates of the chain termination reactions and those of the chain propagation reactions. Because of a significant difference between the thresholds of these reactions (a few thousand degrees for chain propagation and zero energy for three-body reactions of recombination) the value of gas temperature is the main factor which governs the ignition.

The time of explosion induction is about 70 μs under considered conditions (stage 3). A slow accumulation of radicals and slow increase in temperature give way to their explosive rise.

The fourth stage (100 μs and later) is characterized by a slow recombination of radicals at high gas temperature; the system reaches an equilibrium for milliseconds.

The effect of the channel radius on the delay time of ignition was investigated. The results of the 1.5D simulation depend on the radius of the streamer which affects the electric field at the streamer head and the density of electrons and excited particles in the streamer channel.

Figure 10.5 represents the results of active particle production calculation in dependence with the channel radius. It is clearly seen that r_c variation leeds to the significant active particle concentration change.

Figure 10.5 shows the induction time *vs* channel radius r_c. In the range of $r_c = 0.01 - 0.03$ cm the induction time depends on r_c slightly. At higher and lower values of r_c the effect becomes more pronounced.

Reduced electric field value increase and ionic mixture composition change during the gas temperature rise lead to the increase of active and excited particles production 10.5. Together with the total chemical reaction rate increase this leads to the dramatic ignition induction time reduction.

Figure 10.5 shows the effect of initial gas temperature on the delay time of ignition. Calculated induction time as a function of T for the thermal ignition and the ignition which was initiated by the streamer discharge at voltage of 80 kV, the discharge length of 1.4 cm and $r_c = 0.03$ cm were presented. The difference between the thermal ignition time and the time of the ignition by streamer is an order of magnitude at $T = 1200$ K and exceeds 3 orders of magnitude at $T = 800$ K.

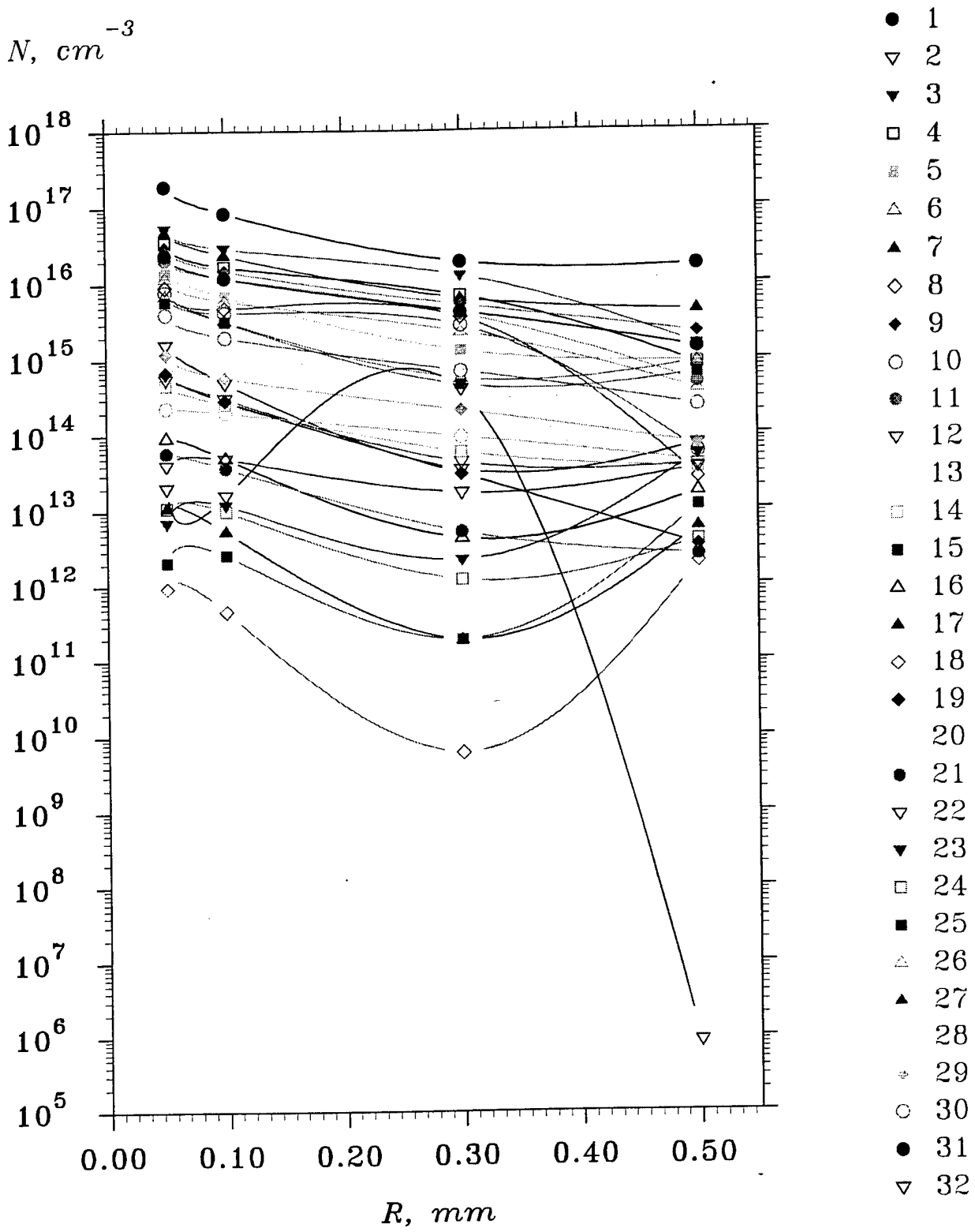

Figure 10.18: Dependence of calculated active particle production in the streamer channel *vs* channel radius. Mixture N_2:O_2:H_2O:CH_4=71:18:2:9. p = 10 atm. U = 80 kV, T_0 = 800 K. Numbers on the graph represents, correspondingly: O, OH, e, $O(^1D_2)$, $O_2(a^1\Delta_g)$, $O_2(b^1\Sigma_g^+)$, $N_2(A^3\Sigma_u^+)$, $N_2(B^3\Pi_g)$, $N_2(a'^1\Sigma_u^-)$, $N_2(C^3\Pi_u)$, O_2^+, O_4^+, H_2O^+, H_3O^+, $O_2^+(H_2O)$, $H_3O^+(H_2O)$, $H_3O^+(H_2O)_2$, $H_3O^+(H_2O)_3$, O^-, O_2^-, OH^-, $O_2^-(H_2O)$, $O_2^-(H_2O)_2$, $OH^-(H_2O)$, $OH^-(H_2O)_2$, CH_4^+, CH_3, CH_2, CH, H_2, H, N_2^+

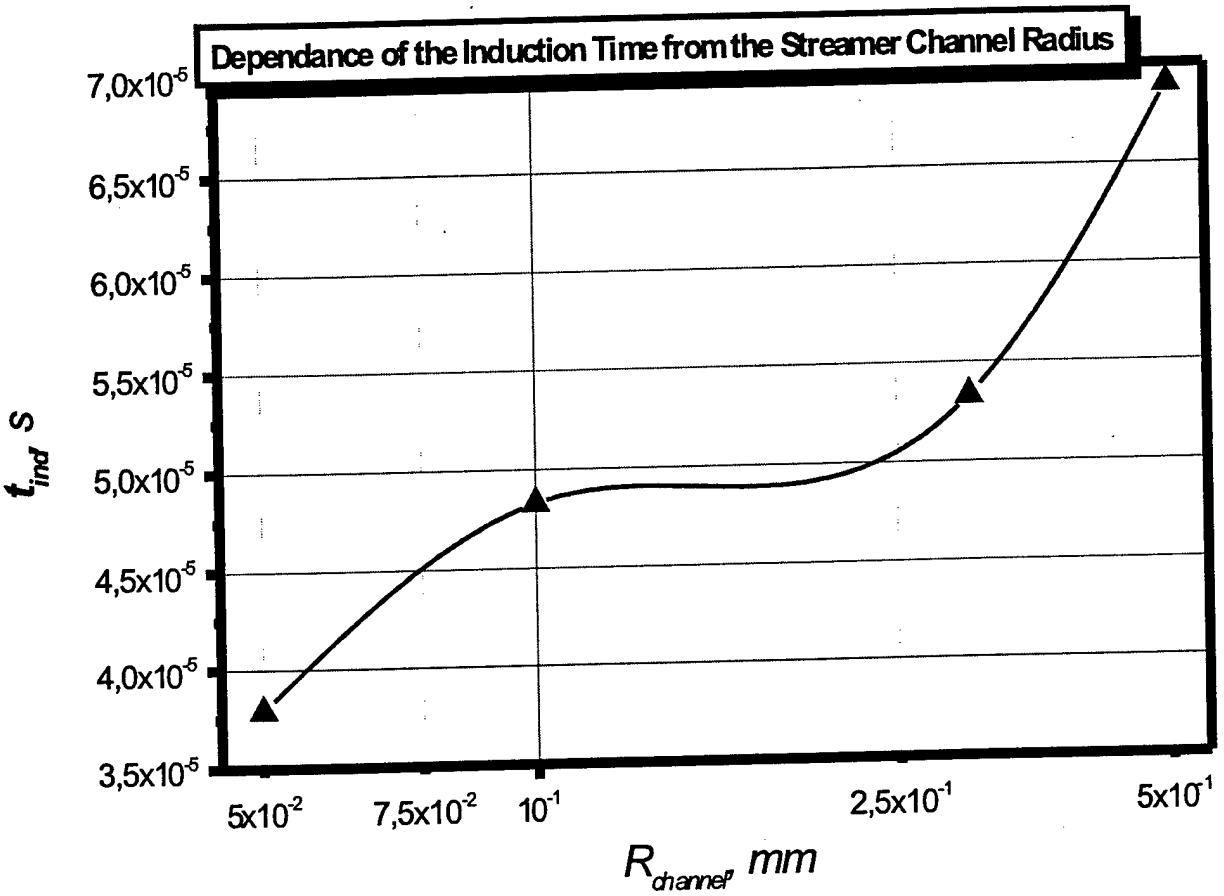

Figure 10.19: Ignition induction time *vs* streamer channel radius r_c N_2:O_2:H_2O:CH_4=71:18:2:9 mixture. $P = 10$ atm. $U = 100$ kV, $T_0 = 800$ K

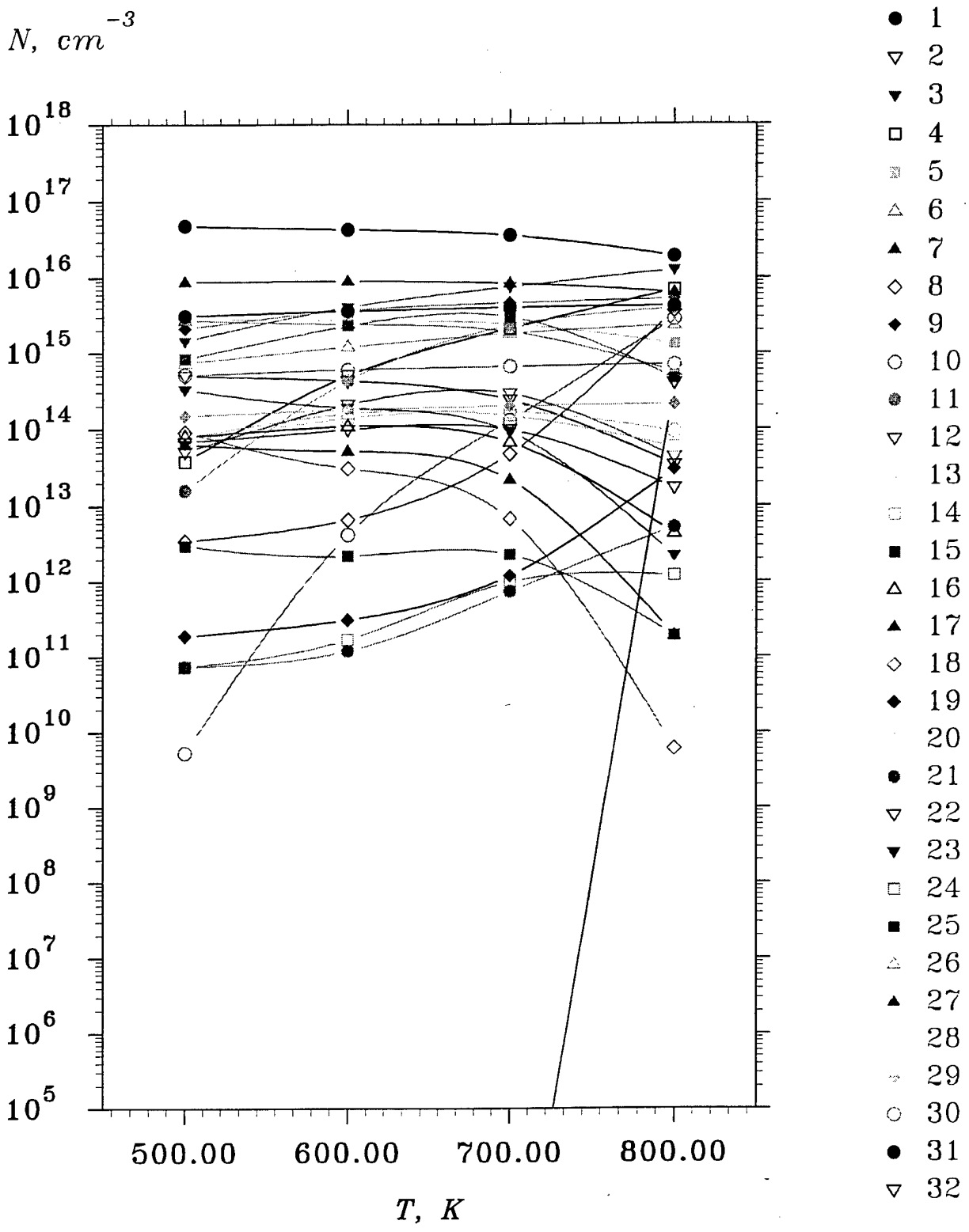

Figure 10.20: Dependence of calculated active particle production in the streamer channel *vs* initial mixture temperature. Mixture N_2:O_2:H_2O:CH_4=71:18:2:9. p = 10 atm. U = 80 kV, $R_{channel}$ = 0.3 mm. Numbers on the graph represents, correspondingly: O, OH, e, $O(^1D_2)$, $O_2(a^1\Delta_g)$, $O_2(b^1\Sigma_g^+)$, $N_2(A^3\Sigma_u^+)$, $N_2(B^3\Pi_g)$, $N_2(a'^1\Sigma_u^-)$, $N_2(C^3\Pi_u)$, O_2^+, O_4^+, H_2O^+, H_3O^+, $O_2^+(H_2O)$, $H_3O^+(H_2O)$, $H_3O^+(H_2O)_2$, $H_3O^+(H_2O)_3$, O^-, O_2^-, OH^-, $O_2^-(H_2O)$, $O_2^-(H_2O)_2$, $OH^-(H_2O)$, $OH^-(H_2O)_2$, CH_4^+, CH_3, CH_2, CH, H_2, H, N_2^+

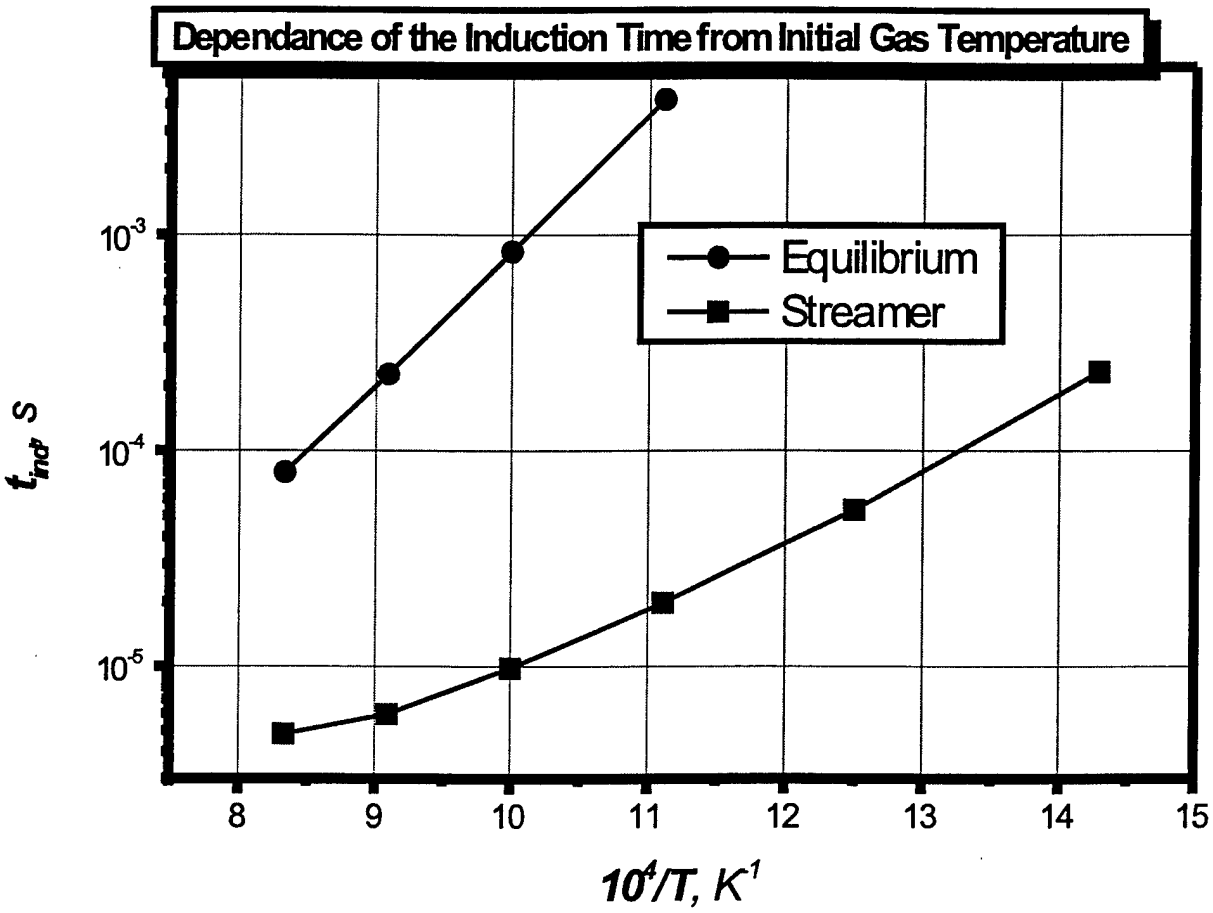

Figure 10.21: Ignition induction time *vs* initial temperature of the gas. N_2:O_2:H_2O:CH_4=71:18:2:9 mixture. $P = 10$ atm. $U = 100$ kV, $r_c = 0.03$ cm

Chapter 11

Experimental Equipment for Investigation of Ignition Threshold under Simultaneous Action of FIW and a Shock Wave.

The installation to investigate superfast homogeneous ignition of supersonic flows (Fig.11.1) consists of the discharge cell connected to a shock tube, the gas evacuation and supply system, the system of various gas discharge initiation, the instrumentation system.

The shock tube is made of the stainless steel has a square cross section of 25×25 mm with the 1.6 m working channel length, high pressure cell length of 60 cm. The working channel is calibrated along the inner cross section, which provides a low level of gas dynamic perturbations in the flow. To evacuate the system roughing-down and diffusive pumps that provide evacuation of the shock tube working channel and its mating dielectric discharge section of the 30 cm length up to 10^{-4} Torr pressure are used. The installation parameters make it possible to obtain the uniformly heated gas volume behind the reflected shock wave, which is motionless relative to the shock tube walls, in pressure range of $P = 0.1 \div 10$ atm, temperature range of $T = 300 \div 5000$ K.

The GIN-9 pulsed voltage generator assembled by the Marks diagram consists of 10 stages. To provide the spark gap operation the pulsed voltage generator column is filled with a nitrogen at pressure from 0.5 to 3 atm, which provides a starting voltage range from 80 to 250 kV. To sharpen the voltage impulse that incomes from the generator to the discharge gap a forming ferrite line of wave resistance Z = 40 was used. At the forming line output the rate of voltage rise in the impulse leading edge is 200 kV/ns, which provides formation of gas breakdown in the form of the fast ionization wave. Velocity of the ionization wave front propagation is $10^9 \div 2 \cdot 10^{10}$ cm/s in dependence on parameters. The pulsed discharge power at voltage $U \simeq 250$ kV is 1.5 GW. The total energy deposition in the discharge depends on its duration which may be controlled in range 10 ns - 1 μs and makes up $5 - 200$ J.

Breakdown in the form of FIW is initiated in a quartz cell of 30 cm length with optical windows for radiation output: quartz KRS $0.4 - 25\mu m$), CaF_2 ($0.12 - 10\mu m$) and LiF ($0.11 - 7\mu m$).

In the problem under consideration the shock wave serves to prepare the gas mixture

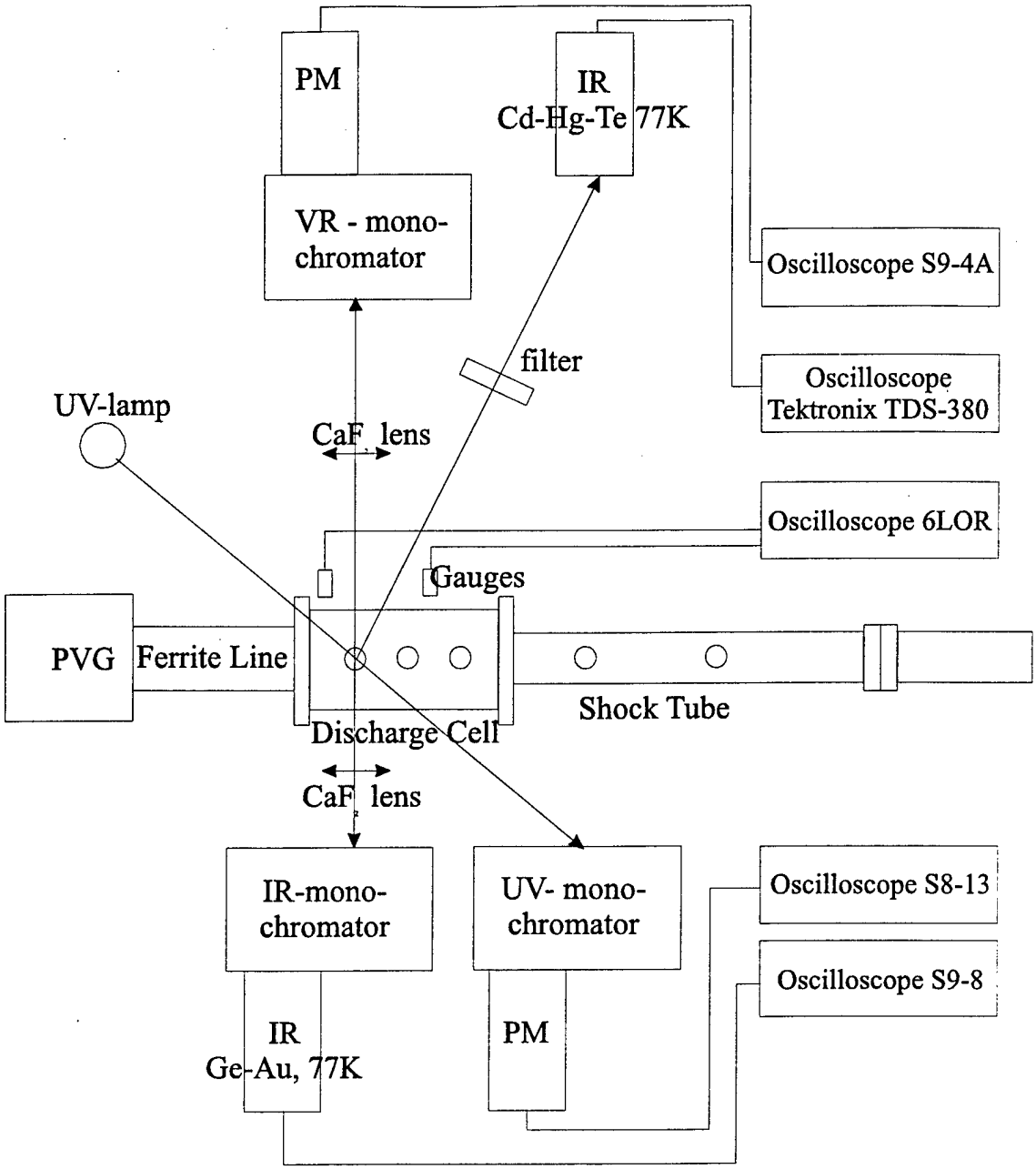

Figure 11.1: Experimental setup.

at the specified temperature (in range $T = 300 \div 5000$ K) and pressure ($P = 0.1 \div 10$ atm). Because the gas dynamic times ($1 - 100\mu$s) are significantly more than the characteristic time of gas excitation by the pulsed breakdown ($1 - 100$ ns) the gas in the shock wave may be regarded as motionless from the view point of the discharge development. A great difference of the characteristic gas dynamic times and the time of discharge development makes it possible to consider that FIW propagates in gas with the parameters distribution (P, T, ρ) corresponding to their instantaneous values behind the shock wave. To exclude the gas parameter change in the observation zone during shock wave interaction with the non-equilibrium plasma of the discharge all experiments will be conducted in a mode of sequential actions on the gas by a shock wave and then FIW. Under these conditions

problems of active particles formation in the discharge and ignition/combustion may be separated in time from the view point of both numerical modeling and experiment.

The system of monitoring of fast nanosecond breakdown electrodynamic parameters includes low-inductive calibrated current shunt to control current impulse parameters and energy deposition in the discharge, the system of electric variable-capacitance transducers and current gauges of various designs to determine the breakdown wave velocity and monitoring of the high-voltage impulse amplitude and shape changes during propagation in the discharge gap. An example of the calibration of gauges is represented in Fig. 11.2. The system of shock wave parameters monitoring includes the system of incident and reflected shock wave velocity measurements by the schlieren method, the system of the initial pressure control and the system of piezoelectric transducers to record the pressure variation in the shock wave. The nanosecond time-resolved emission spectroscopy technique is adjusted in the wavelength region 180–600 nm.

Chapter 12

Summary

- Thus, to understand the basic features of the development and propagation of nanosecond discharge we performed a series of experiments to study the behavior of an electric field and an excitation of electronic degrees of freedom in air and molecular nitrogen under the action of pulsed periodic discharge. Experiments have been performed at 11-15 kV voltage pulse amplitude, 25 ns pulse duration, 2 ns rise time with a repetitive frequency 40 Hz.

  The present experiments have proved that:

  1. The peak value of the electric field in the ionization wave front increases with the growth of pressure, whereas the reduced electric field drops by an order of magnitude from the ~5 kV/ (cm·Torr) at 1 Tor to the ~500 V/(cm·Torr) at 16 Torr. At all the pressures, the electric field peak halfwidth is not more than a few nanoseconds, after that during all the time of the voltage pulse ($\simeq$ 20 ns) electric fields smoothly drop from value optimal for the gas excitation ($\simeq 100 - 500$ Td) to zero. Maximum values of the reduced electric field in the FIW front may significantly exceed the electronic runaway threshold.
  2. There is a strong relationship between electric field behavior and the electronic levels excitation rate. It is shown that the generation of the required electron concentration as well as electron level population take place behind the FIW front in residual fields and sections corresponding to the "electric" and "luminous" FIW fronts are essentially separated in the space.
  3. In a region of relatively low electric fields behind the ionization wave front the average energy, drift velocity of electrons and low-level electron state excitation rate constants can be calculated with a good accuracy using the two-term approximation of Boltzmann stationary equation. Meanwhile, the non-stationary degrading spectrum formed by runaway electrons in the FIW front essentially affects the EEDF formation at high energies. Therewith, the gas ionization rate and high level population essentially increase. The proposed modeling EEDF (2.8) illustrates the stated effect and makes it possible to qualitatively describe the prime regularities of the discharge development in the form of FIW in the whole range of parameters under studies.

- Results obtained in nitrogen and air were applied to describe molecular hydrogen

ignition in the nanosecond high-voltage discharge as a fist step to understand the basic features of ignition of combustible mixtures by this type of breakdown.

The key question for the investigation of ignition in the nonequilibrium conditions is the correlation between different processes on the stage of initiation. The relative importance of electronic (vibrational) levels excitation, dissociation and ionization of molecules is under consideration nowadays.

1. The process of oxidation of molecular hydrogen in the mixture H_2-O_2-N_2 = 0.296 : 0.148 : 0.556 under the action of pulsed nanosecond discharge has been investigated experimentally. The kinetic scheme has been developed for the numerical modelling of the destruction of molecular hydrogen in the discharge. On a base of a comparison of experimental data and results of calculations the analysis of plasmachemical kinetics processes in the system has been performed.
2. Four stages in time were found from the point of view of chemical kinetics; the main processes were determined for each stage. It was proved that up to 100 ns the main role belong to the processes with electronically excited particles, in the microsecond time scale – to the molecular - ion reactions, in the time interval 100 μs – 25 ms – to the reaction with radicals.

- Previously we demonstrated by numerical calculations the fundamental possibility of the FIW application for homogeneous ignition of chemically active mixtures. There was reviewed the problem of ignition of the preliminary heated mixture H_2 - O_2 when the initial active particle concentration is created by the nanosecond pulsed discharge. One of the objectives of this stage of research was a numerical evaluation of efficiency of the FIW application to initiate the H_2 – air and CH_4 – air mixture combustion.

  1. On the basis of numerical modelling a comparative analysis of the shift of ignition threshold in H_2–air and CH_4–air mixtures was performed.
  2. It was found that inasmuch as dissociation degree of CH_4 in discharge substantially smaller then it is for hydrogen, an ignition of an air-methane mixture is much more difficult. The difference between thermal excitation and non-equilibrium initiation of process in methane is not so strong as in hydrogen-containing mixtures.
  3. Absolute value of ignition threshold shift remains significant both for hydrogen - air and for methane - air mixture. For example, for the temperature 1000 K and pressure 1 atm ignition threshold value changes from 10^{-1} to 10^{-5} s for the mixture 29,6% H_2+air and from $3 \cdot 10^{-1}$ to 10^{-2} s for the mixture 9,5% CH_4+air.

- The experimental equipment and a diagnostic system for investigation of ignition threshold under simultaneous action of nanosecond discharge and a shock wave are adjusted and prepared to the next stage of the Project.

- Experimental investigation of the decomposition of N_2O nitrogen oxide in nanosecond pulsed discharge:

1. Relative concentration profiles of electronically excited molecules N_2, NO and N_2^+ during N_2O decomposition in the discharge have been measured;
2. Experimental data of the rate of N_2O decomposition at different pressures have been obtained.

- Theoretical analysis of the elementary exchange reaction AB+C→A+BC with the random distribution of AB reagents over vibration energy.

1. The analytical expressions for microconstants of processes that correspond to certain vibration states of reagents AB(v) and products BC(w) with the use of vibronic terms model have been derived;
2. It has been proved that the values of microconstants are completely determined by the value and temperature dependence of the experimentally measurable rate constant of reaction AB+C→A+BC in thermally equilibrium conditions and value of energy release in reaction ΔH.
3. Comparison of calculations using the proposed model with calculations using other models and experimental data has been performed; the possibility to use the model for a qualitative analysis of vibration excitation effect on kinetics at various conditions of excitation – from strong shock waves at $T_{tr} \gg T_{vib}$ to highly non-equilibrium gas discharge at $T_{tr} \ll T_{vib}$ – has been proved.

- Numerical investigation of the role of vibrationally-excited molecules during the oxidation of molecular hydrogen in H_2-O_2-N_2 stoichiometric mixture in nanosecond pulsed discharge:

1. The numerical model of gas excitation behind the FIW front in the high-current stage taking into account vibrational levels excitation has been developed;
2. The numerical model of chemical kinetics in the complex system taking into account master equations for vibrational levels excitation/relaxation in the discharge afterglow and chemical reactions between excited reagents has been developed;
3. The analysis of the role of reactions with participation of vibrationally excited particles has been performed.

- Numerical simulations of the properties of a positive streamer in CH_4-air mixtures in a nonuniform electric field in 1.5D-formulation.

1. The production of active particles including atoms, radicals and electronically excited molecules by a long positive streamer versus gas composition, pressure, and temperature have been calculated. The results have been used to estimate the efficiency of the streamer-corona ignition of the combustion in the considered gaseous mixtures;
2. The possibility of the ignition at high pressures of CH_4 : Air mixtures by a streamer discharge has been demonstrated. The ignition threshold versus the main parameters of the system has been determined.

- The numerical code for the modelling of discharge development in the form of the fast ionization wave in nitrogen was elaborated. The code is based on the solution of a non-stationary Boltzmann equation by Monte-Carlo Particle-In-Cell method in axial geometry, which corresponds to the majority of experiments with the fast ionization wave.

    1. The governing role of the non-local effects in the propagation of pulsed discharges at high overvoltage and applicability of numerical results together with experimental data on population rates for high-energy emitting electron states for calculation of the energy branching in such a discharges have been demonstrated;
    2. It has been proved that the electron energy distribution function is governed by high-energy electrons in the vicinity of the nanosecond breakdown front.
    3. It has been obtained that the low-energy part of the EEDF in relatively low fields is close to the solution of stationary two-term approximation of Boltzmann equation at the appropriate electric field.
    4. The rates of electron-impact processes near the fast ionization wave front, where the relaxation of the high-energy part of the EEDF leads to the significant differences in constant rate values in comparison with an equilibrium case have been calculated.

Bibliography

[1] Vasilyak L M, Kostyuchenko S V, Kudryavtsev N N, Filyugin I V 1994 *Physics – Uspekhi* **163** 263

[2] Slavin B B, Sopin P I 1990 *High Temp.* **28** 172

[3] Slavin B B, Sopin P I 1992 *High Temp.* **30** 1

[4] Alberta M P, Debontride H, Derouard J, Sadeghi N 1993 *J. Phys. III France* **3** 105

[5] Booth J-P, Fadlallah M, Derouard J and Sadeghi N 1994 *Appl. Phys. Lett.* **65**(7) 819

[6] Booth J-P, Derouard J, Fadlallah M, Sadeghi N 1993 *J. Appl. Phys.* **74** 862

[7] Starikovskaia S.M. 1995 *Plasma Phys. Rep.* **21** 510

[8] Hidaka K, Kouno T, Hayashi I 1989 *Rev.Sci.Instrum.* **60** 1252

[9] Petrov N I, Avanskii V R, Bombenkova N V 1994 *J. Techn. Phys.* **39** 546

[10] Bazelyan E M, Raizer Yu P 1997 *Spark Discharge* (Boca Raton, Florida: CRC Press.)

[11] Akamine Y, Matsuoka S, Hidaka K, Kouno T 1995 *XIth Int. Conf. on Gas Discharges and Their Application, Tokyo* II 210

[12] Kostyuchenko S V, Kudryavtsev N N, Starikovskaia S M, Tretiakov A V, Filiouguine I V 1995 *Chem.Phys.Repts.* **13** 1670

[13] Kolobov V I, Godyak V A 1995 *IEEE Trans. on Plasma Science* **23** 503

[14] Aleksandrov N L, Son E E 1980 *in: Chemistry of Plasma, ed. Smirnov B M* (Atomizdat Press) **7** 35

[15] Phelps A V, Pitchford L C 1985 *Phys. Rev. A.* **31** 2932

[16] Itikawa Y 1974 *Atomic Data and Nuclear Data Tables* **14**

[17] Onda K 1985 *J.Phys.Soc.Japan.* **54** 4544

[18] Schulz G J 1964 *Phys Rev.* **135** A938.

[19] Boness M J W, Schulz G J 1973 *Phys. Rev.* **A8** 2883

[20] Cartwright D C et al 1977 *Phys.Rev. A.* **16**

[21] Spence D , Burrow P D 1979*J.Phys.B.* **12** 179

[22] Winters H F 1966 *J.Chem.Phys.* **44** 1472

[23] Rapp D, Englander-Golden P 1965 *J.Chem.Phys.* **43** 3260

[24] Rapp D et al 1965 *J.Chem.Phys.* **42** 4081

[25] Slinker S P, Ali A W, Taylor R D 1990 *J.Appl.Phys.* **67** 679

[26] Konovalov V P, Skorik M A, Son E E 1992 Plasma Phys. Rep. **18** 778 (In Russian)

[27] Anikin N B, Pancheshnyi S V, Starikovskaia S M, Starikovskii A Yu 1998 *J.Phys.D.: Appl.Phys.* **31** 826

[28] Skubenich V V, Zapesochnui I P 1975 *Chemistry of High Energies* **9** 387

[29] Borst W L, Zipf E C 1970 *Phys.Rev.A.***1** 834

[30] Starikovskaia S M, Starikovskii A Yu, Zatsepin D V 1998 *27th (Int.) Symposium on Combustion* Boulder. WIP Abstracts. P.4.

[31] Morris R A, Viggiano A A, Arnold S T, Maurice L Q, Sutton E A 1998 *27th (Int.) Symposium on Combustion* Boulder. WIP Abstracts. P.343.

[32] Pancheshnyi S V, Starikovskaia S M, Starikovskii A.Yu. 1998 *Plasma Phys. Rep.* **24** 320

[33] Anikin N B, Starikovskaia S M, Starikovskii A Yu 1998 *Plasma Phys.Rep.* **24** 9

[34] Galtsev V E et al 1979 Reprint of the Institute of Atomic Energy

[35] Erwin D A, Kunc J A 1983 *IEEE Transact. On Plasma Science* **11** 266

[36] Spence D, Burrow P D 1979 *J.Phys.B.* **12** 179

[37] Winters H F 1966 *J.Chem.Phys* bf 44 1472

[38] Zipf E C 1978 **Planet Space Sci. 26** 449

[39] Cartwright D.C. 1977 *Phys.Rev. A.* **16** N3

[40] Onda K 1985 *J. Phys. Soc. Japan.* **54** 4544

[41] Schulz G J 1964 *Phys. Rev.* **135** A938

[42] Boness M J W, Schulz G J 1973 *Phys. Rev.* **A8** 2883

[43] Islamov R Sh, Kochetov I V, Pevgov V G 1977 *Reprint FIAN* N169 Moscow: FIAN Publ.

[44] Hake R D, Phelps A V // Phys. Rev. 1967. v.158. No1. p.70.

[45] Gordeev O A, Khmara D V 1998 Proc. IX Conf. on Gas Discharge Physics Russia, Ryazan', P.91.

[46] Melton C E 1972 *J. Chem. Phys.* **57** 4218

[47] Khare S P, Veath W J 1987 *J. Phys. B.* **20** 2101

[48] Hayashi M. "Electron collision cross sections for molecules determined from beam and swarm data" *In: "Swarm Studies and Inelastic Electron-Molecule Collisions* eds. L.C. Pitchford, B.V. McKoy, A. Chutjian, and S. Trajmar. Springer-Verlag, New York, 1987.

[49] Hayashi M. "Electron collision cross sections determined from beam and swarm data by Boltzmann analysis" *In: "Nonequilibrium Processes in Partially Ionized Gases"* eds. M. Capitelli and J.N. Bardsley. Plenum Press, New York, 1990.

[50] Hayashi M. JILA Atomic Collisions Data Center Database. 1987. CITATION 20397.

[51] Physical and chemical processes in gas dynamics. V.1. / Ed. by G.G. Chernyi and S.A. Losev. M. Moscow State Unversity. 1995.

[52] Itikawa Y.1974 *Atomic Data and Nuclear Data Tables* **14** N1

[53] Itikawa Y 1986 *J. Phys. Chem. Ref. Data* **15** 985

[54] Itikawa Y 1989 *J. Phys. Chem. Ref. Data* **18** 23

[55] Rapp D, Englander-Golden P, Briglia D D 1965 *J. Chem. Phys.* **42** 4081

[56] Rapp D, Briglia D D 1965 *J. Chem. Phys.* **43** 1480

[57] Rapp D, Englander-Golden P 1965 *J. Chem. Phys.* **43** 1464

[58] Kostinskii A Yu et al 1990 *Reprint IOF AN N87* Moscow: IOFAN Publ.

[59] Silakov V P 1988 *Plasma Phys. Rep.* **14** 1209

[60] Mitchell J et al. 1986 *in: Physics of ion-ion collisions* M: Atomizdat Publ., P.219

[61] Eremeitsev I G, Piliugin N N 1986 *Applied Mechanics and Technical Physics* N2 P.101

[62] Sal'nikov V.A., Starik A.M. // High Temperature. 1995. V.33. N 1. P.121.

[63] Zyev A.P. // Khimicheskaya Fizika. 1983. V.2. N 7. P.923.

[64] Zyev A.P. // Khimicheskaya Fizika. 1985. V.4. N 11. P.1472.

[65] Zyev A.P., Losev S.A., Osipov A.I., Starik A.M. // Khimicheskaya Fizika. 1992. V.11. N 1. P.4.

[66] Zyev A.P., Tkachenko B.K. // Khimicheskaya Fizika. 1988. V.7. N 11. P.1451.

[67] Achasov O.V., Ragozin D.S. // Vibrational energy exchange rate constants in active laser media with O_2, H_2, H_2O, CO additives. Report N 16. Minsk: ITMO AN BSSR. 1986. 53 P.

[68] Eletskii A V, Smirnov B M 1982 *Physics – Uspekhi* **136** 25

[69] Biondi M et al. 1982 *in: Plasma in lasers* Bekephi J, ed. M: Mir Publ. P.145.

[70] Polak L S et al. 1978 *in: Chemistry of Plasma* Smirnov B M, ed. **5** P.242

[71] Virin L I et al. 1979 *Ion-molecular reactions in gases* M: Nauka Publ.

[72] Aleksandrov N L 1981 *in: Chemistry of Plasma* Smirnov B M, ed. **8** P.90

[73] Rodriguez A E et al. 1991 *J. Appl. Phys.* **70** 2015

[74] Losev S A et al. 1987 *Chem. Phys. Rep.* **6** 1677

[75] Baulch D L et al. 1984 *J. Phys. Chem. Ref. Data* **13** 1259

[76] Del'krya G et al. 1982 *in: Plasma in lasers* Bekephi J, ed. M: Mir Publ. P.176.

[77] Brunet H et al 1985 *J. Appl. Phys.* **57** 1574

[78] Dvoriankin A N et al. 1987 *in: Chemistry of Plasma* Smirnov B M, ed. **14** P.102

[79] Vasilieva A N et al. 1989 *Plasma Phys. Rep.* **15** 190

[80] Golybovskii Yu B et al 1990 *Optics and Spectroscopy* **69** 322

[81] Stott I P, et al 1989 *Proc. R. Soc. Lond.* **424A** 1

[82] Loftus A, Krupenie P H 1977 *J. Phys. Chem. Ref. Data* **6** 113

[83] Ferreira C M et al. 1991 *IEEE Trans. Plasma Science* **19** 229

[84] Pravilov A M 1987 *in: Chemistry of Plasma* Smirnov B M. ed. **14** 65

[85] Capitelli M et al 1989 *in Nonequilibrium vibrational kinetics* M: Mir Publ. P.360

[86] Baulch D L et al. 1980 *J. Phys. Chem. Ref. Data* **9** 295

[87] Nichipor G V et al 1994 *Chem.Phys.Rep.* **13** 69

[88] Wing Tsang, Herron J 1991 *J. Phys. Chem. Ref. Data* **20** 609

[89] Krivonosova O E et al 1987 *in: Chemistry of Plasma* Smirnov B M, ed **14** 3

[90] Kalinenko R A et al 1990 *in: Plasmochemistry-90* Polak L S, ed. M:INKh P.41

[91] Harradine D M et al 1990 *AIAA J.* **28** 1740.

[92] Y.Gardiner, ed. 1998 *Combustion Chemistry* M.: Mir P.217

[93] Krinberg I A 1978 Kinetics of electrons in the ionisphere and plasmosphere of Earth Moscow: Atomizdat.

[94] Jacquin D et al. 1989 *Plasma Chem. And Plasma Proc.* **9** 165

[95] Zuev A P, Starikovskii A Yu 1991 *Sov. J. Chem. Phys.* **8** 1822

[96] Zuev A P, Starikovskii A Yu 1992 *Sov. J. Chem. Phys.* **10** 80

[97] Zuev A P, Starikovskii A Yu 1992 *Sov. J. Chem. Phys.* **10** 255

[98] Zuev A P, Starikovskii A Yu 1992 *Sov. J. Chem. Phys.* **10** 273

[99] Zuev A P, Starikovskii A Yu 1992 *Sov. J. Chem. Phys.* **10** 520

[100] Starikovskii A Yu 1994 *Chem. Phys. Reports* **13** 151

[101] Starikovskii A Yu 1995 *Chem. Phys. Reports* **13** 1422

[102] Pancheshnyi S V, Starikovskaya S M, Starikovskii A Yu 1998 *Chem. Phys. Letters* **294** 523

[103] Sadeghi N, Setser P W 1981 *Chem. Phys. Letters* **77** 304

[104] Sadeghi N, Setser P W 1983 *J. Chem. Phys* **79** 2710

[105] Smirnov B M 1982 *Excited atoms* M.: Energoizdat Publ.

[106] Kyznetsova L A, Kyz'menko N E, Kyziakov Yu A, Plastinin Yu A 1980 *Probabilities of optical transitions for two-atomic molecules* Khokhlov R V, ed. M.: Nauka Publ.

[107] Cahill P 1969 *J. Opt. Soc. Am.* **59** 875

[108] Johnson C E 1972 *Phys. Rev.* **A5** 1026

[109] Allison A C, Dalgarno A 1970 *Atomic Data* **1** 289

[110] Lewis B R 1974 *J. Quant. Spectr. Radiat. Transfer* **14** 537

[111] Hesser J E *J. Chem. Phys. 48* 2518

[112] Stuhl F, Niki H 1971 *J. Chem. Phys.* **55** 3943

[113] Kof L M, Starikovskii A Yu 1996 *26th (Int.) Symposium on Combustion.* Napoli. WIP Abstracts. P.406

[114] Anikin N B, Pancheshnyi S V, Starikovskaia S M, Starikovskii A Yu 1998 *J.Phys.D.: Appl.Phys.* **31** 826

[115] Vasilyak L M, Kostyuchenko S V, Kudryavtsev N N, Filyugin I V 1994 *Physics – Uspekhi* **163**

[116] Electrons in low-temperature plasma. E.E.Son. 1990. Moscow. VZPI Publishing.

[117] Computer Modeling of Gas Lasers. Kenneth Smith, R.M.Thomson. / Plenum Press. New York. 1978.

[118] Frost L.S., Phelps A.V. // Phys.Rev. A13. 471. (1976)

[119] Phelps and Pitchford // Phys. Rev. A 31, 2932 (1985).

[120] Kunhardt and Tzeng // Phys. Rev. A 34, 2148 and 2158 (1986)

[121] Stojanovic and Petrovic // Phys. Rev E (submitted) (1996)

[122] Pitchford // Physics and Applications of Pseudo Sparks, (Wiley, New York, 1990) p. 319.

[123] Jelenkovic and Phelps // Phys. Rev. 36, 5310 (1987).

[124] Itikawa et al. // J. Phys. Chem. Ref. Data 15, 985 (1986)

[125] Malinovskii // Plasma Phys. Rep., 1995 V.21 N 1 P 85.

[126] Anikin N.B., Pancheshnyi S.V., Starikovskaia S.M., Starikovskii A.Yu. // Journal of Physics D: Applied Physics. 1998. V. 31. pp. 826-833.

[127] S.V. Pancheshnyi, S.M. Starikovskaia, A.Yu. Starikovskii // J.Phys.D.: Appl.Phys. **32** (1999) pp.2219-2227.

[128] Nonequilibrium Vibrational Kinetics. // Ed. by M.Capitelli. Springer-Verlag. 1986.

[129] V.D.Rusanov, A.A.Fridman. Physics of Chemically-Active Plasma. Nauka. Moscow. 1984.

[130] Handbook of Chemical Lasers. // Ed. by R.W.F. Gross, J.F. Bott. John Wiley & Sons. 1976.

[131] D.I.Slovetskii. Chemical Reactions Mechanisms in Non-equilibrium Plasma. Nauka. Moscow. 1980.

[132] Adamovich I.V., Macheret S.O., Rich J.W., Treanor C.E., Fridman A.A. // In: Molecular Physics and Hypersonic Flows. Kluwer Academic Publishers. 1996. P. 85-104.

[133] I.S. Zaslonko // Yspekhi Khimii. (In Russian). 1997. V. 66. P.1-27.

[134] Lifshitz A., Teitelbaum H. // Chemical Physics. V.219. 1997. P. 243-256.

[135] Yu.M.Gershenzon, E.E.Nikitin, V.B.Vozenshtein et.al // Khimiya Plazmy. (In Russian). Vol. 5. P.3. Atomizdat. 1978.

[136] S.O.Macheret, V.D.Rusanov, A.A.Fridman // Dokladu Akademii Nayk USSR. (In Russian) 1984. V.276. N.2. P.1420.

[137] Birely J.H., Lyman J.L. // J.Photochem. 1975. V.4. P.269.

[138] A.M.Starik, N.G.Dautov. // Dokladu Akademii Nayk USSR. (In Russian) 1996. V.350. N.6. P.757.

[139] Physical and Chemical Processes in Gas Dymanics. V.1. // Ed. by G.G.Chernyi and S.A.Losev. Moscow. Moscow State University. 1995.

[140] Armenise I., Capitelly M., Colonna G., Gorse C. // Proc. AIAA/ASME 6-th Joint Thermophysics and Heat Transfer Conference, San Diego, USA, 1994.

[141] Computational Methods in Chemical Kinetics. L.S.Polak, M.Ya.Goldenberg, A.A.Levitskii. Moscow. Nauka. 1984.

[142] N.A.Konoplev, A.A.Stepanov, V.A.Sheglov // In: Dymanics of Elementary Atom-Molecular Processes in Gases and Plasma. Lebedev Physical Institute Journal. Moscow. Nauka. 1991. V.213. P.34-60.

[143] Lagana A. // ESCAMPIG 96. European Physical Society. V. 20 E. 1996. P.1-4.

[144] E.E.Nikitin. Theory of Elementary Atom-Molecular Processes in Gases. Moscow. Khimiya. 1970.

[145] Landau L. // Phys. Z. Sow.,1942. V.2. P.46.

[146] Zener C. // Proc. Roy. Soc., 1932. V.A137. P.696.

[147] L.D.Landay, E.M.Lifshits. Quantum Mechanics. Moscow. Nauka. 1983.

[148] Ian W.M. Smith // In: Nonequilibrium Vibrational Kinetics. Ed. by M.Capitelli. Springer-Verlag. 1986. P.137.

[149] Macheret S.O., Rich J.W. // AIAA Paper 93-2860. 1993.

[150] Macheret S.O., Fridman A.A., Adamovich I.V., Rich J.W., Treanor C.E. // AIAA Paper 94-1984. 1994.

[151] Treanor C.E., Marrone P.V. // 1963. Phys.Fluids. V. 6. P.9.

[152] Park C. // J. Thermo.Heat Transfer. 1988. V2. P.1.

[153] Nonequilibrium hypersonic aerodynamics. Park C. J. Wiley & Sons. New York. 1990.

[154] Brun R., Belouaggadia N. // 21st International Symposium on Shock Waves, Paper 1620. Great Keppel Island, 1997.

[155] A.A.Levitsky, S.O.Macheret, L.S.Polak et al. // High Energy Chemistry. (In Russian). 1983. V.17. P.625-632.

[156] C.Park // J. Thermophys. Heat Transfer. 1989. V.3. N 3. P.233.

[157] Combustion Chemistry. // Ed. by W.C.Gardiner, Jr. Springer-Verlag. 1984.

[158] Light G.C. // J.Chem.Phys. 1978. V.68(6). PP.2831-2843.

[159] Johnson B.R., Winter N.W. // J.Chem.Phys. 1977. V.66. P.4116.

[160] Light G.C., Matsumoto J.H. // Chem.Phys.Letters. 1978. V.58. N.4. P 578-581.

[161] Polanyi J.C., Skrlac W.J. // Chem. Phys. 1977. Vol. 23. N2. P.167–194.

[162] . V.D. Rusanov, A.A. Fridman // The Physics of a Chemically Active Plasma. Moscow: Nauka Publ., 1084. 415 P.

[163] . L.S. Polak, P.A. Sergeev, D.I. Slovetskii. // High Energy Chemistry 1973. V.7. N5. P.387.

[164] . M. Capitelli and M. Dilonardo. // Rev.Phys.Appl. 1978. V.13. N.3. P.115.

[165] . N.L. Aleksandrov, A.M. Konchakov, E.E. Son. // Plasma Phys. Rep. 1978. V.4 P.169.

[166] . V.A. Kyz'min, L.S. Polak, P.A. Sergeev, D.I. Slovetskii // High Energy Chemistry 1974. V.8. N2. P.129.

[167] . I.V. Kochetov, V.G. Pevgov, L.S. Polak etc. In the book: Plasmachemical reactions / Polak L.S., ed. Moscow; Inst. of Petroleum-Chemistry Synthesis AS USSR Publ., 1979. P.28.

[168] . Yu.S. Akishev, A.V. Demianov, I.V. Kochetov etc. // High Temp. Teplophys. 1982. Vol.20. N5. P.818.

[169] . D.I. Slovetskii. Nechanisms of the chemical reactions in the nonequilibrium plasma. Moscow: Nauka Publ., 1980. 310 P.

[170] . G.D. Billing, E.R. Fisher. // Chem.Phys. 1979. V.43. P.395.

[171] . A. Lifshitz. J.Chem.Phys. 1974. V.61. P.2478.

[172] B.F. Gordiets, A.I. Osipov, L.A. Shelepin. // Kinetic processes in gases and molecular lasers. Moscow: Nauka Publ., 1980. P.61-64.

[173] . R.C. Millican, D.R. White. J.Chem.Phys. 1963. V.39. P.3209.

[174] . R.C. Millican, D.R. White. J.Chem.Phys. 1963. V.39. P.98; P.3209.

[175] . E.E. Nikitin. The theory of elementary atomic-molecular processes in gases. Moscow: Chemistry Publishing, 1970. P.84.

[176] . G. Billing In a book: Nonequilibrium vibrational kinetics. M.Capitelli, ed. Moscow: Mir Publ., 1989. P.104.

[177] . G.D. Billing, E.R. Fisher. Chem.Phys. 1979. V.43. P.395.

[178] . M. Capitelli and M. Dilonardo. Rev.Phys.Appl. 1978. V.13. N.3. P.115.

[179] V.K. Ablekov, Yu.N. Denisov, F.N.Liubchenko. // Handbook on gasdynamic lasers. Moscow: Machine-building Publ. 1982.

[180] A.P. Zyev, S.A. Losev, A.I. Osipov, A.M. Starik. // Chem. Phys. Rep. 1992. V.11. N 1. P.4-34.

[181] Erwin D.A., et.al. // IEEE Transact. Pl.Sc., 1983, V.11, No4, P.266.

[182] W. Rogowski // Arch. Elektrotech. 1928. V.20. P.99.

[183] Non-Thermal Plasma Techniques for Pollution Control. V.34A of NATO ASI. Series G. / Edited by M. Penetrante and E. Shultheis Springer, Berlin, 1993.

[184] Roeter G. // Electron avalanches and breakdown in gases / Moscow: Mir Publ., 1968.

[185] A. Gilbert, F. Bastien // J.Phys.D:Appl.Phys. 1989. V.22. P.1078.

[186] R.S. Sigmond // J.Appl.Phys. 1984. V.56. N.5. P.1355.

[187] P. Stritzke, I. Sander, H. Raether // J.Phys.D:Appl.Phys. 1977. V.10. P.2285.

[188] M. Simek, V. Babicky, M. Clupek, S. DeBenedictis, G. Dilecce, P. Sunka // J.Phys.D:Appl.Phys. 1998. V.31. P.2591.

[189] N. Spyrou, C. Manassis // J.Phys.D:Appl.Phys. 1989. V.22. P.120.

[190] I.P. Vinogradov // Plasma Sources Sci.Technol. 1999. V.8. P.299.

[191] S.Dali and P.F.Williams // J. Appl. Phys. 1987. V.62. P.4696.

[192] A.A.Kulikovsky // Phys.Rev.E. 1998. V.57. P.7066.

[193] Kinetics Investigations of Avalanche and Streamer Development. E.E.Kunhardt, Y.Tzeng // In: Gaseous Dielectrics IV. / Editors: L.G.Christophorou and M.O.Pace. Pergamon Press. NY. 1984. P.146.

[194] L.E.Kline // J.App.Phys. 1985. V.58. P.3715.

[195] K.Satoh, H.Tagashira, S.Sakamoto // J.App.Phys.D. 1988. V.21. P.922.

[196] J.-M.Guo, C.-H. Wu. Comparisons of Multidimensional Fluid Models for Streamers. // Non-Thermal Plasma Techniques for Pollution Control. V.34A of NATO ASI. Series G. / Edited by M.Penetrante and E.Shultheis Springer, Berlin, 1993. P. 287.

[197] C.Wu and E.E.Kunhardt // Phys.Rev.A. V.37. 1988. P.4396.

[198] P.A.Vitello, B.M.Penetrante, J.N.Bardsley // Phys.Rev.E. 1994. V.49. P. 5574.

[199] A.A.Kulikovsky // J.Phys.D. 1997. V.30. P.441.

[200] A.J.Davies, C.J.Evans // Proc. IEEE. 1967. V.114. P.1547.

[201] P.Bayle and B.Cornebois // Phys.Rev.A. 1985. V.31. P.1046.

[202] R.Morrow and J.J.Lowke // J.Phys.D. 1997. V.30. P.614.

[203] N.L.Alexandrov, E.M.Bazelyan // J.Phys.D. 1996. V.29. P.740.

[204] J.M.Guo and J.Wu // IEEE Trans. Plasma Sci. 1996. V.24 P.1348.

[205] Aleksandrov N.L., Bazelyan A.E., Bazelyan E.M., Kochetov I.V. // Plasma Phys. Rep. 1995. V.21. N1. P.60

[206] Zhelezniak M.B., Mnatsakanian A.H., Sizukh S.V. // High Temp.Teplophys. 1998. V.20. N3. P.423.

[207] Dielectric breakdown in insulating gases: space charge effects and non-uniform fields / by Enrique H.R. Gaxiola. -Eindhoven: Technische Universiteit Eindhoven, 1999

[208] A.F. Djakov, Yu.K. Bobrov, Yu.V. Yourguelenas // XXIV ICPIG (Warsaw, Poland) 1999. V.2. P.208.

[209] S.V. Pancheshnyi, S.V. Sobakin, S.M. Starikovskaia, A.Yu. Starikovskii // J.Phys.D.: Appl.Phys. (will be published)

List of Figures

List of Tables